THE PROPERTIES OF THE SC STARS AND CHEMICAL COMPOSITION OF UY CENTAURI

BY

ROBIN M. CATCHPOLE

South African Astronomical Observatory
P O Box 9, Observatory 7935
SOUTH AFRICA

A Thesis submitted for the Degree of Doctor of Philosophy to the University of Cape Town.

1981

ABSTRACT

This is primarily an observational thesis concerned firstly, with improving our knowledge of the 12 SC stars, defined as a group by Catchpole and Feast (1971) and secondly, with determining the chemical composition of UY Cen, the brightest member of the group.

An atlas, based on 13 A mm^{-1} spectra is presented for the S star π Gru and the C star 19 Psc between 5430 and 6850 Å, while spectra of laboratory CN emission and UY Cen are given between 5430 and 8950 Å. The UY Cen spectra have been measured with a long screw measuring machine and most of the 2484 lines found have been identified. In order to overcome the problems caused by the high density of absorption lines, we use a method of line identification that relies on the statistical interpretation of intensity against wavelength-agreement and Intensity against Excitation diagrams. The objective being to determine which elements are present in the spectrum before assigning identifications to individual lines. The spectrum is found to be rich in 's' process elements and shows weak molecules of both carbides, oxides and hydrides.

U to L (0.36 to 3.4μ) photometry is listed for all the stars and shows them to be a very homogeneous group. Their mean flux distribution is very similar to that of a 2500° black-body but is better approximated by a theoretical model atmosphere showing the H^- opacity minimum at 1.6μ.

A set of wavelengths derived from the line list is used to find the radial velocities of all the stars. These velocities are combined with bolometric apparent magnitudes to investigate SC star kinematics, from which we deduce that they are young Disk population objects with $M_{BOL} = -4.5 \pm 1.0$.

A solar model atmosphere, with pure absorption as the method of line formation, is used to derive astrophysical log gf values from solar equivalent widths and meteor abundances. Spectrum scans of UY Cen are used to obtain the profile and equivalent width of the Na D lines as well as to check the consistency of the adopted photographic continuum, used to measure the equivalent widths of otherwise unblended absorption lines. These data are then used to find the abundances in UY Cen by the curve of growth method and by using Johnson (1974) model atmospheres with pure absorption. The abundances given by the two methods are

in good agreement showing enhancement of 5th and 6th period elements similar to those found in S and C stars and similar to those predicted by Cowley and Downs' (1980) theoretical 's' process calculations. Despite the obvious strength of the Li line, the model atmosphere shows that Li is 0.8 ± 1.0 dex underabundant compared with the Sun. This is mainly a consequence of blending of the Li feature by atomic and molecular lines. Greene's (1972) CN partial pressures are combined with the model atmosphere to deduce that $^{12}C/^{13}C = 40$. The model atmosphere also shows, that for our set of CN equivalent widths, both the CN abundance and the derived isotope ratio depend on the adopted C/O ratio. The variation of the isotope ratio is a consequence of stratification.

We introduce a density contribution function which shows at what depth individual lines are formed in the model atmosphere and demonstrates that stratification is present in UY Cen. The contribution function is also used to investigate the depth dependence of various line forming parameters in the model. The Johnson, Milne-Eddington and Schuster-Schwarzschild models are compared, especially with regard to the wavelength variation of the strong-line-residual-flux; R_o term. This is particularly important in the curve of growth analysis of UY Cen because of the low damping and wide wavelength coverage.

The SC stars are located in the H-R diagram and their abundances are compared with carbon and S stars. A theory is briefly discussed which suggests that there may be two occasions when SC stars are formed, as objects evolve between C and S stars.

The principal results of this thesis have already been published in four papers, namely;

Spectroscopic Observations of SC Stars. Catchpole and Feast (1971)
The Spectrum of the SC Star UY Cen 5413 to 8839 Å. Catchpole (1980)
The Origin of the 6379 Å Absorption in SC and CS Stars. Catchpole (1975)
Metal Abundances in the SC Star UY Cen. Catchpole (1981)

Declaration

I declare the contents of this thesis have not previously been submitted to any University for a degree; and that the work described is entirely my own unless otherwise acknowledged in the text.

Signed by candidate

Signature Removed

R. M. CATCHPOLE

Acknowledgements

I wish to express my sincere thanks to all my dear friends who have encouraged, supported and assisted me, during the production of this thesis.

More specifically I would like to thank, Dr Luis Balona for teaching me how to use a computer, Dr Feast and Professor Warner for their advice and criticism and my employer, the Council for Scientific and Industrial Research, for its material and financial assistance.

LIST OF CONTENTS

CHAPTER 1

History and Definition of SC Stars

1.01 Historical Background

One of the great achievements of 20th century astronomy has been the recognition that the great diversity of spectra, observed amongst the majority of stars, including the sun, can be explained by assuming a fixed composition and varying the conditions of ionization and excitation. As a result of this it is only natural that astronomers, who try and understand the origin of cosmic material, should be most concerned with the exceptions and deviations from this picture.

In 1863 Father Secchii recognised the great diversity of spectra amongst stars redder than the sun and even recognised that carbon played an important role in his class IV, our R and N stars. Fowler (1909) recognised the presence of TiO in Mira, an M star. By 1923 a molecule of Zr, now identified as ZrO, was recognised as the principal origin of S star spectra by Merrill (1923).

Miss Cannon and others (1924) first established the S stars as a class when they recognised three parallel temperature sequences, denoted R-N, M and S, amongst the red stars in the massive Henry Draper catalogue.

It was obvious that the R-N and S stars must in some ways deviate from the Universal abundances. This idea was given added impetus by the discovery of Tc in certain S stars by Merrill (1952). Tc has a half life of $\sim 3 \times 10^5$ years and its presence implies recent nuclear synthesis in these S stars.

In 1954 Keenan (1954) introduced a new scheme of classification for S stars and listed 7 stars that clearly did not fit into this scheme. The stars showed very weak molecules of ZrO and CN, enormous NaD lines and no TiO but, on the basis of their red continuaä , were clearly very cool. One of these stars, FU Mon, was studied at high dispersion by Teske (1956) who showed it contained lines of ZrO and CN while lines of La, Y, Ba, Zr and Sr, which Burbridge et al (1957) describe as 's' processed elements, were all very strong. Bidelman (1950, 1953) following ideas put forward by Fujita in 1938, suggested that these stars were intermediate between S and C stars and had C/O ratios close to unity. His idea was that if all the carbon and oxygen is locked up in CO then

there is none available to form the more usually observed carbides and oxides.

Catchpole and Feast (1971) discovered more members and defined a group, which, on Keenans suggestion, they called SC stars. They used UY Cen, the brightest member of the group, as the type star and listed 12 stars, 6 for the first time. Their definition is stringent and excludes a number of stars that are thought to fall between the S and C stars.

Keenan and Boeshaar (1980) introduced a scheme of classification for S and SC stars which includes both a temperature and C/O parameter. One of the primary objectives of this system is to provide a continuous scheme of classification across the boundary between S and C stars. As a consequence, their SC class includes all the SC stars observed by Catchpole and Feast and an additional 15 objects. Eight of the 15 additional stars have been examined by Catchpole and Feast who class them as CS stars.

The most recent addition to the class is the super lithium rich (SLR) SC star discovered in the Large Magellanic Cloud by Richer and Frogel (1980).

We confine our attention in this thesis to the objects defined as SC stars by Catchpole and Feast. The reason for this is that they form a very homogeneous group of stars, both from the point of view of their colours and their spectra, that probably lie very close to the C/O = unity division. The danger of including too wide a group of objects, when seeking statistical results, is indicated by the SLR star WZ Cas which has usually been called an N star. It is called an SC star by Keenan and Boeshaar and undoubtedly has C/O close to unity. However the complete absence of Zr, reported by Peery (private communication), suggests that it might have quite a different evolutionary origin from the other SC stars. It should also be noted that CS stars are found to scatter more widely in the (J-H) (H-K) diagram than our SC stars.

The importance of studying the SC stars lies in the fact that they are evolved objects which show signs of element synthesis and undoubtedly hold important clues as to the course of stellar evolution. The fact that C/O is very close to unity, which results in the molecules being very weak, means that the SC stars provide an ideal opportunity to study cool evolved star abundances.

1.02 Definition and listing of SC stars

The brightest member of the SC class so far discovered is UY Cen and the SC stars discussed in this thesis are defined as objects spectroscopically similar to UY Cen. The criteria of similarity, applicable at classification dispersion, may be summarised as follows.

1. There must be a marked drop in the continuum intensity for $\lambda < \sim$ 4500 Å. Feast (1954 and 1956) pointed out that AM Cen and GP Ori, which we classify as SC stars, show this strong UV opacity. It is also found in some C stars.

2. The sodium D lines must be strong and in our stars are amongst the strongest seen in any star, with equivalent widths of the order of 50 Å.

3. Spectra of about 80 Å mm^{-1} dispersion should show evidence of both ZrO and CN in the 6000 to 6800 Å spectral region. At this dispersion the ZrO band head at 6473 Å must be clearly visible and diagnostic CN features must be seen at 6444 and 6478.5 Å.

4. The overall match of atomic lines should be similar to those found in UY Cen.

Other interesting spectroscopic features of SC stars are the great strength of SrI 4607 and the simultaneous appearance of both the KI and CaII lines in the 7000 to 8800 Å spectral region.

Although CN is clearly present, low dispersion spectra give the impression of being free of molecules compared with other stars of such red colour. The spectroscopic limits of our definition of SC stars are given by the disappearance of CN towards the S stars and the appearance of C_2 toward the C stars. Similar stars showing very weak C_2 bands are referred to as CS stars by Catchpole and Feast.

The SC stars discussed in this thesis are listed in table 1.01, taken from Catchpole and Feast (1971), and are discussed individually to some extent in the notes. The headings are largely self explanatory indica-

ting either the existence or the comparison of a given feature with that same feature in UY Cen. Entries only appear in the ZrO and CN columns if 15 Å mm^{-1} spectra were available, otherwise there is an entry under "General" based on a comparison with 80 Å mm^{-1} spectra. The evidence for the SrI and ultraviolet opacities are based on blue spectra if available.

Six of the stars listed in table 1.01 already existed in the literature while the remainder are given by Catchpole and Feast (1971) for the first time. The new stars were all discovered on the basis of the Henize objective prism survey. This survey, which lists 264 S or suspected S stars, was never published but is now included in Stephenson's (1976) catalogue of S stars.

TABLE 1.01

Star	α(1900)	δ(1900)	Na D strong	ZrO	CN	Sr I Strong	U.V. Opacity	General
GP Ori	$4^h57^m.1$	+15°11'	Yes	<UY Cen		Yes	Yes	*
FU Mon	$6^h17^m.1$	+ 3°28'	Yes	≈UY Cen	≈UY Cen		*	
V372 Mon	$6^h36^m.5$	- 4°30'	Yes	≈UY Cen			*	≈UY Cen
Henize 244	$8^h46^m.0$	-70°41'	Yes	≈UY Cen	≈UY Cen	Yes	Yes	
Henize 250	$10^h14^m.7$	-60°30'	Yes	≈UY Cen	≈UY Cen	Yes	Yes	
BH Cru	$12^h11^m.0$	-55°43'	Yes	present*		Yes	Yes	≈UY Cen
UY Cen	$13^h10^m.7$	-44°11'	Yes	Yes	Yes	Yes	Yes	
AM Cen	$13^h40^m.9$	-52°51'	Yes	<UY Cen	≈UY Cen	Yes	Yes	
VY Aps	$15^h48^m.9$	-74°12'	Yes	≳UY Cen	≲UY Cen	Yes	Yes	
Henize 166	$16^h33^m.9$	-57°21'	Yes	≈UY Cen	≈UY Cen	Yes	Yes	*
LQ Ara	$16^h42^m.7$	-60°51'	Yes	>UY Cen		Yes	Yes	≈UY Cen
S Lyr	$19^h09^m.1$	+25°50'	Yes	>UY Cen				≈UY Cen

Notes

GP Ori. Slight tendency towards R CMi but more nearly resembles UY Cen. Bidelman (1950) and earlier work by others shows: (1) similarity to FU Mon; (2) strong Na D lines; (3) weakness of bands (suggesting SC type); and (4) strong Sr I 4607 Å. See also Keenan (1954), Spectrum of visual region illustrated by Morgan, Keenan & Kellman (1943) (GP Ori = + 15°726).

Notes continued -

FU Mon. High dispersion study by Teske (1956) with earlier references. Very similar to UY Cen in red (by comparison with Catchpole's high dispersion study of UY Cen). High ultra-violet opacity according to Stephenson (1967).

V372 Mon. Stephenson (1967) places in SC class and finds high ultra-violet opacity.

Henize 244. ZrO possibly slightly weaker than in UY Cen. Henize has doubtful S type and Na D very strong.

Henize 250. Henize has doubtful S type and Na D very strong.

BH Cru. Henize lists as S type but ZrO intensity uncertain and Na D strong. ZrO possibly variable. Also known as Henize 120.

UY Cen. High dispersion study in red (this thesis) shows close similarity to FU Mon. Probably the brightest star of the class. Henize has doubtful S type and Na D very strong. Like GP Ori (Bidelman 1953).

AM Cen. Like GP Ori (Feast 1954, 1956).

VY Aps. Henize has doubtful S type and Na D very strong.

Henize 166. Lithium star. Henize has S type (ZrO intensity uncertain) and Na D possibly very strong.

LQ Ara. ZrO stronger than in UY Cen possibly weaker but ultra-violet opacity and general strength of atomic lines points to SC stars. Henize has S type and Na D strong.

S Lyr. Terrill (1969) (infra-red objective prism) notes that though ZrO is seen, infra-red CN becomes as strong near maximum as is usual only in C stars. This strongly suggests that it is a SC star. Henize has ZrO = $_5$U (i.e. strong but uncertain).

UY Cen is listed in the Henize catalogue as a doubtful S star with very strong Na D lines. Of six other stars with strong Na D lines (Henize intensity >3) five are found to be SC stars and are listed in table 1.01. The exception is TV Vel, which shows C_2 at 4737 Å. Two of the remaining three stars with Na D intensity = 3 are also found to be SC stars. The Henize survey also shows that there are no normal S stars with Na D lines as strong as are found in the SC stars.

Details of the spectra used to discover these stars are given in chapter 2

CHAPTER 2

Line Identification

2.01 Introduction

The object of line identification is to assign a laboratory identification to each absorption line in the star spectrum. This permits us to determine the radial velocity and composition of the star. In a star spectrum rich in both atomic and molecular lines, many of which will form blended features, it is important to strike a useful compromise between identifying only a few lines with great certainty and many lines with little certainty.

2.02 Observational Material and Technique

Red and infrared spectra of UY Cen, covering the wavelengths range from 5400 to 8000Å, were obtained with the coude spectrograph of the Radcliffe 1.88m reflector, while it was still at Pretoria. The spectra used are listed, with details of emulsion and exposure time in Table 2.02.

TABLE 2.02

Plate Number	Star Name & Type	Date	Kodak Emulsion	Exposure time Minutes	Use of Spectrum
DY 940	UY Cen SC	23:4:54	103aF	122	Measured
DY 1422	π Gru S	20:5:65	103aF	74	Plates 1 and 2
DY 2871	UY Cen SC	17:5:71	103aF	90	Plates 1 and 2,analysis
DY 2872	UY Cen SC	17:5:71	103aF	73	Analysis
DY 2873	UY Cen SC	17:5:71	IN Sens	240	Measured,Plate 4,analysis
DY 2878	UY Cen SC	20:5:71	103aD	205	Analysis
DY 2938	19 Psc C	11:7:71	103aF	70	Plates 1 and 2
DY 3559	UY Cen SC	22:5:73	IN Sens	411	Plates 3 and 4,analysis
DY 3563	UY Cen SC	23:5:73	09801	115	Analysis
	CN lab emission		103aF	0.3	Plates 1 and 2
	CN lab emission		IN	0.2	Plates 3 and 4
	CN + LaO emission		IN	0.2	not illustrated

The IN spectra were sensitized by first immersing them in a cold ammonia-distilled water-alcohol solution for 2 minutes. They were then transferred to a pure alcohol drying bath for 2 minutes before drying them in a forced draught. After this the plates were exposed and developed as soon as possible.

The coude spectrograph is mounted on a triangular I beam frame in a separate room which is an integral part of the N telescope pier. The collimator is 15cm in diameter and works at f/30 while the Y camera is a 122cm focal length Schmidt system, with a twice-through corrector plate mounted on the grating. The focal plane is curved and accepts plates of dimensions 23/32 inch x 10 inches. All the spectra listed in Table 2.02 which includes those used in the abundance analysis, were obtained in the first order red at a dispersion of 13 Å mm^{-1}. Spectra used for radial velocity work, which are described in Chapter 4 were obtained with the Z and V cameras. The Z camera is similar to the Y camera except that it has a 53.3cm focal length, giving 31 Å mm^{-1}, while the V camera is a self contained Schmidt system of 20.3cm focal length giving a first order dispersion of 82 Å mm^{-1}.

The coude spectrograph was also used to obtain spectra of lanthanum oxide (LaO) and CN. These were required to help with the identification of these molecules. An arc, struck between carbon electrodes in air, produced a pure CN spectrum. The optical system is shown in Fig. 2.01

The arc consisted of a sharp graphite electrode that could be wound down to strike from a graphite cup, which contained a mixture of graphite powder and LaO. Initial tests with pure LaO in the cup, produced a very dramatic blinding blaze of light. Lens A could be moved to maintain the central image of the arc on the stop. Lens B formed a real image at the stop and lens C transferred this image to the slit of the spectrograph. An order-isolating filter was placed in the beam in front of the stop.

The function of the stop was to isolate the central section of the arc and prevent the continuum radiation from the electrodes swamping the molecular emission. The main purpose of the optical train was to form an enlarged image of the arc at the stop, for the convenience of the observer.

2.03 Plate Measurement and Reduction to Wavelenghts

When seen through a measuring microscope, the absorption lines appear to have a rectangular profile with an apparent width of 0.35 Å, which is also the width at which two lines could be just resolved. The apparent width is largely independant of the strength of the line and bears no direct relation to the widths of the lines judged on density tracings.

A total of 2389 star lines and 322 arc lines, covering a total wavelength range of 5413 to 8839 Å were measured on the plates DY 940 and DY 2873. The plates were measured in both directions using a Hilger long screw measuring machine. Reduction to wavelengths was done in sections using a linear dispersion of 13.1 Å mm^{-1} to calculate star and arc wavelengths. The arc wavelengths were compared with values listed in the MIT lists (Harrison (1939)) and the differences were interpolated with a smooth curve. This curve was then applied to the star lines. The lack of suitable iron lines meant that second order ultraviolet iron arc lines were used. Unlike some old gratings, no systematic difference in the wavelengths given by different orders have been noted with the spectrograph.

The standard error of an individual wavelength determination is ± 0.025 Å, equivalent to ± 2 microns. This is deduced from the internal scatter found in the determination of a mean radial velocity, using 30 lines with good profiles and unique identifications. This velocity was used to convert the observed wavelengths to rest wavelengths. It is the impressive ability of the human eye to bisect a line with an accuracy equal to one tenth its apparent width, that makes this method of wavelength determination and subsequent line identification possible.

2.04 Methods of Line Identification

The usual method of line identification is by the method of multiplets. This requires a rough knowledge of the radial velocity, excitation conditions, and composition of the star. The wavelength of a star line is compared with a list of laboratory wavelengths and a possible identification chosen. In order to confirm this identification other lines of the same element with the same lower energy level (i.e. belonging to the same multiplet) must be found in the star. If these lines are present and they show the same relative intensities in the star as in the laboratory then the identification is confirmed. For the following

reasons, this method is not suitable in a star which is very rich in absorption lines:

1) Many wavelength coincidences can be expected by chance alone.
2) Many of the star lines may be blends having mean wavelengths sufficiently different from the components to escape identification.
3) Blending of star lines will tend to destroy the pattern of multiplet intensities.
4) Some of the more unusual elements or states of excitation may be completely overlooked since they will not be expected.
5) The method can not be applied in cases where multiplet data does not exist, which is the case for several of the elements discussed below.

The UY Cen spectrum has a high density of absorption lines, which means that any set of laboratory wavelengths will show a large number of chance coincidences with the star lines. To overcome these problems a method of identification was adopted, which predicts firstly, whether a given element is present and secondly, if present, which star lines contain contributions from that element. One of the implicit assumptions of this method is that any star line can be formed by more than one laboratory line. The method will be described in detail below after the discussion of the problem of predicting the number of chance identifications.

Except for promethium and technetium, all the laboratory data for the atomic lines have been taken from either Moore (1959) or from Meggers, Corliss and Scribner (1975). Throughout this thesis these works will be referred to as the MPT and the NBS 145 tables respectively.

2.05 Prediction of Coincidences

Russell and Bowen (1929) predict the number of chance coincidences observed when a set of laboratory wavelengths is compared with a star spectrum. The number of chance coincidences C is given by

$$C = N \left\{ 1 - \left(1 - \frac{2x}{X}\right)^M \right\} \qquad (2.01)$$

The standard error σ, of C is given by

$$\sigma^2 = C \left(1 - \frac{C}{N}\right) \qquad (2.02)$$

Here N is the number of laboratory lines to be compared with M star lines all of which lie within a wavelength range of X Angström. A coincidence occurs when a laboratory line lies with ± x Angström of a star line. Havnes and van den Hewvel (1972) suggested that the number of chance coincidences predicted is too small, because the lines in a real star spectrum are much more uniformly distributed than a similar number of randomly distributed lines would be. This uniform distribution arises because lines closer than a certain wavelength interval become blended and are counted as only one line. If the number of lines forming such blends can be estimated, then the parent population, of which the actual number of lines counted in the stellar spectrum is a subset, can be estimated. It is this parent population and not the number of lines counted by the observer, that must be used in the Russell-Bowen formula. The parent population is estimated as follows. Let the wavelength interval X be divided into equal intervals of length S. Let the parent population of lines be equal to M, and let the observed number of lines be M'. Then, provided $S \simeq X/M$, the M lines will be distributed amongst the line intervals S according to a Poisson distribution, denoted $\pi(n)$. The function $\pi(n)$ gives the probability that any particular interval will contain n lines where n can take any integral value from 0 to ∞.

$$\pi(n) = \frac{n_o^{\,n}}{n!} e^{-n_o} \tag{2.03}$$

Here n_o is the true average number of lines in the intervals S given by $n_o = MS/X$. This must not be confused with the observed average number of lines, which is denoted n'_o and given by $n'_o = M'S/X$. Now if S is set equal to the interval at which two absorption lines are just not resolved then no matter how many lines n, actually occur in a given interval S, only one line will be counted by the observer. The problem then is; given M' and S estimate M. The total number of intervals with n lines in each interval equals $\pi(n)X/S$. The total number of lines counted, denoted by M', is then simply equal to the total number of intervals containing one or more lines eg.

$$M' = \frac{X}{S} \sum_{n=1}^{\infty} \pi(n) \tag{2.04}$$

The total parent population M is given by

$$M = \frac{X}{S} \sum_{n=1}^{\infty} n\,\pi(n) \tag{2.05}$$

Combining equations (2.03)(2.04) and (2.05) this gives

$$\frac{M'}{M} = \left\{ \sum_{n=1}^{\infty} \frac{n_o^{\,n}}{n!} \right\} \Big/ \left\{ \sum_{n=1}^{\infty} \frac{n_o^{\,n}}{(n-1)!} \right\} \tag{2.06}$$

M'/M can be found numerically for various values of n_o as the relationship converges rapidly with n. The observed average number of lines n'_o is related to n_o by the relation

$$n'_o = \frac{n_o M'}{M} \tag{2.07}$$

Fig 2.02 shows M'/M as a function of the observed mean number of lines per resolution element. This means that given, the observed line density, the resolution, and the observed total number of lines, Fig 2.02 enables the true number of lines to be estimated. This is then the appropriate number to use in equation 2.01. In the UY Cen spectra, it was found that two moderately strong lines of equal intensity could just be distinguished when they were separated by 0.35 Å. In other words the wavelengths of the two components of the blend, if it was just not resolved, would be at respectively + and - 0.35/2 Å of the measured wavelength. In the extreme case where the two components of the blend are of very different intensity the measured wavelength of the blend would be very close to the true wavelength of the strong line. In which case the weaker component could be up to 0.35 Å on one side or the other of the measured wavelength, depending whether it was on the red side or the blue side of the strong component. It was therefore decided, that if a region 0.70 Å wide, centred on each measured wavelength, was examined, all possible contributions to that feature would be recalled. For reasons that will be further explained in the next section, but which depend on the fact that wavelengths are measured in UY Cen with an accuracy much greater than the resolution limit of 0.35 Å, the 0.70 Å wide region was divided into 5 regions each 0.14 Å wide. The half widths of these regions are the appropriate values of x to use in equation 2.01 if the required chance recovery of lines within the intervals is to be found.

A special case occurs when the coincidence window of width 2x is less than the resolution interval S. In this case, no matter what the distribution of the M' observed star lines, there can never be any overlap of coincidence windows and the number of chance coincidences C is given by

$$C = \frac{M'2x}{X} \qquad (2.08)$$

The data for the red spectrum of UY Cen are given below

S = 0.35
X = 1454
M' = 1158

Using equations 2.06 and 2.07 these data give M=1362 and N'_o = 0.28.

Using this value of M and the values of the wavelength intervals, given in column one of Table 2.02 equations 2.01 and 2.02 give in column 2 the expected percentage recovery of spectral lines due to chance.

The last column of Table 2.02 shows the total number of uranium lines actually found, within the wavelength intervals centred on the lines measured in UY Cen. There are a total of 273 laboratory lines of uranium listed in the wavelength range and the results are expressed as percentages for easy comparison. Uranium is not considered present in UY Cen and the agreement between the predicted chance recovery and observed recovery is considered satisfactory.

TABLE 2.02

Wavelength/intervals in Angström	Expected percentage of chance identifications	Observed percentage of uranium lines identified
± 0.07	11 ± 3%	11%
± 0.21	32 ± 5%	35%
± 0.35	48 ± 5%	52%

2.06 The Method of Identification

The degree of wavelength agreement, between the laboratory and star lines, was noted by assigning each laboratory line to one of five 0.14 Å wide wavelength intervals, centred on the star wavelength.

The process of assigning laboratory lines to their appropriate wavelength intervals was done by hand and was considerably facilitated by the use of a simple cardboard jig illustrated in Fig.2.03

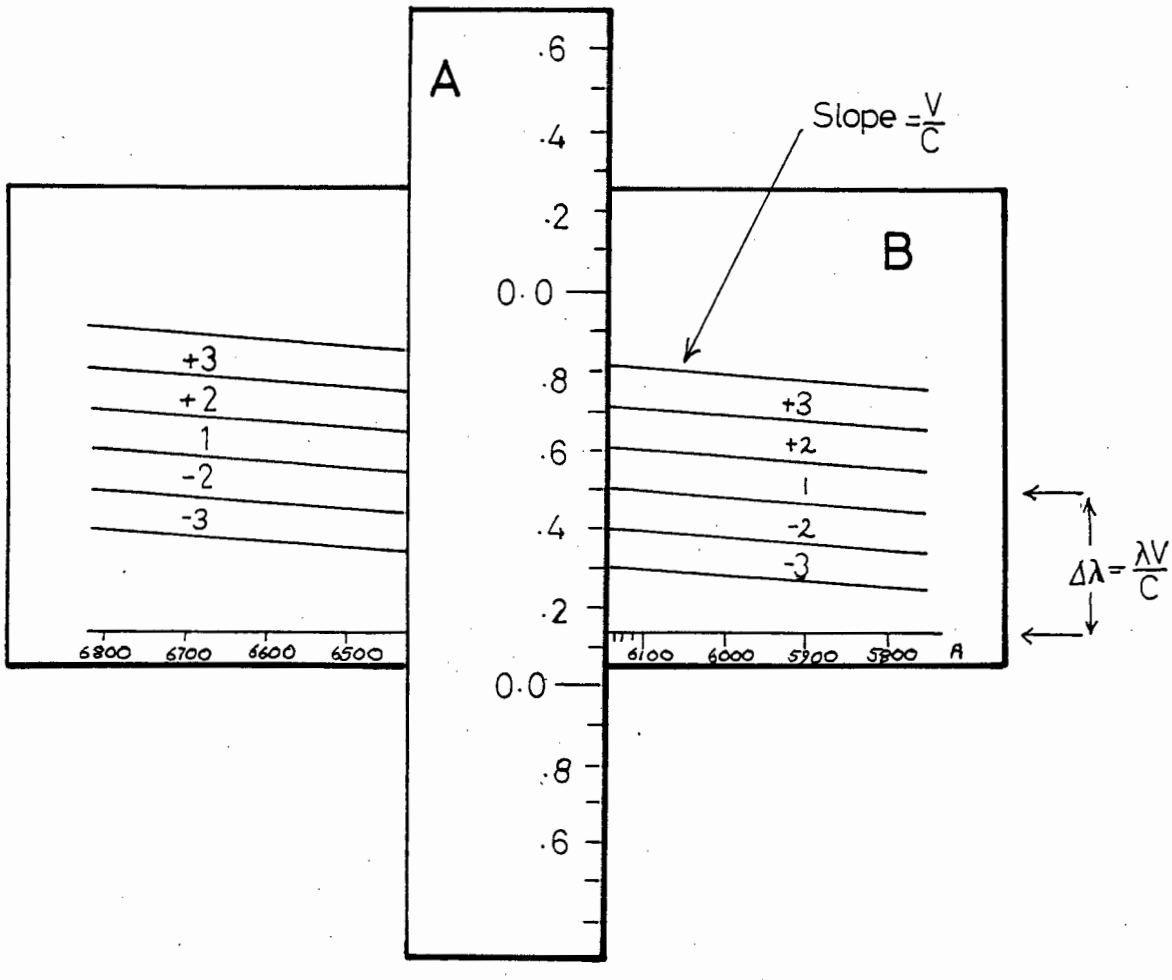

Figure 2.03

The Jig used to assign the correct wavelength interval to laboratory lines. It is set for an observed wavelength of 6135.15 which corresponds to a rest wavelength of 6135.55 A.

The jig consists of two parts marked A and B. Part A is moved horizontally and vertically until the lower scale on part B indicates the measured wavelength of a star line. The decimal part of the wavelength is indicated on part A. The rest wavelength is given on scale A at the point where the centre of the diagonal interval marked 1, intercepts it. The vertical displacement of the diagonal lines corresponds to the doppler velocity of the spectrum. When scanning the laboratory wavelength tables it is then very clear to which wavelength interval each line must be assigned.

For each element the NBS intensity was plotted, on a logarithmic scale, against the degree of wavelength agreement, to give diagrams similar to that shown for lanthanum in Fig. 2.04. In Fig. 2.05 the NBS intensity is plotted, on a logarithmic scale, against the line's lower excitation potential. The data for Fig. 2.04 are for the star lines listed in Table 2.04 while the data for Fig. 2.05 are for lines in both Tables 2.04 and 2.05. Fig. 2.04 has the advantage that it will reveal any systematic shifts in wavelength due to either errors in radial velocity or velocity stratification in the star's atmosphere. This is the main reason for using wavelength intervals smaller than the resolution interval. An implicit assumption of these methods is that the observed laboratory intensities, within a given element, will be well correlated with the intensity distribution of that element within UY Cen.

Visual inspection of Figs. 2.04 and 2.05 show that there are regions of the diagrams, where there is very good wavelength agreement and recovery of lines and other regions, where there is no more than that expected by chance. The degree of recovery can be assessed by using a χ^2 test to compare the observed distribution with the chance distribution given in Table 2.02. This is illustrated in Table 2.03, which gives the percentage recovery in each wavelength agreement interval, for all the possible lines lying in the appropriate intensity interval, delinated by the horizontal lines in Fig. 2.04. The actual distribution is compared with the expected distribution using the χ^2 test to give the probabilities in the last column.

TABLE 2.03

Region of Fig. 2.04	Percentage recovery of lines within interval		Probability the observed distribution is random
	1	+3 to -3	
Top	58	86	< .1%
Middle	23	62	14%
Bottom	12	66	44%
Expected chance recovery	12 ± 3	48 ± 5	

Where possible, the intensity against lower excitation diagrams were used, in preference to the intensity wavelength-interval diagrams, to decide on the presence of lines.

It is interesting to consider the physical meaning of drawing lines to divide regions in Fig.2.05 We can write

$$\log I = \log gf - \theta\chi + C \qquad (2.09)$$

where the symbols have their usual meanings and are defined in chapter 5. Assuming that, for a given element of a given ionization, we only detect lines in UY Cen down to some constant star 'intensity' I_{STAR}, then we can write;

$$\log I_{NBS} = \log I_{STAR} + \chi(\theta_{STAR} - \theta_{NBS}) \qquad (2.10)$$

This equation tells us how the corresponding NBS intensity will change with excitation. Clearly lines of constant star intensity will be straight in Fig. 2.05 with slope $(\theta_{STAR} - \theta_{NBS})$. Examination of Fig. 2.05 shows that lines of unit slope could also divide the diagram very much as indicated, which would imply an excitation temperature of ~ 2500 for UY Cen ($\theta_{NBS} \simeq 0.99$) (Close to the value adopted, see chapter 5).

The main reason for not dividing Fig. 2.05 by straight lines is that this automatically forces the spectrum to obey a model which may be inappropriate or unjustified. We have rather tried to judge the distributions on their own merit.

After the initial identifications had been completed 152 lines remained, unidentified. These lines were compared with Kurucz and Pey-

tremann's (1975) tables, which contain a large number of predicted lines that are not listed in the NBS or MPT. Nearly all the 152 lines were found to have at least one possible identification of which 57 were due to TiI. However, only 9 of these lines were found to be plausible identifications, on the basis of the curve of growth analysis given in chapter 5.

It is quite clear that despite the use of statistical tests the division of the observed distributions into regions of certain indentification, no identification and intermediate regions, must remain highly subjective. This subjectivity is expressed by the division of the identifications in Table 2.04 into three classes designated; certainly present, probably present, and possibly present. These are given under three separate headings in Table 2.05. The three groupings are defined as follows:

CERTAINLY PRESENT

Strong lines of well established elements and or members of complete multiplets.

PROBABLY PRESENT

These are the weaker lines of the well established elements as well as the strong lines of less certain elements. This often applies where an element shows a small number of lines in this spectral region.

POSSIBLY PRESENT

This group includes the weaker lines of less certain elements as well as the stronger lines of doubtful elements.

All three groups are considered very plausible identifications. The object of grouping the identifications has been to assign an order of priority and certainly not to include all possible identifications. No attempt has been made to sub-divide the molecule identifications into different identification classes. For details of the quality of the identifications the reader is referred to the discussion by elements.

Teske (1956), has produced a line list of the SC star FU Mon, based on lower dispersion spectra. He lists 180 lines in the region 6890 to 6790 Å and his identifications are in substantial agreement with those given here.

2.07 Description of the Line Lists in Tables 2.04 and 2.05

The wavelengths and identifications are presented in Tables 2.04 and 2.05. Table 2.04 contains data for lines between 5413 and 6897 Å while Table 2.05 contains data for the lines between 6900 and 8839 Å. This division corresponds to the division between the red and infrared plates used in the original measurements.

The various data given in Tables 2.04 and 2.05 are explained below.

Intensity

The number in column one is on a scale of 10 and indicates the strength of the absorption line. It is a measure of the depth of the line centre, measured from a local continuum and is therefore not directly related to equivalent width, but is intended as an aid to identifying the lines on the plates.

* Indicates the line is broad having a width > 1.5 Å.

[Either the two lines so joined are closely blended or they form the boundaries of a broad absorption region.

Wavelength

Column two contains the rest wavelength in angström units. To obtain rest wavelengths the measured wavelengths were corrected by +23.52 km s^{-1} in Table 2.04 and +8.92 km s^{-1} in Table 2.05. Where two wavelengths are given, the first is the rest wavelength and the second is the measured wavelength. This is only done for lines considered to have atmospheric identifications. When only one number is given after the decimal point this indicates that the wavelength was measured on a microphotometer tracing of the spectrum.

Identifications

Table 2.04 is sub-divided into 'Certainly Present' 'Probably Present' 'Possibly Present' and 'Molecules' according to the criteria given in the previous section.

( ) In Table 2.05 only; this indicates the identification is considered 'probably' or 'possibly present'.

? Indicates uncertain identification.

TiI Indicates $-0.7 < (\lambda_{STAR} - \lambda_{LAB}) < +0.07$ Å for the element, e.g. TiI underlined.

No indication of wavelength agreement is given for multiple CN features, or CN features without quantum data.

* Indicates CN is considered a major contributor.

As a rough guide, identifications in Table 2.05 are given in order of importance, if this is known, otherwise atoms are given before molecules.

In both Tables quantum data are only given for the molecular lines, when the star line corresponds to a unique rotational substate transition.

2.08 Description of the Atlas

Plates 1 and 2 of the atlas cover the wavelength range listed in Table 2.04 while plates 3 and 4 cover the wavelengths listed in Table 2.05. All the spectra are shown as positives so that emission lines appear white. On each plate the spectra are divided into groups. The top spectrum of each group is of the laboratory iron arc. Thereafter the designation on all the plates is as follows:

A = The S star π Gru

B = The SC star UY Cen. Plate 4 contains two spectra of UY Cen exposed to different densities.

C = The C star 19 Psc.

D = The laboratory CN emission spectrum.

On all the plates the wavelength scale is in angström units. The reader is warned that this scale is intended to be used in conjunction with the wavelength Tables and is only accurate to about ±0.2 Å.

PLATE 1(a)

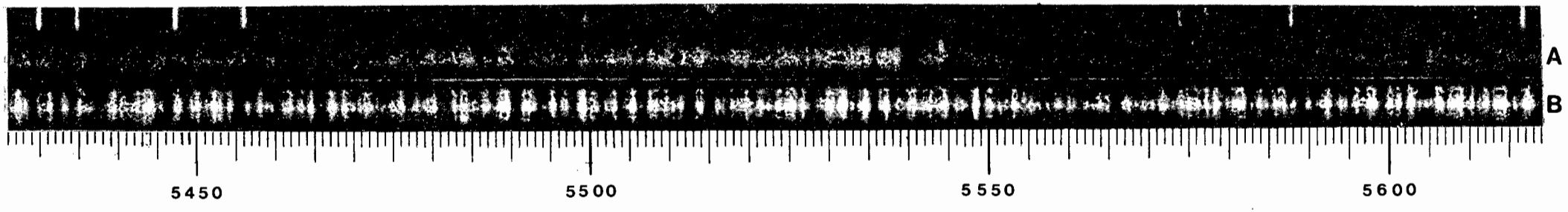

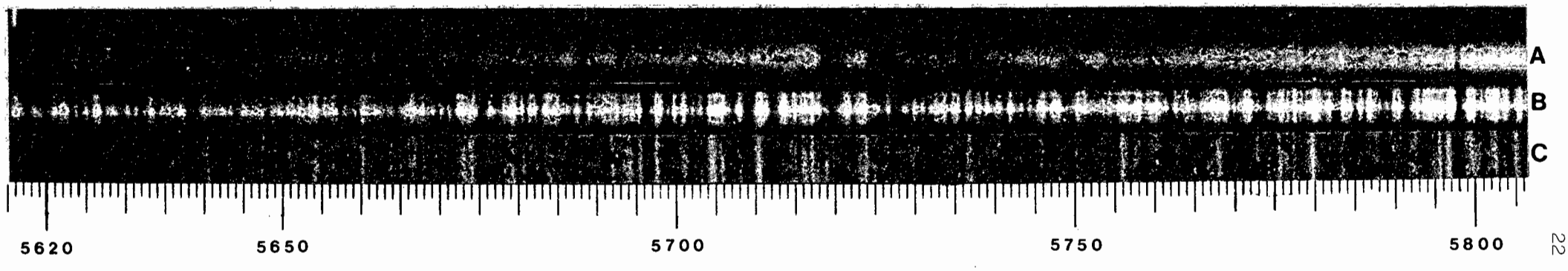

PLATE 2(a)

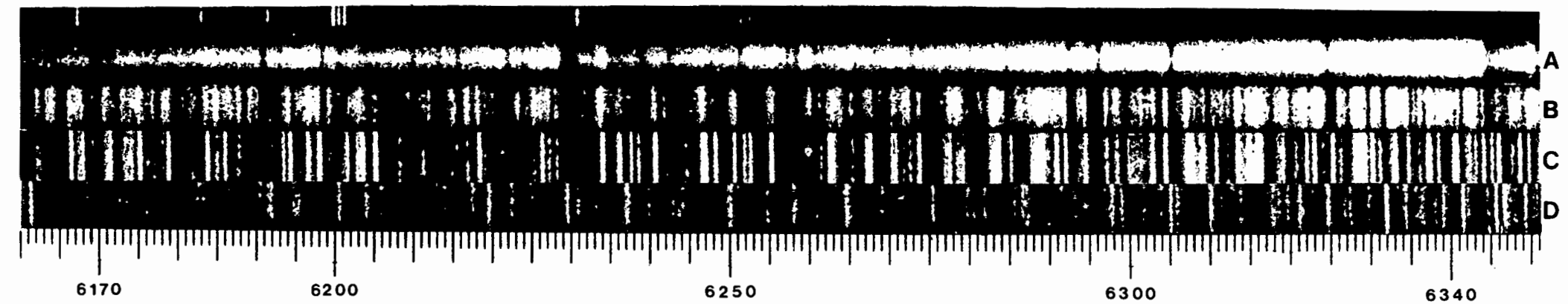
A
B
C
D
6170
6200
6250
6300
6340

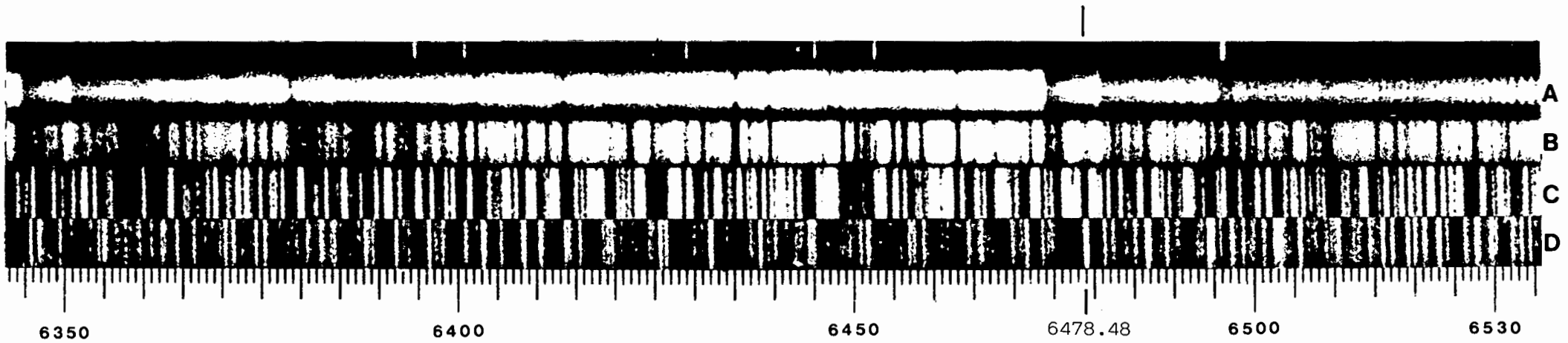
A
B
C
D
6350
6400
6450
6478.48
6500
6530

PLATE 3(a)

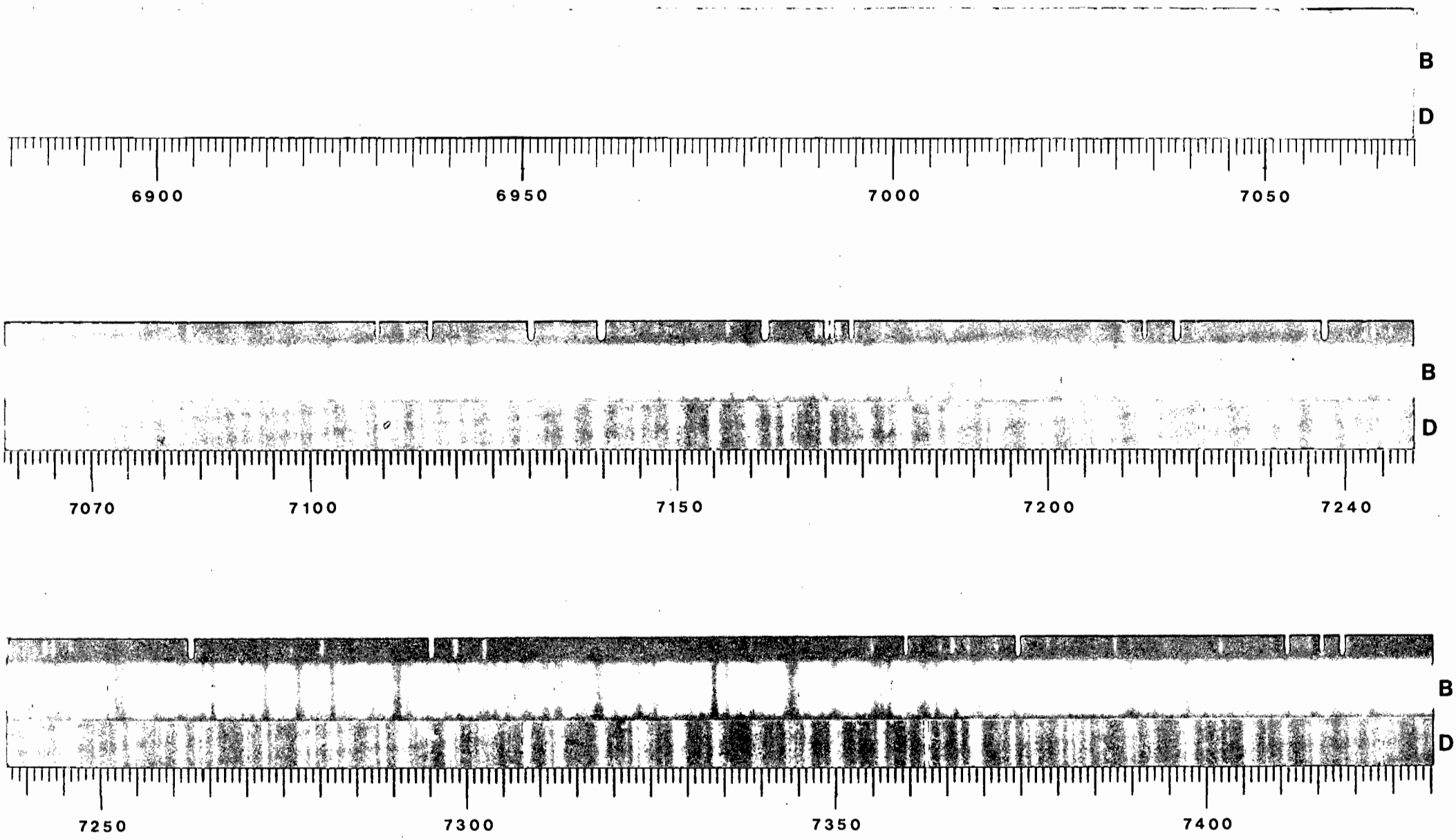
B
D
6900
6950
7000
7050
B
D
7070
7100
7150
7200
7240
B
D
7250
7300
7350
7400

PLATE 4(a)

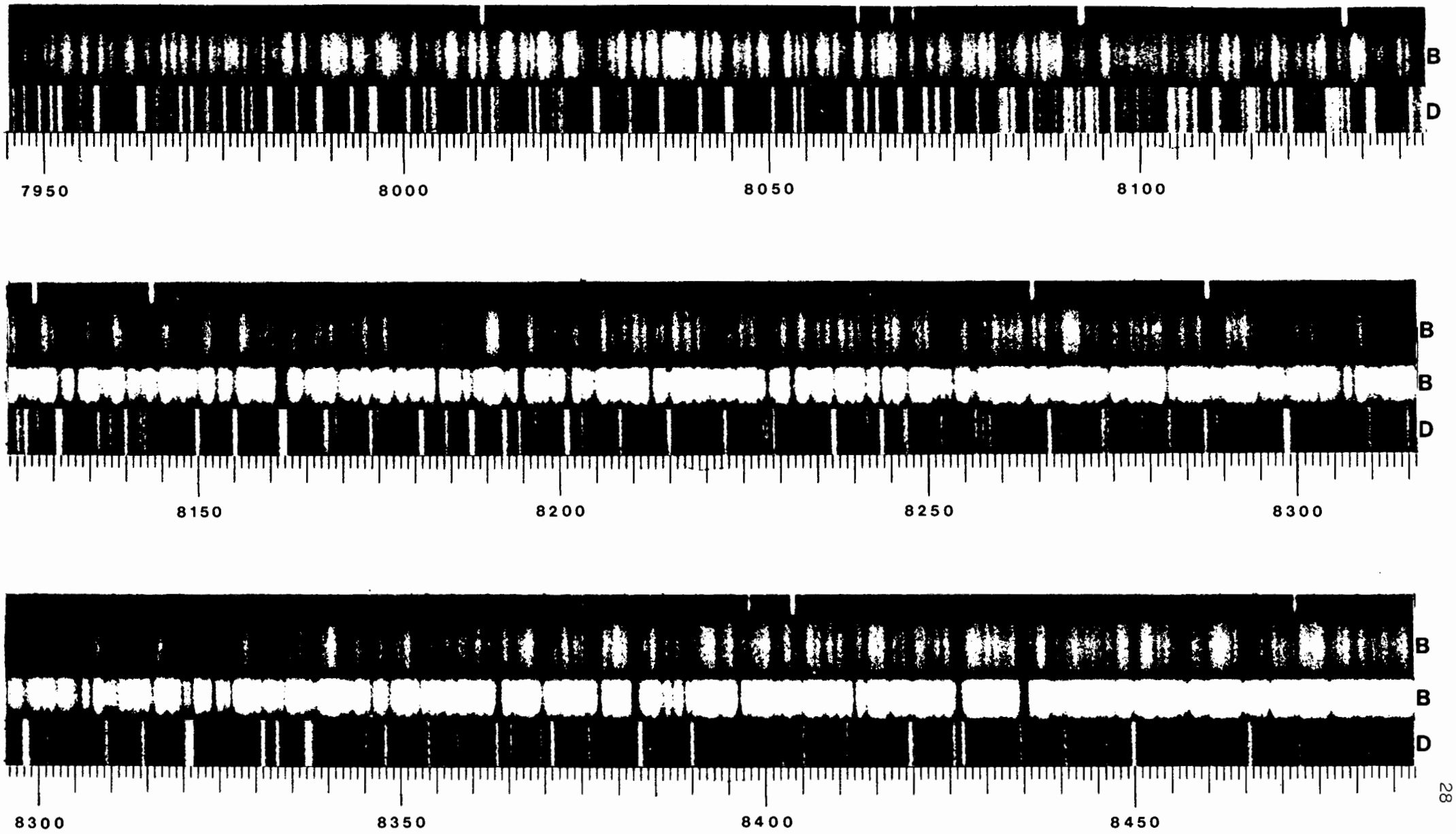
B
D
7950
8000
8050
8100
B
B
D
8150
8200
8250
8300
B
B
D
8300
8350
8400
8450

Int	Wavelength	Certain	Probable	Possible	Molecules
6	5413.17	-	GdI	PrII	-
7	5413.99	ZrI,CeI	-	-	-
5	5415.12	-	VI 130,NdI	-	-
3	5416.34	-	NdII 80	-	-
6	5418.59	CeI	-	-	-
4	5419.57	-	-	-	-
5	5420.42	CeI	MnI 4,NdI	-	-
6	5421.38	NdII 79	GdI	-	-
5	5422.18	CeI	-	NbI	-
4	5423.47	CeI,DyI	-	-	-
5	5424.22	-	BaI 9	YI	-
8	5426.37	TiI 3,CeI	-	ZrI	-
5	5427.32	CeI	-	-	-
4	5428.45	-	-	ZrI	-
10	5429.65	FeI 15	LaI	-	-
6	5431.40	CeI	NdII 80	NbI	-
8	5432.67	-	MnI 1	-	-
10	5434.59	FeI 15	-	-	-
5	5435.95	-	-	-	-
[6	5436.74	[TiI 51	FeI 113	-]	-
6	5439.05	CeI,LaI	NbI,YI,ZrI	HfI	-
5	5440.44	ZrI	-	TiI 107	-
5	5442.04	-	NdII	-	-
5	5443.34	-	-	-	-
5	5445.27	CeI	-	-	-
9	5446.77	FeI 15,FeI 37 TiI 3	-	-	-
7	5448.93	CeI	-	TiI 107	-
5	5450.03	CeI	-	-	-
6	5451.14	DyI	SrI 9	-	-
4	5451.98	CeI	-	-	-
4	5452.87	-	SmI	HfI	-
6	5453.85	CeI	-	TiI 108	-
8	5455.52	FeI 15,LaI	NdII 83	-	-
6	5457.44	CeI	MnI 4	-	-
6	5458.83	CeI	-	-	-
8	5460.50	TiI 3	-	-	-
6	5462.75	-	-	-	-
6	5464.15	-	CeII	LaII	-
6	5465.58	CeI	-	-	-
8	5466.48	YI 12	SmI	-	-
6	5468.33	-	CeII 24,ErI	YI	-
5	5469.63	-	GdI	-	-
6	5470.50	-	MnI 4	TiI 108	-
5	5471.27	TiI 106	-	-	-
6	5472.76	CeI	-	TiI 107	-
7	5473.49	CeI	-	BaI	-
7	5474.35	-	-	TiI 108	-
6	5477.13	ZrI,NiI 59,CeI	-	-	-
6	5478.60	CeI	-	ZrI	-

Int	Wavelength	Certain	Probable	Possible	Molecules
[7	5481.01	ZrI,CeI	SrI 9	-	-
[7	5481.97	TiI 106,ScI 16 CeI	LaII 4	-	-
7	5483.33	CoI 39,CeI	-	-	-
5	5484.99	-	NdII	-	-
6	5485.88	ZrI	NdII 79	-	-
6	5487.76	-	VI 129	-	-
2	5489.15	-	-	-	-
8	5490.57	TiI 3	-	-	-
9	5493.63	LaII 4	SmI	-	-
6	5494.51	-	-	TiI 108	-
6	5495.87	VI 2	-	YI	-
7	5497.72	FeI 15, TiI 51	-	-	-
5	5499.66	-	-	NbI	-
4	5501.44	FeI 15,LaI 3	NdI	-	-
5	5502.47	ZrI,LaI	-	-	-
7	5503.73	LaI	YI	-	-
4	5504.59	-	-	NbI	-
7	5506.01	CeI,LaI	MnI 4	-	-
8	5506.73	FeI 15,CeI	MoI 4	-	-
4	5507.85	-	VI 129	ZrI	-
5	5508.91	-	-	PrII	-
5	5509.89	-	-	YII 19,TbI	-
5	5510.74	CeI	-	-	-
8	5512.37	CeII 24,TiI 106	-	CrI 121,SmI	-
10	5514.50	TiI 106,TiI 106	-	-	-
8	5515.17	VI 1,VI 2,ScI	LaI	-	-
5	5516.31	-	SmI 2	-	-
9	5517.15	ZrI,CeI	LaI	-	-
6	5518.07	ZrI,CeI	-	-	-
6	5520.34	ScI 15	-	-	-
6	5521.74	-	SrI 9	-	-
6	5522.76	CeI	-	PrII	-
5	5524.00	-	NdI	TbI	-
5	5525.86	CeI	NdI	PrII	-
[6	5526.87	CeI	CeII	ScII 31	-
[8	5527.74	VI 1,YI 12	MgI 9	-	-
5	5529.14	-	-	NdI	-
4	5530.65	CoI 38	-	-	-
6	5532.22	ZrI	-	-	-
6	5533.12	-	MoI 4	-	-
4	5533.83	NdI	-	-	-
7	5535.41	BaI 2,VI 1,CeI	NdII	PrII,LaII	-
4	5536.44	-	-	-	-
7	5537.66	CeI	MnI 4,NdII	ZrI	-
6	5539.35	-	NdII	-	-
[5	5540.79	CeI	-	-	-
[4	5541.75	-	-	YI	-
6	5542.75	CeI	-	-	-
6	5544.97	-	-	-	-
6	5547.28	DyI,CeI	-	-	-
7	5548.80	CeI	-	SmI	-
6	5550.54	HfI,CeI	SmI	-	-

Int	Wavelength	Certain	Probable	Possible	Molecules
5	5551.41	CeI	-	NbI	$ZrO\ ^3\Pi - ^3\Delta(0,0)R_{1a}$
7	5552.20	HfI 7,CeI	-	-	-
5	5553.48	-	-	NiI 69	$ZrO\ ^3\Pi - ^3\Delta(0,0)R_{1c}$
6	5554.30	-	-	-	-
6	5555.40	-	-	-	$ZrO\ ^3\Pi - ^3\Delta(0,0)Q_1$
7	5556.42	CeI	YbI	YI,CrI 120, 121	-
6	5557.50	VI 1	-	-	-
6	5559.00	CeI	-	-	-
6	5560.68	VI 1	-	-	-
6	5561.47	NdI	-	SmI	-
6	5562.20	CeI	-	-	-
5	5562.94	CeI	-	-	-
5	5563.94	-	-	-	-
[7	5564.69	CeI	-	TiI 229	-
[8	5566.08	CeI	-	-	-
5	5567.55	CeI	-	YI	-
6	5568.38	LaI	-	-	-
5	5569.49	CeI	-	-	-
6	5570.50	-	MoI 4,LaI	-	-
5	5572.10	CeI	-	-	-
4	5572.99	-	FeI 686	-	-
3	5574.07	-	-	CrI 120	-
3	5575.16	-	CeI	-	-
6	5576.24	-	FeI 686,GdI	NbI	-
4	5577.34	CeI	YI	-	-
6	5578.73	CeI	NiI 47,NdII	-	-
4	5579.68	-	-	-	-
3	5580.35	-	-	-	-
7	5581.88	CaI 21,YI 12	NdII	-	-
6	5582.71	CeI	-	-	-
4	5583.86	-	-	-	-
6	5584.74	VI 37,CeI	VI 85	-	-
6	5586.99	-	FeI 686	NbI	-
[7	5588.06	CeI,LaI	NdII	SmI	-
[8	5588.65	CaI 21	-	-	-
6	5589.99	CaI 21	CeI	-	-
[6	5592.42	VI 37	-	NiI 69	-
[6	5592.87	VI 1	-	-	-
4	5593.69	CeI	-	-	-
7	5594.57	CaI 21	NdII 79	-	-
5	5596.11	CeI	-	-	-
7	5598.58	CaI 21	FeI 113	-	-
4	5600.10	-	-	-	-
6	5601.33	CaI 21,CeI	-	-	-
[6	5602.80	CaI 21	FeI 686	-	-
[4	5603.62	NdII 45	-	NbI,NbI	-
[5	5604.39	-	VI 85	-	-
[6	5605.02	VI 37	-	-	-
6	5606.49	CeI	-	YI	-

Int	Wavelength	Certain	Probable	Possible	Molecules
2	5607.65	-	-	-	-
4	5609.02	-	-	PrII	-
5	5610.29	-	CeII 26	YII 19	-
5	5610.99	CeI	-	-	-
6	5612.16	ZrI	-	-	-
5	5614.51	CeI	GdI	-	-
5	5615.71	CeI	FeI 686	-	-
7	5617.97	GdI 3	-	-	-
6	5620.51	CeI,NdI	ZrI	-	-
4	5621.95	-	VI 85	SmI,PrII	-
7	5623.64	ZrI,CeI,YI 12	-	-	-
5	5624.72	VI 37,VI 37	FeI 686	-	-
5	5625.98	VI 37	-	SmI	-
5	5627.62	VI 37	-	-	$ZrO\ ^3\Pi-{}^3\Delta(0,0)R_2{}_d$
5	5629.5	-	GdI	-	$ZrO\ ^3\Pi-{}^3\Delta(0,0)R_2{}_c$
5	5629.9	YI 12	-	-	-
5	5631.26	LaI	-	-	-
7	5632.29	GdI 3,VI 1,CeI	LaI,MoI	-	-
4	5633.12	CeI	-	-	-
5	5634.40	CeI	-	-	$ZrO\ ^3\Pi-{}^3\Delta(0,0)Q_2$
3	5636.66	-	-	-	-
8	5638.45	CeI,CeI	-	-	-
7	5639.53	DyI	LaI	-	-
5	5641.56	-	-	DyII	-
5	5643.33	GdI 3	-	-	-
7	5644.32	-	-	TiI 240,SmI	-
6	5644.76	-	-	YI	-
5	5645.84	VI 37	EuI	-	-
5	5646.8	CeI	-	-	-
6	5648.32	LaI	-	YI	-
4	5649.42	-	-	-	-
5	5650.51	CeI	-	-	-
3	5651.98	DyI	-	-	-
4	5653.32	-	-	-	-
5	5655.04	CeI	-	-	-
2	5656.30	CeI	-	-	-
8	5657.58	VI 37,LaI	-	-	-
7	5658.92	TiI 50	FeI 686	-	-
6	5659.88	CeI	SmI 2	-	-
7	5663.27	CeI	-	YII 38	-
8	5664.63	CeI	ZrI 47,NbI	-	-
4	5667.40	-	FeI 209	-	-
6	5668.34	VI 37	-	-	-
6	5668.93	CeII 23	NdII	-	-
7	5669.84	CeI,NdI	-	NaI 7	-
7	5670.85	VI 36	-	NbI	-
8	5671.89	ScI 12,CeI	-	NbI	-
1	5673.42	-	-	-	-
8	5675.21	CeI	-	NaI 7,YI TiI 249	-
6	5675.87	NdI	-	-	-

Int	Wavelength	Certain	Probable	Possible	Molecules
5	5677.40	CeI	-	NbI	-
2	5678.66	-	FeI 113	-	-
3	5680.02	-	CeII	BaI	-
6	5680.98	ZrI 25	-	-	-
[3	5681.82	-	-	-	-
[8	5682.71	NaI 6,CeI	-	CaI	-
4	5685.40	-	-	ZrI	-
7	5686.79	ScI 12	GdI	SmI,TbI	-
9	5688.33	NaI 6,NaI 6,CeI	NdII 79	CaI	-
[4	5689.57	-	MoI 5	TiI 249	-
[3	5690.46	-	-	-	-
5	5692.97	CeI	-	-	-
3	5694.04	-	-	-	-
3	5694.94	-	-	NiI 220	-
[9	5696.20	GdI 3,LaI	-	-	-
[4	5697.07	CeI	-	-	-
6	5698.56	VI 35	-	-	-
6	5699.20	CeI	LaI	-	-
6	5700.19	ScI 12	CuI 2	-	-
7	5701.54	GdI 3	FeI 209	-	-
7	5702.46	CeI	NdII 78	TiI 249	-
7	5703.48	VI 35	-	LaII 48	-
1	5704.46	-	-	-	-
1	5705.2	-	-	-	-
5	5706.31	-	-	NbI,SmI	-
8	5706.99	VI 35	YI	CaI 54	-
10	5708.97	CeI,ZrI	NdII 79	-	-
[3	5711.07	MgI 8,MgI 8, MgI 8	LaI	-	-
[8	5712.12	CeI,LaII 20	FeI 686	TiI 249, NiI 69	-
3	5714.13	-	LaI	TiI 249	-
3	5715.24	-	CeII	TiI 228	-
2	5716.52	CeI	-	TiI 249,NbI	-
4	5717.42	-	-	ScI 12	-
6	5718.17	CeI	NdII	CaI 54	$ZrO\ ^3\Pi-^3\Delta(0,0)R_3$
6	5719.8	-	NdII	-	-
6	5720.26	CeI,HfI 6	SmI	TiI 249,LaI	-
[5	5722.06	CeI	-	-	-
[2	5722.76	-	MoI	-	-
4	5724.13	ScI 12	-	-	$ZrO\ ^3\Pi-^3\Delta(0,0)Q_3$
6	5725.80	CeI	VI 35	-	-
[9	5727.09	VI 35,ErI	NdII	LaII 48	-
[9	5727.84	VI 35	-	-	-
8	5729.23	NdI,CeI	NbI	-	-
5	5730.30	-	-	-	-
8	5731.27	VI 36	-	-	-
3	5733.1	-	-	SmI	-
5	5734.03	CeI	VI 135	-	-

Int	Wavelength	Certain	Probable	Possible	Molecules
9	5735.75	ZrI 4,CeI	GdI	CaI 54	-
6	5737.08	VI 35	-	-	-
5	5738.30	-	-	-	-
5	5739.43	-	-	TiI 228	-
7	5741.00	-	NdII	SmI	-
6	5742.47	-	-	-	-
7	5743.57	VI 35,CeI	-	CaI,YI	-
7	5744.61	LaI,CeI	GdI	-	-
5	5746.36	CeI,GdI	-	-	-
5	5748.01	-	NdII,NiI 45	FeI 343	-
7	5749.03	CeI	-	VI 92	-
6	5749.80	-	NdI	-	-
3	5750.53	-	-	-	-
[5	5751.31	-	MoI 5	NbI	-
5	5753.63	NdI	-	-	-
[5	5754.75	-	NiI 68,FeI 113	-	-
4	5755.46	-	-	-	-
3	5756.70	-	-	TiI 228	-
6	5758.40	CeI	-	-	-
6	5760.73	CeI	-	-	-
7	5761.73	LaI,VI 35	-	CaI 54	-
5	5762.83	ErI	-	-	-
[5	5764.23	-	-	CaI,NdI	-
6	5765.23	CeI	EuI	-	-
3	5768.13	-	-	-	-
7	5769.25	LaI 8	-	LaII	-
5	5769.94	CeI,LaI	-	-	-
5	5770.64	CeI	-	-	-
6	5772.23	CeI	-	VI 92	-
[8	5772.96	CeI,CeI	-	-	-
7	5773.55	CeI	-	-	-
[4	5774.41	-	-	-	-
4	5775.15	CeI	-	-	-
[4	5776.04	NdI	-	GdI	-
5	5776.73	VI 36	-	-	-
4	5777.64	BaI 9	-	-	-
5	5778.41	-	FeI 209	-	-
3	5779.13	-	-	SmI	-
5	5780.81	-	-	TiI 214, CrI 188,FeI 552	
[7	5782.18	CeI	CuI 2	KI	
7	5782.75	CeI	-	CrI 188	-
3	5783.76	-	-	VI 141,CrI 188	-
7	5784.73	CeI,NdI	FeI 686	CrI 188,NdI	
6	5785.96	CrI 17		CrI 188,VI 141	-
[5	5787.01	-	-	CrI 119	
7	5788.27	NdI,CeI	-	VI 92,CrI 188,CrI 119,SmI	
7	5789.15	LaI 8	-	-	-
4	5790.02	-	-	-	-
[6	5790.73	CrI 17	-	CrI 188	-
9	5791.29	LaI 8,GdI 3,CeI	-	-	-
4	5792.20	-	-	-	-

Int	Wavelength	Certain	Probable	Possible	Molecules
4	5793.03	-	-	-	-
3	5794.83	CeI	-	-	-
4	5795.99	CeI	NiI 68	-	-
8	5797.76	ZrI 4,LaII 4	-	CrI 185, CrI 185	-
6	5798.43	CrI 17	-	-	-
4	5800.11	BaI 9,NdI	CeII	-	-
4	5800.90	-	-	-	-
2	5801.88	-	-	KI	-
4	5802.93	-	GdI	SmI	-
7	5804.40	CeI	NdII 79	-	-
5	5805.79	LaII 4	-	BaI	-
4	5806.47	-	-	-	-
4	5808.25	LaII 4	-	-	-
5	5809.50	TiI 73	NdII	-	-
3	5810.89	CeI	-	-	-
4	5811.71	CeI	NdII 78	-	-
6	5812.91	CeI	-	-	-
3	5813.95	TiI 73	-	-	-
4	5815.33	CeI	-	-	-
5	5816.29	-	-	-	-
4	5817.08	-	-	VI 92	-
4	5818.75	-	-	EuII 9	-
1	5819.57	-	NbI	-	-
5	5820.58	CeI	NdII	NdI	-
3	5821.90	LaI	-	YI	-
5	5822.90	CeI	-	-	-
6	5823.78	-	GdI,LaI	PrII	-
4	5824.68	-	-	-	-
5	5825.63	-	NdII	-	-
6	5826.68	ErI,NdI	-	-	-
3	5827.85	-	-	-	-
2	5828.87	-	-	-	-
7	5829.91	CeI,LaI	-	-	-
3	5830.59	-	-	VI 142	-
5	5832.00	CeI	-	-	-
6	5834.50	CeI	-	-	-
6	5835.67	CeI	-	FeI 343	-
6	5838.30	CeI	NbI	CrI 119	-
8	5839.55	TiI 105,CeI	LaI	-	-
1	5841.40	-	-	-	-
3	5842.43	-	NdII	NbI	-
3	5842.7	-	-	-	-
* 6	5845.24	-	LaI	-	-
4	5846.19	CeI	-	VI 142	-
5	5847.03	NiI 44	-	ZrI	-
3	5848.30	CeI	LaI	-	-
4	5849.20	-	-	-	$ZrO\ ^1\Pi - {}^1\Sigma^+(0,0)R$
6	5850.73	CeI	-	PrII	-
5	5851.66	GdI 3	-	-	-
6	5852.28	-	LaI	-	-
8	5853.53	BaII 2,CeI,CeI	-	-	-

Int	Wavelength	Certain	Probable	Possible	Molecules
7	5855.23	ErI	-	LaI	-
5	5856.27	GdI 3	-	-	-
7	5857.42	CaI 47,CeI	-	-	-
6	5858.36	CeI	MoI 5	-	-
[4	5859.55	CeI	-	-	$ZrO\ ^1\Sigma-^1\Sigma(0,0)R$
[6	5860.30	-	-	HoI	-
7	5862.58	CeI	-	-	-
5	5863.93	-	-	CrI 185,LaII	-
4	5865.25	-	-	-	-
7	5866.48	TiI 72	-	NbI	-
8	5868.27	ZrI	-	-	-
5	5869.56	-	ZrI	-	-
6	5871.59	CeI	-	-	-
6	5872.91	-	-	EuII 9	-
5	5873.91	CeI	-	LaII 48,SmI	-
4	5874.88	-	LaI	-	-
5	5876.34	-	-	CrI 119	-
6	5877.83	CeI	LaI	NbI	-
5	5878.86	CeI	-	-	-
8	5880.10	TiI 71,ZrI 4	-	-	-
* 10	5892.21	NaI,NaI	-	-	-
9	5910.06	CeI,CeI	-	-	-
4	5912.32	-	-	-	-
5	5912.90	CeI	-	-	-
8	5913.80	TiI 2	-	-	-
7	5914.57	CeI	-	-	-
6	5916.31	-	-	SmI	-
6	5917.51	LaI	-	-	-
6	5918.61	TiI 71	-	-	-
4	5919.38	-	-	-	-
7	5920.20	CeI	-	-	-
8	5922.20	TiI 72	CoI 55	-	-
7	5924.12	CeI	-	-	-
6	5925.14	-	-	ZrI	-
7	5926.33	CeI	-	-	-
3	5927.37	-	-	-	-
7	5928.46	CeI	-	-	-
5	5929.77	CeI	-	-	-
8	5930.64	LaI 2,LaI 2	GdI	-	-
8	5932.40	CeI	-	-	-
4	5933.61	-	CeII	-	-
[7	5934.32	CeI	-	-	-
[9	5935.25	LaI,ZrI 2	CoI 55	-	-
5	5936.26	LaII	-	-	-
5	5936.93	-	GdI	-	-
[7	5937.80	TiI 72,CeI	GdI	-	-
[4	5938.38	CeI	-	-	-
2	5939.26	-	-	-	-
9	5940.72	TiI 2,CeI	-	-	-
7	5941.79	TiI 72	-	-	-
5	5942.78	CeI	-	-	-
3	5943.49	FeI 63	-	-	-

Int	Wavelength	Certain	Probable	Possible	Molecules
9	5944.77	TiI 2,CeI	-	-	-
1	5945.74	-	-	YI	-
5	5947.36	CeI	-	-	-
5	5948.71	-	-	-	-
6	5949.44	FeI 14	-	-	-
5	5950.60	CeI	-	-	-
3	5951.44	CeI	-	-	-
6	5953.23	-	TiI 154	-	-
9	5955.35	ZrI 3	-	-	-
7	5956.69	FeI 14	CeI	-	-
4	5958.30	FeI 14,FeI 63	-	-	-
4	5960.36	-	-	-	-
2	5961.33	-	-	-	-
4	5963.23	FeI 63,CeI	-	-	-
2	5964.73	CeI	-	-	-
7	5965.86	-	TiI 154	EuII 9	-
5	5967.47	-	-	-	-
6	5969.21	-	-	-	-
3	5970.48	-	-	-	-
5	5971.83	BaI 7	-	-	$YO\,^2\Pi_{3/2}-{}^2\Sigma^+(0,0)Q$
4	5972.75	CeI	-	-	-
4	5973.48	-	-	HoI	-
4	5974.48	DyI	-	-	-
6	5975.88	CeI	CeII 30	-	-
3	5976.95	-	GdI	-	-
6	5978.68	-	TiI 154	-	-
6	5979.54	CeI	-	SmI	-
4	5980.89	TiI 72	VI 49,CeI	-	-
[5	5982.30	-	LaI	-	-
[6	5983.01	-	NbI	HoI,CrI 185	-
9	5984.56	TiI 2	ZrI,VI 49	-	-
2	5985.98	-	-	-	-
[8	5988.63	DyI	TiI 154	-	$YO\,^2\Pi_{3/2}-{}^2\Sigma^+(1,1)Q$
[6	5989.27	CeI	NdII	-	-
7	5990.59	TiI	-	-	-
4	5991.89	-	CoI 90	-	-
3	5992.60	CeI	-	-	-
2	5993.90	-	-	-	CN?
5	5995.32	ZrI	-	-	-
4	5995.91	-	TiI 154	-	-
3	5997.01	BaI 7	-	-	-
4	5997.86	-	-	NbI	-
[3	5999.09	-	GdI	TiI 198	-
[6	5999.99	CeI	-	TiI 227	-
3	6001.01	-	ZrI	-	CN
[3	6001.75	CeI	-	-	-
[6	6002.58	VI 34	VI 49	TiI 198	-
3	6004.13	-	-	SmI	-
[8	6006.14	CeI,CeI	-	-	-
[6	6006.77	CeI	-	-	-

Int	Wavelength	Certain	Probable	Possible	Molecules
6	6007.40	CeI,LaI	NiI 42	-	-
4	6008.56	-	VI 49	-	-
4	6009.28	NdII	FeI 64	-	-
4	6010.66	-	DyI	-	-
3	6011.77	-	-	-	-
6	6013.42	MnI 27,CeI	-	-	-
2	6014.51	-	-	-	-
7	6016.55	MnI 27,CeI	-	-	-
6	6017.03	-	-	-	-
6	6017.87	-	VI 49,EuI	PrII	-
7	6018.68	CeI,TiI 70	-	TiI 198	-
5	6019.41	BaI 7	-	-	-
4	6020.29	CeI	-	-	-
4	6021.20	-	GdI	-	-
4	6021.79	MnI 27,FeI 63	-	-	-
8	6023.39	YI 3	-	-	-
7	6024.19	CeI	-	-	-
7	6025.36	ZrI	-	-	-
3	6026.20	-	-	-	-
3	6026.61	-	-	-	-
7	6027.43	CeI	-	SmI	-
4	6028.91	-	-	-	-
3	6029.74	-	-	-	-
5	6030.61	-	MoI 5	-	-
9	6031.61	TiI 2	-	-	-
5	6032.60	-	ZrI	-	-
5	6034.37	-	-	-	-
3	6036.64	-	-	-	$ScO\,^2\Pi - ^2\Sigma(0,0)R_2$
2	6037.62	-	-	-	CN
3	6038.55	-	LaI	-	-
6	6039.73	VI 34	-	-	-
3	6041.22	-	-	-	CN?
3	6042.17	-	-	-	-
3	6043.36	CeII 30	-	-	-
3	6044.96	-	-	SmI	-
4	6045.68	CeI	ZrI	-	-
5	6047.21	CeI	-	-	-
5	6048.62	-	VI 49	-	CN?
5	6049.62	-	-	EuII 9,ZrI	-
4	6051.86	CeII	-	-	-
3	6052.77	-	-	-	CN
3	6053.84	-	-	-	-
4	6054.98	-	-	PrI	-
2	6056.00	-	-	-	-
6	6056.99	-	-	-	-
7	6058.13	VI 34,CeI	-	-	-
4	6059.34	-	-	-	-
4	6060.60	-	-	-	-
3	6061.26	-	-	-	-
10	6062.92	ZrI 3,FeI 63 BaI 7	-	CrI 185	-

Int	Wavelength	Certain	Probable	Possible	Molecules
6	6064.65	TiI 69	-	-	-
5	6065.61	-	FeI 207	-	-
[5	6066.73	CeI	-	-	-
[3	6067.20	-	-	LaII 48	-
1	6067.98	-	-	-	CN?
4	6068.75	-	LaI,CeI	-	-
5	6069.78	CeI,CeI	-	SmI	-
5	6071.92	CeI	-	-	-
2	6073.24	-	-	-	CN?
4	6074.30	-	-	-	-
4	6075.66	-	-	-	-
[5	6076.58	CeI	-	-	-
[6	6077.31	CeI	-	-	-
2	6077.59	-	-	-	-
3	6079.59	-	-	-	$ScO\,^2\Pi-^2\Sigma(0,0)Q_1$
8	6081.38	VI 34,CeI	-	HoI	-
7	6082.68	VI	FeI 64	-	-
3	6084.05	-	-	SmI	CN
7	6085.28	TiI 69	FeI 269	-	-
[4	6086.64	-	VI 49	-	-
[4	6088.33	-	DyI	YI	-
5	6089.56	VI 33	-	-	-
7	6090.30	VI 34,VI 33	-	-	-
4	6091.22	-	-	TiI 238	-
6	6093.12	CoI 37,CeI	-	-	-
6	6093.85	-	-	-	-
1	6095.5	-	-	-	-
5	6097.37	FeI 64,VI 33	-	-	-
4	6098.44	HfI		-	CN
5	6099.84	CeI	-	SmI	-
5	6101.60	-	-	-	-
[9	6102.70	CaI 3	-	-	-
[5	6103.45	-	-	LiI 4	-
4	6104.47	-	-	-	-
[4	6105.42	-	-	-	-
[2	6106.29	-	-	-	-
5	6107.14	-	LaI	VI 60	-
6	6108.30	LaI	NiI 45	-	-
5	6109.13	-	-	-	-
5	6110.27	-	-	-	-
5	6110.77	BaI 7	-	-	-
7	6111.73	VI 34	LaI,CeI	-	-
3	6113.14	-	-	-	-
5	6114.23	GdI 3	-	-	-
3	6115.50	-	-	-	$CN(8,3)R_1 39?$
1	6117.00	CoI 37	-	-	-
4	6117.80	-	-	-	CN?
6	6118.68	CeI,CeI	-	-	-
8	6119.59	CeI,VI 34	-	-	-
[6	6120.31	FeI 14	-	-	-
[7	6120.87	ZrI 24	-	TiI 53	-

Int	Wavelength	Certain	Probable	Possible	Molecules
9	6122.21	CaI 3,ZrI	-	-	-
3	6123.72	CeI	-	-	-
7	6124.83	ZrI 24	-	-	-
6	6126.21	TiI 69	-	LaII	-
8	6127.45	ZrI 2	-	-	-
6	6128.45	VI 33	-	-	-
4	6129.80	-	-	LaII 47	-
4	6131.14	-	-	-	-
6	6132.23	-	-	-	$YO\ ^2\Pi_{1/2}-{}^2\Sigma^+(0,1)Q$
6	6133.56	-	-	HoI	-
9	6134.51	ZrI 2	LaI	-	-
7	6135.33	VI 34	CeI,YI	VI 60	-
8	6136.64	FeI 62	FeI 169	-	-
6	6137.72	-	FeI 207	-	-
8	6138.49	-	YI 3	TiI 197	-
7	6140.45	ZrI 24	-	-	-
8	6141.68	BaII 2	-	FeI 816	-
9	6143.20	ZrI 2,CeI	-	LaI	-
2	6144.72	-	-	-	-
6	6146.34	CeI	LaII 4	TiI 153	-
[3	6147.69	CeI	-	-	-
6	6148.62	-	-	-	$YO\ ^2\Pi_{1/2}-{}^2\Sigma^+(1,1)Q$
8	6150.13	VI 20	-	-	-
6	6151.68	CeI,VI 33, FeI 62	-	-	-
4	6152.58	-	-	-	-
3	6153.31	-	-	-	-
7	6154.25	NaI 5	-	-	$ZrO\ ^1\Pi-{}^1\Sigma(1,0)$
6	6154.89	-	-	-	-
[5	6155.9	CaI 20	ZrI	-	-
5	6156.73	-	-	-	-
6	6157.75	-	NdII	ZrI	CN?
7	6158.95	-	-	-	-
6	6160.78	NaI 5	-	-	-
8	6161.30	CaI 20	-	PrII	-
10	6162.18	CaI 3,CeI	-	-	-
8	6163.69	CaI 20	FeI 64	-	-
8	6165.69	LaI	CeI	PrII	-
7	6166.52	CaI 20	-	-	-
5	6167.77	-	-	-	-
[9	6169.12	CaI 20	-	-	-
9	6169.52	CaI 20	-	-	-
[9	6170.44	VI 20	-	-	-
5	6171.03	-	-	-	-
[5	6172.71	LaII 4	-	-	-
5	6173.41	FeI 62	-	EuII 9	-
3	6174.44	-	LaII 47	SmI	-
3	6175.21	CeI	-	-	-
3	6176.39	-	-	-	-
8	6178.22	-	-	-	-
5	6180.27	-	NiI 65,FeI 269	-	-
5	6181.14	-	-	-	-

Int	Wavelength	Certain	Probable	Possible	Molecules
5	6181.95	-	-	-	-
5	6183.75	-	-	-	-
4	6185.08	HfI	-	-	-
4	6186.21	CeI	-	TiI 197	-
5	6187.94	CeI	-	-	-
7	6189.26	CoI 37, VI 20	-	ZrI	-
3	6190.45	-	-	-	-
9	6191.63	YI 2	NiI 45, FeI 169	-	-
7	6192.30	-	-	-	CN(4,0)R_2head
6	6193.03	ZrI 24	-	-	-
6	6193.73	ScI 3	-	-	-
3	6194.37	-	-	SmI	-
6	6195.43	CeI, CeI	-	-	CN
3	6196.80	-	-	-	-
2	6197.91	CeI	-	-	-
8	6199.27	VI 19	-	-	-
5	6200.72	-	-	-	CN
6	6201.94	-	-	-	-
7	6204.97	-	-	-	-
5	6206.65	-	-	-	CN(4,0)R_1head
6	6207.36	VI 20	-	-	CN
5	6208.34	-	-	-	CN
6	6209.41	CeI	-	-	-
9	6210.72	ScI 2	-	-	-
8	6213.07	FeI 62, ZrI 24	-	-	-
8	6213.87	VI 20	-	-	-
4	6215.17	-	TiI 293	-	-
9	6216.44	VI 19	-	-	-
5	6218.14	-	-	-	CN
5	6219.34	FeI 62	-	-	-
7	6221.22	ErI	-	-	-
9	6222.54	-	YI 2	-	-
5	6223.25	CeI	-	-	-
8	6224.50	VI 20	-	-	-
4	6225.32	-	-	-	-
2	6226.50	-	-	NdI, SmI	-
6	6228.21	CeI	-	-	-
5	6229.15	-	-	-	ZrO $^3\Phi$-$^3\Delta$(0,0)R_3
7	6229.95	-	-	-	-
9	6230.87	VI 19, CoI 37	FeI 207	-	-
7	6233.33	VI 20	LaI	-	-
3	6235.01	-	LaI	-	ZrO $^3\Phi$-$^3\Delta$(0,0)Q_3
3	6235.81	-	-	-	-
6	6237.34	CeI	-	-	CN
6	6238.64	CeI	-	HfI	-
10	6239.77	ScI 3, VI 20	-	-	-
7	6241.77	CeI	-	-	-
9	6243.07	VI 19, VI 19	-	-	-
7	6245.12	VI 20	-	-	-
4	6246.43	-	-	FeI 816	-
6	6247.78	-	-	-	-

Int	Wavelength	Certain	Probable	Possible	Molecules
4	6248.6	–	–	–	–
7	6249.90	LaI 7	–	–	–
8	6251.77	VI 19	–	–	–
6	6252.66	–	FeI 169	–	–
6	6253.65	CeI	–	–	–
6	6254.27	–	FeI 111	–	–
5	6255.02	–	–	–	–
5	6256.30	NiI 43	FeI 169	–	–
8	6256.92	VI 19	ZrI	–	–
9	6257.96	TiI 1,TiI 104	–	–	–
9	6258.75	TiI 104,VI 19 ScI 3,DyI	–	–	–
5	6260.02	–	–	–	–
8	6261.22	TiI 104,VI 20	–	–	–
5	6262.34	LaII 33	–	–	–
2	6263.76	–	–	–	CN
6	6265.11	FeI 62	–	TiI 144	CN
8	6266.25	VI 20,LaI	–	TiI 144	–
6	6266.94	–	EuI,ZrI	SmII	–
8	6268.71	VI 20,TiI 103	–	–	–
6	6270.14	–	CeI	–	–
3	6271.71	–	–	–	–
8	6273.45	TiI 1	–	–	–
8	6274.73	VI 19	–	–	–
8	6276.40	ScI 2,CeI	–	–	–
5	6277.29	–	–	TiI 144	–
2	6278.50	–	–	–	CN(4,0)$P_2$22
8	6280.67	FeI 13	–	–	–
5	6282.70	CoI 37	–	–	–
7	6285.15	VI 19	–	–	–
5	6285.95	–	–	–	CN
4	6287.49	–	–	–	CN
3	6288.21	–	–	–	–
3	6289.79	–	–	–	–
3	6290.81	–	–	–	–
3	6291.82	–	–	–	CN
9	6292.83	VI 19,NdII, TiI 103	GdI	–	–
6	6293.46	LaI	–	–	–
4	6294.33	–	–	–	–
9	6295.37	TiI 1,CeI	–	TiI 144	–
10	6296.66	TiI 1,VI 19, (LaII)	–	–	–
5	6297.97	FeI 62	–	TiI 144	CN
6	6299.70	–	ZrI	–	CN
4	6301.26	–	–	–	–
4	6302.37	–	–	–	–
7	6304.04	TiI 104,ZrI 24	–	–	–

Int	Wavelength	Certain	Probable	Possible	Molecules
[10	6305.73	ScI 2,ScI 3	LaII 5	-	-
[5	6306.92	-	-	-	-
5	6308.03	-	-	-	-
5	6308.84	ErI	-	-	-
7	6310.16	CeI	-	NdI	CN
5	6311.39	TiI 103	-	-	-
5	6312.28	TiI 104	-	-	-
6	6313.09	ZrI 65	-	-	-
5	6314.58	ZrI	NiI 67	-	-
3	6315.60	-	-	-	-
3	6316.62	-	-	-	-
6	6318.11	TiI 103	-	CaI 53	CN
5	6320.47	LaII 19	-	-	CN?
[4	6321.24	-	ZrI	-	CN
[3	6321.90	-	-	-	CN
4	6322.75	-	FeI 207	-	CN?
9	6325.14	TiI 1	-	-	CN
8	6325.84	LaI 2	-	-	-
[4	6326.99	-	VI 84	-	CN(4,0)$Q_1$34
[6	6327.55	NiI 44	-	-	CN?
1	6328.9	-	-	-	-
7	6330.16	CrI 6	-	-	-
7	6332.02	CeI	-	-	CN(5,1)R_2head
4	6334.14	-	-	-	-
6	6335.37	FeI 62,CeI	-	-	-
5	6336.14	TiI 103	-	-	-
5	6337.04	CeI	-	FeI 816	-
4	6338.31	-	-	-	CN
3	6339.16	-	VI 84	-	-
4	6339.99	-	-	-	-
5	6340.80	CeI	-	-	-
6	6341.73	BaI 6	-	-	-
5	6344.03	-	CeII,FeI 169	-	-
8	6345.02	ScI 1	ZrI	-	ZrO $^3\Phi-{}^3\Delta$(0,0)R_2
6	6346.02	-	-	-	-
5	6347.25	-	-	-	CN(5,1)R_1head
4	6348.54	-	-	-	-
5	6349.55	-	VI 84	-	-
3	6350.49	-	-	-	-
4	6351.25	-	-	-	ZrO $^3\Phi-{}^3\Delta$(0,0)Q_2
5	6352.18	-	-	-	-
5	6353.64	FeI 13	CeI	-	CN
6	6355.12	-	-	-	CN
4	6356.21	-	-	-	-
7	6357.10	ZrI 2	VI 84	-	-
8	6358.71	FeI 13	-	-	-
8	6359.97	TiI 1	LaI	-	-
[6	6362.29	ScI	-	-	CN
[7	6362.88	CrI 6	-	-	CN
8	6364.75	TiI 1	NiI 67	-	-

Int	Wavelength	Certain	Probable	Possible	Molecules
6	6366.48	TiI 103	-	-	CN
4	6367.50	-	-	SmI	-
4	6369.13	-	-	-	-
4	6369.89	-	-	-	-
4	6370.80	-	-	SmI	CN
4	6371.68	-	-	-	CN
5	6372.68	CeI	-	-	-
5	6374.43	-	-	-	CaH CN
5	6375.94	-	-	-	CN
3	6377.00	-	-	-	-
5	6378.07	-	-	-	-
8	6378.80	ScI 1	-	-	CaH
6	6379.68	-	-	-	-
5	6380.54	-	SrI	-	CaH
6	6381.13	-	-	-	-
6	6381.95	-	-	-	CaH $^2\Sigma-^2\Sigma(0,0)P_2$head
6	6382.81	-	-	-	CN
5	6383.86	-	-	-	-
5	6384.89	-	NdII 85	-	-
5	6385.80	-	-	-	-
6	6387.06	CeI	-	-	-
7	6388.84	-	-	-	CN
5	6389.36	-	-	-	CaH $^2\Sigma-^2\Sigma(0,0)P_1$head
6	6390.42	LaII 33,CeI	-	-	CN?
6	6392.17	-	-	-	CN
5	6392.65	-	FeI 109	-	-
8	6394.19	LaI 7	-	-	-
5	6396.00	CeI	-	-	-
5	6397.91	-	-	-	-
4	6398.84	-	-	-	CN
8	6400.29	FeI 13	-	FeI 816	-
7	6402.05	YI 2	-	-	-
4	6403.05	-	-	-	CN*
2	6404.66	-	-	-	CN*
4	6405.67	-	-	CaI	CN
5	6407.05	ZrI 2	-	-	-
6	6408.27	-	SrI 8	FeI 816	CN
4	6409.81	-	-	-	CN*
7	6411.03	LaI 7	-	-	-
4	6412.45	-	FeI 169	-	-
9	6413.32	TiI 1,ScI 1	-	-	-
4	6415.40	-	-	-	CN*(5,1)$Q_1$25
3	6416.09	-	-	-	CN*(5,1)$P_2$21
2	6416.86	-	-	-	-
3	6417.94	-	-	-	-
5	6419.22	-	-	TiI 196	CN
4	6420.57	-	-	-	-
6	6421.57	DyI	FeI 111	-	-

Int	Wavelength	Certain	Probable	Possible	Molecules
1	6423.20	-	-	-	-
6	6424.38	-	-	-	CN
5	6425.63	-	-	-	CN
4	6426.40	-	-	ZrI	CN
5	6428.69	NdII	-	-	-
7	6430.73	FeI 62	VI 107	NbI	-
5	6431.70	-	VI 107	-	CN
5	6432.43	-	-	-	-
3	6433.36	-	VI 107	NbI	-
[7	6434.50	CeI	-	ZrI	-
[8	6435.04	YI 2	VI 107	-	-
5	6436.51	CeI	-	-	-
5	6437.84	-	-	EuII 8	CN
7	6439.10	CaI 18	-	-	-
4	6440.01	CeI	-	-	-
4	6440.89	-	-	-	-
3	6442.6	-	-	-	CN
2	6443.3	-	-	-	CN
4	6444.3	-	-	-	CN
3	6445.1	-	-	-	CN
5	6445.85	CeI	ZrI 57	-	-
8	6448.21	ScI 1	LaI	-	-
4	6449.13	-	-	-	-
8	6450.07	CaI 19,CoI 37	-	-	-
6	6450.92	BaI 6	-	-	-
6	6451.65	ZrI	-	-	-
6	6452.33	-	VI 48	-	-
7	6454.54	LaI	-	-	-
8	6455.91	LaI 1,CaI 19	-	-	-
4	6456.91	-	-	-	CN*
7	6458.05	CeI	-	-	-
2	6459.9	-	-	-	-
1	6460.8	-	-	-	-
8	6462.65	CaI 18,FeI 33	-	-	-
[4	6464.03	-	-	-	CN*
[4	6464.70	FeI 13,CaI 19	-	-	-
2	6465.81	-	-	-	CN*(5,1)$Q_2$34
5	6467.17	VI 32,CeI	-	-	-
3	6468.49	-	-	-	-
2	6469.38	-	-	-	-
5	6470.35	ZrI 65	-	-	-
6	6471.62	CaI 18	-	-	-
2	6472.53	-	-	SmII 60	-
* 7	6473.89	-	-	-	$ZrO\ ^3\Phi-^3\Delta(0,0)R_1$head
* 7	6475.13	-	-	-	-
5	6478.48	-	-	-	CN*
5	6480.60	-	-	-	$ZrO\ ^3\Phi-^3\Delta(0,0)Q_1$head
7	6481.98	-	FeI 109	-	-
6	6482.80	BaI	NiI 66	-	-
6	6484.35	ZrI	-	-	-
[6	6485.96	-	-	NdI	CN
[4	6486.61	-	-	-	-

Int	Wavelength	Certain	Probable	Possible	Molecules
4	6487.97	-	-	-	-
5	6488.83	-	-	-	CN
5	6489.67	ZrI 65	-	-	-
4	6491.18	CeI	-	-	-
5	6493.06	-	ZrI	-	-
7	6493.80	CaI 18	-	-	CN(6,2)R_1head
[7	6495.12	-	FeI 168	-	-
[6	6495.60	-	-	-	ZrO $^1\Pi$-$^1\Sigma$(0,0)?
[8	6496.90	BaII 2	-	-	-
[6	6497.75	-	-	NbI	-
8	6498.87	BaI 6,FeI 13	-	-	-
6	6499.73	CaI 18	-	-	-
3	6500.35	-	-	-	-
6	6501.12	CrI 16	-	-	-
4	6502.33	-	-	-	CN*
[3	6503.23	-	ZrI	-	CN
[4	6504.16	CeI	VI 48,SrI 8	-	-
5	6505.43	-	-	-	-
2	6506.33	ZrI	-	-	CN
6	6507.19	-	-	-	-
5	6508.19	TiI 102	-	-	CN
6	6508.97	CaI 18,CeI	-	-	-
3	6510.46	-	-	-	CN*
2	6511.24	-	-	-	ZrO Rot
3	6512.36	-	-	-	ZrO Rot
2	6513.33	-	-	-	ZrO Rot
6	6514.90	NdII	-	-	ZrO Rot Atm H_2O?
3	6516.0	-	-	-	-
6	6517.29	CeI	-	-	Atm H_2O?
4	6518.66	-	-	-	ZrO Rot CN
3	6519.80	-	-	-	ZrO Rot CN
3	6521.09	-	-	-	ZrO Rot CN?
6	6522.67	-	-	EuI	-
3	6523.96	-	-	-	ZrO Rot
4	6525.05	-	-	-	ZrO Rot
3	6526.05	-	-	-	ZrO Rot CN?
[7	6527.29	LaII 33,BaI 6	-	-	ZrO Rot
[4	6528.13	-	-	SmI	ZrO Rot
4	6529.32	-	-	-	ZrO Rot CN
5	6530.44	CeI	-	-	ZrO Rot
6	6531.29	-	VI 48	-	ZrO Rot
4	6532.62	-	NiI 64	-	ZrO Rot
3	6534.10	-	-	-	ZrO Rot CN
2	6534.88	-	-	-	ZrO Rot
4	6537.11	-	-	-	ZrO Rot CN
[5	6538.08	CrI 16	-	-	ZrO Rot
[1	6539.28	-	-	-	ZrO Rot
2	6540.20	-	-	-	ZrO Rot
3	6541.35	-	-	-	ZrO Rot CN
8	6543.23	LaI 7	VI 48	-	-

Int	Wavelength	Certain	Probable	Possible	Molecules
5	6544.91	-	-	NbI	CN
5	6546.29	TiI 102	FeI 268	-	-
4	6547.65	FeI 13	-	-	CN
[6	6549.56	NdII	-	-	-
[6	6550.44	-	SrI 12,NdII	ZrI	-
6	6551.72	FeI 13,CeI CoI 54	-	SmI	-
5	6552.87	-	-	-	CN*
6	6554.17	TiI 102	-	-	-
[4	6554.97	-	-	-	-
[7	6556.01	TiI 102	-	-	-
[8	6557.35	YI 1	-	-	-
[5	6558.19	-	VI 59	-	CN(6,2)$Q_2$25
5	6559.69	-	-	-	-
3	6560.75	CeI	-	-	CN(5,1)$Q_2$45
5	6563.16	-	CoI 80	-	CN
5	6564.19	-	-	-	CN*
7	6565.55	-	LaI,VI 48,CeI	-	-
4	6566.74	-	-	PrII	CN
5	6568.74	-	-	-	-
[6	6569.42	ZrI	-	SmII 62	-
[4	6570.15	-	-	-	CN(6,2)$R_2$34
4	6570.96	-	LaII 47	-	CN
9	6572.76	CaI 1,CrI 16	-	-	-
[8	6574.25	FeI 13	-	-	-
[6	6575.08	-	FeI 206	-	-
8	6576.63	ZrI	-	YI	CN?
4	6577.42	CeI	-	-	-
8	6578.54	LaI 1	-	-	-
6	6579.36	DyI	-	-	-
[7	6581.13	CrI 16,FeI 34	-	-	-
[3	6581.83	-	-	-	-
5	6583.37	ErI	-	-	-
7	6584.88	YI 1	-	-	-
4	6585.44	-	-	-	CN
4	6586.40	-	NiI 64	-	-
3	6587.16	-	-	-	CN(6,2)P,23
2	6587.86	-	-	-	-
5	6589.10	-	SmI 1	-	CN
3	6590.28	-	-	-	-
5	6591.49	-	GdI	-	-
[6	6593.07	TiI 102	FeI 268	-	-
[7	6593.64	LaI	-	-	-
5	6595.26	BaI 6	-	-	-
5	6596.68	-	-	ZrI	-
9	6598.98	ZrI,TiI 49	-	-	-
6	6600.18	LaI	-	-	-
3	6602.54	-	-	-	CN

Int	Wavelength	Certain	Probable	Possible	Molecules
4	6603.29	-	-	ZrI	CN(6,2)$Q_2$32
5	6604.55	-	-	HoI, SmII ScII 19	-
7	6606.23	CeI	VI 48	-	-
6	6607.82	-	FeI 109, VI 59	-	-
5	6609.47	FeI 13	-	-	-
2	6610.75	-	-	-	CN*(6,2)$Q_2$33
3	6612.22	-	-	-	CN
6	6613.80	FeI 13	YII 26	-	-
3	6614.88	-	-	-	CN
6	6616.68	LaI	-	-	CN
4	6618.4	-	-	-	CN*(6,2)$Q_2$34
4	6619.20	-	MoI	-	-
3	6621.21	-	-	-	-
6	6622.92	CeI	-	-	-
7	6625.03	FeI 13	VI 48	-	-
3	6626.28	-	-	-	CN*(6,2)$Q_2$35
3	6627.61	-	-	-	CN (6,2)$R_2$42
6	6628.91	CeI	-	HoI	-
6	6630.07	CrI 16	-	NdI	-
7	6631.23	-	-	LaI	-
4	6632.42	-	-	-	CN
3	6633.4	-	-	-	CN*(7,3)$R_2$8
3	6634.2	-	-	-	CN*
2	6634.9	-	-	-	CN*
2	6637.2	-	-	-	-
3	6637.8	-	-	-	CN*
3	6638.5	-	-	-	CN*(7,3)$R_2$12
5	6639.90	-	GdI	-	CN
4	6641.22	-	-	-	-
7	6643.53	NiI 43	SrI 8	-	-
[7	6644.43	LaI	-	-	-
3	6645.03	-	-	EuII 8, LaI	-
4	6646.84	-	FeI 206	-	CN
5	6648.09	FeI 13	-	-	CN(7,3)R_1head
5	6649.29	-	-	-	CN
8	6650.79	LaI	CeI	YI	-
3	6651.42	CeI	-	-	-
3	6653.35	-	-	-	CN *
4	6654.32	-	-	-	-
5	6655.59	-	-	-	-
[5	6657.00	-	-	-	CN
4	6657.76	-	-	-	-
3	6658.7	-	-	-	CN*
4	6659.2	-	-	-	-
5	6659.7	-	-	-	CN*
7	6661.37	LaI, CeI	-	-	-
5	6662.53	-	-	-	-
6	6663.45	-	FeI 111	-	-
5	6664.50	-	-	YI	-
6	6665.50	FeI 34, CeI	-	-	-

Int	Wavelength	Certain	Probable	Possible	Molecules
6	6666.42	TiI	–	–	–
4	6667.51	–	–	–	CN
4	6669.67	–	–	–	CN* (7,3)P,7
3	6670.40	–	–	NdI	CN* (7,3)Q,16
5	6671.50	LaII 33	SmI 1	–	–
4	6672.53	–	FeI 205	–	CN(7,3)P,8
5	6673.99	–	–	–	–
6	6675.28	BaI 6	–	–	–
3	6676.64	–	–	–	CN
5	6677.37	–	NbI	–	–
6	6678.01	–	FeI 205, FeI 268	–	CN
6	6678.68	CoI 54	–	TiI 213	CN
4	6679.93	CeI,CeI	–	–	–
5	6681.38	–	–	–	CN*
3	6682.5	–	–	–	CN*
5	6683.36	–	–	–	CN*
4	6684.88	–	–	–	CN*
3	6686.11	–	–	–	–
8	6687.53	YI 1	–	–	–
6	6688.16	ZrI	–	–	–
5	6689.43	–	–	–	$BaH\ ^2\Pi - ^2\Sigma(0,0)P_2$head
4	6690.99	–	–	–	CN
2	6692.1	–	–	–	–
5	6692.81	LaI	–	–	CN
5	6693.54	BaI 6	–	–	–
4	6694.53	–	–	–	CN *
5	6696.05	–	–	AlI 5	–
5	6697.23	–	–	–	CN*
5	6698.10	–	–	–	CN
5	6698.63	–	–	AlI 5	–
4	6700.62	CeI	–	–	CN(6,2)P,37
3	6701.26	–	–	NbI	–
5	6702.03	–	ZrI	–	CN?
4	6702.64	–	–	TbI	CN?
5	6703.35	–	FeI 268	–	CN
6	6704.21	CeI	–	–	–
5	6704.86	–	–	–	CN(6,2)P,38
3	6705.83	–	–	–	–
8	6707.78	LiI 1	–	–	–
7	6709.54	LaI 6, ZrI	–	CaI 45	–
6	6710.28	FeI 34, CeI	–	–	–
2	6711.1	–	–	–	–
5	6712.4	–	–	–	CN(6,2)Q,44
3	6713.44	CeI	–	YI	–
4	6715.65	–	–	–	CN
7	6717.71	CaI 32	–	ZrI	–
4	6719.91	–	–	–	–
3	6720.8	–	–	–	CN(7,3)Q,26
5	6721.86	–	–	–	CN *
6	6722.56	–	–	–	CN *
4	6723.75	–	NbI	–	CN
4	6726.12	–	–	SmI	CN

Int	Wavelength	Certain	Probable	Possible	Molecules
5	6728.57	CeI	–	–	CN
4	6729.62	CeI	–	CrI 301	–
5	6730.80	GdI 2	–	–	–
4	6732.15	–	–	SmII 59	–
4	6733.82	–	MoI	–	–
[5	6735.00	–	–	–	–
[4	6735.8	–	–	YI	–
4	6736.9	–	–	–	CN
4	6737.8	–	ScI 8	–	CN
[6	6739.6	FeI 34	–	NbI	–
[7	6740.09	NdII	–	–	–
4	6742.36	–	–	–	–
7	6743.20	TiI 48	–	–	–
[5	6747.25	–	FeI 205	–	CN
[4	6747.96	–	LaI	–	CN
4	6749.48	CeI	–	–	–
6	6750.19	–	FeI 111	–	CN
4	6751.34	–	–	–	–
8	6752.97	LaI, VI 31, ZrI	–	–	–
5	6754.77	–	–	–	CN
4	6755.80	–	–	–	–
3	6757.0	–	–	–	–
4	6759.23	–	–	–	$CN^*(6,2)P_2 43$
3	6760.37	–	–	–	–
3	6761.38	–	–	–	CN^*
8	6762.35	ZrI 1	–	–	–
[5	6764.17	–	CeI	–	–
[4	6765.00	–	–	–	–
7	6766.53	VI 31	–	–	–
6	6767.79	CeI, NiI 57	–	–	–
[7	6769.09	–	ZrI	–	–
[5	6769.68	–	–	–	CN
6	6771.00	CoI 54	–	–	–
[4	6772.13	–	–	BaI	CN
[6	6772.96	–	ZrI	–	CN
7	6774.22	LaII 2	–	–	–
2	6775.25	CeI	–	–	–
4	6776.31	–	–	–	$CN(7,3)Q_1 33$
[5	6777.53	–	–	–	CN^*
[6	6778.38	CeI	–	–	–
4	6780.31	–	–	–	$CN(7,3)R_2 41$
4	6781.47	–	–	–	–
4	6782.47	–	–	–	CN?
5	6783.50	–	FeI 206, FeI 205	–	–
6	6785.03	VI 31	–	–	–
4	6785.97	–	–	–	CN
4	6787.06	–	–	–	–

Int	Wavelength	Certain	Probable	Possible	Molecules
3	6788.23	-	-	-	-
5	6789.23	-	-	HfI	CN?
6	6790.36	NdII	-	-	-
7	6791.03	SrI 3	ZrI	-	-
6	6791.57	-	-	-	-
5	6792.26	-	-	-	CN(7,3)Q,35
8	6793.70	YI 1	-	-	-
4	6794.90	-	-	-	-
4	6795.38	-	-	YII 26	-
5	6796.69	-	-	ZrI	-
5	6798.51	CaI 31	-	-	-
3	6799.82	-	-	-	CN
5	6800.98	-	-	-	CN
4	6801.69	FeI 34,CeI	-	-	-
5	6802.96	CeI	-	SmI	-
4	6803.99	-	-	-	-
3	6804.7	-	-	-	-
4	6805.62	-	-	-	-
5	6806.92	-	FeI 268	-	-
5	6807.78	CeI	-	-	-
6	6808.88	LaII I,CeI	FeI 340	-	CN(8,4)R$_1$head
5	6810.31	-	-	-	-
4	6811.38	-	CeI	-	-
6	6812.52	VI 31	-	-	-
2	6813.76	-	-	-	CN?
6	6815.07	CoI 54	-	YI	-
5	6816.02	-	NdII	-	-
4	6816.59	-	GdI	-	-
4	6817.40	-	-	-	-
5	6818.19	CeI	-	-	CN
4	6819.04	HfI	-	-	-
5	6819.74	-	-	-	-
4	6822.30	-	-	-	-
6	6823.74	-	LaI	-	-
3	6825.06	-	-	-	CN
5	6826.84	-	-	-	BaH $^2\Pi$-$^2\Sigma$(1,1)P$_1$head
6	6828.30	GdI	-	NbI	-
5	6830.05	VI 31	-	-	-
4	6830.82	-	-	-	-
6	6832.16	-	-	YII 26	-
8	6832.93	ZrI 1,VI 31	-	-	-
5	6833.66	-	-	ZrI	-
5	6834.16	LaII 3	-	-	-
5	6835.26	DyI	-	-	-
4	6836.11	-	-	-	-
5	6836.77	-	-	-	CN
4	6838.05	LaII 33	-	-	-
5	6839.83	-	FeI 205	-	-
4	6841.23	-	-	-	-
5	6841.71	VI 31	-	-	-
3	6842.90	-	-	-	-
4	6844.00	CeI	-	-	-

Int	Wavelength	Certain	Probable	Possible	Molecules
5	6845.21	YI 16	-	ZrI	-
7	6846.58	ZrI	-	-	CN
7	6847.30	CeI,ZrI	-	-	-
5	6848.53	-	-	-	-
5	6849.42	-	-	ZrI,NbI	-
3	6850.04	-	-	-	$BaH\ ^2\Pi-^2\Sigma(0,0)P_1$head
4	6850.60	-	-	-	-
5	6851.76	FeI 34	-	-	-
4	6852.89	-	-	ZrI	-
5	6853.80	-	CeI	-	-
5	6854.55	ZrI	-	-	-
4	6855.71	-	-	-	-
5	6856.46	CeI	-	-	-
4	6857.94	-	-	ZrI	-
5	6859.58	-	FeI 340	-	-
5	6861.24	-	SmI	TiI 237	-
5	6862.17	-	FeI 109	-	-
4	6863.26	-	-	-	-
2	6864.72	-	EuI	-	-
4	6865.58	-	-	BaI	-
6	6866.08	-	-	-	-
4	6866.36	-	-	-	-
6	6867.95/67.41	-	-	-	Atmos O_2,B band
7	6868.95/68.41	-	-	-	"
7	6869.59/69.05	-	-	-	"
8	6870.56/70.02	-	-	-	"
7	6871.67/71.13	-	-	-	"
6	6872.67/72.13	CoI 54	-	-	"
7	6874.39/73.85	-	-	-	"
7	6875.94/75.40	-	-	-	"
6	6877.22/76.68	-	-	-	"
6	6878.19/77.65	SrI 3	-	-	"
3	6879.59/79.05	-	-	-	"
6	6880.56/80.02	-	-	-	-
6	6881.02	-	-	-	-
3	6881.91	-	-	-	-
5	6883.24	-	-	ZrI	-
5	6883.92/83.38	-	-	-	Atmos O_2,B band
6	6885.69/85.15	CeI,CeI	-	-	"
7	6886.67/86.13	-	-	-	"
4	6888.31	-	ZrI	-	-
6	6889.61/89.07	-	-	-	Atmos O_2,B band
6	6890.39/89.85	-	-	-	"
4	6891.50	-	-	-	-
7	6892.76/92.22	SrI 1	-	-	Atmos O_2,B band
5	6893.86/93.32	-	CeI	-	"
4	6894.56	CeI	-	-	-
5	6895.81	-	-	YII 26	-
5	6896.53/95.99	-	-	-	Atmos O_2,B band
5	6897.47/96.93	-	-	-	"

Int	Wavelength	Identification
8	6900.52	ZrI
6	6902.42	CaH $^2\Pi-^2\Sigma(1,1)Q_2$head
7	6904.43/04.23	ZrI, Atmos O_2
5	6906.11	-
5	6908.59/08.39	Atmos O_2
6	6909.86/09.66	Atmos O_2
6	6911.62	(FeI 109), (HfI)
5	6913.20	-
6	6914.52	NiI 62
8	6916.60	GdI 2, ZrI
7	6918.30	LaI
[6	6919.32	CaH $^2\Pi-^2\Sigma(0,0)Q_2$head
[4	6920.13	-
4	6922.46	-
6	6924.23	NdI, CeI
5	6925.97	CN(3,0)R_2head, (LaI)
5	6927.74	-
5	6929.36	CaH?
4	6930.33	CN, ZrO $^1\Pi-^1\Sigma^+(0,1)R$ head
6	6932.36	CN?, (ZrI)
[7	6933.45	CN?, YI 1
[6	6933.99	-
5	6935.33	LaI
5	6937.05	-
[4	6938.66	(KI)
[6	6939.52	CeI, CN
5	6941.19	CN(3,0)$Q_2$8
5	6942.55	CN(3,0)R_1head, CaH?
6	6943.89	-
6	6945.07	(FeI 111), CN
7	6948.99	-
5	6950.88	(FeI 205), CN
6	6952.29	CN
[8	6953.67	ZrI, CN(3,0)Q_1head
[6	6954.37	LaII 1, CN
7	6957.80	LaII, DyI, CN
5	6959.07	CN *
6	6960.88	-
6	6963.66	CN *
7	6966.27	ZrI, CN
5	6968.79	CN
6	6970.69	CeI, FeI 463, CN
5	6972.16	-
6	6974.60	CN *
4	6975.87	ZrI
7	6978.12	(FeI 111), CN
6	6979.71	(YI), CN
6	6981.62	CN
5	6983.64	CN(7,3)$Q_1$53 ?
6	6984.5	CN *
7	6986.07	CeI, CN

Int	Wavelength	Identification
6	6989.47	CN *
7	6990.79	ZrI
7	6991.83	GdI 2
7	6994.67	ZrI, CN
6	6996.66	(TiI 256), CN
5	6997.92	CN(3,0)$P_2$17
6	6999.08	CN *
6	6999.99	CeI
5	7001.85	CN
3	7002.92	-
6	7004.15	CN
5	7006.21	CN, CaH?
5	7007.86	TiI 100, CN
5	7009.18	CN
4	7010.25	CN(3,0)$P_2$19
5	7011.63	CN *
4	7012.78	CN(3,0)$R_2$33
4	7013.29	CN(3,0)$R_1$32 (CeI)
5	7014.70	CN (CeI)
6	7016.27	CN FeI 109, CoI 54
4	7017.23	CeI
5	7018.05	CN(3,0)$Q_2$26
5	7019.02	CN, CeI
4	7020.21	CN(3,0)$Q_1$25, (SmII 59)
4	7021.06	-
3	7022.14	-
6	7023.60	LaI
6	7024.49	CN(3,0)$Q_2$27, NdII
5	7025.62	CN
7	7027.27	ZrI, CN
4	7029.04	-
5	7031.01	CN(3,0)$Q_2$28
6	7032.22	CN *
7	7033.64	-
2	7035.72	CaH $^2\Pi - ^2\Sigma$(0,0)P_2
5	7037.65	CN, NdII
5	7038.77	CN, (TiI 256)
5	7039.74	CN *
2	7040.84	-
2	7042.15	(SmII 58)
6	7045.16	CN *
7	7045.87	LaI 6, CN
5	7046.89	NbI, CN
2	7049.55	CeI, (CeI)
4	7050.78	(TiI 256)
6	7052.61	CN, GdI, CoI 54 (YI)
4	7054.28	CN, (CeI)
3	7055.38	-
4	7057.32	ZrI
4	7057.92	(ZrI)

Int	Wavelength	Identification
6	7060.00	CN,BaI 5
4	7061.22	CN(3,0)$P_1$25
4	7062.63	CN,(NiI 64)
3	7063.6	HfI
4	7065.12	TiI 100
7	7066.43	LaII 1,NDII, CN
6	7068.39	LaI 1,CN
5	7070.07	SrI 3
2	7072.0	TiI
3	7072.63	CN(4,1)R_{21}head
4	7074.43	CN(3,0)$Q_1$33
4	7075.13	(YI),(NbI)
4	7076.04	CN
4	7076.87	CN,EuII 8
2	7077.84	-
3	7078.89	CN(3,0)$R_2$42
2	7081.33	-
4	7082.59	CN,(SmII 55)
[4	7084.52	CN
5	7084.98	CoI 54
3	7086.47	-
7	7087.31	ZrI 42
4	7088.99	CN(4,1)R_2head
4	7090.69	CN
6	7092.51	CN
5	7094.11	NdI
5	7095.58	ZrI,(SmI)
4	7096.45	CN,(SmI)
6	7097.77	ZrI 42
4	7098.92	GdI,CN
2	7100.13	CN(4,1)Q,10
5	7101.63	CN *
[7	7102.98	ZrI 42
7	7103.74	ZrI 42,CN
3	7104.71	(SmI)
4	7106.89	CN(4,1)R_1head,(EuI)
4	7107.98	CN
3	7108.94	CN
[5	7110.2	CN
5	7110.6	NiI 64,CN
6	7111.73	ZrI 23
5	7113.15	ZrI,(CeI),CN
4	7114.88	CN
4	7117.55	CN *
3	7118.68	CN
6	7120.20	BaI,CN
6	7122.45	CN,GdI,(NiI 126)
3	7124.76	CeI
4	7125.87	CN *
3	7127.36	CN *

Int	Wavelength	Identification
2	7128.3	CN
5	7129.46	NdII,CN
5	7130.37	TiI 100,CN
6	7131.92	HfI,(SmI),CN
3	7133.15	(ZrI),CN
2	7134.49	CN
5	7135.58	CN *
2	7136.50	CN(4,1)$Q_1$14
4	7138.05	TiI 99
5	7138.87	TiI 99,CN
5	7139.68	CN
5	7141.51	CeI
4	7143.45	CN
5	7145.20	CN
2	7146.6	-
2	7147.3	CN(4,1)$Q_1$17
6	7148.14	CaI 30,CN
5	7149.80	CN,(SmII)
5	7151.61	CeI,FeI 109,CN
3	7153.45	CN
5	7155.53	CN,(CeI)
3	7156.81	CeII
6	7158.10	LaI, CN
3	7159.4	NbI,CN
6	7160.67	TiI 98,LaI,CN
4	7163.50	CN
2	7164.3	-
4	7165.53	CN
3	7166.66	CN(4,1)$Q_2$23
4	7167.43	CN(4,1)$R_2$31
5	7168.33	GdI 1
6	7169.09	ZrI 42,CN
5	7170.42	CN
4	7172.65	(SmI),CN
4	7174.37	CN
5	7176.04/75.83	CN,Atmos H_2O
4	7177.52/77.31	(CeI),Atmos H_2O
3	7178.72	CN(4,1)Q,25
5	7179.98	FeI 33 CN
6	7181.79/81.58	CN,(NiI 126),Atmos H_2O *
2	7183.30	CN(4,1)$P_2$20
6	7185.05/84.84	CN,Atmos H_2O
7	7187.34	CN,(FeI 1051)
5	7188.4	TiI 99
5	7189.3	NdII,(FeI 463)
4	7190.32	CN(4,1)$P_2$21,(FeI 463)
6	7191.80/91.59	CN,CeI,(YI),Atmos H_2O
4	7192.94	CN(3,0)$Q_2$46
6	7193.92/93.71	CN,Atmos,H_2O
3	7195.15	BaI,10,EuII 8
2	7195.98	CN(4,1)P,,216
4	7196.95	NiI 62

Int	Wavelength	Identification
5	7198.09	CN
5	7198.99	NdII, CN
[5	7201.0	CN
[8	7201.93/01.72	CaI 29, CeI, ZrI, (Atmos H_2O)
3	7203.42	CeI, CN?
4	7204.49/04.28	CN(3,0)$Q_2$47, Atmos H_2O
6	7206.73/06.52	CN, Atmos H_2O
5	7208.04	-
7	7209.55/09.34	TiI 99, Atmos H_2O
3	7210.68	-
5	7213.66	CN, (SmI)
4	7214.99	CN *
6	7216.23	TiI 98, CN
4	7217.38	CeI, (CoI 126), EuII 8
3	7218.38	-
4	7219.86	LaI
5	7221.03	CN
3	7222.51	CN
5	7223.96	(FeI 463), CN
3	7226.69	CN *
5	7228.75	CN *
3	7230.17	CN
6	7233.17/32.95	CN, GdI, Atmos H_2O
4	7234.91/34.70	Atmos H_2O
7	7236.47/36.26	NdII, HfI, CN, (Atmos H_2O)
3	7238.85	CN
7	7240.89/40.68	HfI, (CN), Atmos H_2O
[4	7242.27	-
[5	7243.05	-
6	7244.78	TiI 99
5	7246.20	CN *
3	7248.34	-
3	7250.06	CoI 53
6	7251.68	TiI 99
7	7252.72/52.51	(CN), Atmos H_2O
7	7253.55	TiI 143, CN
[5	7254.76	CN
[4	7255.43	-
5	7258.14	(ZrI), CN
4	7259.01	CN(5,2)R_2head
6	7261.67	NiI 62, CN
4	7262.64	GdI, CeI
[4	7263.69	CN
[6	7264.68	ZrI, CN
6	7265.99/65.78	CN, Atmos H_2O
3	7268.38	CN
6	7270.14	LaI, LaI, CN
5	7271.38	TiI 97
[6	7272.96/72.75	CN, Atmos H_2O
[4	7273.65	CN (TiI 212)

Int	Wavelength	Identification
4	7275.67/75.46	Atmos H_2O
3	7276.57/76.36	CN(5,2)$P_2$5, Atmos H_2O
6	7277.97/77.76	CeI, CN, CN(5,2)R_1head, Atmos H_2O
5	7279.36	SmI, CN
6	7280.30	BaI 5, CN
5	7281.27	CN
7	7282.29	LaII 1, CN
5	7283.76	CN, (MnI 50)
4	7284.87	CN, (ZrI)
5	7287.51	CN
[5	7288.77	CN, (FeI 1077)
[4	7289.10	CN(5,2)Q_1head
[6	7290.81/90.60	CN, Atmos H_2O
[7	7291.40	GdI, NiI 63, CN
[5	7292.71	CN
[3	7293.8	CN*
4	7295.08	CN
3	7296.05	CeI
4	7297.80	CN*
5	7299.50	CN*, TiI 97
4	7301.20	CN, (EuII 8)
4	7302.65	CN, (MnI 50)
4	7303.49	CN
5	7304.73	CN
[5	7305.93	TiI 143, CN
[2	7306.56	(ZrI), (FeI 1077), CN
5	7308.26	CN*
4	7309.27	SrI
[5	7311.11	(FeI 1077)
[5	7311.63	CN, ZrI
[6	7312.80	CN*
[5	7313.43	GdI, ZrI, CN
4	7315.54	CoI 89, TiI
4	7316.69	NdII
6	7318.21	(ZrI), (TiI 212), CN
[5	7318.76	CN
[5	7320.80	LaI, CN
3	7322.11	CN
4	7323.15	NdII, CN
6	7323.92	CN
4	7324.89	CN
6	7326.08	CaI 44, (MnI 50), CN
2	7327.0	CN(5,2)$R_1$27
4	7329.01	CN
4	7330.01	CN, CeI
5	7331.04/30.83	TiI 143, CN, Atmos H_2O
5	7332.33	TiI 143, CN
8	7334.22	LaI, CN
6	7336.02	ZrI 23, CN
3	7336.87	-
4	7337.72	TiI 212
4	7339.10	(VI 117), CN
2	7341.83	-

Int	Wavelength	Identification
6	7343.82	ZrI, CN
7	7344.52	TiI 97, CN
6	7345.08	LaI, CN
4	7346.67	(YI), CN*
3	7348.57	CN*
4	7350.45	CN*
3	7352.01	(TiI 272)
4	7353.11	(NbI), CN
3	7354.34	CN
* 5	7356.21	CrI 93, (VI 117), CN
6	7357.74	TiI 97, CN
1	7359.24	-
3	7360.33	CN
6	7362.26	CeI, CeI, (VI 117), CN
6	7364.07	TiI 97
5	7366.53	TiI 96, CN
5	7369.27	CN
3	7370.1	CN, (EuII 8)
4	7372.50	NbI, CN
5	7374.39	CN*
4	7376.02	CN*
4	7376.86	CN*
4	7380.75	CN*
5	7381.87	CN, NdII
4	7382.77	LaI
3	7383.56	ZrI
3	7384.44	CN
4	7385.29	NiI 84
3	7386.13	CN(4,1)$Q_1$47
2	7387.47	-
3	7388.68	CN
3	7389.28	(FeI 1077)
6	7390.32	CeII, CN
4	7391.36	CN
4	7392.44	BaI 10
4	7393.35	CeI
3	7395.70	-
6	7397.74	CeI, CN
4	7398.59	CN
5	7400.12	CrI 93, CN
4	7401.09	(ZrI), CeI
3	7401.97	CN
5	7403.62	($LaO\,^2\Pi_{3/2} - {}^2\Sigma$ Q(0,0)head)
5	7406.26	CN
4	7408.45	CN
4	7409.49	NiI 139
5	7411.11	CN, (ZrI), (NdII), (FeI 1077)
3	7412.95	-
6	7414.73	NiI 62, CN
5	7417.51	CoI 89, (BaI)

Int	Wavelength	Identification	Int	Wavelength	Identification
5	7419.44	-	5	7495.99	CN,(TiI 225)
6	7421.03	CeI	2	7497.54	CN(6,3)$Q_1$16
6	7422.21	NiI 139,(ZrI)	4	7498.91	LaI
[5	7423.15	TiI 97	5	7500.42	CN,CeI
[5	7423.88	CN*	3	7501.87	-
5	7424.50	TiI	4	7503.02	CN,(ZrI)
3	7427.88	-	[3	7504.54	CN*
4	7428.90	CN	[4	7505.26	CN*(5,2)$Q_2$42
4	7430.70	-	3	7506.14	CN,(ZrI)
4	7432.00	TiI 142,CN(4,1)$Q_2$51	4	7507.25	CN
6	7432.97	CN,ZrI,CeI	2	7508.5	CN(4,1)$P_2$50,CeI
3	7434.57	-	3	7509.73	(CeI)
5	7437.21	CN(6,3)R_2head	4	7511.01	CN,(FeI 1077)
4	7438.55	CeI	3	7512.41	-
7	7440.19	ZrI,CN	4	7514.07	CN
[5	7441.96	GdI,CN	3	7516.36	CN*
[5	7442.60	CN	[3	7518.29	CN,(ZrI)
5	7444.47	CeI,CN(5,2)$R_1$43	[2	7519.40	-
4	7445.51	CN,FeI,1077	[3	7521.12	(ZrI)
4	7448.84	-	[3	7521.4	CN
⌐4	7451.38	CN *	4	7522.82	NiI 126,CN
| 4	7452.08	CN *	[3	7523.7	-
⌊3	7452.81	CN *	[3	7525.00	NiI 139,CN
3	7454.27	CN	5	7527.26	(CeI)
5	7456.45	CN	3	7528.24	CN*
4	7459.13	CN	3	7529.42	CN*
4	7461.07	CN	4	7531.09	(FeI 1137),CN
5	7462.28	CeI,CrI 93,CN	5	7533.53	LaI
4	7462.98	LaI	3	7534.83	CN
5	7464.33	GdI,CN	3	7536.46	CN
2	7465.50	-	3	7538.19	CN(4,1)$Q_1$58
4	7466.37	TiI 142	7	7539.26	LaI,CN
4	7467.40	(ZrI)	4	7540.74	ZrI,CN
4	7468.75	CN(6,3)Q_1head	3	7543.23	CN
5	7469.94	TiI	3	7544.62	ZrI
5	7471.18	TiI	[3	7545.86	-
4	7472.27	(CeI)	[4	7546.76	CN*
4	7473.59	CN	2	7548.24	-
5	7475.23	TiI 142,CN	3	7549.88	CN*
5	7478.70	CeI,CN	5	7551.32	CeI,ZrI
4	7479.58	CN,(ZrI)	5	7552.95	ZrI,CN
2	7480.3	-	[6	7554.74	ZrI,CN
4	7481.39	NdII,CN	[4	7555.55	(NiI 187)
7	7483.34	LaII 1	4	7558.48	ZrI,CN
4	7484.92	CN	4	7559.96	(ZrI)
4	7487.96	BaI 5	4	7560.7	(ZrI)
5	7489.57	CN,(TiI 225)	[6	7562.26	ZrI,CeI,CN
4	7491.34	-	[6	7562.92	GdI,(HfI),CeI
4	7493.71	CN	5	7565.07	CN
5	7494.94	FeI 33,(FeI 1077)	3	7566.2	CN(6,3)$Q_2$29

Int	Wavelength	Identification
4	7567.33	CN
4	7568.68	CN, FeI 1077
3	7569.8	CN
3	7571.2	-
2	7572.9	-
4	7574.86	CN*, NbI
4	7577.46	NdII
3	7578.72	-
4	7580.31	TiI
4	7581.71	CN
4	7583.71	(FeI 402)
4	7586.09	(FeI 1137), (CeI)
2	7587.7	-
4	7588.37	-
2	7589.71	-
5	7590.64	CoI 89, NdII
[4	7591.82	CN
[2	7592.53	CN(6,3)$Q_1$31
	Atmospheric A band of O_2	
4	7647.85	CeI, CN
[3	7651.98	-
[4	7652.72	-
7	7654.32/54.09	Atmos O_2
7	7655.37/55.14	Atmos O_2
3	7657.65	(MgI 22)
6	7658.62	ZrI
7	7659.63/59.40	Atmos O_2
[7	7660.73/60.50	Atmos O_2
[6	7661.19	(FeI 1077), CN
	7662.2	(DyI)
10	7664.80	KI 1
6	7665.19/64.96	Atmos O_2
3	7667.17	-
4	7668.62	CN
5	7670.81/70.58	Atmos O_2
7	7672.07/71.84	BaI, Atmos O_2
[4	7673.30	CN
[2	7674.48	-
4	7676.79/76.56	Atmos O_2
5	7677.90/77.67	Atmos O_2
2	7679.9	-
4	7681.53	CN
4	7682.59/82.36	Atmos O_2
4	7684.05/83.82	Atmos O_2
3	7687.59	CN*
3	7689.12	(CeII)?, CN
4	7690.69/90.46	ZrI Atmos O_2
3	7691.66/91.43	Atmos O_2
5	7693.48	-
[4	7695.7	CN, Atmos O_2
[4	7696.39/96.16	Atmos O_2
[9	7698.77	KI 1
[3	7699.99	-
4	7702.74/02.51	(CeI), Atmos O_2
[4	7704.06/03.83	(ZrI), Atmos O_2
[4	7704.7	CN(6,3)$P_1$36
3	7705.59	-
3	7707.39	CN?
3	7708.43	(ZrI)
2	7709.51	CN*
3	7710.47	CN, (FeI 1077)
1	7711.5	-
4	7712.65	(CoI 126)
6	7714.42	NiI 62, CN
4	7717.63	CeII
3	7719.19	-
3	7720.53	CN*
2	7722.09	-
4	7723.15	FeI 108
5	7723.93	ZrI
3	7724.6	-
4	7726.48	(NbI)
3	7727.75	(NiI 156)
3	7729.61	CN
3	7731.20	CN
4	7732.30	CeI
4	7733.54	GdI 1
3	7735.66	-
2	7737.17	-
3	7739.00	-
3	7740.21	HfI
3	7742.4	-
[3	7743.90	-
[3	7745.42	CN
2	7746.62	CeII
[6	7748.26	(FeI 402), CeI, (NiI 156)
[4	7749.41	GdI
4	7751.02	NdII
[3	7752.84	CeII
[2	7753.73	-
2	7755.08	-
2	7756.86	-
2	7759.35	CN
1	7761.5	CN(6,3)$P_2$41
3	7762.96	CeI
3	7764.25	-
5	7765.57	ZrI, CN
[5	7766.8	(ZrI)
[5	7767.13	-
3	7769.63	CeI
2	7771.39	-
[5	7773.04	NdII
[2	7773.74	TiI

Int	Wavelength	Identification
4	7775.87	-
3	7777.28	-
2	7778.84	CN(6,3)Q,48
5	7780.44	BaI 5
3	7781.82	CN
2	7782.82	-
2	7784.0	-
3	7785.3	-
4	7786.24	-
5	7788.85	NiI 62
3	7789.98	-
4	7791.34	TiI
3	7793.22	-
3	7793.8	CN?
3	7795.91	CN?
3	7796.45	TiI
4	7797.73	CeI,(NiI 201)
2	7799.23	CN(5,2)Q,62
6	7800.23	RbI
3	7802.89	-
3	7804.22	-
4	7806.83	CeI
4	7808.50	NdII
3	7810.8	-
3	7812.63	CeI
2	7814.32	-
5	7816.28	ZrI,CN
2	7817.2	CN(5,2)Q,63
4	7818.79	-
5	7819.32	ZrI
3	7820.16	-
3	7820.87	-
2	7821.68	CN(6,3)Q,51
4	7822.92	ZrI
2	7824.2	CN(7,4)Q,35
4	7826.63	ZrI
3	7827.88	-
3	7829.47	-
3	7830.88	CN
4	7831.92	-
4	7832.85	-
4	7834.50	TiI
5	7835.73	CeI
2	7836.6	CN
3	7837.8	-
3	7838.91	-
5	7840.52	-
5	7841.86	LaI
5	7842.66	CeI
5	7845.22	HfI
2	7847.77	-
6	7849.32	ZrI 40

Int	Wavelength	Identification
6	7850.36	-
3	7851.7	CN?
6	7852.70	TiI 34
4	7853.79	-
4	7855.24	-
6	7857.05	GdI
4	7859.05	-
3	7860.82	(NiI 156)
3	7861.59	-
5	7863.07	NdII
5	7864.33	CeI
5	7866.05	CeI
4	7868.56	-
6	7869.96	ZrI 41
7	7872.89	$CN(2,0)R_2 3,4,5,6$
5	7873.87	$CN(2,0)R_2 1,2,7,8$
4	7874.83	$CN(2,0)R_2 0,9$
5	7875.89	$CN(2,0)R_2 10$
5	7877.23	$CN(2,0)Q_2 1, R_2 11$, $LaO\,^2\Pi - {}^2\Sigma(0,0)$R head
5	7878.75	$CN(2,0)Q_2 2, R_2 12$
6	7880.57	$CN(2,0)Q_2 3, R_2 13$
7	7882.09	ZrI, (YII 32), CN
5	7882.72	CN*
4	7884.43	$CN(2,0)Q_2 5$
7	7885.04	TiI 34, CN
4	7886.71	$CN(2,0)Q_2 6$
5	7887.79	$CN(2,0)R_2 16$
5	7889.43	CN
4	7890.58	$CN(2,0)R_2 17$
4	7892.09	$CN(2,0)Q_2 18$
3	7892.97	CN
7	7894.09	$CN(2,0)R_1$head
7	7894.69	CN
7	7895.20	TiI 34, CN
6	7896.74	CN*
7	7898.14	ZrI, CN
5	7899.61	CN
5	7900.76	CN
6	7901.75	CN
4	7903.12	CN*
6	7904.35	CN
5	7905.63	BaI 10, $CN(2,0)Q_2 12$
5	7906.67	CN
8	7908.56	ZrI, CN, $CN(2,0)Q_1$head
6	7909.30	CN*
4	7910.86	$LaO\,^2\Pi_{1/2} - {}^2\Sigma(0,0)$Q head, CN
5	7911.35	BaI $1^{1/2}$
8	7913.27	CN, FeI 12
6	7915.43	CN*
6	7916.3	CN*

Int	Wavelength	Identification
[7	7917.88	CN*
[5	7918.56	CN*
6	7920.22	CN,HfI
4	7921.82	-
6	7922.95	CN*
6	7924.14	CN,(ZrI)
5	7926.18	CN(2,0)$Q_1$13
*6	7927.98	CN,SmII,CeI,6
[6	7929.86	CN
[4	7931.59	-
7	7933.33	CuI 6,CN
5	7934.96	CN*
4	7936.23	CN(2,0)$P_2$13
[6	7937.72	CN(2,0)$Q_1$16
[6	7938.0	CN(2,0)$R_1$26
[6	7938.94	CN*
5	7940.47	ZrI
6	7942.06	CN(2,0)$Q_1$17
7	7944.68	ZrI 40,CN
5	7945.9	-
5	7946.68	CN(2,0)$Q_1$18
[7	7947.74	RbI
[7	7948.28	-
[7	7949.09	TiI 125,CN
5	7950.38	CN(2,0)$Q_2$21
6	7951.69	CN
5	7954.13	CN
7	7956.71	ZrI 41,CN
7	7958.32	CN
[7	7959.85	ZrI
[5	7960.62	CN(2,0)$R_1$30
5	7962.61	CN(2,0)$Q_1$21
6	7963.41/63.18	CN(2,0)$P_2$17 (ZrI),Atmos H_2O
*7	7965.28	CN,LaI,NdII
4	7967.11	CN(2,0)$R_1$31
4	7968.50	CN(2,0)$Q_1$22
[5	7970.11	CN(2,0)$Q_2$24
[4	7970.55	CN
7	7972.04	CN,CeI,CeII
3	7973.74	CN(2,0)$R_1$32
5	7974.62	CN(2,0)$Q_1$23
3	7975.4	-
3	7976.26	-
5	7977.22	CN(2,0)$Q_1$25
7	7978.56	TiI 151,CN
5	7979.73	CN(2,0)$R_2$34
6	7981.01	CN
5	7982.72	NdII
6	7984.87	CN
5	7986.39	CN
7	7987.71	CN *

Int	Wavelength	Identification
3	7989.37	(CrI 300)
2	7991.1	-
5	7992.33	CN
2	7993.5	-
6	7994.87	CN,HfI
5	7995.60	-
3	7996.46	(TiI 308)
2	7998.89	CN,(FeI 1136)
3	7999.4	CN
6	8000.03	CN
5	8001.93	LaI
6	8002.39	CN(2,0)$Q_1$27
5	8003.63	CN
5	8005.25	ZrI,CN?
0	8006.1	^{13}CN(2,0)$R_2$32
5	8007.63/07.40	CN(2,0)$P_1$21,Atmos H_2O
5	8008.47	CN(2,0)$Q_2$29
5	8010.07	CN(2,0)$Q_1$28
6	8011.80	CN
5	8012.65	CN(2,0)$R_2$38
5	8015.31	(ZrI),CN
4	8017.03	CN(2,0)$Q_2$30
5	8018.05	CN(2,0)$Q_1$29
2	8019.3	^{13}CN(2,0)$P_2$19
4	8020.18	CN(2,0)$R_1$38
5	8021.28	CN
2	8022.69	^{13}CN(2,0)$Q_1$24
5	8024.02	CN(2,0)$P_1$23
5	8024.83	TiI 151
8	8025.92	CN,CeII,SmII 63,SmII 67
7	8027.37	VI 30
4	8028.98	CN(2,0)$R_1$39
5	8030.62	CeII,CN
4	8031.33	CeI
5	8032.67	CN(2,0)$P_1$24
1	8033.7	^{13}CN(2,0)$P_1$19
5	8034.92	CN
2	8036.0	-
3	8038.05	CN(2,0)$R_1$40
6	8040.16	CeI,ZrI,CN
5	8041.79	CN(2,0)$P_1$25,(CN(8,5)$Q_1$36)
7	8044.13	CN
4	8045.96	ZrI
6	8047.60	FeI 12,CN(2,0)$R_1$41
1	8048.8	SmII 67
6	8050.01	CN
7	8051.28	LaI,NdII,CN

Int	Wavelength	Identification
5	8052.98	CN,(ZrI)
5	8054.02	CN(2,0)$Q_2$34
7	8055.47	ZrI,ZrI
4	8057.19	CN
5	8058.10	ZrI 41
[5	8059.39	-
[6	8060.59	-
[5	8062.71	CN
[7	8063.06	ZrI 40
4	8064.13	CN(2,0)$Q_2$35
1	8065.2	-
3	8065.97	TiI 151,(CN)
6	8067.11	CN(3,1)R_2head,(CeI)
6	8068.29	TiI 151,(CN)
*8	8070.18	ZrI 40,(CeI),CN
6	8072.27	CN,FeI 108
7	8075.16	FeI 12
3	8077.0	CN
5	8077.81	CN
4	8079.27	CeI,CN(3,1)$Q_2$5
6	8080.59	CN
6	8081.57	CN
[5	8082.42	CN(2,0)$Q_1$36
[4	8082.92	CN
[3	8083.89	-
[5	8084.96	CN*
5	8086.16	LaI,CN
4	8087.47	CN(3,1)$Q_2$8
4	8088.27	CN(2,0)$R_1$45
7	8089.62	CN(3,1)R_1band head,CN
5	8091.36	CN
7	8092.72	CuI 6,CN
7	8093.42	VI 30,CeI,CN
6	8094.24	CeI,CN
6	8096.04	NiI 290,CN
5	8096.86	CN(3,1)$R_2$20
6	8097.60	CN
5	8099.15	CN
5	8099.97	CN?
5	8101.02	CN
5	8102.28	CN
6	8103.90	CN*
6	8105.25	CN
5	8107.13	-
5	8108.18	CN
*7	8109.56	CN
5	8112.08	CN*
5	8113.31	CN*
7	8114.57	CN,ZrI
5	8115.82	CN*
8	8116.88	VI 30,CN

Int	Wavelength	Identification
5	8118.82	CN(2,0)$Q_2$40
7	8120.11	CeI, ZrI, CN
5	8122.03	NdII, CN
5	8123.19	CN(3,1)$Q_1$13
3	8124.08	CN(3,1)$P_1$7
6	8125.16	CN*
6	8125.92	CN, (Li)?
5	8127.00	CN*
5	8127.82	CN*
3	8129.34	-
7	8130.71	CN*
4	8132.07	CN(3,1)$P_1$9
7	8133.12	ZrI 40
5	8134.13/33.89	CN, Atmos H_2O
5	8135.18/34.94	CN, Atmos H_2O
6	8136.53/36.29	CN, (Atmos H_2O)
5	8137.64	CN*
6	8140.08/39.84	CN, (Atmos H_2O)
6	8141.48	CN*
6	8142.12/41.88	CN, Atmos H_2O
5	8142.73	CN(2,0)$Q_2$42
6	8143.98/43.74	CN, Atmos H_2O
6	8144.58	VI 30, CN
5	8146.59/46.35	CN, Atmos H_2O
6	8147.42/47.18	CN, Atmos H_2O
6	8148.54/48.30	CN, Atmos H_2O
6	8149.25	CN
7	8150.02/49.88	CN, Atmos H_2O
7	8152.71/52.47	ZrI, CN, Atmos H_2O
5	8154.0/53.8	CN?, Atmos H_2O
8	8155.20/54.96	CN, Atmos H_2O
6	8157.92	CN
4	8159.22	CN
3	8160.06	CN(3,1)$R_1$30
* 9	8161.74/61.50	CN, VI 30, Atmos H_2O
7	8164.79/64.55	(CN), Atmos H_2O
6	8165.73	CN
3	8166.77	CN(3,1)$R_1$31
5	8167.80	CN
7	8169.46/69.22	CN, Atmos H_2O
6	8171.38	CeI
6	8172.47	NdII, CN
6	8174.10	CN
5	8175.23	CN(2,0)$Q_1$44
7	8177.32	CN, Atmos H_2O
6	8179.18/78.94	CN, Atmos H_2O
6	8181.10	CN *
5	8182.05/81.81	Atmos H_2O
8	8183.27	NaI 4
6	8184.61	CN *
7	8186.74/86.50	VI 30, Atmos H_2O

Int	Wavelength	Identification
7	8187.94	CN*
6	8189.55/89.31	Atmos H_2O
*6	8192.80/92.56	CN, Atmos H_2O
9	8194.86	NaI 4, NaI 4, ZrI, CN
4	8196.93	CN
5	8197.89/97.65	Atmos H_2O
6	8198.98	VI 30, CN
5	8200.10	CN(3,1)$P_1$20
[7	8201.16/00.92	CN*
7	8201.66	ZrI 40; CN
6	8203.25	CN, (LaI)
[6	8204.1	FeI 12
*7	8204.94	FeI 12, HfI, CN
5	8206.95	CN
5	8208.27	CN
5	8209.74/09.50	CN, Atmos H_2O?
3	8211.26	CN(3,1)$Q_1$28
7	8212.64/12.40	ZrI 40, (CN), (Atmos H_2O)
3	8213.95	CN(3,1)$R_1$37
6	8215.07	CN*
3	8216.91	-
5	8218.56/18.32	CN, Atmos H_2O
4	8219.60	CN(3,1)$Q_1$29
[4	8220.52	CeI
4	8221.11	CN
5	8222.43/22.19	CN, Atmos H_2O
[4	8223.62	CeI
5	8224.26/24.02	CeII, (CrI 98), CN
4	8225.41	CN(3,1)$P_1$23
6	8227.22/26.98	CN, Atmos H_2O
8	8228.42/28.12	CN, Atmos H_2O
7	8229.22	CN
3	8229.98/29.74	Atmos H_2O
*8	8231.79/31.57	NdII, CN, Atmos H_2O
*6	8234.17/33.93	CN, Atmos H_2O
4	8235.90	CN
6	8237.45/37.21	CN, Atmos H_2O
4	8239.22	FeI 108, (CeI)
4	8240.32/40.08	ZrI, Atmos H_2O
*6	8241.70	VI 30, CeII, CN
7	8243.75/43.51	CN*, Atmos H_2O
3	8245.17	CeI
*6	8247.38	LaI, CN
3	8249.61	NdII
5	8250.76	CeII, CN
5	8251.65	CN
5	8252.58	(CN)
7	8253.55	VI 30, CN
[6	8255.85	VI 30
7	8256.67/56.43	CN, Atmos H_2O ?

Int	Wavelength	Identification
5	8258.50	CN
2	8260.0/59.8	Atmos H_2O
3	8261.05	CeI
3	8261.91	CN(3,1)$R_1$42 (CrI 98)
6	8263.62/63.38	CN, Atmos H_2O
3	8265.04	CN(3,1)$R_2$43
5	8266.45	CN *
4	8268.05	CN(3,1)$Q_2$35
4	8271.23	CN(4,2)R_2head
5	8272.46/72.22	CN, Atmos H_2O
5	8273.70	CN
7	8274.50/74.26	Atmos H_2O
5	8276.14	CN
6	8276.82/76.58	CN, (HfI), Atmos H_2O
3	8278.02	CN(4,2)$R_2$12
4	8278.89	CN(3,1)$Q_2$36
4	8279.99/79.75	(CN), Atmos H_2O
8	8282.26/82.02	CN, Atmos H_2O
5	8283.60	ZrI, CN
4	8285.05	CN
4	8286.12	CN
5	8287.38	CN
6	8288.08/87.84	Atmos H_2O
* 6	8289.85/89.61	Atmos H_2O
3	8291.19	CN(4,2)$R_2$17
3	8292.09	CN(4,2)$Q_2$8
3	8293.61	FeI 623
7	8294.72/94.48	CN, Atmos H_2O
5	8296.24	CN
4	8297.34	CN(3,1)$P_2$31
* 7	8298.48	CN *
5	8299.43	CN(4.2)$R_1$14
5	8300.64/00.40	CeI, Atmos H_2O
5	8301.46	CN*
6	8302.71	(CN)
4	8303.75	CN
6	8304.63	CN
7	8305.28/05.04	CN, Atmos H_2O
8	8305.94	ZrI 40, CN
7	8307.50	TiI 33, FeI 12, CN
6	8309.38	(ZrI) CN
5	8310.22	CeI, CN(4,2)Q_1head
6	8311.09	FeI 12, CN
5	8312.31/12.07	CeI, CN, Atmos H_2O
4	8313.21	CN(3,1)$Q_2$39
5	8314.58	CN *
6	8316.03	LaI, (CN)
5	8318.03/17.79	CN, Atmos H_2O
4	8319.21	CN(3,1)$P_1$32
7	8320.16	ZrI, (CN)

	Int	Wavelength	Identification
	8	8321.58/21.34	CN, Atmos H_2O
	5	8323.25	CN
	7	8324.62	LaI
	6	8326.13	DyI, CN
	7	8327.01	FeI 60, CN
	4	8328.59	CN(4,2)$R_1$23
	5	8330.09/29.85	CN, Atmos H_2O
	6	8331.40	CN
	6	8333.39	CN
	7	8334.35	TiI 33, CN
	5	8336.24	CN
[	6	8337.28	CN
[	6	8338.81	CN
	3	8339.8	-
[	5	8342.19/41.95	(Fe 401), CN, Atmos H_2O
[	6	8343.69	CN
	5	8345.55	CN*
[	7	8346.45	LaI, NdII
[	5	8347.22	CN
[	5	8348.32	(CrI 56), CN(2,0)$Q_2$56
[	7	8348.94	FeI 12, CN
[	5	8349.72/49.48	CN(4,2)$Q_2$20, Atmos H_2O
	4	8350.71	CN(3,1)$Q_2$42
	5	8352.25	CN*
	6	8353.14	TiI 33
	6	8354.18	CN*
	4	8355.26	CN(2,0)$P_1$49
	5	8356.28	CN*
	5	8358.05	CN
	3	8359.17	CN(4,2)$R_2$30
	5	8360.31	CN
	5	8362.36/62.01	CN, Atmos H_2O
*	8	8364.15	TiI 33, CN
	6	8365.78	(FeI 623), CN
	4	8366.42	CN
	2	8367.5	(ErII)
[	5	8369.38	CN
[	7	8370.20	ZrI 40, CN
	5	8371.43	CN
	5	8372.56	CN
	4	8374.17	CN
	4	8375.24	-
	5	8376.29	CN*
	8	8377.88	TiI 33, CN
	3	8379.30	(CN)
	2	8381.10	-
*	9	8382.61	TiI 33, TiI 33, FeI 12, CN
	4	8384.64	CN
	7	8386.38	TiI 182, CN
	7	8387.80	FeI 60
	7	8389.41	ZrI 40, TiI 182, CN
	6	8390.34	CN*
	4	8391.35	CN*

Int	Wavelength	Identification
5	8394.27	CN
3	8395.15	CN
8	8396.87	TiI 33, CN
4	8398.43	CN
2	8399.76	CN(4,2)$R_1$34
5	8401.68	FeI 108, CN
5	8402.64	CN, (TiI 224)
4	8404.17	CN
6	8405.41	CN, (CeII)
3	8407.15	CN(2,0)$Q_1$59
5	8408.30	CN
5	8409.92	ErI
5	8411.24	CN
8	8412.37	TiI 33, CN
6	8413.96	ZrI 40, CN
2	8415.44	CN?
6	8417.17	(NiI 156), (TiI 224), TiI 182, CN
4	8418.49	CN
[5	8419.78	CN*
5	8420.44	CN
2	8421.5	CN?
4	8422.36	CN(4,2)$Q_1$28
4	8423.10	TiI 150
5	8424.39	TiI 182
*9	8426.57	TiI 33, (FeI 12), CN
3	8429.89	CN(4,2)$Q_2$30
3	8431.11	CN(4,2)$Q_1$29
3	8432.34	CN(3,1)$P_2$41
3	8433.45	(CN)
[9	8434.97	TiI 33, CN
9	8435.51	TiI 33
4	8436.74	CN
[6	8438.95	TiI 224, CN
5	8439.53	CN
5	8440.71	CN*
3	8441.66	CN(3,1)$Q_1$48
4	8443.28	(TiI 210)
5	8446.16	CN
5	8447.62	FeI 12, CN
[6	8449.92	CN*
5	8450.68	CrI 56, (TiI 224)
4	8453.12	ZrI
3	8454.13	CN(4,2)$P_2$26
4	8455.33	CN(4,2)$R_1$40, (CrI 56)
5	8456.05	CN
7	8457.29	TiI 141, (ZrI), CN
4	8458.6	CN(2,0)$P_2$55
5	8459.83	CN
4	8463.43	CN
*6	8464.72	ZrI 40, CN
5	8467.18	TiI 182

Int	Wavelength	Identification
7	8468.43	TiI 150, FeI 60
3	8469.83	CN(4,2)$Q_1$33
3	8470.94	CN(4,2)$Q_2$34
4	8471.68	CN
5	8472.37	ErI,CN
2	8484.1	-
2	8475.2	-
6	8476.57	LaI,CN
3	8478.6	-
4	8479.98	CN
4	8481.82	CN
4	8483.34	TiI 150,CN
4	8484.85	CN
*6	8488.08	CN*
2	8490.4	-
4	8491.29	CN
4	8493.13	CN
5	8494.43	TiI 141
6	8495.95	(TiI 209),(TiI 210),(ZrI),CeI,(CN)
9	8498.20	CaII 2,ZrI 40
4	8502.57	CN*
4	8503.78	CN
4	8504.92	CN
3	8506.58	-
2	8507.96	-
4	8510.2	CN(5,3)R_1head
5	8511.22	CN
4	8511.5	CN
7	8513.91	CN,FeI 60, ZrI
5	8515.07	(FeI 401),(ZrI)
3	8517.07	CN(5,3)$R_1$15
6	8518.13	TiI 182,TiI 150
3	8519.21	-
5	8520.90	(CsI)
4	8522.53	CN
5	8523.33	CeI,CN
5	8525.37	CN*
4	8526.88	CN
3	8527.78	-
4	8528.53	CN(4,2)$R_2$47
5	8530.47	NdII,CN
5	8531.58	TiI 141,CN
3	8533.0	CN?
4	8535.16	-
4	8536.77	CN *
6	8538.05	-
6	8539.17	CeII,(TiI 209)
*10	8542.12	CaII 2
6	8545.49	LaI
5	8546.48	HfI,(CN(2,0)$P_1$59)

Int	Wavelength	Identification	Int	Wavelength	Identification
6	8548.06	TiI 150, CN	4	8618.22	(TiI 209), CN
4	8549.09	(CrI 56), CN	5	8619.35	CN(4,2)Q$_1$45
5	8550.70	TiI 141, CN	3	8620.56	-
2	8552.41	-	5	8621.63	(FeI 401)
4	8554.46	CN(5,3)Q$_2$18	5	8623.01	CN
6	8555.39	(CrI 56), CN	3	8624.18	(LaI)
4	8556.93	(CN)	4	8626.41	CN*
5	8560.00	BaI, CN(2,0)Q$_2$67	5	8629.15	CN
4	8561.10	CN	4	8631.62	CN*
3	8562.12	CN(4,2)R$_1$49	4	8633.98	CN*
4	8563.71	CN(4,2)Q$_1$41	3	8635.01	-
5	8564.64	CeI, CN	5	8636.54	(CrI 56)
4	8565.65	TiI 141, CN	3	8638.43	CN
5	8567.54	CeI, CN	4	8639.56	HfI
5	8568.62	CN	5	8641.93	CN*
4	8570.81	(CN)	5	8642.9	(CrI 56)
2	8571.96	-	4	8643.9	-
4	8573.25	CN*	4	8645.7	-
4	8574.50	-	4	8647.67	CeI
3	8576.13	(CN)	* 4	8649.04	CN*
2	8577.03	CN	4	8651.44	CN
4	8578.42	TiI 141, CN	5	8653.96	-
2	8580.0	-	4	8654.67	CN(2,0)Q$_1$71
5	8581.98	CN	4	8657.35	CN
4	8583.02	CN	4	8658.76	CN
4	8584.27	(ZrI), CN	5	8660.28	(CN)
2	8585.20	CN(3,1)Q$_2$57	*10	8662.11	CaII 2, FeI 60
3	8586.09	-	5	8664.32	-
2	8586.93	CN(2,0)Q$_1$68	* 4	8668.40	CN
3	8587.95	CN, (ZrI)	4	8672.61	CN
*3	8589.1	CN*	7	8674.63	LaI, (FeI 339)
*4	8591.39	CN*	7	8675.39	TiI 68
3	8592.96	-	3	8677.56	-
3	8594.38	-	3	8678.88	CN(4,2)P$_1$42
3	8595.64	CN(5,3)Q$_1$22	3	8680.80	CN
4	8597.08	CN*	7	8683.02	TiI 68, CN
4	8598.39	(TiI 236)	4	8684.12	-
2	8599.99	-	3	8686.69	CN(4,2)P$_2$43
3	8600.94	TiI 141, (TiI 209)	8	8688.62	FeI 60, (CN)
4	8602.54	CN	4	8689.85	CN(4,2)Q$_2$50
4	8604.00	CN*	4	8691.01	-
4	8605.54	CN*	7	8692.27	TiI 68, (CN)
2	8606.7	CN	4	8693.88	CN
3	8607.81	CN	5	8695.16	CN
2	8608.9	CN(2,0)R$_2$77	3	8696.32	CN
5	8610.18	CN, (ZrI)	4	8697.43	-
5	8611.67	(FeI 339), CN	* 3	8698.55	FeI 400, CN
5	8612.66	CeI, TiI 141, CN	3	8700.77	MnI 49
5	8614.07	CN	5	8702.37	CeII, NiI 83, CN
5	8615.88	-	3	8704.46	-
3	8616.74	-			

Int	Wavelength	Identification	Int	Wavelength	Identification
4	8706.73	CN	4	8796.39	CN
4	8709.51	CN	5	8798.85	-
4	8712.03	-	7	8800.61	YI 1
4	8713.2	(FeI 400)	4	8802.88	-
5	8714.09	CN	4	8804.69	FeI 106, (ZrI)
5	8716.48	CeII	5	8806.77	MgI 7, MgI 7, MgI 7
4	8717.7	-	2	8809.16	(NiI 200)
5	8719.54	TiI 140	5	8810.87	CeI
4	8721.07	CN	4	8812.90	CN
3	8722.63	-	3	8813.73	-
*5	8724.24	CN	4	8819.41	TiI 68
3	8725.85	TiI 139, CN	4	8821.16	TiI 139
3	8726.84	CN(4,2)$R_2$60	6	8824.21	FeI 60
4	8729.20	CN*	3	8825.99	LaI
*5	8730.74	CN*	2	8830.51	-
2	8733.17	-			
6	8734.75	TiI 68, (MnI 49), (ZrI)			
4	8736.10	-			
3	8737.51	(MnI 49)	3	8832.65	-
4	8738.72	-	3	8833.54	-
3	8740.97	(MnI 49)	5	8835.99	ZrI
3	8743.64	-	*7	8839.04	NdII
4	8745.48	CN			
4	8747.02	-			
5	8748.45	LaI			
6	8749.47	ZrI			
	8751.15	CN			
3	8753.21	(CN(5,3)$Q_1$38)			
3	8755.71	-			
5	8757.05	FeI 339, CN			
2	8758.83	-			
	8759.6	-			
3	8761.39	TiI 139			
4	8763.59	-			
6	8766.70	CN			
5	8767.30	CN			
3	8769.92	-			
3	8770.64	NiI 82			
5	8772.08	CeII			
4	8772.77	AlI 9			
4	8773.94	AlI 9			
3	8775.55	CN			
5	8778.59	TiI 140			
3	8780.25	-			
4	8782.46	(CeI)			
3	8784.52	-			
3	8786.39	(ZrI)			
4	8788.28	-			
3	8789.75	-			
3	8793.02	-			
2	8794.40	-			

2.09 Results of line identification

This section is divided into two parts. In the first part elements are listed according to increasing atomic number while individual molecules are discussed in the second part.

The following points should be borne in mind while reading this discussion. The abbreviation 'mpt' refers to the multiplet designations given in Moore (1959). Voltages refer to the excitation of the lower level of an electronic transition in electron volts. Wavelengths, where given, refer to laboratory values. The 'red' and 'infrared' refer to the regions covered by Tables 2.04 and 2.05 respectively. Lastly any other comments are only to be considered relevant to the region from 5413 to 8839 Å.

Main regions of terrestrial Absorption

Atmos H_2O	7170 to 7300 Å	
	8130 to 8350 Å	
Atmos O_2	6860 - 6920 Å	B band
	7600 - 7700 Å	A band

Lithium LiI

The resonance line at 6707 Å is strong and has a wavelength of 6707.78 which indicates it is largely composed of Li^7.

Possibly present: 6103.62 Å in wing of strong CaI 1.

Sodium NaI

The D lines are exceedingly strong with a width at half intensity of about 32 Å.

Certainly present: mpts 1,4,5,6,7.

Magnesium MgI

Certainly present: mpts 7 and 8.

Possibly present: mpt 22.

Aluminium AlI

Certainly present: mpts 5,9.

Mpts 10 and 11 not listed but may contribute to strong absorption features.

Potassium KI

Certainly present: Strong resonance lines at 7665 and 7699 Å.

Possibly present: mpt 7 (1.6 volt).

Calcium

CaI

Certainly present: mpts 1,3,18,19,20,21,29,30,32,44,47.

CaII

Certainly present: mpt 3. These three lines are amongst the strongest in UY Cen.

Scandium

ScI

Certainly present: mpts 1,2,3 and strongest members of mpts 12,15,16.

ScII

Possibly present: 6604.6 mpt 19 and 5526.8 Å mpt 31. (These are two of the strongest lines of ScII).

Titanium TiI

Certainly present: mpts 1,2,3,33,34,48,49,50,51,68,69,71,72, 73,96,97,98,99,100,101,102,103,104,105,106,125, 139,140,141,142,143,150,151,154,182.

Probably present: mpts 107,108,144,153,197,198,209,210,224, 225,236,237,238,239,240.

Possibly present: mpts 249,256,272.

Vanadium VI

Certainly present: mpts 1,2,19,20,30,31,33,34,35,36,37.

Probably present: mpts 48,49,59,84,85,107,117,129,130,135.

Possibly present: mpts 60,92,142.

Chromium CrI

Certainly present: mpts 6,16.

Probably present: mpts 93.

Possibly present: Certain lines of mpts 56,93,119,185 and 7989.36 of mpt 300. It is possible that mpts 298,299 and 300 may be present in the infrared but all members, except for 7989.36, have competing CN identifications.

Manganese MnI

Certainly present: mpt 27(all 3 lines have alternative identification).

Probably present: mpts 1,4,50.

Possibly present: mpt 49. The line at 8740.97 of mpt 49 is the only unblended line of MnI observed.

Iron FeI

Certainly present: mpts 12,13,14,15,33,60,62,63.

Probably present: mpts 64,108,109,111,113,168,169,205,206, 207,209,268,269,339,340,343,400,401,402,463, 623,686,816. Weaker members are bracketed in Table 3.

Possibly present: mpt 1077. 7164.5 of mpt 1051, 7998.97 of mpt 1136, 7586.04 and 7531.17 of mpt 1137. All bracketed in Table 3.

Cobalt CoI

Certainly present: mpts 37,38,39,54 and certain lines of 89,90.

Probably present: mpt 55.

Possibly present: mpt 126.

Nickel NiI

Certainly present: mpts 43,44,57,59,62,63,82,83,84,126,139.

Probably present: mpts 45,47,64,66,67,68,187,200.

Possibly present: mpts 69,156.

Copper CuI

Copper is considered certainly present. All four copper lines in this spectral region are observed. The wavelength agreement is good but all four lines have alternative identifications. The two lines observed at 8092.72 Å and 7933.33 Å are considered to be mainly due to copper but are blended with CN lines.

Rubidium RbI

Certainly present: Resonance lines at 7800.2 and 7947.6.

Strontium SrI

Certainly present: mpts 1,3. 4607.3 mpt 2 is one of the strongest lines in the blue.

Probably present: Strongest members of mpts 8,9,12.

Yttrium

YI

Certainly present: mpts 1,2,3,12,16.

Probably present: 5 remaining lines with NBS intensity > 100.

Possibly present: Lines with NBS intensity >20.

YII

Possibly present: mpts 19,26,27,32,38.

Zirconium ZrI

Certainly present: mpts 1,2,3,4,23,24,25,40,41,42,47,57,65. All remaining lines <1 volt.

Probably present: Lines, 1 $\leq$ volt <2 and with NBS intensity >20.

Possibly present: All the remaining recovered lines. These are bracketed in Table 3.

Niobium NbI

Probably present: All lines with NBS intensity >100.

Possibly present: Remaining recovered lines with NBS intensity >55 and less than 1 volt. These are not bracketed in Table 3.

Molybdenum MoI

Probably present: mpts 4,5. Also the 4 recovered lines <1.5 volts and with NBS intensity >100.

Technetium TcI

There is no evidence for TcI. Meggers and Scribner (1950) list 356 lines, which have been compared with UY Cen and show only the number of coincidences expected from chance. The strongest TcI lines occur at 4238 and 4297 and have been observed in M, S and C stars; Peery (1971). A comparable estimate of the TcI abundance in UY Cen can only be made by observing the same spectral region.

Caesium CsI

There is a double unidentified feature at 8520.90 Å which may contain the strong line of CsI at 8521.24. No other caesium lines are found.

Barium

BaI

Certainly present: mpts 1,2,5,6,7,10. All lines with NBS intensity >400.

BaII

Certainly present: mpt 2.

Lanthanum

LaI

Certainly present: mpts 1,2,3,6,7,8. All lines with NBS intensity >70. All lines <0.65 volts and with NBS intensity >30.

Probably present: Remaining recovered lines <0.65 volts and with NBS intensity >9. The remaining recovered lines with NBS intensity >30.

LaII

Certainly present: All lines <0.62 volts and with NBS intensity >16.

Possibly present: All remaining recovered lines <1.2 volts and with NBS intensity >16.

Cerium

CeI

Certainly present: All recovered lines <0.6 volts.
Recovered lines <1.2 volts and with NBS intensity $\geqslant$10. Remaining recovered lines with NBS intensity >20.

Probably present: Recovered lines 5$\leqslant$ (NBS intensity) <10 and with 0.6< volts <1.2.
Recovered lines 10$\leqslant$ (NBS intensity) <20 and volts >1.2.

CeII

Probably present: All recovered lines with NBS intensity >100.
All recovered lines <1.2 volts and with NBS intensity >30. All remaining <0.6 volt lines.
The probably present CeII lines are not bracketed in Table 3.

Praseodymium

PrI

Possibly present: 6055.13 is the strongest laboratory line and has no other competing identifications.

PrII

Possibly present: All recovered lines with NBS intensity >130.
All recovered lines <0.4 volts and with NBS intensity >25.

Neodymium

NdI

Certainly present: All lines <0.8 volts and with NBS intensity >30.

Probably present: All remaining recovered lines <0.9 volts and with NBS intensity >15.

NdII

Certainly present: All lines <0.4 volts and with NBS intensity >14.

Probably present: All remaining recovered lines with NBS intensity >50. All remaining recovered lines <0.8 volt. None of these lines are bracketed in Table 3.

Promethium PmI

There is no evidence for PmI. Unfortunately the strongest and lowest excitation lines of PmI lie in the region 4600 - 5000 Å which has not been observed in UY Cen. Davis (1971) has tentatively identified some of the strongest PmI lines in blue spectra of the S stars V Cnc and T Sgr.

81 of the PmI lines classified by Reader and Davis (1967) have been compared with UY Cen and show exactly the number of coincidences expected from chance. All of these lines have lower excitations below 1.1 volts and 27 have intensities ≥100. The strongest PmI lines have been assigned intensities between 700 and 900 by Reader and Davis (1967) and until these blue lines are looked for in UY Cen the identification of PmI can not be rejected at the strengths at which it is found in T Sgr and V Cnc.

Samarium

SmI

Probably present: All lines with NBS intensity >100 and excitation <0.6 volts. This identification could have been upgraded to 'certain' if 5 of the 7 lines did not have 'certain' competing identifications.

Possibly present: All the remaining recovered lines <0.6 volts.

SmII

Possibly present: All recovered lines with NBS intensity >90.

Europium

EuI

Probably present: All 0 volt lines.

EuII

Possibly present: All lines with NBS intensity greater than 400. Members of mpts 8,9.

Gadolinium GdI

Certainly present: mpts 1,2,3. All remaining <0.3 volt lines with NBS intensity >70.

Possibly present: All remaining recovered <0.3 volt lines. Lines <1.1 volts with NBS intensity >30.

Terbium TbI

Possibly present: Four <1.1 volt lines with NBS intensity >30.

Dysprosium

DyI

Certainly present: All 0 volt lines with NBS intensity >30.

Probably present: 2 lines <0.6 volts and NBS intensity >30.

DyII

Possibly present: 0.1 volt line at 5641.5.

Holmium HoI

Possibly present: 6 zero volt lines with NBS intensity >80. Of these, lines at 5860.3 and 5973.5 have no competing identification.

Erbium ErI

Certainly present: All zero volt lines of NBS intensity >35 5/9 of these lines have no competing identification.

Thulium TmI

Three out of the four available ground state lines of TmI are recovered in UY Cen. The unrecovered line has an NBS intensity of 190 and is the weakest of the four lines. This line is certainly not present in UY Cen. The strongest ground state line with an NBS intensity of 580 shows very good wavelength agreement with a feature in UY Cen. Unfortunately this feature at 5678.87 has the same wavelength as a NdI line which is considered certainly present. On this evidence thulium is not considered present. The NBS wavelengths of the 3 recovered lines are 5631.41, 5675.84 and 5764.29 Å. Culver (1971) considers that 5675 is due to Thulium in 63 Cygni and CY Cygni.

Ytterbium YbI

YbI has a strong ground state line, with an NBS intensity of 2400, at 5556.47 Å, which coincides with a strong line at 5556.42 Å, in the spectrum UY Cen. In UY Cen YI, CeI and CrI are all considered to contribute to this line so that it can not certainly be identified with YbI. However Culver (1971) identifies the line with YbI in CY Cygni and 63 Cygni and it is on the basis of his identification that it is marked probably present in Table 2.

Hafnium HfI

Certainly present: All recovered <1.3 volt lines with NBS intensity >100.

HfI continued

Possibly present: Remaining recovered <1.3 volt lines with NBS intensity >20.

Molecules

The spectra of normal C, M and S stars are dominated by molecules containing either carbon or oxygen, which have dissociation energies of between 4 and 9 volts. Hydrogen is also an important constituent but since hydrides have lower dissociation energies of about 2.5 volts and show more open rotational structure they are generally much less conspicuous.

The molecular spectrum of UY Cen is peculiar in two ways. Firstly it shows carbides, oxides and hydrides and secondly all the molecules are rather weak. This is well illustrated in the plates, where features seen in either the S star π Gru or the C star 19 Psc can be seen in UY Cen. A good example of this occurs in plate 2(a) between 6470 and 6490 Å where the red degraded absorption band of ZrO, which is very strong in π Gru can be weakly seen in UY Cen. In the middle of this region at 6478.48 Å there is a diffuse absorption line in UY Cen caused by CN. This line appears very strongly in 19 Psc and as a bright emission line in the CN spectrum. The correspondence in wavelength between the CN emission lines and many of the absorption lines in 19 Psc is very obvious.

Individual molecules are discussed in detail below. Wavelength and classification data for the oxides, unless otherwise acknowledged, come from Gatterer, Junkes and Salpeter (1957). Data for other molecules, unless otherwise acknowledged, have been taken from Pearse and Gaydon (1976).

CN

Lines of the $A\ ^2\Pi - x^2\Sigma$ electronic transition of CN are observed throughout the spectrum from 6000 to 8000 Å. The most conspicuous CN feature is the triple headed 2,0 vibrational band system degraded to red of 7872 Å. The CN spectrum appears very complex because of extensive overlapping and blending of lines, arising from different vibrational and rotational systems. This blending tends to obscure the pattern of band heads. The laboratory emission spectrum of CN, which is illustrated in the plates, was compared with the star spectrum, in order to distinguish the atomic lines and to help assess the relative contributions and intensities of the CN lines. Davis and Phillips' (1963) analysis of the CN molecule

was then used to discover the blended composition of each line. The symbol CN is asterisked in Tables 2.04 and 2.05, only when it is considered the major contributor to an absorption line. Quantum numbers are only given to the CN identifications in Tables 2.04 and 2.05, when the absorption line can be identified with a single rotational transition. Members of the following vibrational bands are considered present in UY Cen (5,3)(4,2)(3,1)(2,0)(6,3)(5,2)(4,1)(3,0)(7,3)(6,2)(5,1)(4,0)(8,3)(7,2).

A preliminary discussion of the $^{12}C/^{13}C$ ratio is given by Catchpole (1979). Several of the lines used in that paper are now considered to be blends as a result of the more thorough line identification given here.

Wyller (1966) has made a detailed study of the laboratory spectrum of the (2,0) and (3,1) bands of $^{13}C/^{14}N$. As a result he lists 25 features that are sensitive to ^{13}C and which are visible at moderately high dispersion. All these features have been examined on our spectra and four have been selected as being identifiable with individual rotational lines which are otherwise free from blends. The ^{12}CN lines were selected to have good profiles and to cover as wide as possible range of equivalent width. The CN lines used in the analysis are listed in Table 5.07 of chapter 5.

CaH

Calcium hydride is present and its identification has been discussed in detail by Catchpole (1975). CaH is characterized by two regions of general absorption, the A band, which stretches between 7035 Å and 6850 Å and the B band, which lies between 6400 and about 6370 Å. The A band consists of a series of blue degraded band heads of the $^2\Pi-^2\Sigma$ system. The two most conspicuous heads, which are clearly seen in UY Cen, are the $(0,0)Q_2$ head at 6919.8 and the $(1,1)Q_2$ head at 6902.6 Å. The B band arising from the $^2\Sigma-^2\Sigma$ transition shows, a $P_1(0,0)$ head at 6389.3 and a $P_2(0,0)$ head at 6382.1 Å.

CaCl

Catchpole and Feast (1971) did not observe CaCl at 80Åmm^{-1} dispersion in any of their SC stars of which UY Cen is the prototype. CaCl is however strongly present in the CS star VX Aql (Case 621 in Catchpole and Feast (1971)). Clegg and Wyckoff (1977) discuss the occurance of CaCl in cool stars and show that it is only found in stars with C/O ≈ 1. They also conclude that the abundance of CaCl is strongly dependent on atmospheric structure. It is therefore of interest to see if CaCl is present at high dispersion in UY Cen.

The band heads, which Clegg and Wyckoff indicate are the strongest observed in stars, are listed below, along with wavelength data from Pearse and Gaydon (1976).

		Laboratory		UY Cen		
			λ Å	λ Å	Int.	Ident.
B $^2\Sigma-x^2\Sigma$	(0,0)	red degraded	5934.0	34.32	4	CeI
A $^2\Pi-x^2\Sigma$	(1,0) Q_2	blue degraded	6051.6	51.86	4	CeII
	(1,0) Q_1	blue degraded	6076.6	76.58	4	CeI
	(0,0) Q_2	blue degraded	6184.9	85.08	3	HfI
	(0,0) P_2	blue degraded	6193.4	93.73	5	ScI 3
	(0,0) Q_1	blue degraded	6211.6	10.72	8	ScI 2

The wavelength, intensities and identifications, of the nearest lines found in UY Cen are also given. The wavelength agreement with the CaCl lines is good for all but the last line. However all the lines have 'certain' alternative identifications and all but the first line have wavelength agreements with these identifications of within ±0.07 Å. Careful examination of these lines, on both tracings and prints, show that none of them, with the possible exception of 6076.6 show band head like structure. There is therefore insufficient evidence to identify CaCl.

ScO

Two of the strongest bands of ScO have red degraded band heads at 6036.17 and 6079.30 Å. Both of these heads coincide with faint otherwise unidentified lines. The next two strongest bands, if present with similar intensities, would be masked by strong atomic

lines. ScO is only listed as possibly present at 6036.17 and 6079.30 Å.

YO

Yttrium oxide is present. Red degraded bands of the $^2\Pi-^2\Sigma$ system are considered certainly present at 6132 and 6148 Å, while bands at 5988 and 5971 Å are marked probably present. The bands at 5988 and 5971 Å are blended with atomic lines.

ZrO

Zirconium oxide is certainly present. The γ system, arising from the $^3\Phi-^3\Delta$ electronic transition, is the strongest band system in this spectral region. All three of the red degraded double headed bands of the (0,0) system are certainly present. The reddest double headed band of the rather similar β (0,0) $^3\Pi-^3\Delta$ system is also considered certainly present, while the remaining bands of this system are considered possibly present.

There are two other important band systems in this region, the $^1\Sigma-^1\Sigma$ system Phillips and Davis (1976a) and the $^1\Pi-^1\Sigma^+$ system Phillips and Davis (1976b). Both of these band systems are red degraded. The (0,0) band of the $^1\Sigma-^1\Sigma$ system is considered possibly present as are also the (0,0) (1,0) (2,0) and (0,1) bands of the $^1\Pi-^1\Sigma^+$ system.

BaH

There is a diffuse, otherwise unidentified absorption line at 6689.43 Å, which may be identified with the blue degraded (0,0) P_2 head of the $^2\Pi-^2\Sigma$ system of BaH at 6689.5 Å. Very weak, otherwise unidentified absorption lines, occur at 6826.84 and 6850.04 Å, which may be identified with BaH lines at 6827.4 (1,1) P_1 and 6850.2 (0,0)P_1. All these lines are entered as possibly present in Table 2.04. The laboratory wavelengths are from Pearse and Gaydon (1976). The barium halides and barium hydride have been identified at low dispersions in cool stars by Dubois (1977). However these identifications have not been confirmed by Wyckoff and Clegg (1978) who have observed one of Dubois' stars (R Cyg) at higher dispersion.

Wyckoff and Clegg show theoretically that BaF and BaCl should be the most easily detectable of the barium compounds. The band heads of BaF and BaCl, listed in Pearse and Gaydon (1976), are not found in UY Cen, which may therefore cast some doubt on the identification of BaH.

LaO

Lanthanum oxide is certainly present although it is very weak and masked by CN. Two band heads; a Q head with a wavelength of 7910.5 Å and an R head at 7877.18 Å, are certainly present although blended with CN lines. Both are (0,0) heads of the $^2\Pi_{1/2}-^2\Sigma$ transition. The Q head of the (0,0) $^2\Pi_{3/2}-^2\Sigma$ band with a wavelength of 7403.52 Å is considered possibly present. Identification was greatly facilitated by comparing a spectrum of a mixture of LaO and carbon with that of UY Cen obtained on the same spectrograph.

CeO

There is no evidence for CeO in UY Cen. CeO has been tentatively identified by Wyckoff and Wehinger (1977) in the spectrum of the S star R Cyg at minimum light. Detailed comparison of the laboratory wavelengths quoted by them as well as comparison with the CeO emission spectrum of Gatterer et al. (1957) shows that despite a number of coincidences with strong absorption lines, there is no evidence for CeO in UY Cen. The most convincing evidence for the absence of CeO in UY Cen is the absence of the band heads at 7235.5 and 7241.5 Å and the absence of the broad absorption feature starting at 7560 Å. All of these features are clearly seen in R Cyg.

Wyckoff and Clegg (1978) suggest, that since La and Ce are chemically very similar, when the one oxide is present the other should also be seen. LaO is present in UY Cen but is very much weaker than in R Cyg, which could explain the absence of CeO in UY Cen. Wyckoff and Wehinger (1977) also find very good correspondence between stellar and laboratory features of CeO in the region 4790-4830 Å. This region has not been examined by us in UY Cen.

Unidentified Molecules

The following molecules have been searched for but have not been identified in UY Cen, C_2, TiO, NbO, SrH. Wojslaw and Peery (1976) have identified CuH, ZnH, GeH and SnH in the C star 19 Psc. Unfortunately SnH is the only molecule with lines visible in this spectral region but it is not observed.

CHAPTER 3

Photometry

3.01 General Principles

The objectives of stellar photometry are to determine the wavelength and time variation of the flux emitted by a star. When this information is known it is possible, by comparison with theoretical models, to draw conclusions about the star's evolutionary status and physical properties.

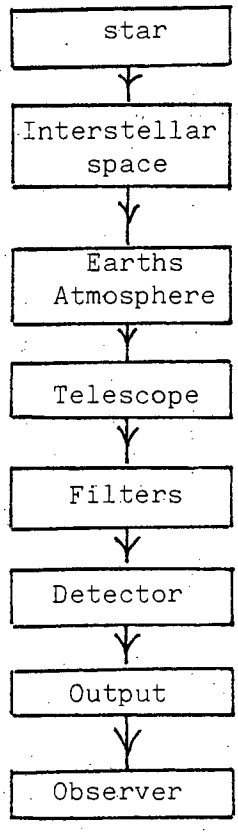

Fig. 3.01

Fig. 3.01 illustrates the factors that modify the signal between the star and the observer and demonstrates that neither the flux nor its variation with wavelength can be directly observed.

The problem can be conveniently divided into two parts; firstly to determine the star's flux above the earth's atmosphere and secondly determine the flux at the star's surface.

For the sake of comparison and convenience astronomers usually observe stars using one of the standard photometric systems.

The method used, is to observe both program and standard stars, through a set of filters and with a detector, that matches as closely as possible those used to define the photometric system. The instrumental deflections observed for each star are corrected for the effects of atmospheric extinction and converted to a set of natural magnitudes. The natural magnitudes are then converted to apparent magnitudes using the standard stars observed on the same night.

Although the initial observations can be made with an error of typically only 0.1%, conversion to the standard system introduces a further uncertainty, caused by the fact that each filter spans a finite wave-

length interval. The resulting uncertainty can be 5% or more when the energy distributions of the standard and program stars are quite different, as in the case of the SC stars.

3.02 Flux Calibration of the Magnitude Scale and Bolometric Magnitude

In order to compare our observations with theoretical models we must be able to convert our magnitudes to fluxes. In principle this could be done by observing a standard source with our telescope-filter-detector system. In practice this is a difficult observation and we therefore rely on values given by Johnson (1965) and Wilson et al. (1972). The adopted values are given in Table 3.01.

Johnson's method is to determine the apparent visual magnitude and colours of the sun, for which the flux distribution with wavelength, above the earths atmosphere, is well known. Johnson then assumes that the broadband magnitudes can be approximated by a monochromatic magnitude at the mean effective wavelengths of each filter. The star fluxes are then found by interpolating the suns flux distribution at the appropriate wavelength and scaling it by the appropriate magnitude difference between the sun and the star.

Johnson's (1965) calibration is used for $UBVR_JI_J$ where the subscript J refers to Johnson. The subscript KC refers to Kron Cape; the magnitude system used at the Cape observatory. The sensitivities of the Kron Cape colours are given by Bessell (1979).

The JHKL calibration is taken from Wilson et al. (1972) and is based on the flux distribution of Vega, which they assume has an apparent magnitude of 0.00 at JHKL. This thesis used JHKL magnitudes based on the Glass (1974) system of standards in which Glass (private communication) says that Vega has J=H=K=L= -0.02. Therefore the JHKL fluxes given in Table 3.01 are the Wilson et al. (1972) values reduced by 2%.

The relationship between the bolometric correction and the apparent v magnitude is

$$M_{bol} = M_v - BC_v \qquad (3.01)$$

By definition BC = 0 for the sum. If the solar constant (1.388×10^6 erg cm^{-2} s^{-1}) is combined with Johnson's adopted apparent v magnitude of the sun (-26.74) this leads to the flux at the earth for an $M_{bol} = 0$ star:

$$2.795 \times 10^{-12} \text{ W cm}^{-2}$$

Johnson (1966) sets BC = 0 for a G 2 V star but, comparison of his mean colours for a G 2 V star with his observed colours for the sun, show that the sun emits about 5% more flux than a G 2 V star, of the same apparent magnitude. This implies that the calibration of $M_{bol} = 0$, appropriate to his 1966 article, should be about 5% smaller than the value stated above. Since the sensitivities of the different bands are based on the observed colours of the sun, it seems more appropriate to use the corresponding calibration of M_{bol} given above.

3.03 Description of the Infra-Red Photometer and observing Technique

The detector used with the infra-red photometer was originally a PbS but more recently an InSb photodiode. This is mounted behind a CaF_2 Fabry lens and appropriate filters and apertures, all of which are maintained at liquid nitrogen temperature (77°K) in a vacuum. It is essential to maintain a low temperature to reduce the radiation emitted by the interior of the photometer and detector, which would otherwise overwhelm the star signal at 3.4μ. The vacuum merely provides suitable thermal insulation. The star to be observed is imaged at the aperture via a rotating chopper mirror. A second fixed mirror is set behind the chopper mirror so that the detector alternately views two nearby areas of sky either one of which contains the star. The photocurrent produced by the detector is amplified by an operational amplifier, whose first stage is maintained at liquid nitrogen temperature. The chopper frequency of (12.5 HZ) is matched to the response time of the detector and generates an AC signal at the preamp, which is then amplified by a lock-in amplifier, phase locked to the rotating chopper. This produces a DC voltage, which is monitored on a chart recorder and also passed to a vol-

tage to frequency converter, followed by a counter. At the instigation of the observer, the number of cycles counted per 10 seconds is punched onto paper tape, along with the filter, and aperture data.

The observing technique is designed to overcome problems associated with the large background radiation from the telescope. The fixed and rotating mirrors each allow the detector to see a slightly different aspect of the telescope structure. At the beginning of the night a fine-tilting adjustment is made to the fixed mirror so that, when no star is in either beam, the telescope flux is exactly balanced and no AC signal is generated. However this is only a first approximation that is anyway subject to drift because of changing telescope aspect and temperature.

The method of observing is to place the star first on the rotating mirror for a 10 second integration and then on the stationary mirror for another 10 second integration. Because the telescope signals cancel, the difference between the two signals is equal to twice the intrinsic star deflection. The phaselocked amplifier is required to maintain the correct phase relation, when the star is observed on either of the mirrors. Observation is confined to 10 second pairs to minimise the effects of background drifts.

Standard stars are observed during the course of the night and each colour is reduced to the system defined by them, allowing corrections to be made for atmospheric extinction and zero point drifts. Details of transformation and saturation problems are discussed by Robertson and Catchpole (1981).

3.04 Data

The photometry used in this thesis is listed in Table 3.02. Column twelve gives the date of observation and column thirteen the source of the data. The data are drawn from four sources. 'Eggen' refers to Eggen (1972) in which he discussed the photometry of the SC stars. The values quoted in Table 3.02 are the mean values of his data listed in his Table 8 but transformed to the Johnson system using Eggen's transformations. 'Walker T' refers to data published by Walker (1976) in his thesis while 'Walker' refers to his individual measures, mean values for which are given in Walker (1979). This material was obtained with the 20" and 30" telescopes at the S.A. Astronomical Observatory. 'MkI' refers to data obtained with the MkI infrared photometer by I.S. Glass, mainly with the 18" reflector at Cape Town. MkII refers to data obtained mainly by the author using the MkII infrared photometer on the

30" reflector at Sutherland.

Mean values of the magnitudes are formed for each colour of each star and are listed in the first row for each star, in Table 3.03. The second row of Table 3.03 contains the unreddened colours. The method of obtaining these is explained in the next section.

TABLE 3.02

U	B	V	R_{KC}	R_J	I_{KC}	I_J	J	H	K	L	Date	Source
GP Ori												
	12.23	9.27		6.74		5.01					1972	Eggen
							3.81	2.61	2.16	1.85	17:11:72	MkI
							3.65	2.49	2.09	1.69	9:12:73	MkI
		9.43	7.66		6.10						9:12:75	Walker
		9.52	7.82		6.15						5:12:76	Walker
FU Mon												
	12.32	9.05		6.35		4.53					1972	Eggen
							3.12	1.95	1.51	1.12	26:11:72	MkI
16.83	12.36	9.06	7.24		5.59						9:12:75	Walker
		9.02	7.26		5.53						5:12:76	Walker
V372 Mon												
							4.38	3.28	2.87	2.55	12:12:72	MkI
17.42	13.09	9.98	8.19		6.65						9:12:75	Walker
		9.65	8.01		6.46						1: 1:77	Walker
Henize 244												
	12.18	9.33		7.14		5.50					1972	Eggen
							4.23	3.05	2.64	2.42	:11:72	MkI
							4.15	3.05	2.67	2.39	: 6:74	MkI
							4.11	3.03	2.67	2.32	18: 4:75	MkII
16.25	11.92	8.97	7.40		6.04						9:12:75	Walker
		9.57	7.96		6.37						1: 1:77	Walker
Henize 250												
							5.10	3.96	3.60	3.32	23: 1:73	MkI
							5.10	3.97	3.61	3.27	26: 6:73	MkI
							5.19	3.99	3.61	3.19	31: 5:74	MkI
		9.83	8.41		6.99						31:12:76	Walker
BH Cru												
	11.77	8.35		6.01		4.46					1972	Eggen
							5.14	3.97	3.61	3.27	: 1:73	MkI
15.13		8.33	6.74								17: 7:75	Walker T
13.03	10.12	7.41	5.94		4.79						26: 2:76	Walker
		7.61	6.28		5.08						31:12:76	Walker

TABLE 3.02 Continued

U	B	V	R_{KC}	R_J	I_{KC}	I_J	J	H	K	L	Date	Source
UY Cen												
	9.22	7.14		4.74		3.14					1970	Eggen
							2.00	0.96	0.62	0.21	3: 6:72	MkI
							2.02	0.93	0.54	0.17	23: 1:73	MkI
							2.01	0.93	0.57	0.22	1: 6:74	MkI
							2.15	1.04	0.68	0.25	15: 4:75	MkII
							2.09	1.03	0.62	0.26	17: 5:75	MkII
							2.06	0.97	0.59	0.22	5: 7:75	MkII
							2.09	1.01	0.62	0.26	20: 2:76	MkII
		7.07	5.58		3.95						23: 2:76	Walker
14.09	10.03	7.13	5.54		4.00						26: 2:76	Walker
							2.08	0.99	0.61	0.24	25: 3:76	MkII
							2.05	0.97	0.58	0.18	10: 4:76	MkII
							2.06	0.96	0.56	0.20	11: 6:76	MkII
							2.08	1.02	0.61	0.19	12: 7:76	MkII
		7.28	5.72		4.12						31:12:76	Walker
							2.11	1.01	0.61	0.27	3: 1:77	MkII
							2.20	1.00	0.58	0.26	2: 2:77	MkII
AM Cen												
	11.61	8.68		5.94		4.28					1972	Eggen
							3.31	2.12	1.72	1.35	3: 6:72	MkI
							3.13	2.00	1.63	1.30	23: 1:73	MkI
							3.29	2.15	1.76	1.40	1: 6:74	MkI
14.83		8.58	6.93								15: 7:75	Walker T
14.87		8.55	6.90								17: 7:75	Walker T
		8.75	7.15		5.46						23: 2:76	Walker
15.41	11.70	(8.12)	7.09		5.72						26: 2:76	Walker
VY Aps												
							4.14	3.04	2.64	2.35	14: 6:72	MkI
							4.03	2.93	2.53	2.19	26: 6:73	MkI
							3.92	2.82	2.53		15: 4:75	MkII
15.15	11.96	9.12	7.53								21: 5:75	Walker T
15.50		9.25	7.62								17: 7:75	Walker T
		9.29									5: 5:76	Walker
		9.18	7.65		5.94						23: 6:76	Walker
Henize 166												
							5.35	4.18	3.76	3.42	26: 6:73	MkI
							5.46	4.27	3.83		1: 6:74	MkI
							5.37	4.25	3.83	3.49	18: 4:75	MkII
16.41	13.45	10.51	8.96								21: 5:75	Walker T
16.54		10.94	9.38								17: 7:75	Walker T
		10.92	9.34		7.52						23: 2:76	Walker
16.84	14.19	(11.29)									5: 5:76	Walker
LQ Ara												
							4.54	3.28	2.81	2.40	8: 9:72	MkI
							4.29	3.13	2.69	2.29	15: 4:75	MkII
16.38	13.34	10.28	8.43								21: 5:75	Walker T
17.48		10.08	8.26								5: 9:75	Walker T
16.61	13.40										5: 5:76	Walker
		10.44	8.68		6.71						6: 5:76	Walker
		10.49	8.73		6.75						23: 2:76	Walker

TABLE 3.03

	U	B	V	R_{KC}	R_J	I_{KC}	I_J	J	H	K	L	A_v
GP Ori		12.23	9.41	7.74	6.74	6.12	5.01	3.73	2.55	2.12	1.77	0.43
		10.80	8.34	7.40	6.42	5.87	4.81	3.63	2.48	2.08	1.75	
FU Mon	16.83	12.34	9.05	7.25	6.35	5.56	4.53	3.12	1.95	1.51	1.12	0.57
	15.94	11.58	8.48	6.79	5.93	5.23	4.26	2.98	1.86	1.46	1.10	
V372 Mon	17.42	13.09	9.82	8.10		6.55		4.38	3.28	2.87	2.55	0.93
	15.97	11.85	8.89	7.36		6.01		4.16	3.13	2.79	2.51	
Hen 244	16.25	12.18	9.33	7.68	7.14	6.20	5.50	4.16	3.05	2.66	2.38	0.44
	15.56	11.59	8.89	7.33	6.81	5.94	5.29	4.05	2.98	2.62	2.36	
Hen 250			9.83	8.41		6.99		5.13	3.97	3.61	3.26	0.99
			8.84	7.62		6.42		4.89	3.81	3.52	3.22	
BH Cru	14.08	10.94	7.92	6.32	6.01	4.94	4.46	5.14	3.97	3.61	3.27	0.89
	12.69	9.76	7.03	5.61	5.35	4.42	4.04	4.93	3.83	3.53	3.23	
UY Cen	13.44	9.95	7.10	5.54	4.74	4.02	3.14	2.07	0.99	0.60	0.22	0.29
	12.99	9.56	6.81	5.31	4.53	3.85	3.00	2.00	0.94	0.57	0.21	
AM Cen	15.04	11.65	8.64	7.02	5.94	5.59	4.28	3.24	2.09	1.70	1.35	0.50
	14.26	10.99	8.14	6.62	5.57	5.30	4.05	3.12	2.01	1.66	1.33	
VY Aps	15.33	11.96	9.21	7.60		5.94		4.02	2.93	2.56	2.27	0.45
	14.63	11.36	8.76	7.24		5.68		3.91	2.86	2.52	2.25	
Hen 166	16.61	13.82	10.87	9.30		7.58		5.38	4.23	3.80	3.45	0.86
	15.27	12.68	10.01	8.61		7.08		5.17	4.09	3.72	3.42	
LQ Ara	16.82	13.37	10.32	8.52		6.73		4.39	3.20	2.74	2.34	0.61
	15.87	12.56	9.71	8.03		6.38		4.24	3.10	2.69	2.32	

3.05 Interstellar Absorption and Reddening

Light travelling through interstellar space is partially absorbed. The absorption per unit distance is stronger at shorter wavelengths, causing a distant star to appear intrinsically redder and fainter than it should be. Both these effects must be removed before the intrinsic properties of the SC stars can be discussed.

From studies of early type stars, the amount of absorption per unit distance and its variation with wavelength, are known to vary around the sky. This variation is known to be very patchy and has not been determined for the regions near the SC stars. Accordingly van Herk's(1965) law is used. This law assumes that the absorption coefficient depends only on height above the galactic plane, and can be written

$$a\,(h) = a_o e^{-h/\beta_o} \qquad (3.02)$$

Here a(h) = the absorption coefficient

h = the height above the galactic plane

β_o = the scale height, set = 100 pc

a_o = the absorption in the galactic plane

set = 1.9 mag kpc^{-1}

This leads to the relation

$$A_v = \frac{0.75 a_o \beta}{\mathrm{Sin}b} \left\{ 1 - \exp\left(\frac{r\ \mathrm{Sin}b}{\beta} \right) \right\} \qquad (3.03)$$

where b is the galactic latitude of a star at a distance of r parsecs and experiencing an absorption of A_v magnitudes in the V filter band. Van der Hulst's theoretical curve No 15 is used to find the variation of the absorption A with wavelength. This curve is given by Johnson (1968). Both these relations are considered good mean approximations for the galaxy.

Before these relations can be used the approximate distance to the SC stars must be known. From radial velocity data alone, Catchpole and Feast (1971) deduce a mean distance for the SC stars of 0.8 ± 0.9 kpc. When combined with the observed apparent H magnitudes this gives a mean H absolute magnitude of -6.4. As no allowance has been made for interstellar absorption, this will be a slight underestimate of the true value of the H absolute magnitude. Feast, Catchpole and Glass have discussed the absolute magnitudes of a number of S stars, of known distances and obtain values of M_H, of -7.96, -8.52 and -8.42 for the stars TT9 T12 and T Sgr

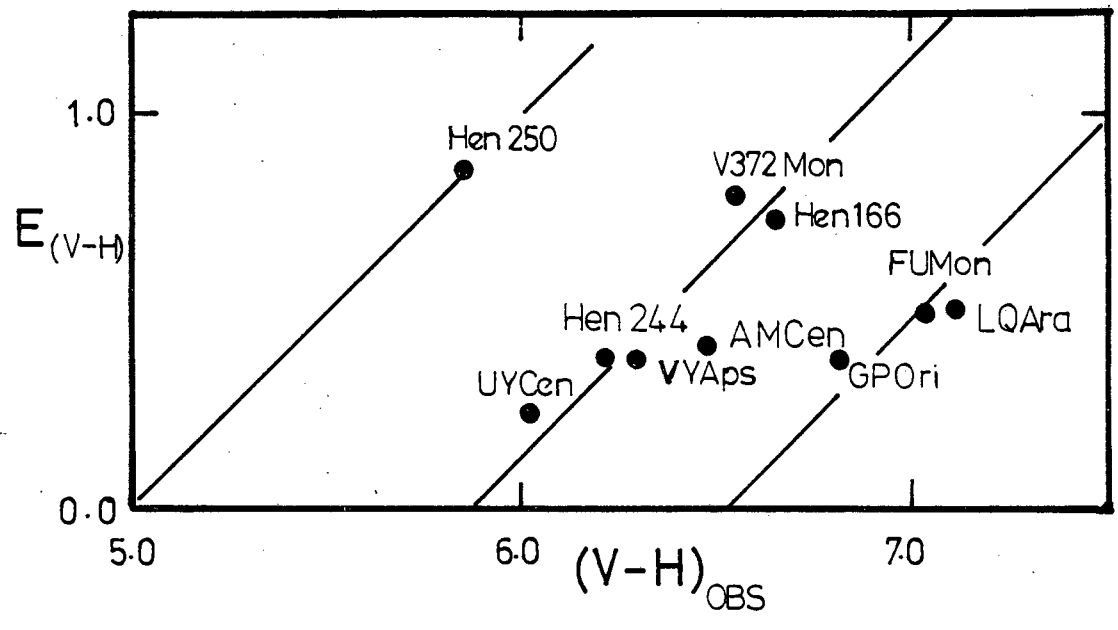

Figure 3.02

Theoretical colour excess is shown as a function of the observed colour. The spread of stars suggests that either they do not all have the same intrinsic colours or the model of the reddening is not correct.

respectively. A value of $M_H = -7.0$ is chosen as a good approximation for the absolute magnitudes of the SC stars. This value is then combined with the observed apparent magnitude M_H to give the distance, from which can be found the appropriate value of the absorption A_V. The values of A_V are not very sensitive to the adopted value of the absolute magnitude. For $M_H = -7.0$ the mean value of $A_V = .82$, which only increases to $A_V = .84$ when the absolute magnitude is raised to $M_H = -8.5$.

It is often possible to deduce the amount of reddening a star suffers by comparing its observed colours with the intrinsic colours of stars of similar or adjacent types. In (V-H)/(H-K) and (V-H)/(J-H) diagrams, the observed distribution of M and SC stars is found to run parallel to a reddening line. This makes it impossible to distinguish between an intrinsic spread in colours and a spread due to the effects of reddening.

Values of $E(V-H) \equiv A_V - A_H$, calculated from equation 3.03 with an absolute magnitude of $M_H = -7.0$, are plotted in Fig. 3.02 against the observed (V-H). If all the stars obeyed the same reddening law and all had the same intrinsic value of (V-H) they would lie about the same line of slope one. The intercept of this line with the $E(V-H) = 0$ axis would give the intrinsic value of (V-H). All dereddened intrinsic values are designated by the subscript $_o$ eg $(V-H)_o$.

It is clear from Fig. 3.02 that all the stars do not fall along the same reddening line. To give the stars the same value of $(V-H)_o$. We would have to assume that Henize 250 suffered no reddening and that LQ Ara, GP Ori and FU Mon lay in a direction of above average reddening. Eggen (1972) finds time variations of the order of 0.5 magnitudes in V for the SC stars he has observed, which would go some way to explain the scatter in Fig. 3.02.

With the information available it is not possible to improve on the values of A_V deduced from equation 3.03. These values of A_V are therefore used to correct the observed magnitudes, listed in the first line of Table 3.03, to give the reddening-free values in the second line.

3.06 Reduction of Data to fluxes and bolometric magnitudes

The dereddened values of the apparent magnitudes are converted to fluxes using the calibration given in Table 3.01. The total flux is then found by integrating a curve drawn by hand through the points in a flux frequency diagram. This integral is converted to a bolometric apparent magnitude using the calibration given in Table 3.01. The bolometric apparent magnitudes and bolometric corrections are given in Table 3.04. The results in Table 3.04 all contain a correction of 0.03m for the CO bands, which is discussed in the section 3.08.

The conventional bolometric correction BC_V, as well as the bolometric correction to the H apparent magnitude BC_H, are both given by equations similar to equation 3.01. The bolometric apparent magnitude for BH Cru is found by applying the mean value of BC_H found for the remaining stars, to the observed value of H. This was done because it is clear that the JHKL magnitudes of BH Cru are not compatible with the visual colours.

The total flux from each star was arbitrarily normalized to a value of 2×10^{-10} W M^{-2}. The normalization factor was applied to the observed flux in each waveband for all the stars. These normalized fluxes are listed in Table 3.05. The mean fluxes and the standard errors of the means are also given. It is clear from inspection of this table that the SC stars form a very homogeneous photometric group which is the justification for using mean fluxes for all the stars in the following discussion.

TABLE 3.04

	m_{Ho}	m_{Vo}	m_{BOL}	BC_H	BC_V	$dx10^{-3''}$
GP Ori	2.48	8.34	5.39	-2.91	2.95	3.9
FU Mon	1.86	8.48	4.80	-2.94	3.68	5.2
V372 Mon	3.13	8.89	6.04	-2.91	2.85	2.9
Hen 244	2.98	8.81	5.88	-2.90	3.01	3.1
Hen 250	3.81	8.84	6.68	-2.87	2.16	2.2
BH Cru	3.83	7.03	(6.73)			2.1
UY Cen	0.94	6.81	3.76	-2.82	3.05	8.3
AM Cen	2.01	8.14	4.90	-2.89	3.24	4.9
VY Aps	2.86	8.76	5.78	-2.91	2.98	3.3
Hen 166	4.09	10.01	7.08	-2.99	2.93	1.8
LQ Ara	3.10	9.71	6.05	-2.95	3.63	2.9

TABLE 3.05

Fluxes in units of 10^{-27} watt M^{-2} HZ^{-1}

	U	B	V	R_{KC}	R_J	I_{KC}	I_J	J	H	K	L
GP Ori		0.97	9.7	33	77	110	266	624	1070	955	588
FU Mon	0.004	0.59	8.9	34	70	114	256	565	1020	923	583
V372 Mon	0.014	1.46	19.1	63		175		597	990	854	501
Hen 244	0.017	1.60	16.6	56	85	161	269	570	984	866	499
Hen 250			36.4	90		218		551	958	791	472
UY Cen	0.027	1.48	15.9	51	98	157	313	532	914	812	512
AM Cen	0.024	1.13	13.4	44	109	119	324	548	975	854	525
VY Nps	0.038	1.82	17.0	55		187		594	1004	868	504
Hen 166		1.78		52		171		610	1069	946	568
LQ Ara	0.015	0.77	9.1	34		126		558	1026	948	604
Mean	0.019	1.29	16.2	51	88	154	286	575	1001	882	535
Standard error	±.004	±.15	±3.0	±6	±8	±12	±15	±9	±16	±19	±15

3.07 Discussions of the SC star fluxes

In Fig. 3.03 the log of the mean flux for each waveband is plotted against frequency. It is clear that the distribution of flux is smooth and that the flux falls off rapidly in the blue and visual regions of the spectrum. The simplest physically plausible model that can be compared with the observed flux distribution is that of a black-body. Black-body flux distributions are calculated for temperatures of 2400, 2500 and 2600°K and normalized to a total flux of $2 \times 10^{-10} W M^{-2}$. The observed mean star flux and the black-body fluxes, are differenced with the 2500°K flux, giving the results shown in Fig.3.04, where $\Delta F_\nu = F_{\nu \text{ observed}} - F_{\nu 2500}$. In order to appreciate how much actual energy is involved at each wavelength, it is important to compare Fig.3.04 with Fig.3.03.

To a first approximation it is clear that the over all distribution of flux in the SC stars from say B to L, which covers a range of 10^3 in total flux, differs nowhere by more than a factor of about 1.6 from that of a 2400° black body. However, the more detailed shape of the flux distribution in the region JHKL, where most of the flux is emitted, is in very poor agreement with a black body. For instance the colour temperature indicated by the slope J to H, is very much less than 2400° but the colour temperature given by H to L, is greater than 2600°. This effect is seen in a wide range of stars, from G giants (Catchpole and Glass (1974)) to S and carbon stars. For early G to late K giants, Catchpole and Glass have shown that this excess of flux in the H band is reproduced by the model atmospheres calculated by Carbon and Gingerich (1969).

The peak, which was predicted by Gingerich and Kumar (1964) is caused by a minimum in the H^- opacity. Because of the complications expected from molecules and uncertain sources of opacity, few model atmospheres have been calculated for very cool stars. Gingerich et al. (1966) have constructed five models with an effective temperature of 2500°K and a range of gravities. Inspection of their paper, shows that changing the gravity changes the relative importance of H^- as a source of opacity. In the high gravity model H_2^- and He^- become proportionately more important, and obliterate the opacity minimum at 1.6μ. Their low gravity model, with log g = 1 is also shown in Figs. 3.03 and 3.04 and clearly reproduces the flux distribution in the JHKL region. A value of log g = 1 is rather low for a giant and is more appropriate to a supergiant.

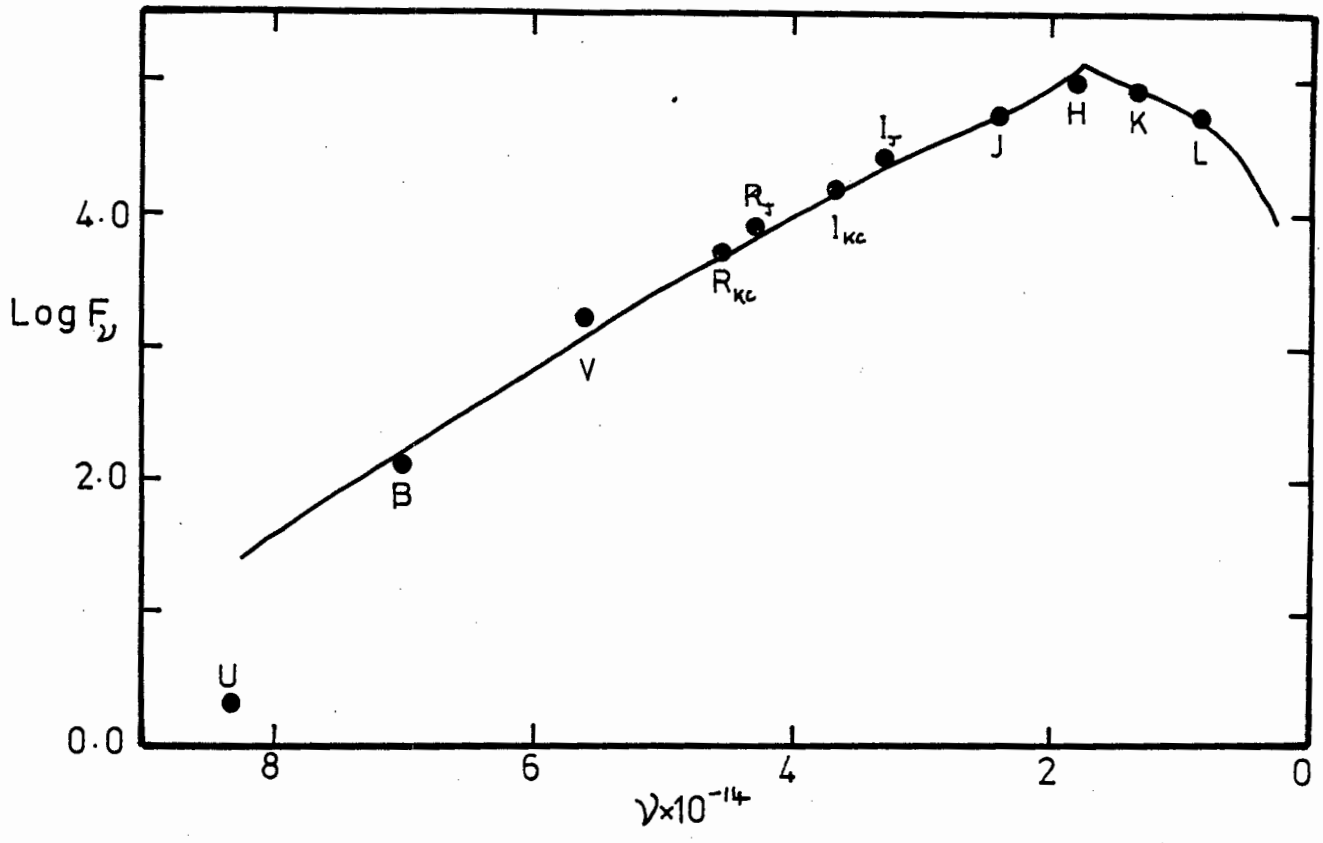

Figure 3.03

The mean monochromatic flux of the SC stars is shown as a function of frequency and compared with the Gingerich et al. (1966) model atmosphere which is indicated by the solid line.

However if the gravity is increased, the peak at H^- is reduced and the predicted flux in the BVR region will be increased.

Two important conclusions can be drawn. Firstly the effective temperature of the SC stars is 2500° with an uncertainty of plus or minus one hundred degrees. Secondly, despite the rich absorption spectrum, the broad-band fluxes in the VRI region do not appear to be strongly blanketed.

The observed flux is seen to fall off very rapidly in the U band, an effect first noted by Feast (1954). It is clear that the total flux removed from the U band, by comparison with either the black-body or the model, is small compared with the integrated stellar flux.

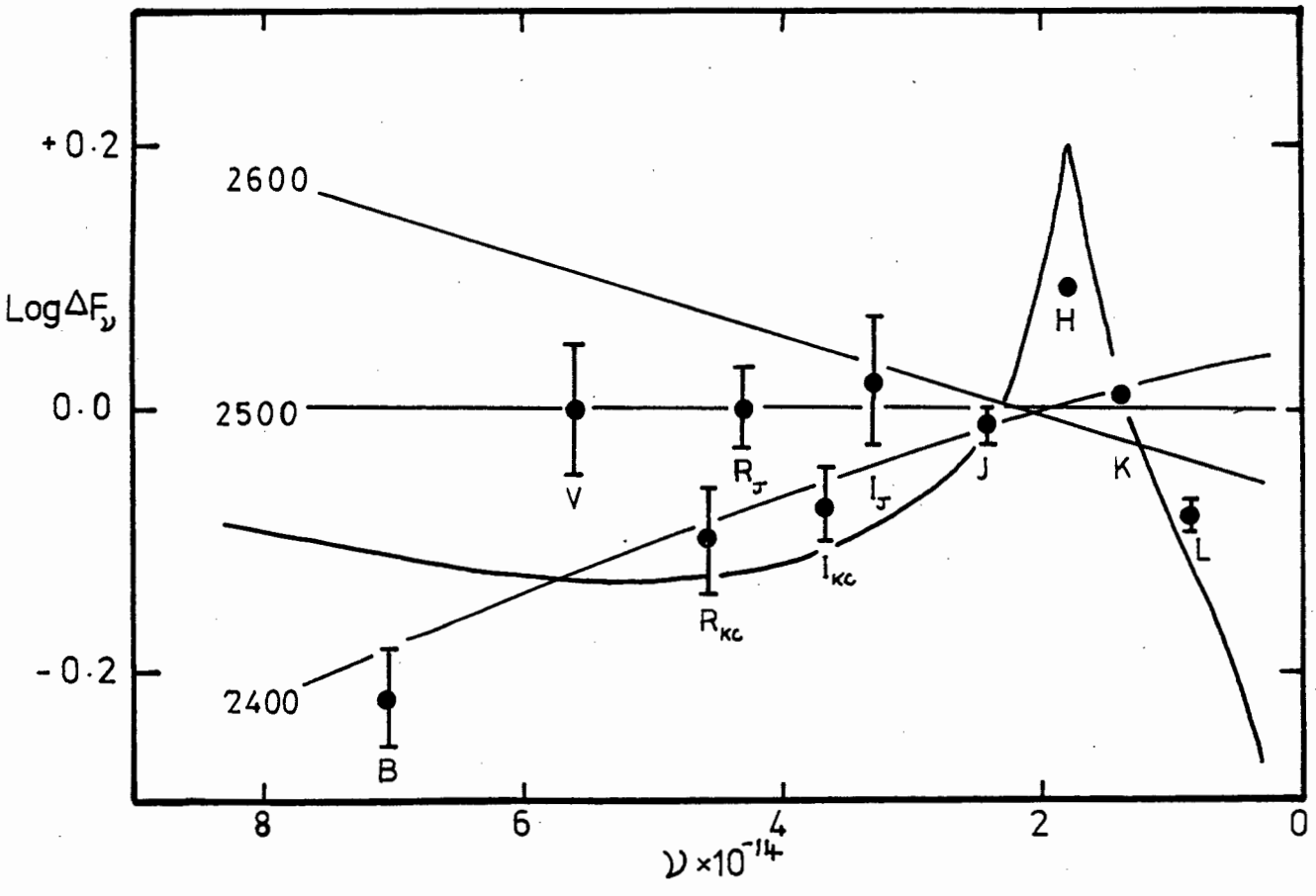

Figure 3.04

Black-bodies, appropriately labelled by temperature, and the Gingerich et al. (1966) atmosphere, shown by the heavy curve, are compared with the mean monochromatic fluxes of the SC stars. Note the much better fit of the model in the JHKL region where most of the flux is emitted.

3.08 Errors

There are three important sources of error. One is connected with the photometry and the other two intrinsic to the star.

Initially we did not have flux calibrations for the Kron system so that Eggen's (1972) observations were transformed to the Johnson system. Inspection of Fig. 3.04 shows that the R and I Kron Cape fluxes are 20% smaller than the R and I Johnson fluxes. This difference is increased to 35% if the Kron Cape calibrations are used with Eggen's untransformed data, which indicates that the two Kron systems are not identical. There are two possible explanations for the difference between these adjacent filters. Either there are strong absorption features in the star at the wavelengths of the Kron Cape bands not found in Eggen's filters, or the effective wavelengths of the bands are changed by observing such red stars. The spectrum of UY Cen shows absorption bands at R_{KC} caused by ZrO and CN, and at I_{KC} strong absorption due to the CN(2,0) and CN(3,1) bands. The R_J band on the other hand lies in a region of absorption caused by the CaH (0,0) band, so that the effect of absorption will be partly balanced. Inspection of Fig. 3.03 shows that for broad bands, that are typically several hundred angstrom wide, the actual star flux changes across the band. When the flux is convolved with the transmission functions of the filter and sensitivity of the photomultipliers, it can give an effective wavelength, for the band, which when compared with another star, is displaced to the red. Both these effects must play some part in causing the irregularities shown in Fig. 3.04. However the error they introduce, in the determination of the bolometric magnitudes, will be quite negligible.

A much more serious uncertainty is caused by assuming that the infrared fluxes can be interpolated by a smooth curve. This is equivalent to assuming that there are no strong absorption bands lying between the infrared bands. This is not so in the case of certain Mira M stars; for instance Omicron Ceti shows very strong stellar water vapour absorption bands that lie exactly between the J,H and K filters. These water vapour bands coincide with the terrestial bands which makes their observation difficult from ground based observatories.

Merrill and Stein (1976) have obtained spectral scans of a number of stars in the 2 to 4 micron region, including the SC star GP Ori. The

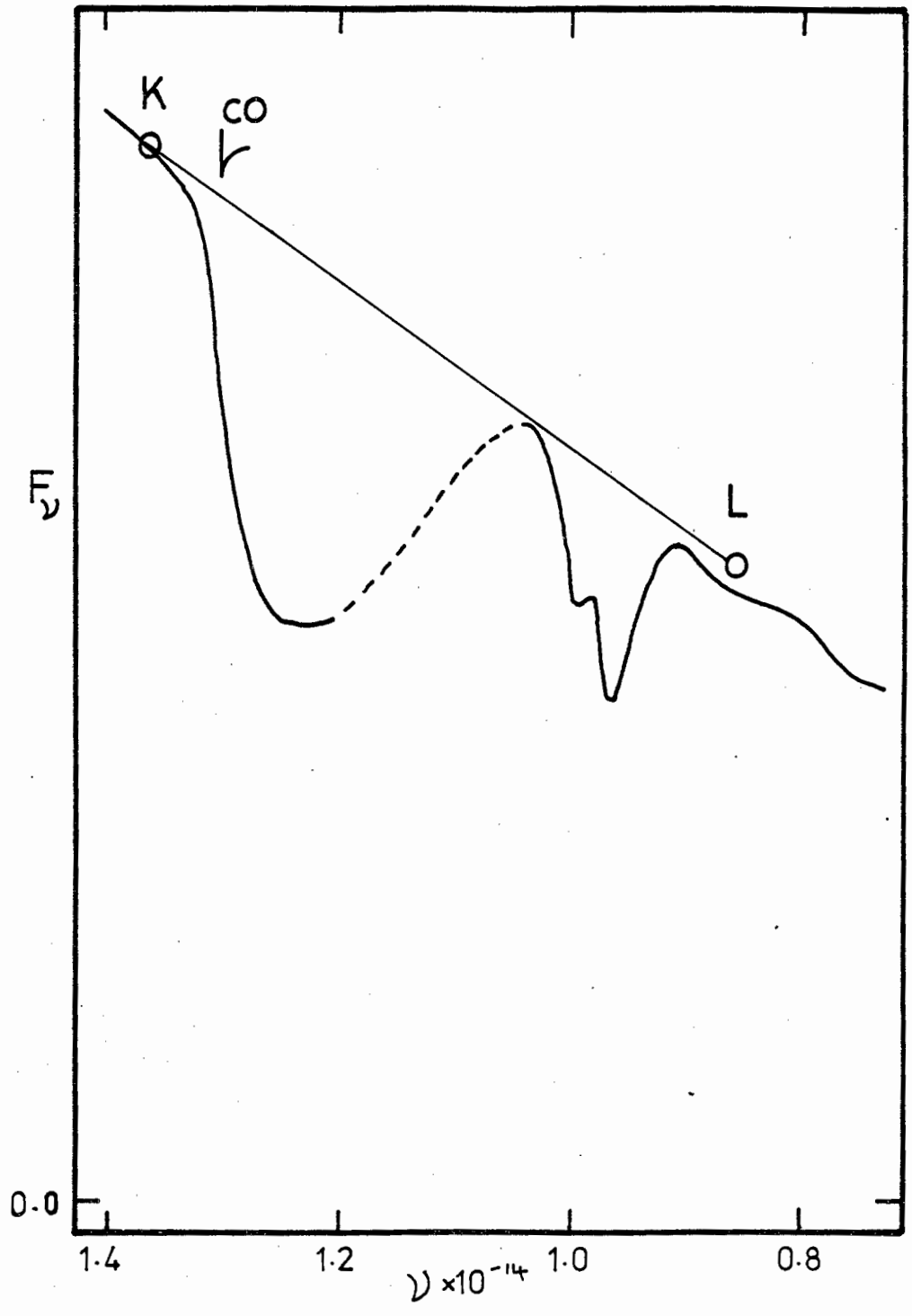

Figure 3.05

Merrill and Stein's (1976) spectrum scan of GP Ori is compared with our arbitrarily normalised K and L colours and illustrates the amount of flux removed from the spectrum by absorption features.

scans show that CO is stronger in GP Ori, than in any other of their carbon or M stars, but that water vapour is not present. In Fig. 3.05 their scan of GP Ori has been transformed to a frequency scale. Also shown are the mean K and L, SC star fluxes, arbitrarily normalized to the flux in the continuum of GP Ori, at the effective wavelength of the K filter. The agreement between the K to L slope and the observed scan slope, is encouraging. The dotted curve is a hand drawn interpolation across the region of the spectrum which is obliterated by the atmospheric water vapour band. The area of the two absorption features corresponds to 3% of the total flux of the star, which in turn implies that the bolometric apparent magnitudes must be made 0.03m fainter. This correction has been applied to the results given in Table 3.04.

The final important source of error is that made in extrapolating the flux beyond the frequency limits of the photometry. There is at present no evidence, either from UV satellite data or from infrared sky surveys, to suggest that any of the SC stars show large fluxes in either of these regions. Changes in the form of the extrapolation between L and zero frequency will result in errors of no more than few percent in the total flux.

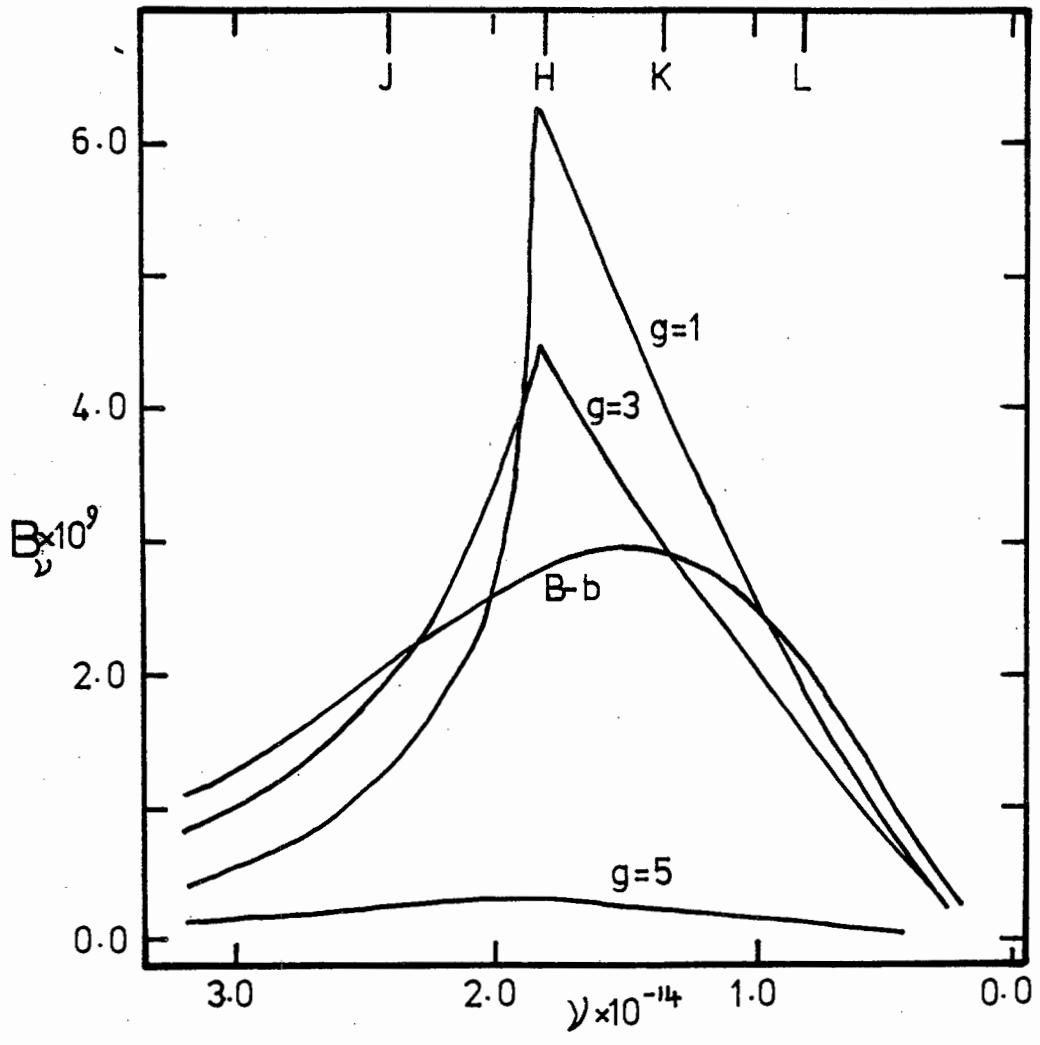

Figure 3.06

The intensity of the three 2500 model atmospheres, labelled by log gravity, is shown as a function of frequency. A 2500° black-body marked B-b is also shown.

3.09 Comparison with Published results

Eggen (1972) has discussed the photometry of 6 of the SC stars, which can be identified as the only stars listed in Table 3.03, having values of R_J and I_J. Eggen uses Johnson's (1966) calibration of $(R-I)_o$ against T_e for giants, to deduce the effective temperatures of the SC stars. The mean value of $(R-I)_{o_J}$ is 1.53, which corresponds to a Johnson temperature of 3200° as opposed to the temperature of 2500° adopted here. The black body temperature of $(R-I)_J = 1.53$ is 2550°.

Through a study of stellar angular diameters, Barnes et al (1976 and 1978) present, what they claim is a widely applicable relationship between various colour indices and visual surface brightness. Using equation 1 of Barnes et al. (1976), it is possible to relate visual surface brightness and bolometric corrections, to effective temperature. Using the relationships given in the two papers cited above we find

$$T_e\ (V-R)_J = 682^\circ \quad \text{and} \quad T_e\ (R-I)_J = 877^\circ$$

These estimates are clearly incompatible with either the black body or the model atmosphere estimates of T_e.

Eggen uses the relation $M_{bol} = M_{IJ} + 1$ and the observed relationship between M_{BOL} and $(R-I)_o$ for old disk population stars, to deduce values of M_{BOL} and the distance modulus. This method gives a mean value of $M_{BOL} = -3.4$ and a mean distance of 0.6 kpc, for the six stars. This is in reasonable agreement with the Oort constant solution of $M_{BOL} = -3.5$ given in the next chapter, but in poor agreement with the best compromise value $M_{BOL} = -4.5$ finally adopted. It follows from Eggen's method that his stars will lie on an old disk population line in his M_{BOL}, T_e diagrams. The values of $M_{BOL} = -4.5$ and $\log T_e = 3.4$ adopted here, while lying outside the range of his diagram, place the stars below his line. The uncertainties in the distance scale prevent any strong conclusions being drawn from this.

3.10 Angular diameters

The effective temperatures is related to the angular diameter of a star by the following relation

$$\theta^2 = \frac{4F_{OBS}}{\sigma T^4} \qquad (3.04)$$

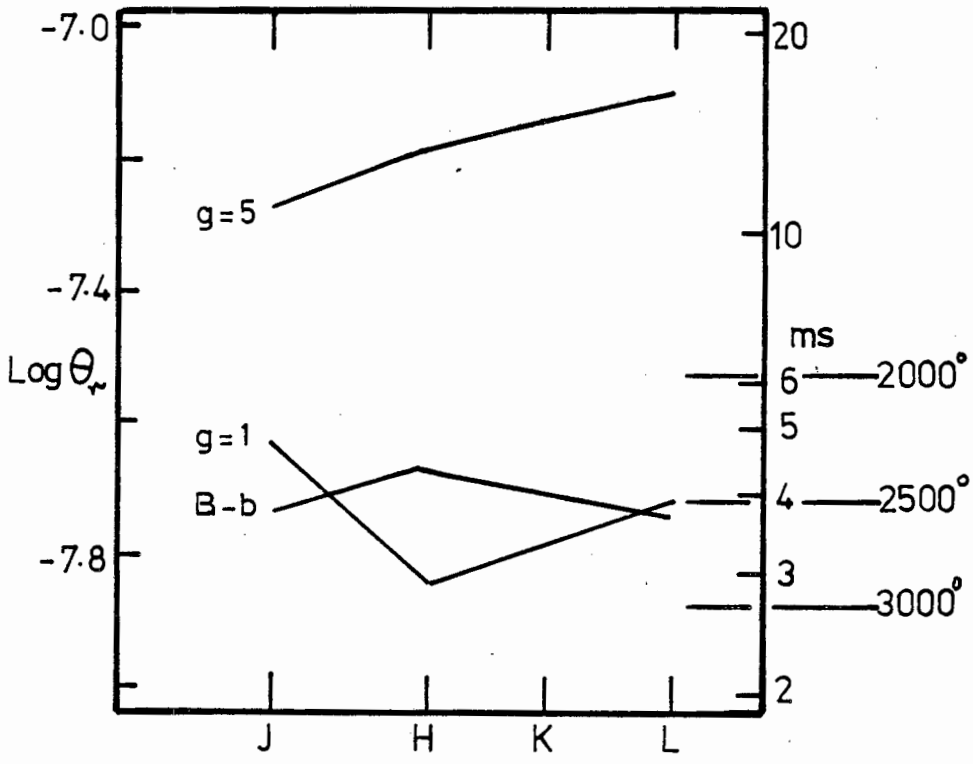

Figure 3.07

The angular diameter, in radians on the left and milliarcseconds on the right, is given for various colours by equation 3.05, using the models and black-body given in Fig. 3.06. The temperatures on the left indicate diameters given by equation 3.04. The scale is for a star having the mean SC star flux distribution and a total flux at the earth of 2×10^{-10}watt cm^{-2} s^{-1}.

Where θ = the angular diameter in radians, F_{OBS} is the total observed flux at the earth and σ is Steffan's constant. The angular diameter is also given by the relation,

$$\theta = 2\sqrt{F_{obs\ \nu}/F_{star\ \nu}} \qquad (3.05)$$

where $F_{obs\ \nu}$ is the flux observed per unit area at the earth and $F_{star\ \nu}$ is the flux emitted per unit area over 2π steradian at the surface of the star. $F_{star\ \nu}$ can be calculated either from the Planck function or from a model atmosphere. In calculating $F_{star\ \nu}$ some allowance should be made for the limb darkening, but to a first approximation in the infra red, this may be ignored. In Fig. 3.06 the intensity at the star's surface is plotted as a function of frequency; for a black-body at 2500° and for three values of the gravity, for the Gingerich et al. 2500 model. This diagram illustrates the strong deviation from a black-body shown by these models. Fig. 3.07 shows the resulting diameters for an SC star having a total flux at the earth of 2×10^{-10} watt $cm^{-2}s^{-1}$ with the fluxes given in Fig. 3.06 and using equation 3.05. Also shown in Fig. 3.07 is the angular diameter obtained from equation 3.04 for various values of the effective temperatures. It is clear that the predicted angular diameter depends critically on the choice of model and that if the angular diameters could be observed this would be a sensitive test of the model.

The agreement between the angular diameters given by equation 3.04 and 3.05 for the black-body model is a further illustration that the over all flux distribution of the SC stars most closely follows that of a 2500° black-body.

Robertson (1980) has compared angular diameters determined from JHKL photometry (using equation 3.04) with measured diameters. He shows that the methods are in good agreement for stars hotter than 4000° but disagree by as much as a factor 2 for the cooler Miras S Psc and U Ari. He points out that the diameters for these stars were determined in the visible, whereas the 1.2 and 1.6μ diameters, given for the two Miras by Ridgway et al. (1979), are within 10% of the black-body diameters. This again suggests that, despite the quite marked wavelength dependant structure in cool star atmospheres, black-bodies provide a good first approximation.

Angular diameters deduced from equation 3.04 and a temperature 2500° are given in Table 3.04 column 7.

At present occultations provide the most accurate measurements of angular diameter. Walker (private communication) indicates that errors are typically about 0.5 milliarcseconds. Therefore both FU Mon and GP Ori would be worth observing, should the opportunity arise. Under good conditions it would be possible to determine their diameter with an error of about 10%, which would allow comparison between the black-body and model results at H.

3.11 Conclusions and Results

This discussion of the photometry enables the following conclusions to be drawn.

1) The SC stars are a photometrically very homogeneous group of stars.
2) The effective temperature of the group is 2500°K ± 100.
3) The energy distribution of the SC stars, while lying close to that of a 2500° black-body, shows structure in the 1.6μ region, which is described by a model in which H^- is still an important source of opacity.
4) It should be possible to measure the angular diameters of FU Mon and GP Ori with an error of ~ 10%, by the lunar occultation method.

We also present a set of bolometric apparent magnitudes, which should be largely free from reddening and which can be used in the galactic rotation studies, given in the next chapter.

CHAPTER 4
Kinematics and Galactic Distribution

4.01 Introduction

This chapter is divided into two main parts. In the first part, under the title Data, the method of obtaining radial velocities is described and the results presented. In the second part these data are used to draw conclusions about the possible age and luminosity of the SC stars. Proper motion data are only available for the stars UY Cen and FU Mon. These data are not considered to be of sufficient extent or accuracy to add to the discussion and are therefore ignored.

The bolometric apparent magnitudes, obtained in the photometery section, when combined with the known galactic latitudes and longitudes of the SC stars, enable a model of their galactic distribution to be constructed. The problem of finding the absolute magnitudes is essentially the problem of placing a scale on this model. This can be done by considering the radial velocities of the stars. The velocity dispersion will depend on the age of the objects while the actual velocities will show the effects of the differential rotation of the galaxy, the magnitude of which will depend on the distances of the stars. Their distribution above and in the galactic plane will also depend on age, and places further constraints on the results of the velocity dispersion and galactic rotation methods. The details of these methods will be discussed in the appropriate sections.

The application of these methods assumes that the SC stars are a homogeneous group of objects that have shared in the dynamical evolution of the galaxy. Without this assumption no progress can be made toward determining their ages and absolute magnitudes. The possibility that these stars are Runaway stars, or are not a homogeneous group, is discussed below and is rejected.

4.02 Derivation of Wavelength system and Measurement of Velocities

Radial velocities are available in the literature for the stars FU Mon and GP Ori. Velocities for the remaining stars were derived from spectra of three different dispersions, using wavelengths based on the line list for UY Cen. For both the Y and Z camera dispersions of 13 and 32 Å mm^{-1} respectively, it is possible to select a sufficient number of lines which have unique laboratory indentification and which have good profiles in UY Cen. The laboratory wavelengths and the wavelengths measured in UY Cen are identical for these lines so the velocities derived from the Z camera spectra are based entirely on laboratory wavelengths. At a dispersion of 80 Å mm^{-1}, although many absorption lines are observed, very few of them have unique identifications and most of them are blends of four or more lines. The problem is then to find the effective wavelengths of each of these blends and to establish that this effective wavelength remains constant for all the stars. The problem is aggravated by the fact that the velocities of the stars do not remain constant, but is simplified by the fact that spectroscopically they form a very homogeneous group.

Thirty one sharp absorption features were identified on an 80 Å mm^{-1} V camera spectrum of UY Cen. These features were compared with high dispersion spectra and tracings of UY Cen. Each feature could then be resolved into its separate component absorption lines. The effective wavelength of each feature was found by forming the weighted mean wavelength of the component lines. The weighting is proportional to the observed intensity of each component line as given in the line list of UY Cen. This initial set of wavelengths is called λ_1.

All the visible λ_1, lines were then measured on four V camera spectra of UY Cen. All the spectra were measured on a Hilger long screw measuring machine identical with that used to produce the UY Cen line list. A similar measuring technique was used. A mean velocity was determined for each plate and differences from this mean were found for all the lines on all the plates. A mean difference was then found for each line on all the plates and this difference was used to correct the initial set of wavelengths, λ_1 to give a set λ_2. It should be noted that no assumption is made about either the value or the constancy of the velocity of UY Cen from one plate to the next. The λ_2 set of wavelengths was then applied to 45 spectra of all the SC stars and a similar procedure followed to get a set of wavelengths λ_3. These λ_3 wavelengths, with their principal

TABLE 4.01

λ_3	main contributor
5983.65	TiI(2)
5989.07	CeI
6006.66	CeI
6031.42	TiI(2)
6057.59	VI(34)
6063.29	BaI(7)
6102.50	CaI(3)
6120.76	CaI(3)
6142.17	BaII(2) ZrI(2)
6161.87	CaI(3)
6169.92	CaI(20)
6191.92	YI(2)
6222.59	YI(2)
6258.40	TiI(1)
6280.91	FeI(13)
6305.56	ScI(2)(3)
6325.76	TiI(1)
6413.31	TiI(1)
6449.98	CaI(19) ScI(1) BaI(6)
6456.22	CaI(19) LaI
6462.82	FeI(13)
6543.17	LaI(7)
(6562.82	Hα measured only in emission and not included in means)
6565.03	VI(48)
6599.26	TiI(49)
6643.89	NiI 43
6650.82	LaI
6687.86	YI (1)

contributors are listed in Table 4.01 and are used to derive the velocities and standard errors given in Table 4.03. The velocities listed in Table 4.03 are heliocentric radial velocities and include the declination term discussed below

It should be noted that if all the lines could be measured in all the spectra of all the stars, the iterative procedure described would not change the velocities derived but would merely reduce the standard errors of the mean velocities. In practice not all the lines are visible in each star so that iteration is necessary to ensure that spectra with few lines visible, do not give systematically different results.

4.03 Declination Term

When a star is observed away from the zenith the light from that star becomes dispersed by the earths atmosphere, so that instead of a simple image, an impure spectrum of the star is formed on the slit of the spectrograph. The dispersion of this spectrum depends on the tangent of the zenith distance of the star. When the observer centres a star on the slit he does so in a way that depends on a convolution of the star's flux distribution with the sensitivity response of his eye. If the peak of this convolution is different from the region of the spectrum being recorded, the observer will tend to hold the region being observed systematically off the centre of the slit. The V camera employs a wide slit, having a projected width at the spectrum of 2.3 Å, equivalent to 108 km s^{-1}. It is clear that a systematic failure to centre the star will appear as a systematic shift in velocity.

Because there is a strong tendency to observe stars near the meridian, this effect, which depends on zenith distance Z, is referred to as a declination term and we may assume the relationship $Z = \delta - \phi$, where δ is the declination and ϕ is the latitude of the observatory.

The convention, when observing stars for velocity with the V camera, is to set the star on the slit so that the north direction is upward. This is done with the aid of a Dove prism, (which rotates the field), mounted ahead of the slit.

The declination term was investigated by observing pairs of spectra set respectively N and S up, as seen on the slit. Table 4.02 shows the results of these observations which are displayed graphically in Fig. 4.01 Also shown are the results of similar observations on late type velocity

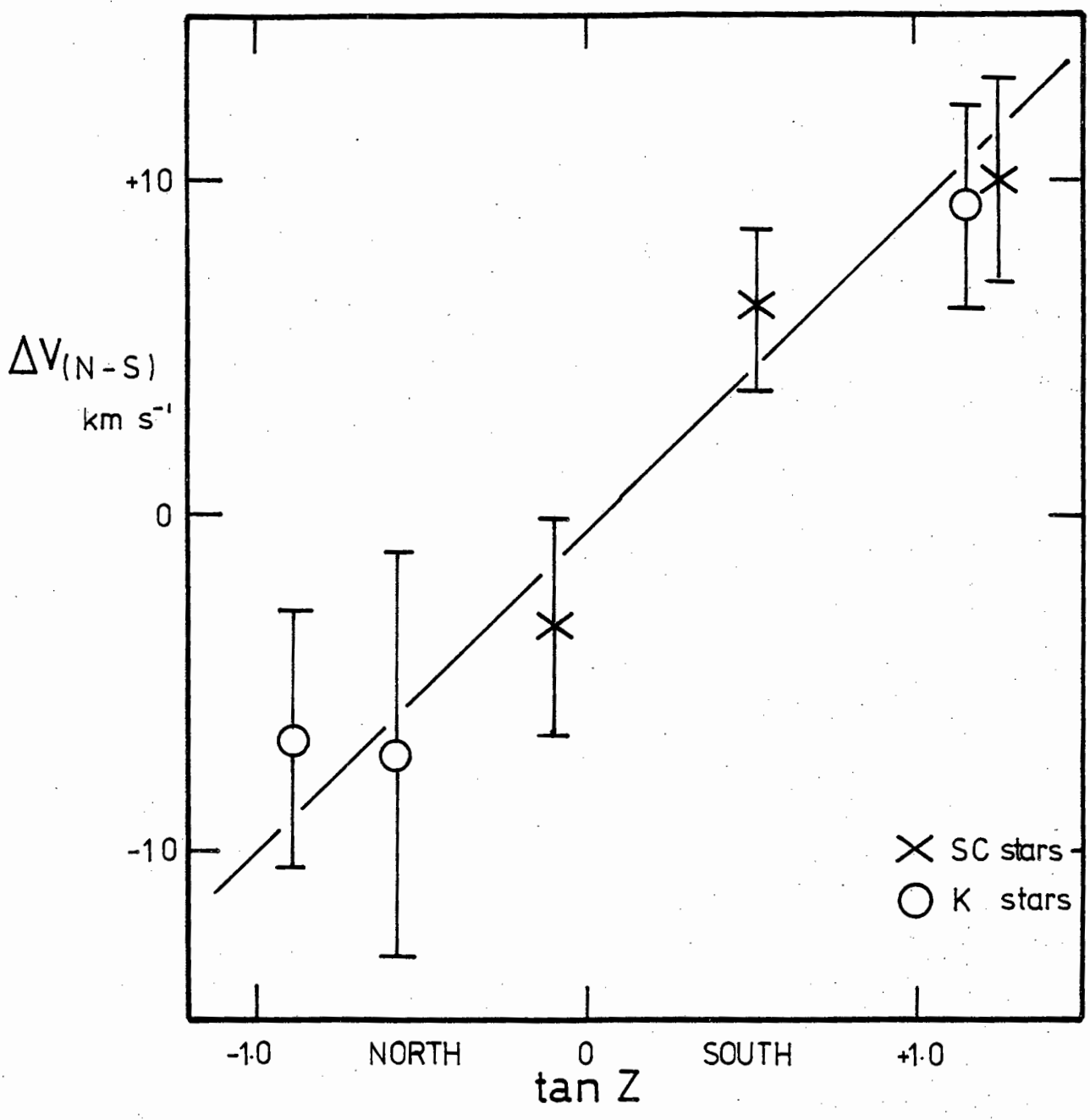

Figure 4.01

Velocity differences, using two sky orientations on the slit, are shown for various types of star, as a function of zenith distance.

standards. The error bars are the standard errors of the differences.

TABLE 4.02

SC STARS

	V_{Nup}	V_{sup}	$\Delta_{V(N-S)}$	s e	tan Z	No of points
GP Ori	+80.2	+86.9	-6.7	±3.8	-0.87 North	6
FU Mon	-25.2	-18.1	-7.1	±6.0	-0.56 North	3
VY Aps	-27.1	-36.3	+9.2	±3.0	+1.14 South	2
			K Standards			
HD203638	+22.2	+25.6	-3.4	±3.2	-0.08 North	10
θ Oct	+28.7	+18.7	+10.1	±3.1	+1.26 South	11
Π Phe	- 8.3	-14.4	+6.1	±2.4	+0.51 South	4

The agreement between the SC stars and the K velocity standards is good and suggests that the declination correction does not depend strongly on the colour of the star. All the SC star velocities listed in Table 4.03 have been corrected for the declination term according to the relation

$$V_{corrected} = V_{measured} - \frac{\Delta V_{(n-s)}}{2} \qquad (4.01)$$

4.04 Systematic Corrections and Final Velocities

The V camera velocities for the SC stars are listed in Table 4.03 along with their internal standard errors. Inspection of this Table, and more particularly of the pairs of spectra of GP Ori, indicates that the true errors may be somewhat larger than is indicated by the internal standard error. These rather larger errors will mask the intrinsic variations of velocity which were found in the high dispersion observations made by Catchpole and Feast (1971). Mean velocities and standard

TABLE 4.03

Star	Plate No	HJD 2440000	R.V.	s.e.	Mean	s.e.
GP Ori	2496	581.263	+105.5	±3.6		
	2496	581.277	+103.3	±2.2	+86.9	± 2
	2505	599.343	+ 90.2	±3.6		
	2508	601.298	+ 88.4	±3.0		
	2642	807.637	+ 82.5	±2.2		
	2642	807.651	+ 83.6	±1.8		
	2651	817.645	+ 81.2	±2.2		
	2651	817.658	+ 81.0	±2.2		
	2728	877.558	+ 77.9	±2.6		
	2728	877.577	+ 92.0	±3.6		
	2733	904.505	+ 93.0	±4.3		
	2733	904.601	+ 79.7	±2.0		
	2739	933.407	+ 86.8	±2.4		
	2739	933.431	+ 80.4	±3.4		
	2749	962.368	+ 81.9	±3.0		
	2750	962.389	+ 82.7	±3.0		
FU Mon	2497	581.386	- 16.1	±2.8		
	2502	585.409	- 12.2	±2.5	-19.9	± 3
	2534	677.299	- 34.8	±6.2		
	2537	678.221	- 6.3	±3.2		
	2734	905.555	- 19.2	±2.7		
	2734	905.566	- 10.0	±3.8		
	2739	933.452	- 23.6	±3.2		
	2739	933.468	- 23.2	±2.1		
	2748	961.378	- 31.4	±2.8		
	2748	961.393	- 22.4	±2.8		
V372 Mon	2497	581.464	+ 19.6	±3.9		
	2508	601.416	+ 25.3	±2.9	+21.4	± 2
	2534	677.318	+ 19.4	±4.9		
Hen 244	2498	581.527	+ 26.1	±2.9		
	2515	644.390	+ 35.7	±4.1	+30.9	
Hen 250	2326	402.300	+ 21.3	±3.0		
	2516	644.510	+ 20.6	±3.6	+19.3	± 2
	2541	701.459	+ 21.1	±4.1		
	2564	734.330	+ 14.1	±4.7		
BH Cru	2511	611.535	+ 6.9	±4.1		
	2516	611.549	+ 12.2	±2.8	+ 9.5	
UY Cen	2310	373.448	- 15.0	±2.9		
	2516	644.553	- 12.1	±2.4	-15.0	± 1
	2537	678.511	- 13.8	±5.0		
	2551	705.464	- 18.1	±2.9		
	2562	733.413	- 16.0	±3.1		
AM Cen	2517	644.570	- 22.5	±2.0		
	2537	678.519	- 27.5	±4.3	-21.0	± 3
	2538	678.586	- 18.7	±2.7		
	2542	701.577	- 15.5	±2.4		

TABLE 4.03 Continued

Star	Plate No	HJD 2440000	R.V.	s.e.	Mean	s.e.
VY Aps	2311	373.567	-30.7	±3.1		
	2322	401.294	-30.9	±2.5	-32.1	± 1
	2552	705.591	-36.3	±3.2		
	2639	807.337	-31.9	±3.3		
	2639	807.363	-29.0	±3.6		
	2643	808.247	-32.2	±2.6		
	2643	808.273	-33.5	±3.6		
Hen 166	2273	341.576	- 8.3	±5.0		
	2535	677.610	- 7.0	±12.0	-13.1	± 5
	2554	706.550	-25.2	±5.2		
	2565	734.566	-11.8	±3.9		
LQ Ara	2395	433.463	+ 5.3	±4.4		
	2554	706.585	+ 3.2	±3.7	+ 4.1	± 1
	2577	756.477	+ 3.8	±3.1		

errors are given in Table 4.04 for each star seperately for both the high and low dispersion spectra. The results from high dispersion spectra are those given by Catchpole and Feast, with the exception that one new velocity has been measured for UY Cen (JD2441089, DY2871, V = 17.6 ± 1.04) and the velocity of FU Mon has been changed. Teske's velocity for FU Mon has been made 1.4 km s^{-1} more positive as comparison between the line list of UY Cen and that of FU Mon showed the FU Mon line list to have a residual velocity of -1.4 km s^{-1}.

The V camera velocities and other velocities are compared in Table 4.04. There is a systematic difference between the two sets of velocities in the sense that the V camera velocities are +4.8 km s^{-1} too red shifted. A systematic shift of + 2 km s^{-1} for K stars has also been found by the author. When the SC stars are compared individually the evidence for this shift is not strong, as comparison is frequently made with only one high dispersion measure, which frequently lies within two standard deviations of the dispersion of the V camera results. However, for UY Cen the high dispersion measures bracket the low dispersion measures in time, and the systematic difference therefore seems better established.

The corrected V camera velocities, listed in column 9 of Table 4.04 are found by subtracting 4.8 km s^{-1} from all the velocities in column 2. These corrected velocities are combined with the high dispersion velocities in column 5 to give the final mean velocities listed in column 10.

TABLE 4.04

	V Camera			High Dispersion					
	Mean	σ	N	Mean	σ	N	V-High	V Camera corrected	V_{final}
GP Ori	+86.9	8.2	16	+79		1	+7.9	82.1	80
FU Mon	-19.9	9.1	10	-22.2		1	+2.3	-24.7	-23
V372 Mon	+21.4		3					+16.6	17
Hen 244	+30.9		2	+26		2	+4.9	+26.1	26
Hen 250	+19.3	3.5	4	+12		1	+7.3	+14.5	13
BH Cru	+ 9.5		2	+5		1	+4.5	+ 4.7	5
UY Cen	-15.0	2.2	5	-19	3.3	5	+4.0	-19.8	-19
AM Cen	-21.0	5.2	4	-22		2	+1.0	-25.8	-24
VY Aps	-32.1	2.2	7	-40		1	+7.9	-36.9	-38
Hen 166	-13.1		4	-13		2	-0.1	-17.9	-15
LQ Ara	+ 4.1		3	-4		2	+8.1	- 0.7	-2

TABLE 4.05

	ℓ	b	ρ
GP Ori	186.0	-15.8	70
FU Mon	206.6	- 4.9	-36
V372 Mon	207.9	- 0.10	4
Hen 244	285.6	-17.0	14
Hen 250	285.4	- 3.5	2
BH Cru	298.0	6.3	-2
UY Cen	307.6	17.9	-22
AM Cen	311.3	8.6	-28
VY Aps	314.8	-16.1	-44
Hen 166	330.2	- 7.4	-16
LQ Ara	328.2	-10.6	-4

4.05 Reduction of Velocities to the Local Standard of Rest

The final set of velocities given in Table 4.04 are heliocentric radial velocities. Before they can be interpreted with a model of the galaxy they must be referred to the Local Standard of Rest (LSR) This is defined as a frame of reference that rotates in a circular orbit about the galactic centre at the distance of the sun. For practical purposes the standard of rest can be defined as the mean motion of young stars in a volume of space centred on the sun. The best estimate of this, based on radial velocities, is that given by Balona and Feast (1974):

$U_o = +7.4$
$V_o = +13.0$
$W_o = +7.0$

Where U_o V_o W_o are the sun's motion (km s^{-1}) with respect to the standard of rest defined by OB stars. The frame of reference is defined such that U points to the galactic centre, V in the direction of galactic rotation and W above the galactic plane.

The radial velocities of the SC stars in column 4 of Table 4.05 are referred to this local standard of rest.

4.06 Peculiar Motion and Velocity Dispersion

As the galaxy has evolved, the gas which was probably initially spherically distributed about the galactic centre and moving with large random velocities, has become more and more concentrated toward the galactic plane. This progressive relaxation is a result of the frequent interaction of gas and dust. The density of stars in space is so low, that they almost never encounter each other and once formed tend to preserve the motion of the material out of which they were created. As a result, older stars appear less confined to the galactic plane and show a larger velocity dispersion than younger stars. Older stars also show a much greater proportion of high eccentricity orbits, when compared with young stars. The mean circular velocity of these old high eccentricity stars is found to be less than that of the LSR. This can be deduced as follows for a simple model of the galaxy where all the mass is considered to be concentrated at the galactic centre. In this model, stars which are at their maximum distance from the galactic centre when near the sun, will have tangential velocities

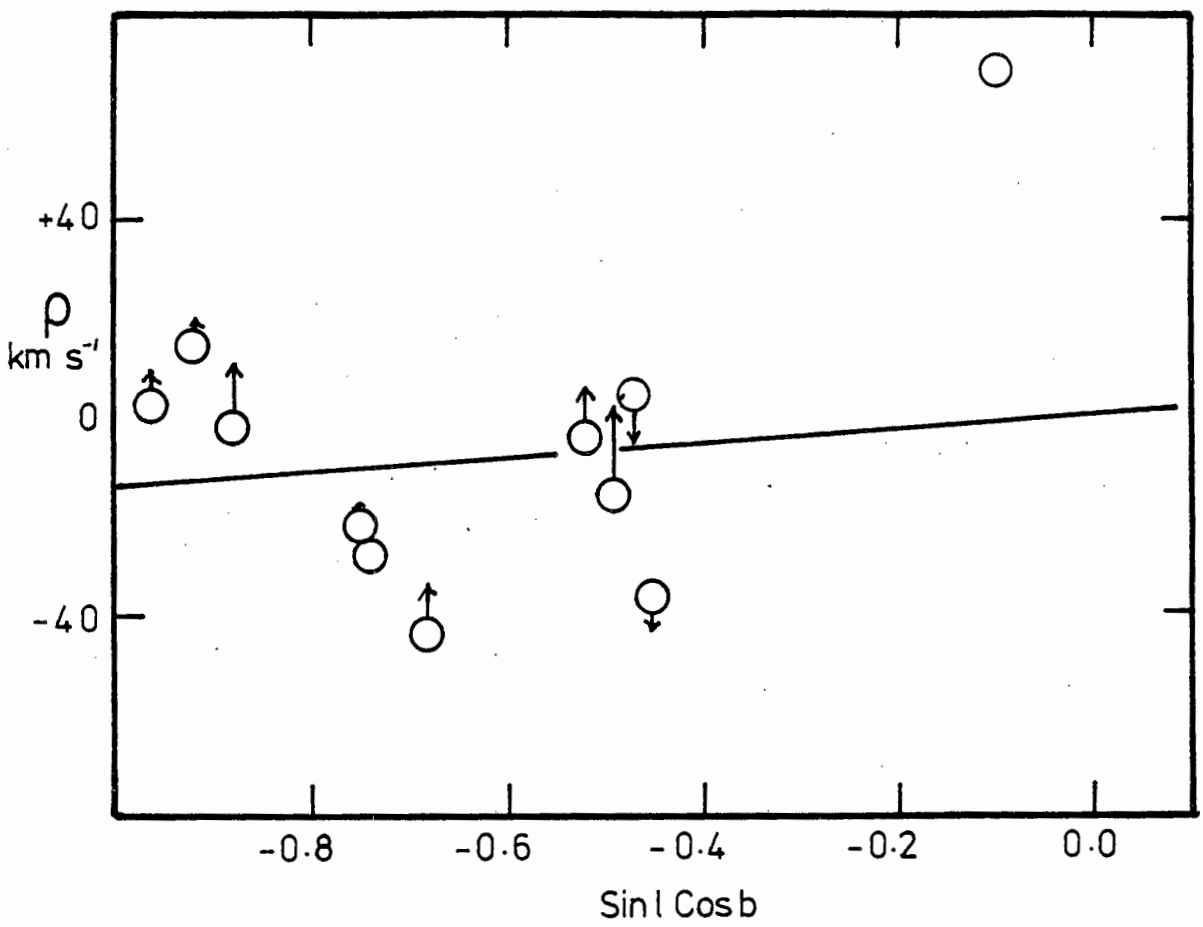

Figure 4.02

The radial velocity, corrected for the standard solar motion is shown as a function of "sin ℓ cos b" for the SC stars. The straight line is a least squares fit constrained to go through the origin. The arrows indicate the effect of correcting for galactic rotation.

given by:

$$\theta_x = \theta_{LSR} \sqrt{(1-e)} \qquad (4.02)$$

where θ_x is the tangential velocity of a star at the sun, in an orbit of eccentricity e. This equation is derived from equation 53 of Smart (1962). As the eccentricity varies between the limits $0 < e < 1$ then θ_x will vary between the limits $\theta_{LSR} > \theta_x > 0$. Such objects will therefore always lag behind the Local Standard of Rest. For stars at their minimum distance from the galactic centre at the distance of the sun, the simple theory predicts;

$$\theta_x = \theta_{LSR} \sqrt{(1+e)} \qquad (4.03)$$

As the eccentricity varies between $0 < e < 1$, θ_x varies between $\theta_{LSR} < \theta_x < \theta_{LSR}\sqrt{2} = Vel_{escape}$

Since the sun lies towards the edge of the galaxy, there are more stars with mean distances to the galactic centre, less than that of the sun in the solar neighbourhood, so the high velocity stars will show velocities which are negative with respect to the Local Standard of Rest. More advanced theory given by Oort (1965 page 455) predicts a relationship between velocity dispersion in the U direction and deviation from the standard solar motion. This is illustrated by Delhaye (1965 page 72).

Feast (1963), discussing the motions of the long period variables, showed that the only significant deviations from the standard solar motion do indeed occur in the V direction.

V_o, the deviation from the local standard of rest, can be found from;

$$V_o \text{Sin } \ell \text{Cos} b = \rho, \qquad (4.04)$$

where ρ is the radial velocity corrected for the standard solar motion.

A weighted mean value of $V_o = 14 \pm 14$ km s^{-1} is found when the weight is $(\text{Sin } \ell \text{ Cos } b)^2$. The dispersion of velocity about zero is 31 ± 7 km s^{-1}. This value does not include a correction for the instrumental dispersion which, judged on the basis of the standard errors given in Table 4.04, will be negligible. The results are shown in Fig. 4.02. When the effects of differential galactic rotation are removed (as discussed in the next section) the deviation from the LSR becomes $V_o = 5 \pm 13$ km s^{-1} and the velocity dispersion is reduced to 30 km s^{-1}. The deviation from the LSR does not differ significantly from zero. This sets an upper limit on

the age of the SC stars of less than that of Intermediate Population II objects (Blaauw 1965). The velocity dispersion sets a lower limit on the age. The velocity dispersion given here can be compared with the dispersions given by Delhaye (1965). Since the SC stars lie in the galactic plane, the appropriate comparison is with

$$\frac{\Pi^2 + \Theta^2}{2}$$

in Delhaye's notation. This is important as it is clear that the dispersion in Π, the direction away from the galactic centre, is greater and more sensitive to population type than that in the direction of galactic rotation Θ. Comparison with Delhaye's Table 2 and Blaauw's Table 3 indicates that the SC stars lie somewhere in the region of Old Pop I and Disk Population objects.

Dean (1976) has discussed the kinematics of 180 carbon stars. None of his subgroupings show a significant deviation from the standard solar motion but his early carbon stars show a velocity dispersion of 33 km s^{-1} in the plane, similar to the value found here.

4.07 Differential Galactic Rotation

The galaxy does not rotate as a rigid body but to a first approximation the stars in the plane can be considered to rotate in orbits about a mass concentrated at the centre. Therefore the closer a star is to the galactic centre the shorter will be its period and the greater its orbital velocity. When viewed from a frame of reference on a circular orbit, for instance the LSR, stars toward the galactic centre ($\ell = 0°$) will overtake, while stars away from the galactic centre $\ell = 180°$ will trail behind. Stars at $\ell = 90°$ and $\ell = 270°$ will be on the same circular orbit and will therefore not appear to move. It is clear from this that not only is a star's radial velocity zero at $\ell = 90°$ and $\ell = 270°$ but also at $\ell = 0°$ and $\ell = 180°$ where its motion is entirely tangential to the line of sight. A star's radial velocity will be at a positive maximum at $\ell = 45°$ and $\ell = 225°$ at a negative maximum at $\ell = 135°$ and $\ell = 315°$.

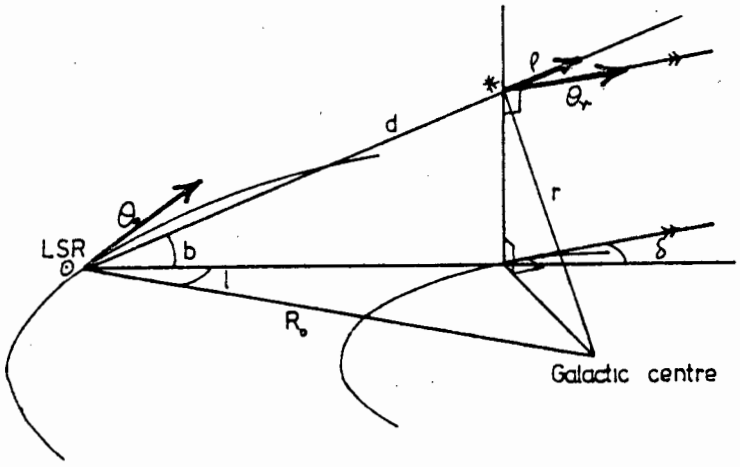

Fig. 4.03

Consider a star ✳ as illustrated in Fig. 4.03, at a distance d and at Galactic longitude ℓ and galactic latitude b with respect to the LSR. Let the star have velocity θ_r at a distance r from the galactic centre. Let the LSR have velocity θ_o at distance R_o. Let ρ = the radial velocity of ✳ as seen from the LSR and given in column 4 of Table 4.05.

Then

$$\rho = \theta_r \cos\delta \cos b - \theta_o \sin \ell \cos b \qquad (4.05)$$

It can be seen by use of the sine formula that

$$R_o/\sin(90 + \delta) = (r^2 - d^2 \sin^2 b)^{1/2}/\sin \ell \qquad (4.06)$$

which gives

$$\rho = \sin \ell \cos b \left(\frac{R_o \theta_r}{(r^2 - d^2 \sin^2 b)^{1/2}} - \theta_o\right) \qquad (4.07)$$

This relation is exact and assumes only that the stars are on concentric orbits. Since the stars considered are close to the sun r>>d and (4.07) becomes

$$\rho = \sin \ell \cos b \left(\frac{R_o \theta_r}{r} - \theta_o\right) \qquad (4.08)$$

to a first approximation

$$\theta_r = \theta_o + \left(\frac{d\theta}{dr}\right)_{R_o} (r-R) \qquad (4.09)$$

In a Keplerion system, $\frac{d\theta}{dr} \sim \frac{1}{r^2}$ whereas $\frac{d\omega}{dr} \sim \frac{1}{r^3}$, so that (4.09) might be expected to be a better approximation than working in terms of ω.

Substituting (4.08) in (4.09) gives

$$\rho = (R_o - r)\left\{\frac{\theta_o}{r} - \frac{R_o}{r}\left(\frac{d\theta}{dr}\right)\right\} \sin \ell \cos b \qquad (4.10)$$

The Oort constant A is defined by

$$A = \frac{1}{2}\left\{\frac{\theta_o}{R_o} - \left(\frac{d\theta}{dr}\right)_{R_o}\right\} \qquad (4.11)$$

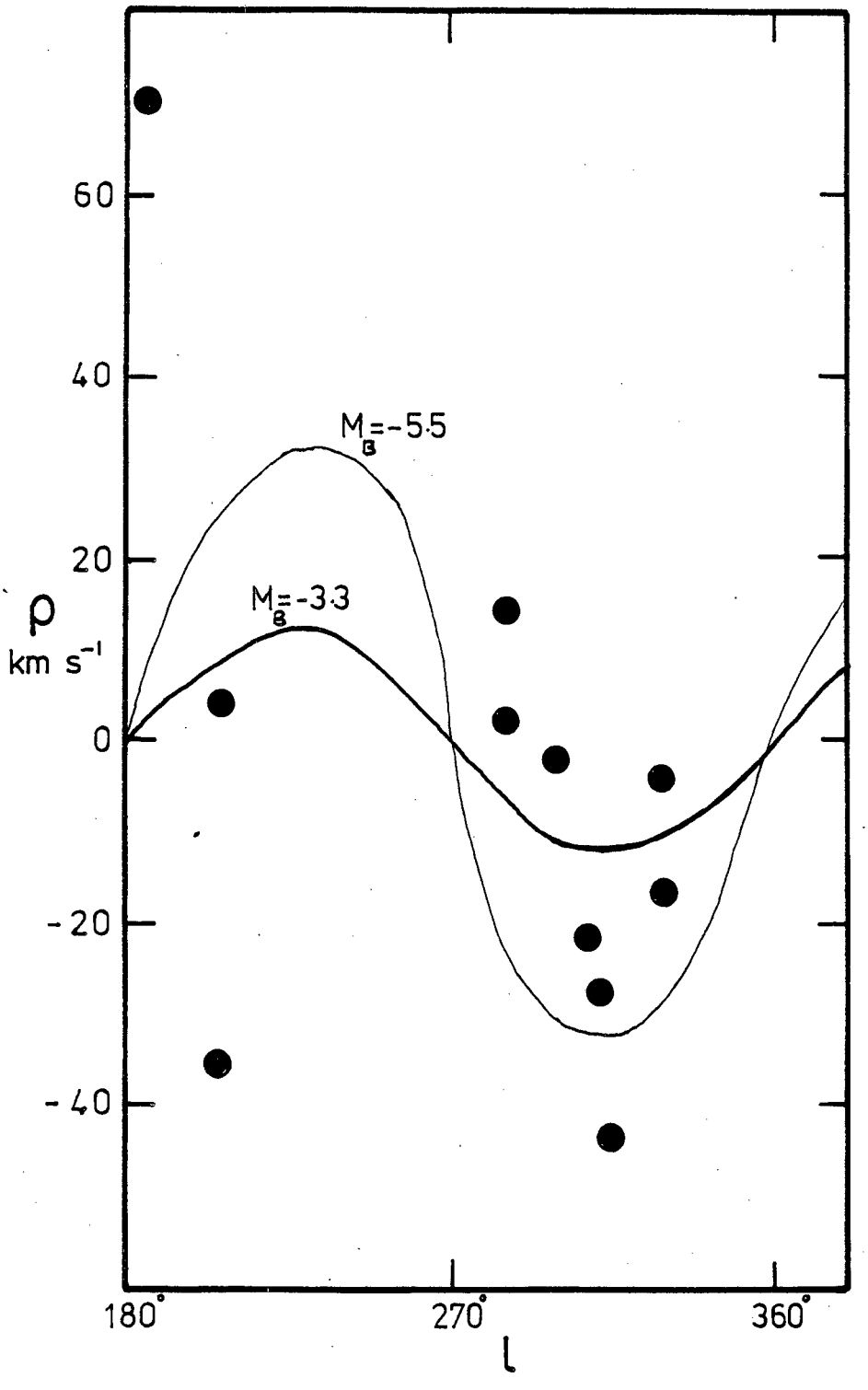

Figure 4.04

The radial velocity, corrected for the standard solar motion is shown as a function of galactic longitude. The two curves give the galactic rotation curves, if all the stars were at the mean distance indicated by the absolute magnitudes.

Comparing equations 4.10 and 4.11 and assuming that $\frac{\Theta_o}{r} \simeq \frac{\Theta_o}{R_o}$ and that $\frac{R_o}{r} \simeq \frac{\Theta_o}{R_o}$ and that $\frac{R_o}{r} \simeq 1$, equation 4.10 reduces to

$$\rho = 2A(R_o - r) \text{ Sin } \ell \text{ Cos } b \qquad (4.12)$$

The apparent and absolute bolometric magnitudes are related by

$$m_{bol} - M_{bol} = 5 \log\{100d\} \qquad (4.13)$$

where d is in kiloparsec. While d is related to R_o and r by

$$r^2 = d^2 + R_o^2 - 2d\, R \text{ Cos } b \text{ Cos } \ell \qquad (4.14)$$

The values of ρ are used to obtain a weighted mean value for A, where weights are given by $((R_o - r) \text{ Sin } \ell \text{ Cos } b)^2$. The distance to the galactic centre is taken as $R_o = 9$ kpc

Using an initial $M_{BOL} = -3.5$ we find

$$A = 16 \pm 15 \text{ km s}^{-1} \text{ kpc}^{-1}$$

Assuming that the true value of A = 17 km s^{-1} kpc^{-1}, as given by Balona and Feast (1974), then the derived value of M_{BOL} becomes -3.3. The one standard deviation error limits indicate that it is improbable that the absolute magnitude will be brighter than -4.8. Fig. 4.04 shows values of ρ for individual stars, and also galactic rotation curves for two values of M_{BOL}. These curves would only apply if all the stars were at the same distance, but do illustrate the size of the rotation effect and the relative importance of different stars in determining the Oort constant.

4.08 Galactic Distribution

The luminosities obtained in the previous section enable the distribution of these objects in the galaxy to be studied.

It is clear from inspection of Table 4.05 that the SC stars have small galactic latitudes, which is in itself an indication that they are not old objects. Examination of the stars' distribution in galactic longitude, shows that despite the fact that the galactic plane extends in the southern hemisphere from 210° to 30°, all but three of the objects lie between $\ell = 285°$ and $\ell = 330°$. Were this non uniform distribution to reflect an observational selection effect, it would imply that there should be 50 SC in the sky. Yorka (1976) has shown that both the S and

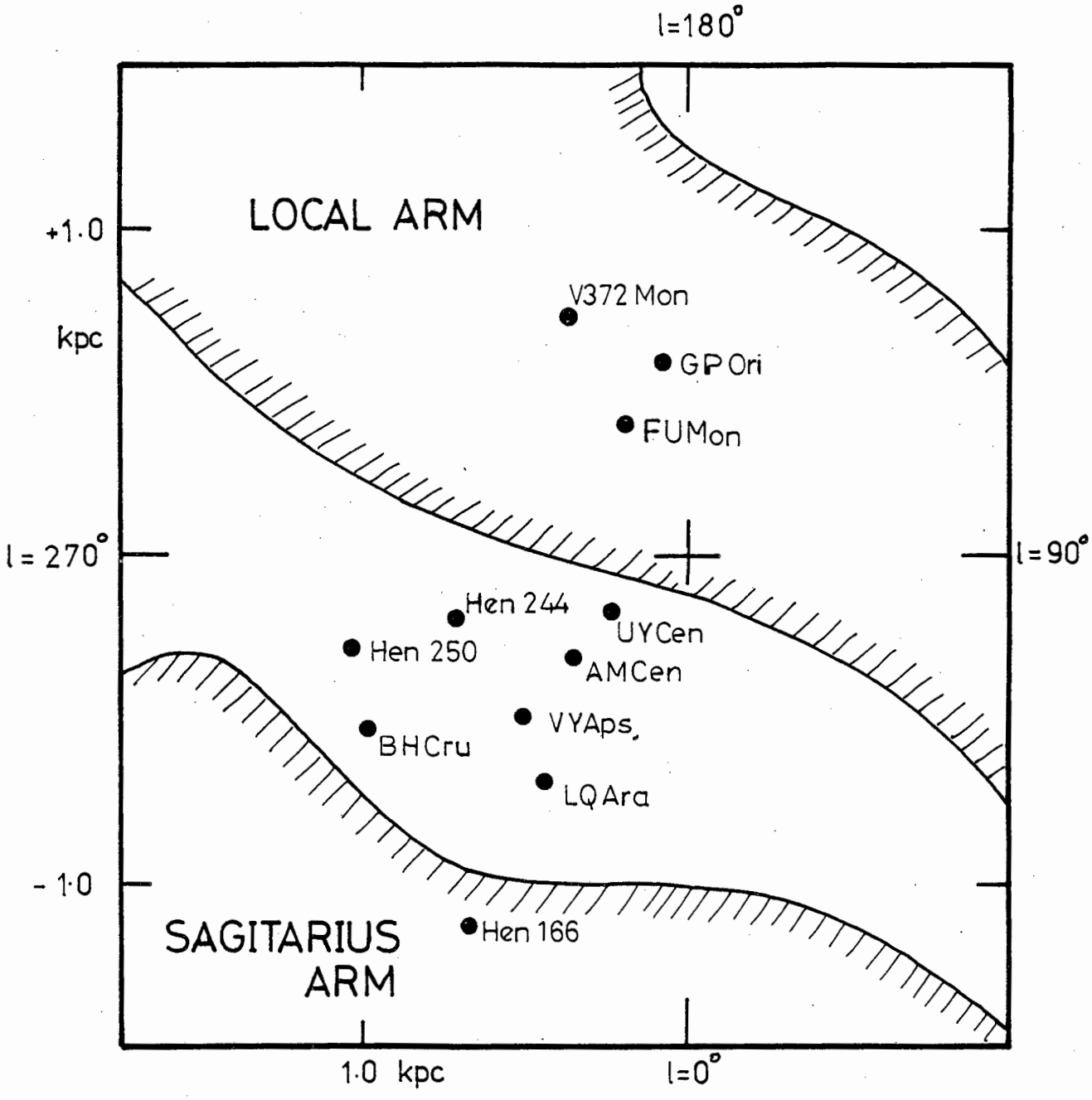

Figure 4.05

The distribution of the SC stars in the galactic plane using M_{BOL} = -3.5. The large cross marks the sun while two nearby spiral arms are also shown.

the C stars are more strongly concentrated in the region 210° to 280° but the M giants within 2° of the galactic plane from Blanco (1965), show a concentration in the direction 285 to 340°. It is interesting to note that the SC stars show a longitude distribution more like that of M giants than that of carbon or S stars. The distribution of SC stars in the plane is shown in Fig. 4.05. Also outlined are spiral arms, as defined by the young galactic clusters and HII regions, and illustrated by Becker and Fenkart (1970). It is clear from this diagram that the maximum in the number of S and C stars, between 210° and 280°, is in the direction between two spiral arms, where less absorption would be expected. On the other hand the M star concentration lies in the direction of the Sagitarius arm, which indicates that these objects are probably associated with that arm.

The SC stars have been plotted at distances corresponding to an absolute magnitude of $M_{BOL} = -3.5$. With this absolute magnitude it is clear that only one of the eight SC stars lying in the direction of the Sagitarius arm is actually inside the arm. The percentage of stars inside a spiral arm is shown as a function of absolute magnitude in Fig.4.06.At the right hand side of the figure the mean modulus height, $\overline{|Z|}$ of the SC stars, above the galactic plane is also shown. The population types marked are taken from Blaauw (1965) (Stellar Populations page 444).

It is clear from Fig. 4.06 that if all the stars are forced to be in spiral arms, then their mean height will be too great for a spiral population. Alternatively, if the SC stars are allowed to remain between the spiral arms, as in a disk population, then they are too strongly confined to the galactic plane and would imply that there are many as yet undiscovered SC stars of similar brightness not only at high galactic latitudes but at other galactic longitudes. Neither of these limiting situations seems very probable.

4.09 Possible Mixed Population or Runaway Origin of the SC Stars

We have made the assumption, throughout the previous sections, that the SC stars are a kinematically homogeneous group of objects. However the large peculiar radial velocity of 70 km s^{-1} shown by GP Ori, casts doubt on this assumption and suggests that GP Ori is either a much older object or a runaway star. The long run of V camera plates

rules out the possibility that the high radial velocity of GP Ori is caused by binary motion.

Population II C stars, known as CH stars, are well known e.g. Keenan (1958) while Catchpole and Feast (1971b) have identified a population II S star. This star has a radial velocity of 300 km s^{-1} and has a spectrum which at 80 Am^{-1} is otherwise indistinguishable from that of a normal S star. It therefore seems quite possible that Population II objects might exist amongst the SC stars.

Although unfortunately no proper motion is available for GP Ori the radial velocity is not as great as that seen in extreme Pop II objects and is not unusual for that found in Disk or Intermediate Pop II objects. For example Catchpole et al. (1977) discussing the Ba stars, identify a group of 27 metal weak stars, which have a velocity dispersion of 33 ± 4.5 km s^{-1} but which includes two stars with velocities of about 80 km s^{-1}. They consider that these stars are probably disk population or intermediate Pop II objects.

The position of GP Ori near a node of the galactic rotation curve means that it has a low weight in the determination of the Oort constant A.

If the SC stars were considered very young objects with a velocity dispersion of about 12 km s^{-1} then FU Mon and GP Ori, having velocities at least 3 x the dispersion, would both qualify as runaway stars. In order to have a Z distribution similar to that of extreme Pop I objects the SC stars would have to have an absolute magnitude of less than -3, which is itself quite reasonable. However their space distribution would then not resemble Pop I objects unless they were all brought into the local arm, which would require an absolute magnitude of about 0.0. This would make the SC stars rather less luminous than S and C stars and would leave unexplained their uneven distribution in galactic longitude. On present evidence the runaway hypothesis need not be further considered.

4.10 The SC Star in the LMC

Richer and Frogel (1980) report the discovery of a super-lithium-rich (SLR) SC star in the LMC (LMC 89). This is very exciting as the probability of discovering an SC star, at a time when no S and few C stars have been found, is very low. The well determined distance of the LMC allows Richer to give an

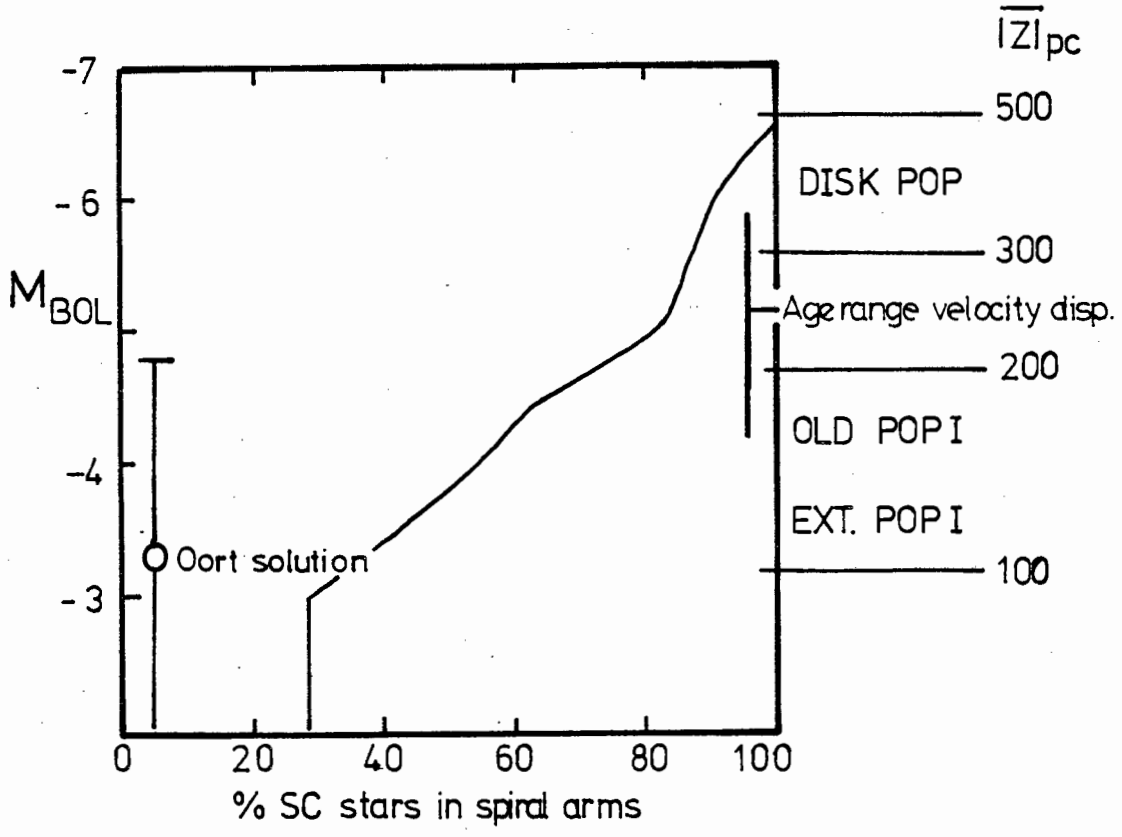

Figure 4.06

A composite diagram representing the galactic distribution and absolute magnitude data for the SC stars. The M_{BOL} and galactic height, Z, scales are coupled by the actual SC star distribution. The age calibration is from Blaauw (1965). The % of SC stars in spiral arms is based on Fig. 4.05.

accurate value of $M_{BOL} = -5.45$ for this star. This is very similar to the values found by Feast, Catchpole and Glass (1976) for certain S and SLR S stars, but is about 2 magnitudes brighter than the mean value, given for our SC stars, by the Oort constant solution.

Examination of Fig. 4.06 shows that the higher luminosity would have two advantages in that it would place more of the SC stars in spiral arms and would imply a greater degree of compatibility between the observed velocity dispersion and the mean height above the plane. Were the SC stars at the distance implied by the LMC SC star, then the light line drawn in Fig. 4.04 shows the expected rotation curve. It is clear that the derived Oort constant depends heavily on the stars between $\ell = 290°$ and $330°$ and they are not wildly uncompatible with the larger amplitude curve implying the brighter M_{BOL}.

It is of course not certain that the LMC SLR SC star has the same intrinsic luminosity as the galactic SC stars.

4.11 Conclusion

The small number of SC stars available makes it very difficult to determine their properties from statistical arguments. By simultaneously considering all the available evidence it is possible to set reasonable limits on their age and luminosity. The evidence is all presented in Fig. 4.06. Fig. 4.06 has the advantage of allowing one to see, the way in which the spatial distribution of the SC stars in and above the galactic plane, depends on the adopted M_{BOL}.

The compromise that must be struck between, the space distribution, velocity dispersion, Oort constant solution and the LMC luminosity, is highly subjective.

We suggest that the best compromise is to assume that the SC stars are intermediate between old population I and disk objects, with an absolute Bolometric magnitude in the range -3.5 to -5.5 and a mean value of -4.5. This corresponds to a value of $M_V = -1.5$. The adopted age implies that these are objects of about 1.5 solar mass.

CHAPTER 5

The Chemical Composition of UY Cen

5.01 Introduction General Survey

The wide diversity of spectra amongst cool stars indicates that these objects possess a range of abundances. This range of abundances has been confirmed by curve of growth analyses which indicate that the major variations occur in the C/O ratio, the Li abundance and the relative proportion of s-process elements. The great interest in these abundance variations arises because these stars may constitute an important source of such elements in the universe. The appearance of abundance anomalies in some but not all cool giants, must also provide important clues as to their evolutionary history.

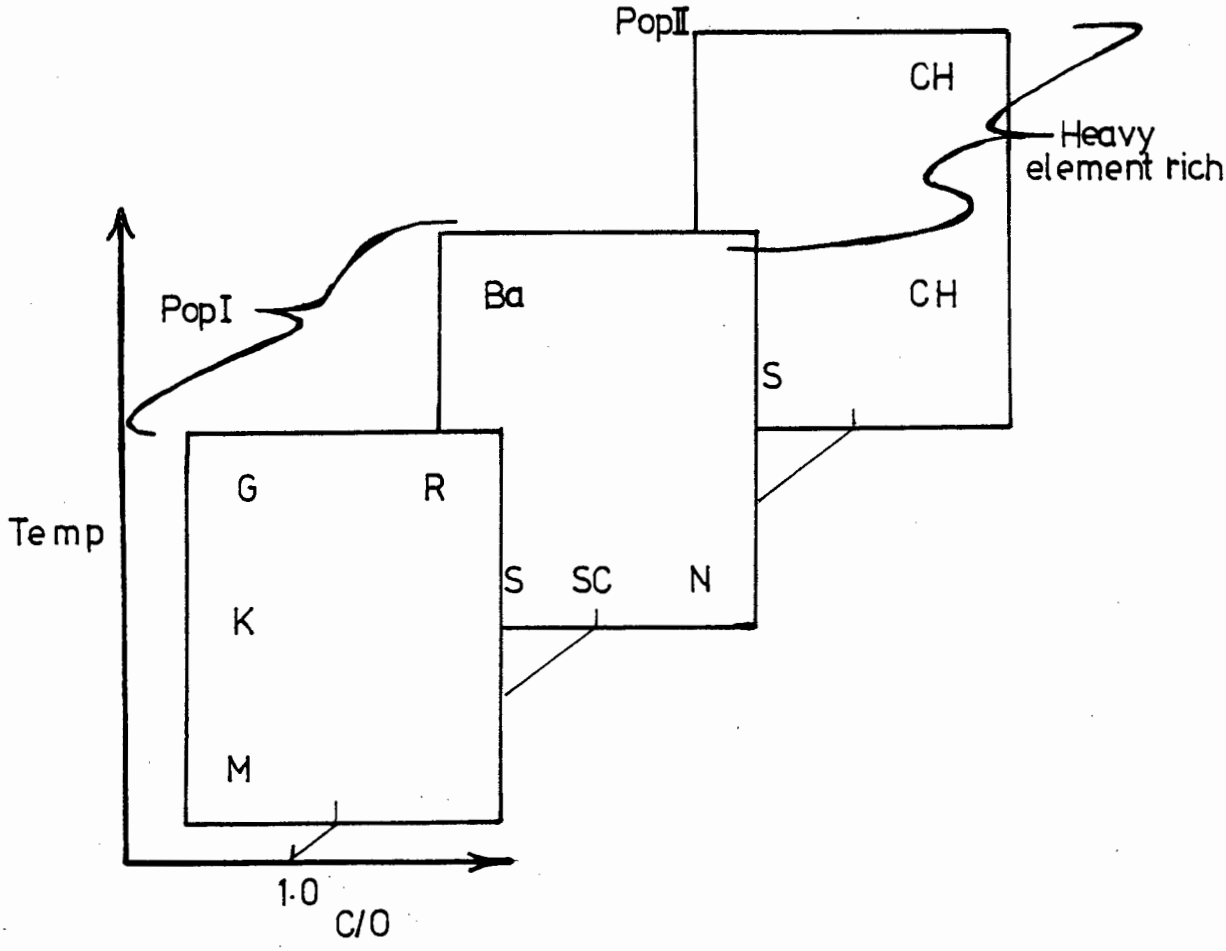

Figure 5.01

The distribution of cool stars as a function of C/O, Population Type and temperature.

Fig. 5.01 summarizes the distribution of the different types of cool star with temperature, population, s-process richness and C/O ratio. The temperature axis may also correspond to an inverse luminosity axis although this would not necessarily imply there is evidence for evolution directly from one type of object to another.

Abundance analyses of cool stars by, among others, Utsumi (1970) 22 cool stars, Tsuji (1962) 2 S stars, Kilston (1975) 8 N stars, Yamashita (1973) GP Ori FU Mon, Culver (1971) the SC star CY Cygni and Catchpole Feast (1976) SLR S star RZ Sgr, have, with the exception of Kilston, (1975) all been based on a simple curve of growth analysis. Kilston undertook a spectrum synthesis in an attempt to overcome the severe blending problems, introduced by CN in carbon stars. These analyses show that amongst the heavy element rich stars, the variations of heavy metal abundance with atomic weight can be divided into two distinct classes. The first class, characterized by overabundances of elements of both the 5th (Rb Sr Y Zr..) and 6th (Cs Ba La Ce..)periods, is shown by Ba, S, SC, N and SLR S stars. The second, showing only an enhancement of 6th period elements, is found in CH stars and ^{13}C rich N stars, including the SLR N star WZ Cas. It is possible that the RCB star U Aqr may represent a 3rd class in which only elements of the 5th period are enhanced. Bond et al.(1979) report that U Aqr shows Sr and Y enhancements relative to Fe of the order 2 dex, while the heavier elements appear normal. Because their atmospheres are relatively free of the effects of either CN or TiO and ZrO the SC stars present an ideal opportunity to examine. cool star abundances. This is undoubtedly due to the fact that C/O ≈ 1 so that all the carbon and oxygen is locked up in CO. Yamashita (1973) has analysed the SC stars GP Ori and FU Mon, using 40 A mm^{-1} spectra and Culver (1971) has analysed the SC star CY Cygni, using spectra of between 8 A mm^{-1} and 17 A mm^{-1} dispersions. The major advantage of the present analysis is the more extensive wavelength coverage of the spectra and the fact that it has been preceded by a detailed line identification program.

5.02 The Model Atmosphere

The spectrum of a star is formed in its outermost layers down to depths at which a photon when once emitted can just escape from the star's surface, without further scattering or absorption. The physical depth over which this occurs depends on the opacity of the star's atmosphere. The mean opacity of the atmosphere controls the temperature gradient, which exists as a consequence of the outward flow of radiation from the stars interior. The star's opacity can be thought of as consisting of two parts: a part which varies slowly with wavelength and which controls the flux distribution in the continuum and a rapidly varying part, which forms the absorption lines. The opacity is high in the centre of a strong absorption line so that radiation only escapes from the highest and coolest parts of the star's atmosphere. The lower emissivity of this cooler region results in the line appearing dark in contrast to the adjacent continuum. The strength of an absorption line will depend on the number of atoms capable of forming the line. The total number of atoms present in the line forming region will depend partly on the abundance of the element and its degree of ionization but will also depend on the continuum opacity. The higher the continuum opacity the less deep will the radiation emerge and the less atoms will be present in the line of sight. The problem of relating the number of atoms present to the observed strength of an absorption line is the problem of constructing a model atmosphere. Models can only be successfully constructed where there is accurate information regarding the sources of continuous opacity. H.R. Johnson (1974) has constructed model atmospheres that are appropriate to very cool stars; these will be used to derive abundances and to give clues as to possible effects of stratification that may occur in UY Cen.

The effects and origins of the opacity are not known with sufficient accuracy in UY Cen, to justify attempting to construct a model but useful abundance information can be obtained from a simple curve of growth analysis and by comparison with already existing models.

The curve of growth analysis is itself based on a simple model. The two simplest models of a star's atmosphere are the Milne-Eddington (ME) and the Schuster-Schwarzchild (SS) models. Both models, which constitute opposite limiting approximations to what happens in a star, assume the star's atmosphere can be described as a parallel slab. In

the ME model, lines are formed by pure scattering and throughout the line forming region the ratio of the selective (line forming) absorption to the continuous absorption, is considered constant. Exact curves of growth for this model have been computed by Wrubel (1949). In the SS model, lines are formed by pure absorption above the source of continuous opacity and exact curves of growth have been computed by van der Held (1931). More generally the curve of growth can be thought of as a saturation curve that relates the observed strength of a line to the strength it would have in the weak line approximation, where its strength is simply proportional to the number of atoms forming the line.

The derivation of the relation between the observed equivalent width and the number of atoms present is divided into parts. The equation of transfer, describing the flow of radiation through the star's atmosphere is derived in the first part. In the second part the ME and SS models are described, compared, and then linked to the equation of transfer. The variation of the line absorption coefficient with frequency is found in the third part, while the form of the curve of growth is described in the last part. The theoretical derivation described below is based on the following sources. Mihalas (1977), Powell (1969), Aller (1963) and Cowley (1970).

5.03 The Theory of Line Formation

The Equation of Transfer

Consider a volume element, δs long, having area $\delta\sigma$ in the S direction, in a plane parallel atmosphere, as illustrated in Fig. 5.02 where Z is the direction of the outward normal.

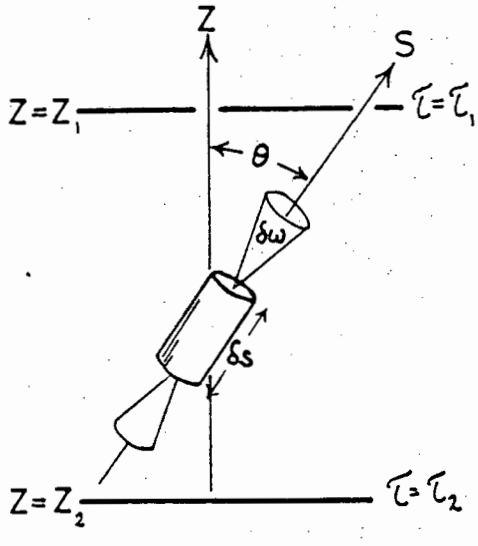

Fig. 5.02

The amount of energy δe_{in}, that enters the volume element $\delta s \delta\sigma$ along the direction S, through solid angle $\delta\omega$ in frequency interval $\delta\nu$ in time δt, is given by

$$\delta e_{in} = I(\nu,s,\theta)\delta\omega\ \delta\sigma\ \delta\nu\ \delta t \qquad (5.01)$$

where $I(\nu,s,\theta)$ is the intensity at frequency ν position S and in the direction θ along the line S.

The amount of energy δe_{out} that leaves the volume element along the same direction is given by

$$\delta e_{out} = I(\nu,s+\delta s,\theta)\delta\omega\delta\sigma\delta\nu\delta t \qquad (5.02)$$

Let γ equal the emission coefficient per atom of the material in the volume element and let K equal the absorption coefficient per atom. Let there be N atoms per cubic centimetre in the volume element. The difference between the amount of energy entering the volume element and the amount leaving must be equal to the difference between the amount created and the amount absorbed. Equations (5.01) and (5.02) can be re-written

$$\{I(\nu,s+\delta s,\theta)-I(\nu,s,\theta)\}\delta\omega\delta\sigma\delta\nu\delta t=\{\gamma(\nu,s,\theta)-K(\nu,s,\theta)I(s,\theta,\nu)\}N\delta\omega\delta\sigma\delta\nu\delta t\delta s$$

In the limit this may be written

$$\frac{I}{N}\frac{dI}{ds}(s,\theta,\nu) = \gamma(s,\theta,\nu) - K(s,\nu,\theta)I(s,\theta) \qquad (5.03)$$

For a two dimensional plane parallel atmosphere

$$dz/ds = \text{Cos } \theta \equiv \mu$$

The source function $S_\nu(z)$ is defined to be

$$S_\nu(z) = \gamma_\nu(z)/K_\nu(z)$$

The optical depth is defined by the relation

$$\tau_\nu(-z) = \int_{z_1}^{z_2} N(z)K(z)dz$$

The optical depth is defined to increase inward from the surface by the relation

$$d\tau_\nu(z) = -N(z)K_\nu(z)dz$$

Using all these relations equation 5.03 can be rewritten

$$\mu\left(\frac{dI_\nu}{d\tau_\nu}\right) = I_\nu - S_\nu \qquad (5.04)$$

This is a first order linear differential equation which can be solved by multiplying through by the integrating factor $e^{-\tau/\mu}$
Equation 5.04 becomes

$$\exp(-\tau/\mu)\frac{dI_\nu}{d\tau_\nu} - \frac{1}{\mu} I_\nu \exp(-\tau/\mu) = -\frac{1}{\mu} S_\nu \exp(-\tau/\mu)$$

$$\frac{d}{d\tau_\nu}\left[I_\nu \exp(-\tau/\mu)\right] = -\frac{1}{\mu} S_\nu \exp(-\tau/\mu)$$

This is integrated to give

$$I_\nu \exp(-\tau/\mu) = -\frac{1}{\mu}\int S_\nu \exp(-\tau/\mu)\, d\tau + C \qquad (5.05)$$

Consider the boundary conditions for outward flowing radiation through the plane parallel slab illustrated in Fig.5.02.At the base of the slab where $\tau = \tau_2$ the slab receives radiation of intensity $I_\nu(\tau_2)$. But at the base of the slab the integral of the source function for outward flowing radiation must equal zero. Hence from equation 5.05

$$C = I_\nu(\tau_2) \exp(-\tau_2/\mu)$$

Now consider the top boundary of the slab at $\tau = \tau_1$ equation 5.05 with the above value of the constant becomes.

$$I_\nu(\tau_1) \exp(-\tau_1/\mu) = -\frac{1}{\mu}\int_{\tau_2}^{\tau_1} S_\nu \exp(-\tau/\mu)\, d\tau + I_\nu(\tau_2) \exp(-\tau_2/\mu)$$

This can be rewritten as

$$I_\nu(\tau_1) = \frac{1}{\mu}\exp(\tau_1/\mu)\int_{\tau_1}^{\tau_2} S_\nu \exp(-\tau/\mu)\, d\tau + I_\nu(\tau_2)\exp(-(\tau_2-\tau_1)/\mu)$$

$$= \frac{1}{\mu}\int_{\tau_1}^{\tau_2} S_\nu \exp(-(\tau-\tau_1)/\mu)\, d\tau + I_\nu(\tau_2)\exp(-(\tau_2-\tau_1)/\mu)$$

When $\tau_1 = 0$, which is the case at the surface of a star

$$I_\nu(\tau_1=0) = \frac{1}{\mu}\int_0^{\tau_2} S_\nu \exp(-\tau/\mu)\, d\tau + I_\nu(\tau_2)\exp(-\tau_2/\mu) \qquad (5.06)$$

This is the form of the equation of transfer appropriate to radiation flowing out of a plane parallel slab.

The Schuster-Schwarzchild Model

The Schuster-Schwarzchild (SS) model is the simplest approximation to a stellar atmosphere in which lines are formed by pure absorption in a plane parallel isothermal slab. This model, illustrated in Fig. 5.03 corresponds closely to the traditional view that the solar absorption spectrum was formed in a cool reversing layer above a hotter photosphere.

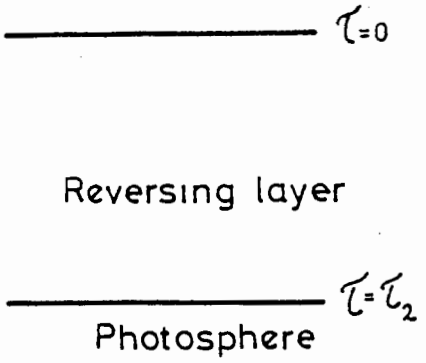

Fig. 5.03

Curves of growth for the SS model were first computed by van der Held (1931) and have recently been extensively tabulated by Powell (1969). Cowley and Cowley (1964), in their study of the sun and Gasson (1966) in her study of Arcturus, find that their empirical curves of growth correspond closely to van der Held curves.

The SS model ignores the sphericity of the star and also assumes that local thermodynamic equilibrium (LTE) exists in the slab. This second assumption means that S_ν can be replaced by the Planck function B_ν. Using all these conditions equation 5.06 of the previous section, which is for the equation of transfer, becomes;

$$I_\nu(\tau=0)\ \text{continuum} = I_\nu(\tau_2)\ \text{continuum} \qquad (5.07)$$

$$I_\nu\ (\tau=0)_{\text{line}} = I_\nu(\tau_2)\ \exp(-\tau'_2) + B_\nu\ (1 - \exp(-\tau'_2)) \qquad (5.08)$$

Here τ'_2 is the optical depth in the line at the physical depth defined by $\tau_{\text{continuum}} = \tau_2$.

The Equivalent Width (EW) is a very convenient measure of the strength of an absorption line and is defined in Fig.5.04. Fig.5.04 shows the intensity distribution or spectrum of the star, in the region of an absorption line A, with EW = W_ν. The EW is defined such that the amount of energy represented by $W_\nu X\ I_{\text{cont}}$ is equal to the amount of energy removed from the star spectrum by the absorption line. In otherwords area A equals area B in Fig.5.04. W_ν has the dimensions of frequency.

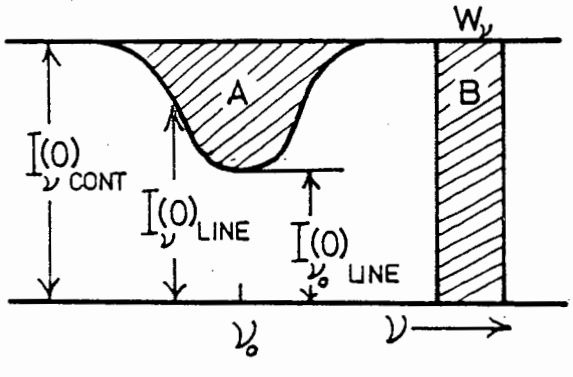

Fig. 5.04

Let r_ν = the depth of the line at frequency ν where r_ν is defined by

$$r_\nu = \frac{I_\nu(o)_{\text{cont}} - I_\nu(o)_{\text{line}}}{I_{\nu\ \text{cont}}} \qquad (5.09)$$

The equivalent width W is then given by the equation

$$W_\nu = \int_0^{+\infty} r_\nu d\nu \qquad (5.10)$$

If equations 5.07 and 5.08 are substituted in equation 5.09

$$r = (1 - \exp(-\tau'_2(\nu))(1 - \frac{B(\nu)}{I_{\tau_2}(\nu)}) \qquad (5.11)$$

In this equation τ'_2 is shown as a function of ν and $I_{\nu cont}(\tau_2)$ has been replaced by $I_{\tau_2}(\nu)$ to make the notation more convenient. The term $(1 - \frac{B(\nu)}{I_{\tau_2}(\nu)})$ is considered to be constant across the width of an absorption line.

Consider the centre of a very strong absorption line in which $\tau'_2(\nu) \to \infty$ and let the central depth of this line $r_{\nu_o} = r_o$ then

$$r_o = (1 - \frac{B(\nu)}{I_{\tau_2}(\nu)}) \qquad (5.12)$$

This implies that the central intensity of strong absorption lines will be given by the Planck function having a temperature equal to that of the reversing layer. In a real stellar atmosphere this will not be exactly true as the central intensity will have a contribution, from the source of continuous opacity, as well from line radiation returned to its original direction of travel toward the observer, by secondary scattering.

Equation 5.11 can be rewritten to include r_o and combined with equation 5.10 to give

$$W_\nu = r_o \int_0^{\infty} (1 - \exp(-\tau'_2(\nu))\, d\nu \qquad (5.13)$$

This is the exact relation for the equivalent width of an absorption line in an SS model atmosphere.

The Milne-Eddington Atmosphere

We will now consider the solution of the equation of transfer in the Milne-Eddington (ME) atmosphere. This is a more sophisticated model in which the line and continuum radiation are formed at the same levels throughout a region where there is a temperature gradient. The ME atmosphere is still highly idealized in order to allow an analytical solution and contains the following assumptions:

1. The continuum is formed by pure absorption although the lines can be formed by either pure absorption or pure isotropic coherent scattering.
2. The ratio of the line to continuous absorption coefficients remains constant with depth.
3. The source function in the continuum is a Planck function and can be approximated by a relationship of the form $B(\tau) = B_o + B_1\tau$

Where τ is the continuum optical depth.

Chandrasekhar has given an exact solution of the transfer equation in the ME atmosphere. The solution given here is based on Eddingtons 'first approximation' which is;that everywhere within the atmosphere the radiation is isotropic,while at the surface only an outward going hemisphere of radiation exists. Although this is clearly artificial, Eddington's approximation has been found to give a more accurate description of real atmospheres than the more exact solutions. Wrubel (1949) gives curves of growth for pure scattering and Wrubel (1960) gives curves of growth for pure absorption, in the ME atmosphere.

Equation of Transfer in the ME Atmosphere

As before the first stage is to write down the equation of transfer for which we consider Fig.5.02. The total line absorption coefficient K is divided into a pure absorption part ℓ and a pure scattering part S by a factor E such that:

$$\ell = EK \quad \text{and} \quad S = (1-E)K$$

Let the continuum absorption coefficient = K'_c. For ease of explanation this is somewhat unconventionally defined as the continuum absorption coefficient per line forming atom. Thus,

$$K'_c N'_o = K_H N_H$$

where N'_o is the number of line forming atoms per cm^3, N_H is the number of hydrogen atoms per cm^3 and K_H is the continuum absorption coefficient per hydrogen atom.

The total number of quanta of frequency ν absorbed in our volume element δs is given equal to $(K'_c + K)N'_o\delta s \int I(\nu\, s,\theta)d\omega$ where the inte-

gral is over a sphere. Of these a fraction

$$\frac{\delta\omega}{4\Pi}\,(1-E)KN'_{o}ds\int I(\nu,s,\theta)d\omega$$

are scattered into the cone $\delta\omega$.

Adding gains and losses we find that analagous to equation 5.03

$$\frac{I}{N_o}\frac{dI}{ds} = (1-E)K\int\frac{I}{4\Pi}\,d\omega + \gamma - (K'_c + K)I \qquad (5.14)$$

Assuming that the continuum radiation is not scattered and that the non-scattered part of the line radiation is thermalized then the emission coefficient can be written as

$$\gamma = B(T)\,(EK+K'_c) \qquad (5.15)$$

As before $\frac{dz}{ds} = \text{Cos}\theta \equiv \mu$, also $dt = -(K+K'_c)N'_o dz$, where dt is the increment of line plus continuum optical depth. The continuum optical depth is $d\tau = -K'_c N'_o dz$.

We now introduce the following simplifying relations

$$\eta = \frac{K}{K'_c}, \quad L = \frac{1+E\eta}{1+\eta}, \quad M = \frac{1}{1+\eta} \qquad (5.16)$$

Following Eddington we introduce the quantities.

$$J=\int I\,\frac{d\omega}{4\Pi} \qquad H=\int \text{Cos}\theta\; I\,\frac{d\omega}{4\Pi} \qquad K=\int \text{Cos}^2\theta\; I\,\frac{d\omega}{4\Pi} \qquad (5.17)$$

The integrals are taken over a sphere and the quantities have the following meanings. J is the mean intensity. H is the net outward flow of energy and K gives the radiation pressure multiplied by the velocity of light.

Equation 5.14 can now be rewritten by making use where appropriate of equations 5.15, 5.16 and 5.17 to give,

$$\mu\frac{dI}{dt} = I - J(1-L) - B(T)L \qquad (5.18)$$

This is exactly equivalent to equation 5.04 of the previous section with a source function $S_\nu = J(1-L)+B(T)L$.

In order to determine the variation of line depth with frequency, we wish to express the flux at the stars surface as a function of L and M. This is done as follows.

multiply equation 5.18 by $\frac{d\omega}{4\pi}$ and integrate over a sphere

$$\frac{d}{dt}\int \frac{I\mu d\omega}{4\pi} = \int \frac{I d\omega}{4\pi} - J(1-L)\int \frac{d\omega}{4\pi} - B(\tau)L\int \frac{d\omega}{4\pi}$$

using 5.17 this gives

$$\frac{dH}{dt} = L(J-B(\tau)) \qquad (5.19)$$

Similarily multiplying 5.18 by $\mu\frac{d\omega}{4\pi}$ and integrating gives

$$\frac{dK}{dt} = H \qquad (5.20)$$

We now consider Eddingtons two 'first approximations'. Consider a sphere at the surface of the star. Over the upper hemisphere the intensity is zero, while the first of the approximations is to assume, that over the lower hemisphere the intensity is independent of θ. Since the mean value of the cosine averaged over a hemisphere is ½ it follows that from equation 5.17

$$H_o = J_o/2$$

The other approximation is to assume that even in the surface layers $K = \frac{1}{3} J$. This is exact deep in the atmosphere where I is uniform over the entire sphere so that from equation 5.17, $J = 1$ and $K = \frac{1}{3} I$

If $K = \frac{1}{3} J$ then $\frac{dK}{dt} = \frac{1}{3}\frac{dJ}{dt}$

which substituted in 5.20 gives $H = \frac{1}{3}\frac{dJ}{dt}$

which substituted in 5.19 gives $\frac{d^2J}{dt^2} = 3L(J-B(\tau))$ (5.21)

Before continuing note that by definition

$$dt = -(K + K_c')N_o' dz$$
$$= -(1+\eta)K_c'N_o' dz$$

also $d\tau = -K_c N_o' dz$

$$\therefore \frac{d\tau}{dt} = \frac{1}{1+\eta} = M$$

Take condition 3 that $B(\tau) = B_o + B_1\tau$ and differentiate w.r.t. τ

$$\frac{d}{dt}B(\tau) = B_1 \quad \text{and} \quad \frac{d}{dt}B(\tau) = MB_1 \tag{5.22}$$

note also that $\frac{d^2}{dt^2}B(\tau) = 0$ (5.23)

We now continue and note that relation 5.23 enables us to rewrite equation 5.21 in the form

$$\frac{d^2}{dt^2}(J-B(\tau)) = 3L(J-B(\tau)) \tag{5.24}$$

This equation has a simple solution allowing a positive or negative exponential. However on physical grounds it is clear that when t is large $J-B(\tau) \to 0$ so that the positive exponential is excluded.

The solution to equation 5.24 can be written as

$$J = B(\tau) + Ae^{-\sqrt{3L}\ t} \tag{5.25}$$

We must now find A. Equation 5.25 is differentiated with respect to t and combined with equation 5.22 to give

$$\frac{dJ}{dt} = MB_1 - \sqrt{3L}\ Ae^{-\sqrt{3L}\ t} \tag{5.26}$$

Recalling Eddingtons approximations that $J(t=0) = 2H(t=0)$ and $H = \frac{1}{3}\frac{dJ}{dt}$ and substituting these into equations 5.25 and 5.26 respectively with $t = 0$ gives the relations;

$$2H = B_o + A \quad \text{and} \quad 3H = MB_1 - \sqrt{3L}\ A \tag{5.27}$$

These are combined to give

$$A = (2B_1M - 3B_o)/(3 + 2\sqrt{3L}) \tag{5.28}$$

Since we are interested in the flux at the surface of the star, A is substituted in the relation $2H = B_o + A$ of equation 5.27. We now recall that we can write the line depth $r_\nu = \frac{H_{cont} - H_{line}}{H_{cont}}$ (5.29)

and also the equivalent width $W_\nu = \int_o^\infty r_\nu d\nu$ (5.30)

Noting that in the continuum $\eta = 0$, $\therefore$ $M = 1$ and $L = 1$, we can combine 5.30, 5.29, 5.28 and 5.27 to give after same algebra

$$W_\nu = \int_0^\infty \left\{ 1 - \frac{(\sqrt{3L} + \frac{B_1}{B_0} M)(1 + \frac{2}{\sqrt{3}})}{(\sqrt{3} + \frac{B_1}{B_0})(1 + \frac{2\sqrt{L}}{3})} \right\} d\nu \qquad (5.31)$$

This ME equation for the equivalent width is equivalent to equation 5.13 of the previous section.

Comparison of the ME and SS solutions for weak lines

Consider first the SS solution:

Equation 5.12 for r_o is rewritten in the form

$$r_o = (1 - \frac{B_{line}}{B_{continuum}})$$

which expresses the assumption that the continuum intensity can be represented by a Planck function at the continuum temperature while B_{line} represents the temperature of the reversing layer. Equation 5.13 becomes

$$W_\nu = (1 - \frac{B_{line}}{B_{cont}}) \int_0^\infty (1 - \exp(-\tau'_2 \nu))d\nu \qquad (5.32)$$

for a weak line, $\tau' \to 0$ and $\exp(-\tau'_2(\nu)) \simeq 1 - \tau'_2(\nu)$

Now $\tau'_2(\nu) = K(\nu)\, H_o N'_o$ where H_o is the scale height and N'_o is the number density of line forming atoms at the point τ_2 (τ_2 is the continuum optical depth). The use of the scale height is further discussed below. $H_o N'_o$ has the dimensions NL^{-2} and can be thought of as the total number of atoms per square cm, observed in the line of sight.

Equation 5.32 can now be written as

$$W_\nu = (1 - \frac{B_{line}}{B_{cont}})\, H_o N'_o \int_0^\infty K(\nu)d\nu \qquad (5.33)$$

Now from equation 5.54 below $H_o = \tau_{2\,cont}/K_H N_H$

Now if $\tau_{2\,cont} = 1$ then $H_o = \frac{1}{K_H N_H}$ and equation 5.33 becomes

$$W_\nu = \left(1 - \frac{B_{line}}{B_{cont}}\right) \frac{N_o'}{N_H K_H} \int_o^\infty K(\nu)d\nu \qquad (5.34)$$

which is the weak line limiting case for the SS model.

For the ME model there are two limiting solutions to equation 5.31 The first is for pure absorption in which case;

$$E = 1 \quad \therefore \quad L = 1$$

The second is for pure scattering in which case;

$$E = 0 \quad \therefore \quad L = M$$

For weak lines we can make the approximations ;

$$M = \frac{1}{1+\eta} \simeq (1-\eta) \quad \text{and} \quad \sqrt{M} \simeq (1-\frac{1}{2}\eta)$$

Equation 5.31 now reduces to two limiting values:

Pure Absorption	Pure Scattering
$W_\nu = \left(\frac{\frac{B_1}{B_o}}{\sqrt{3}+\frac{B_1}{B_o}}\right) \frac{N_o'}{K_H N_H} \int_o^\infty K(\nu)d\nu$	$W_\nu = \frac{(\frac{3}{2}+(1+\sqrt{3})\frac{B_1}{B_o})}{(\sqrt{3}+2)(\sqrt{3}+\frac{B_1}{B_o})} \frac{N_o'}{K_H N_H} \int_o^\infty K(\nu)d\nu$

(5.35)

Comparison of equations 5.34 and 5.35 shows that all three models predict the same type of relationship between the weak line equivalent width and the absorption coefficients and they can be generalised to the form ;

$$W_\nu = r_o \frac{N_o'}{K_H N_H} \int_o^\infty K(\nu)d\nu \qquad (5.36)$$

It is important to realise that r_o is a function of frequency and that this functional relationship differs amongst the three models. In the ME atmosphere (which is grey)

$$\frac{B_1}{B_o} = \frac{3}{8} \frac{h\nu}{kT_o} \left(1 - \exp(-\frac{h\nu}{kT_o})\right)^{-1} \qquad (5.37)$$

where T_o is the boundary temperature related to the effective temperature by

$$T_e = 1.19\ T_o$$

The Curve of Growth

This section considers the solutions of equations 5.13 and 5.31 as a function of N_o'. In order to do this we need to know the variation of K with frequency, as well as the relationship between K and the total number of atoms, of the appropriate element, in the star's atmosphere. More generally the curve of growth can be considered as a saturation curve, that relates the observed equivalent width, to the equivalent width computed in the weak line approximation, where the effects of saturation and damping are ignored. This is a useful approach because, very broadly speaking, the shape of the curve of growth is independent of the details of the model. This means that whatever the formalism of our star model we are free to use any suitable theoretical, or even an empirical curve of growth, that best fits the data.

Elementary theory of the simple oscillator gives the relationship;

$$\int_o^\infty K(\nu)d\nu = \frac{\Pi e^2 f}{mc} \quad \text{or} \quad \int_o^\infty K_\lambda d\lambda = \frac{\Pi e^2 \lambda^2 f}{mc^2} \tag{5.38}$$

which combined with equation 5.36 of the previous section gives;

$$\frac{W_\nu}{r_o(\nu)} = \frac{N_o' \Pi e^2 f}{K_H N_H mc} \tag{5.39}$$

In this equation e and m are the charge and mass of the electron f is the oscillator strength, which is always less than one and c is the speed of light.

We will now follow the derivation of the curves of growth for pure absorption in the SS atmosphere. This corresponds to the solution of equation 5.13 (analagous of course to equation 5.31 in the ME case) where

$$\tau'_2(\nu) = K(\nu)H_o N_o' \tag{5.40}$$

The frequency variation of $\tau'(\nu)$ or $K(\nu)$ is a convolution of the doppler broadening, due to the turbulent and thermal motions of the radiating atoms and the natural and collisional broadening of the energy levels involved in the transition.

The absorption coefficient can be written in the form

$$K(\nu) = K_o H(a,v) \tag{5.41}$$

where K_o is the absorption coefficient at the line centre for zero damping, H(a,V) is the Hjerting function, a is a damping parameter and V is the distance from the line centre in units of the doppler width $\Delta\nu_D$. More explicitly:

$$K_o = \frac{\sqrt{\pi}e^2 f}{mc \Delta\nu_D} \quad V = \frac{\nu-\nu_o}{\Delta\nu_D} \quad a = \frac{\Gamma}{4\pi\Delta\nu_D} \qquad \Delta\nu_D = \frac{\nu_o}{c} \frac{2kT}{M_a} + \xi^2 \tag{5.42}$$

Here Γ is the combined natural and collisional damping T is the kinetic temperature of the atoms of mass M_a, forming the absorption line of central frequency ν_o and ξ is the microturbulent velocity of the line forming gas. In cool stars $\xi^2 > \frac{2kT}{M_a}$ and dominates $\Delta\nu_D$.

Equations 5.13 and 5.41 were first solved by van der Held (1931) for various values of a. In practice it is more practical to use log $W/\lambda r_o$ instead of log $W\nu/\Delta\nu_D$. For this reason Powell (1969) tabulates log $W/\lambda r_o$ as a function of log X for a doppler width of 1.69 km s^{-1} and for various values of the damping constant a. He assumes $r_o = 1$.

For weak lines log X is defined by the relation,

Log X = log $W/\lambda r_o(\lambda)$

From equation 5.39 and using wavelengths in angstroms instead of frequencies Log X can be written

$$\text{Log } X = \log \{\frac{H_o N_o' \pi e^2 f \lambda_A}{mc^2}\}$$

$$= \log N_o' H_o f \lambda_A - 20.05 \tag{5.43}$$

The family of curves corresponding to different values of the damping parameters 'a' are saturation curves that relate the observed equivalent width of a strong line to its unsaturated weak line value given by equation 5.43.

Fig. 5.05 shows, schematically, the dependence of the shape of the curve of growth on both the doppler width and the damping constant.

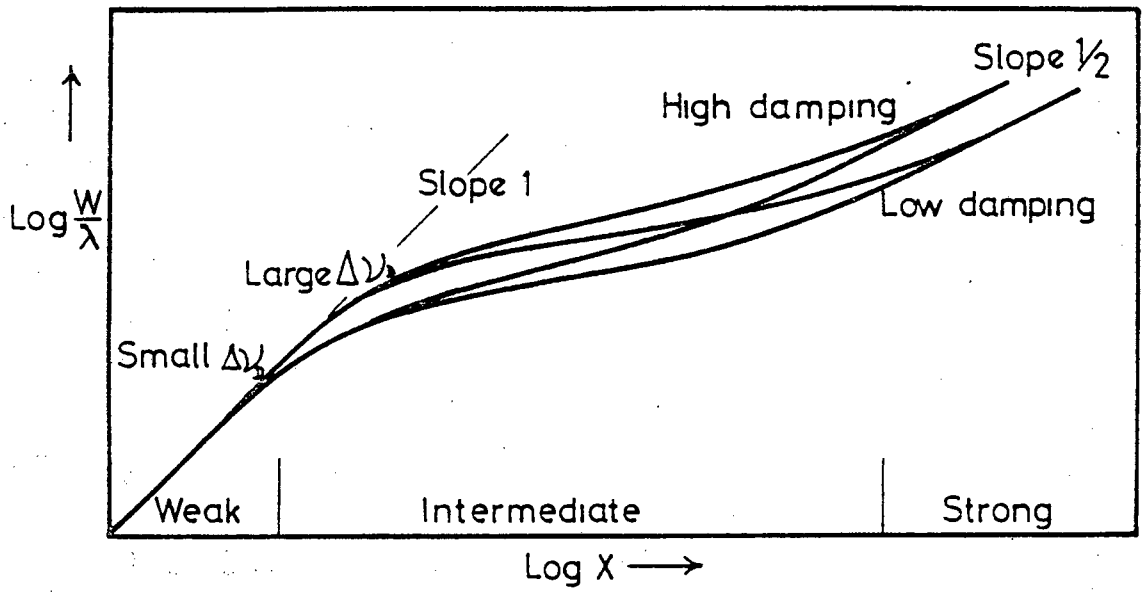

A schematic Curve of Growth.

Fig. 5.05

The curve of growth divides into three regions, the weak line region where Log W/λ = log X, the intermediate region where log W/λ depends on both the damping and the doppler width, and the strong line region where log $\frac{W}{\lambda}$ only depends on the damping.

Most star lines fall on the intermediate part of the curve of growth. An exact relation, analogous to equation 5.39, between W_λ and $\hat{N}'H_o$ can be written for lines on the strong line region.

$$\frac{W_\lambda}{\lambda r_o}\ \text{STRONG} = \left(\frac{e^2\Pi}{4mc^3}\ N_o' H_o f \gamma \lambda^2\right)^{1/2} \qquad (5.44)$$

If $\gamma = \gamma_{\text{classical}}$, as is frequently found in cool stars with extended atmospheres and $\gamma_{\text{classical}} = 0.222/\lambda^2$ (λ in cm) then 5.44 becomes

$$\log \frac{W_\lambda}{r_o \lambda}\ \text{STRONG} = \frac{1}{2} \log N_o' f H_o - 11.89 \qquad (5.45)$$

The number of atoms capable of forming a given absorption line, down to some continuum optical depth τ_2, can now be predicted, if a curve of growth is chosen with the appropriate doppler width and damping constant.

The final stage in interpreting line strengths, is to relate this number, to the total number of atoms of the given element per cubic centimetre in the atmosphere, by allowing for the effects of excitation, ionization and the continuous opacity. The theoretical curves of growth in the ME atmosphere with pure scattering, have B_1/B_0 as an additional parameter. These curves are tabulated by Wrubel (1949).

Excitation and Ionization Corrections

In LTE the Boltzmann equation relates the number of atoms in a given energy level N_o', to the total number of atoms in the appropriate degree of ionization say N_{oI}

$$N_{oI} = N_o' \frac{U}{g} e^{\chi/kT} \tag{5.46}$$

Where U is the partition function, T is the excitation temperature and χ is the excitation energy in electron volts, of the appropriate level having statistical weight g.

In LTE the Saha equation relates the number of atoms in different ionization levels say I and II, to the ionization temperature T, the ionization potential in electron volts χ_{ion} and the electron pressure P_e.

$$\frac{N_{oII}}{N_{oI}} = 2 \frac{UII}{UI} \frac{(2\pi M)^{3/2}(kT)^{5/2}}{P_e h^3} e^{-\frac{\chi_{ion}}{kT}} \tag{5.47}$$

Where UII and UI are the appropriate partition functions. If N is the total number of atoms of a given element and $a = N_{oII}/N_{oI}$ then a useful notation is

$$N = N_{oI}(1+a) = N_{oII}(1+\frac{1}{a}) \tag{5.48}$$

The Continuous Opacity

In this section we justify the use of the expression $N_o'H_o$, introduced in equation 5.33, which represents the total number of element atoms observed above one square cm in the line of sight. We also show how the number density of element atoms can be related directly to the number density of hydrogen atoms, which provides a much more practical way of

expressing the results.

Equation 5.07defines the thickness of the line forming atmosphere to be the distance into the star at which the optical depth in the continuum $\tau_{continuum} = \tau_2$. The numerical value of τ_2 is about unity. In order to relate $\tau_{continuum}$ to atomic parameters let:

N = The total number of atoms per cc of all elements.

M = The average mass of an atom.

K_c = The continuum absorption coefficient per atom.

By definition $$\tau_{cont} = \int_0^z K_c N \, dz \qquad (5.49)$$

where z is a depth measured in cm.

If N is constant throughout the atmosphere then 5.49 gives

$$z = \frac{\tau_2}{K_c N} \qquad (5.50)$$

which is the appropriate value of z to use in equation 5.13 to evaluate the line optical depth. However a more realistic atmosphere is one that is in hydrostatic equilibrium which is defined by the equation

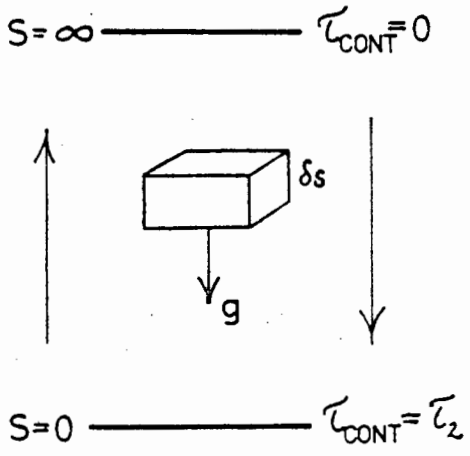

Fig. 5.06

$$dp = - \rho g ds \qquad (5.51)$$

where P is the pressure, ρ the density, g the gravitational force per gram and s the distance as defined in Fig. 5.06.

With the assumptions, that there is no radiation pressure contribution to P and that the temperature T is constant, then equation 5.51 can be written,

$$\frac{dN}{N} = - \frac{Mg}{kT} ds \qquad (5.52)$$

where $\rho = MN$ and $P = NkT$. The factor $\frac{kT}{Mg} \equiv H_o$ has the dimensions length and is known as the scale height. Integrating equation 5.52 gives;

$$N(s) = N(s=o)e^{-\frac{s}{H_o}} \qquad (5.53)$$

substituting 5.53 in the equation: $\tau_{2\,cont} = \int_{s=o}^{\infty} K_c N(s)ds$ gives

$$\tau_{2\,cont} = K_c N(s=o) \int_o^{\infty} e^{-\frac{s}{H_o}}\, ds$$

$$= K_c N(s=o) H_o$$

Where N(s=o) is the number of atoms per cubic centimetre at the point where $\tau_{cont} = \tau_2$. In practice K_c may be re-defined as the absorption coefficient per hydrogen atom in the continuum hereafter K_H, and N(s=o) may be replaced by N_H so that

$$\tau_{2\,cont} = K_H N_H H_o \qquad (5.54)$$

In a well mixed atmosphere the scale height is the same for all elements so that the value of H_o given by 5.54 is the appropriate value to use in equation 5.33 and relates the number of element atoms to the number of hydrogen atoms.

Conclusion

We now conclude the derivation by combining equations 5.43, 5.46 and 5.54 to give

$$\log X = \log gf\lambda - \theta\chi + \log \frac{N_o}{N_H} - \log U - \log \frac{K_H(\lambda)}{\tau_2} - 20.05 \qquad (5.55)$$

where λ is given in angstrom units, $\theta = 5040/T$ and T is the excitation temperature. There is a practical problem in using equation 5.55 in that it is correctly normalized when used with the equivalent width parameter $\log {}^{W}/\lambda r_o(\lambda)$. In practice $r_o(\lambda)$ and more important its wavelength variation, are best treated as an unknowns. We therefore use a modified form of 5.55, suitably normalised for use with $\log {}^{W}/\lambda$, given by:

$$\log X = \log gf\lambda - \theta\chi + \log \frac{N_o}{N_H} - \log U - \log \frac{K_H(\lambda)}{\tau_2} + \gamma \log r_o(\lambda) - 20.05 \qquad (5.56)$$

The factor γ is the reciprocal of the observed slope of the curve of

growth at the corresponding value of log W/λ. This must be included now that r_o has been brought over to the log X side of the equation.

5.04 The Method of Analysis

The practical details of the analysis will be described more fully below but for the sake of continuity the basic method is outlined here.

A stellar curve of growth is constructed by choosing a suitable value of θ and plotting log W/λ against log X_{star} where

$$\log X_{star} = \log gf\lambda - \theta\chi - \log \frac{K_H(\lambda)}{K_H(\lambda_o)} + \gamma \log \frac{r_o(\lambda)}{r_o(\lambda_o)} \qquad (5.57)$$

The last two terms are convenient ways of handling the wavelength variation of K and r_o. A theoretical curve of growth is fitted to the stellar curve to determine the microturbulent velocity and damping. The difference in abscissae, $\Delta\log X_o$, between the theoretical and observed curves of growth is found for each line and defined by;

$$\Delta\log X = \log X_{STR} - \log X_{THEOR} \qquad (5.58)$$

θ is adjusted until there is no trend of $\Delta\log X$ with χ.

The term $\gamma\log \frac{r_o(\lambda)}{r_o(\lambda_o)} - \log \frac{K_H(\lambda)}{K_H(\lambda_o)}$ is given by the observed systematic trend of $\Delta\log X$ with wavelength.

Finally combining equations 5.48, 5.56, 5.57 and 5.58;

$$\log \frac{N}{N_H} = -\Delta\log X + \log \left(\frac{K_H(\lambda_o)}{\tau_2} \right) - \gamma \log r_o(\lambda_o) + \log I + 20.05 \qquad (5.59)$$

where $\log I = \log(1+a) + \log UI$ for neutral lines

$= \log(1+\frac{1}{a}) + \log UII$ for ionized lines

and a is defined by equation 5.47

5.05 The Empirical Model Atmosphere Theory

This section reviews the theoretical background necessary to estimate abundances from observed equivalent widths using an empirical model atmosphere. The construction of such an atmosphere is beyond the scope of this thesis. For the sun we have used the Harvard Smithsonian Reference Atmosphere (HSRA), published by Gingerich et al (1971). For UY Cen we have used a series of models, published by Johnson (1974) and also an atmosphere, published by Gingerich et al (1966).

The principal advantage of using a model atmosphere is that it provides an important second approximation to a simple curve of growth analysis in that it allows for stratification. It also removes the artificial constraint of the ME atmosphere that the ratio of the line to continuous absorption coefficients must remain constant with depth.

We use a model of line formation in which both the line and continuum radiation are formed by pure absorption. The intensity of the emergent beam at an angle θ, to the normal defining the atmosphere, is given by

$$I_\lambda(\theta) = \int_0^\infty B(\tau_\lambda) \exp(- t_\lambda \sec \theta) \sec \theta \, dt_\lambda \qquad (5.60)$$

The residual intensity in an absorption line is the ratio of the fraction of the intensity in the line to the intensity in the continuum

$$R(\lambda) = \frac{I_\lambda(\theta)}{I^c_\lambda(\theta)} \qquad (5.61)$$

The equivalent width is given by the relation

$$W = 2 \int_{\lambda_o}^\infty (1 - R(\lambda))d\lambda \qquad (5.62)$$

In these equations λ_o is the central wavelength of the line under consideration, $B(\tau_\lambda)$ is the value of the Planck function at the continuum optical depth τ and at the appropriate wavelength λ.

The continuum optical depth at λ is related to the optical depth at the standard wavelength, at which the model is tabulated by the relation.

$$\tau_\lambda (x) = \int_o^x K_{STD} \left(\frac{K_\lambda}{K_{STD}}\right) \rho (x)dx \qquad (5.63)$$

In this equation x is the depth in cm, measured from the surface of the stellar atmosphere, $\rho(x)$ is the density and K is the absorption coefficient. The line plus continuum optical depth t_λ, is given by the relation

$$t_\lambda(x) = \int_0^x (K_\lambda^{cont} + K_\lambda^{line})\ \rho(x)dx \qquad (5.64)$$

Solar atlases are constructed from radiation from the centre of the solar disk, in which case the appropriate form of equation 5.60 has $\theta = 0$. For the star, we observe the integrated flux F_λ, from the entire hemisphere of the star where;

$$F_\lambda = 2 \int_0^{\pi/2} I_\lambda(\theta)\ \mathrm{Cos}\theta\ \mathrm{Sin}\theta\ d\theta \qquad (5.65)$$

which reduces to

$$F_\lambda = 2 \int_0^{\infty} B(\tau_\lambda)E_2(t_\lambda)dt_\lambda \qquad (5.66)$$

where $E_2(....)$ is the exponential integral given by

$$E_2(x) = \int_{y=1}^{\infty} \frac{e^{-xy}}{y^2}\ dy \qquad (5.67)$$

Equation 5.66 now gives the flux with which to compute the residual intensity and equivalent width. In practice the equivalent widths, computed in terms of either the intensity or the flux, only differ by a few percent.

The continuous absorption is considered as constant across the line profile, which is a satisfactory approximation. The wavelength variation of the line absorption coefficient is related to the fictitious coefficient at the line centre by equation 5.41 above, and the values of the Hjerting function are taken from Gray (1976 page 252).

At each level in the atmosphere the Saha and Boltzman equations are solved, using the appropriate atomic data for the line under consideration and the fictitious line absorption coefficient is found. The damping parameters used in the Hjerting function depend on both natural

and van der Waal damping. The microturbulent velocity is an input parameter taken to be independant of depth in the atmosphere. All the integrals are evaluated numerically using the trapezoidal method. This simple method is perfectly adequate for most lines but breaks down for the central regions of the strong lines in the coolest atmospheres.

Breakdown occurs within the uppermost layers, when $t_\lambda(x) >> 1.0$. This results in the physically unrealistic situation of the emissivity greatly exceeding the value given by the Planck function in the top layer even though $\exp(-t_{\lambda 0}) \simeq 0.0$ for the second layer.

The problem is overcome by subdividing the outer layers of the atmosphere and interpolating the tabulated temperatures, densities and pressures. It must be remembered that this is a mathematical artifice, which does not remove the physical uncertainty inherent in relating the central brightness of strong lines to the outer structure of the model atmosphere.

Equivalent widths are evaluated separately for each line from the appropriate atomic data. The number of element atoms per hydrogen atom is iterated until the observed equivalent width equals the calculated equivalent width. No attempt has been made to simulate blends except for the sodium and lithium doublets. In these cases the absorption coefficients of each doublet are added at each wavelength across the line.

5.06 The H.S.R.A. Model Atmosphere

The Harvard Smithsonian Reference Atmosphere (HSRA) described by Gingerich et al. (1971) has been used to model the solar atmosphere. This is not the most recent, nor the most accurate solar model atmosphere but Table 19 of Lambert and Luck (1978) shows that the uncertainties introduced by its use are typically no greater than 0.05 dex. (y dex indicates a numerical value of 10^y) This is well within the uncertainty required of our empirical log gf values. We adopt a solar microturbulent velocity of 1.0 km s^{-1}, as recommended by Lambert and Luck (1978).

The wavelength variation of the continuous absorption coefficient

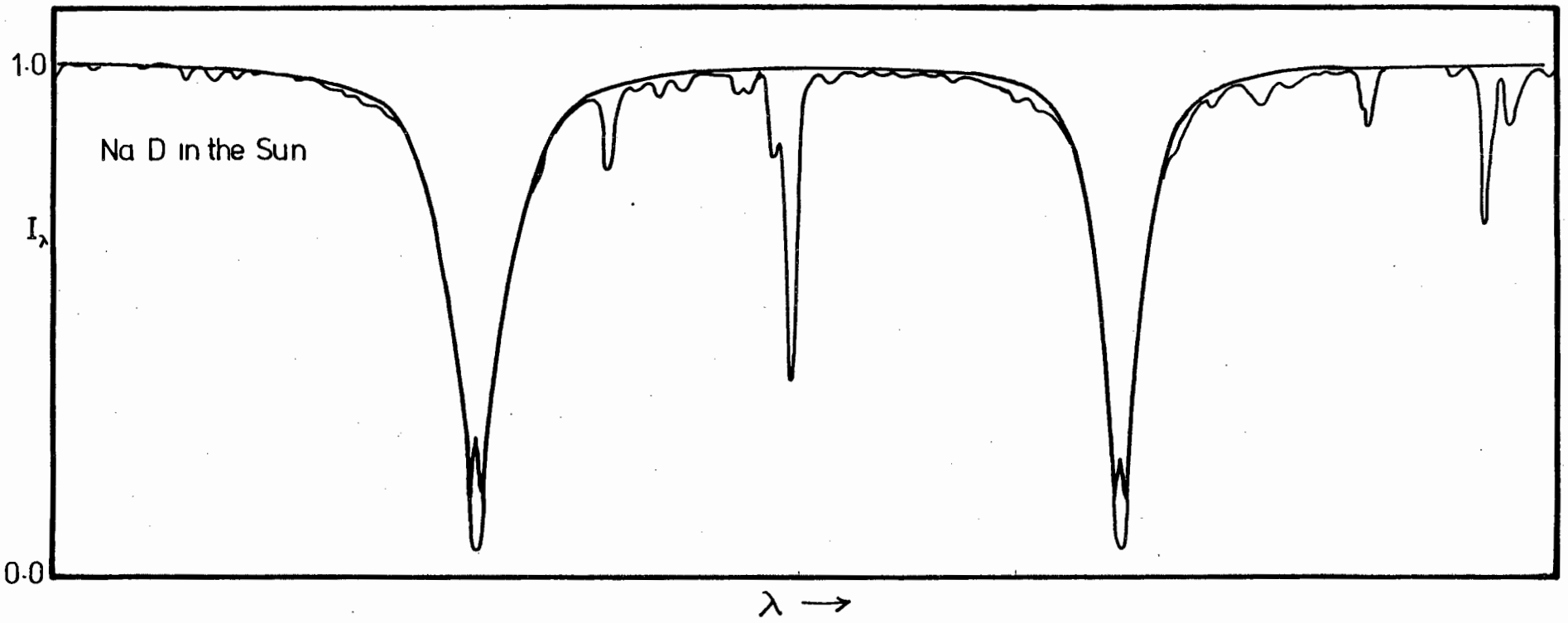

Figure 5.07

The Na D lines in the sun compared with the predictions of the HSRA with pure absorption. Note the poor agreement in the line cores, a consequence of the temperature reversal and caused by ignoring the effects of scattering.

was modelled by scaling the tabulated values, at the standard wavelength of the atmosphere (5000 Å), by the wavelength variation of H^- bound-free H^- free-free, He^- free-free and electron scattering. The formulae for these were taken from Gray (1976).

Fig.5.07 shows the NaD lines modelled with the HSRA, assuming theoretical values of log gf = 0.11 and -0.19 given by Lambert and Warner (1968) and solar abundance of 6.32 dex (H=12 dex). The solar abundance is taken from Lambert and Luck (1978) and is based on weak Na lines. The model is compared with the Delbouille et al. (1973) solar atlas. The agreement in the wings is considered to be good, but, note the poor agreement in the line centres. The model shows a reversal in the line centre, which is a consequence of the reversal in the temperature gradient at the top of the solar model atmosphere combined with the fact that pure absorption is the only method of line formation. Scattering is important in the outer layers of the sun and if included in the model would remove this line reversal. The problem only arises in the case of strong lines and is not important in deducing astrophysical log gf values for which the solar lines are all weak.

5.07 The Johnson Model Atmospheres

H.R.Johnson (1974) has published a series of model atmospheres covering a range of temperature, pressure and composition, for cool stars. A number of these atmospheres are used to investigate the UY Cen data.

The Johnson models take account of convection and include the effects of 54 molecules in determining the equation of state. The wavelength variation of opacity, apart from the usual hydrogenic sources, includes the effects of CN, CO, H_2O, HCO, HCN, NH_2, CH_2 and C_3 as well the effects of blocking by line opacity. The cool models clearly show the molecular bands of CO and H_2O in the region beyond 1.0 micron.

We have used his models J30, J31, J32, which all have a value of log g = 1.0, a solar composition and effective temperatures of 3000°, 2800° and 2500° respectively. To a first approximation, the temperature pressure structure of the models does not appear as sensitive as the wavelength variation of the emergent flux, to changes of composition. For the purpose of

investigating line formation in UY Cen, we consider it more important to cover the probable range of effective temperature rather than that of C/O, which is only given for the hotter models. We have modelled the wavelength variation of opacity in the same way as for the sun. UY Cen, with its intrinsically weak molecules, should be a better candidate for a simple model atmosphere analysis than most cool stars.

5.08 Contribution Functions

The purpose of a contribution function is to indicate where the flux within an absorption line originates and how the atoms forming the line are distributed within the atmosphere. There are three kinds that we can use. These are the residual flux contribution function, the absorption contribution function and a number density contribution function which we introduce for the first time. Throughout this discussion we confine ourselves to the case of pure absorption at the centre of the disk.

Rather than working in terms of residual intensity, R, as defined by equation 5.61, we work in terms of line depth r_λ as given by equation 5.09. In which case, using equations of the form of 5.60 and working in terms of λ, 5.09 becomes;

$$r_\lambda = \frac{1}{F_c} \left(\int_0^\infty B(\tau_\lambda)\exp(-\tau_\lambda)d\tau_\lambda - \int_0^\infty B(\tau_\lambda)\exp(-t_\lambda)dt_\lambda \right) \qquad (5.68)$$

where F_c is the flux in the continuum, given by the first term inside the brackets of equation 5.68. For the sake of uniform comparison, it is convenient to work in terms of the parameters used to specify the model atmosphere which are; τ_{STD}, the continuum optical depth, and K_{STD} the continuum absorption coefficient. It is also more convenient to visualise the results in terms of log τ_{TSD}. These requirements are satisfied by the following substitutions and identities:

$$\left.\begin{aligned} dt_\lambda &= (K_\lambda + \ell_\lambda)\rho dx, \quad d\tau_\lambda = K_\lambda \rho dx \quad \text{so that} \quad dt_\lambda = \frac{(K_\lambda + \ell_\lambda)}{K_\lambda} d\tau_\lambda \\ d\tau_\lambda &= \frac{K_\lambda}{K_{STD}} d\tau_{STD} \quad , \quad d\tau_{STD} = \tau_{STD}\, d \log_e \tau_{STD} \end{aligned}\right\} \qquad (5.69)$$

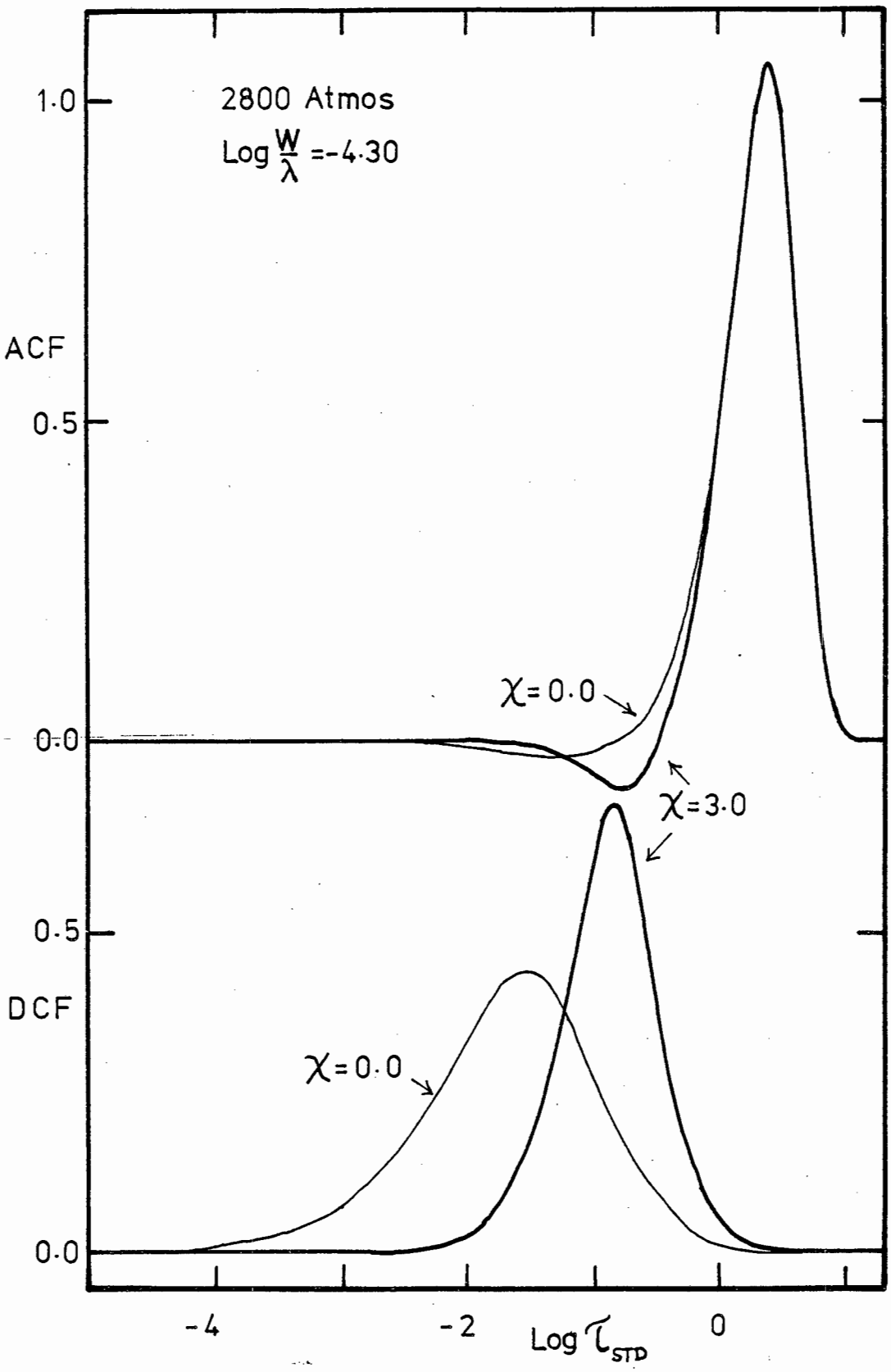

Figure 5.08

The absorption and density contribution functions are shown as a function of optical depth. Note how the two lines of different excitation level are much more clearly distinguished by the DCF. The ACF mainly shows the continuum flux distribution.

Equation 5.68 now becomes

$$r_\lambda = \frac{1}{F_c}\frac{K_\lambda}{K_{STD}}\left\{\int_{-\infty}^{+\infty} B(\tau_{STD})\left(e^{-\tau} - \frac{(K_\lambda-\ell_\lambda)}{K_{STD}}e^{-t}\right)\frac{\tau_{STD}}{\log_e 10}\, d\log\tau_{STD}\right\} \quad (5.70)$$

Residual Contribution function

The residual flux contribution function is the integrand of the second term of equation 5.70 which is;

$$RFCF = \frac{1}{F_c \log_e 10}\,\tau_{STD}\frac{(K_\lambda-\ell_\lambda)}{K_o}\,B(\tau_o)e^{-t} \quad (5.71)$$

The RFCF illustrates quantitively where the flux forming the line originates in the atmosphere. It is clear that when the line absorption ℓ is small, equation 5.71 becomes equal to the integrand of the first term in equation 5.70 in which case the RFCF gives the continuum flux distribution, but tells us nothing about where the line is formed.

Absorption Contribution Function

The ACF is the entire integrand of equation 5.70

$$ACF = \frac{1}{F_c \log_e 10}\,\tau_{STD}\,B(\tau_{STD})\left(e^{-\tau} - \frac{(K_\lambda-\ell_\lambda)}{K_{STD}}e^{-t}\right) \quad (5.72)$$

and is illustrated in the top part of Fig.5.08, for two lines having lower energy levels χ = 0 and 3 volts and the same log W/λ. The curve is negative in the part of the atmosphere where the line emisivity is greater than the continuum emisivity. Note the poor discrimination between the two curves and the fact that the majority of the flux still comes from the continuum forming levels.

The Density Contribution function

The two preceding contribution functions only give an idea of where the line forming atoms are in the atmosphere, in the case of very strong lines. In order to investigate stratification effects

it is important to know at what depth the line forming atoms are found. In order to do this we introduce a density contribution function (DCF).

Let $N'(\tau_{STD})$ equal the number of line forming atoms per gram at standard optical depth τ_{STD}. The effective number of line forming atoms in the line of sight is then;

$$N = \int_0^\infty N(\tau_{STD})\rho(\tau_{STD})e^{-t}dx \qquad (5.73)$$

The DCF is then simply the integrand of equation 5.73. It is convenient to normalise the DCF by the total number of line forming atoms in the line of sight outside the line in the adjacent continuum.

$$N_{total} = \int_0^\infty N'(\tau_{STD})\rho(\tau_{STD})e^{-\tau}dx \qquad (5.74)$$

All the contribution functions so far mentioned have only applied to one wavelength in the line. For practical purposes we use a weighted contribution function across the line, where weighting is according to the line depth r_λ. Using this and combining equations 5.73 and 5.74 obtain;

$$DCF = \int_{\lambda_0}^\infty R_\lambda N'(\tau_{STD})\rho(\tau_{STD})e^{-t}d\lambda \Big/ \int_{\lambda_0}^\infty R_\lambda d\lambda \int_0^\infty N'(\tau_{STD})\rho(\tau_{STD})e^{-\tau}dx \qquad (5.75)$$

The DCF is plotted as a function of log τ_{STD} in the lower part of Fig. 5.08 and now clearly illustrates the different levels of formation of the 0 and 3 volt lines.

The mean effective temperature, pressure or density, of formation of a given line can be found by simply using the relation that,

$$\bar{X} = \int DCF\ X\ dX \Big/ \int DCF\ dX \qquad (5.76)$$

where X is the appropriate parameter. Equations 5.75 and 5.76 are both very easily applied to a computer. They are used to define mean temperatures and electron pressures for individual absorption lines which are discussed in the model atmosphere section.

OBSERVATIONAL DATA

5.09 Plate Material. Calibration and Conversion to Intensities

All the spectra used in this analysis were obtained with the Y camera, at the coude focus of the 1.88m reflector, while it was at Pretoria. Details of the plates are listed in Table 2.01. The spectrograph has already been described in Chapter 2 as has the technique for sensitizing the IN emulsions.

Calibration spectra were obtained using a calibration spectrograph. This uses a stepped slit as the graded light source. The light is chopped every few seconds, to simulate the intermitancy effect of guiding. The spectrograph is situated next to the coude room and the star and calibration plates are exposed and developed together, in order to standardize the conditions. In its original form, the calibration spectrograph produced a series of bands across the spectra, caused by interference between the sandwich of glass in which the stepped slit was mounted. A correction must be applied to the narrowest slits to allow for the light loss due to diffraction away from the collimator. The finally adopted calibration intensities should be good to 3%.

All plates were developed using violent agitation while holding them in a gloved hand. This is considered less destructive than brush developing and more likely to produce non laminar flow across the plate than bubble development.

All the spectra and calibration spectra, were scanned with the PDS microdensitometer at the Royal Greenwich Observatory.

Each spectrum was scanned 3 times using a 5 micron wide slit stepping 4 microns. The slit length was fixed and required 2 partly overlapping scans to cover the entire width of the spectrum. The third scan was of clear plate. The calibration plates were also scanned and the data obtained were used to draw density-intensity curves. These curves were then used to produce intensity tracings. I am very grateful to Dr D Clarke of the RGO for supplying the necessary software. The main scientific advantage of the PDS is its high sensitivity. This means that on dense parts of the emulsion the photometer noise is negligable. This is very important as it is these dense regions that

TABLE 5.01

CONTINUUM HIGH POINTS

log I

λ	09801	103aF	103aD
6825	1.98	1.76	
6813	1.96	1.76	
6802	2.02	1.81	
6771	2.05	1.92	
6762	2.01	1.94	
6723	2.04	1.98	
6718	2.08	2.07	
6708	2.04	1.99	
6669	1.97	1.99	
6640	1.96	2.05	
6632	1.94	2.03	
6600	1.89	1.96	
6570	1.84	1.92	
6535	1.71	1.86	
6471	1.69	1.93	
6452	1.72	1.99	
6422	1.66	1.90	
6374	1.53	1.71	
6332	1.54	1.79	
6328	1.58	1.78	
6288	1.53	1.68	1.75
6233	1.50	1.59	1.88
6194	1.50	1.59	1.93
6129	1.60	1.75	2.16
6097	1.58	1.74	2.13
6080	1.56	1.72	2.06
6071	1.58	1.73	2.07
6049	1.57	1.68	2.04
5983	1.50		1.95
5960	1.51		1.95
5908	1.41		1.64
5839	1.48		1.80

are required to define the continuum.

5.10 Continuum

The correct location of the continuum remains one of the most difficult and contentious aspects of the curve of growth analysis of cool stars. In the single layer model, the continuum is correctly placed when the effect of removing the absorption line under study is to restore the emergent flux to the continuum level. This definition does not help locate the continuum but it does provide the rationale for defining the continuum, by joining the highest points by straight lines, over no more than a few tens of angstroms at a time. If continuum points occur much less frequently, then it is unlikely that any of the lines under study will be unblended. Yamashita and Unno (1963) have investigated the effect of incorrectly placing the continuum The effect is most marked on the equivalent widths of strong and weak lines and will interfere with the deduction of parameters which depend on the shape of the curve of growth. It should not affect the determination of excitation temperature and relative abundances, for which the curve of growth is merely an interpolation curve. If the continuum fluctuates rapidly with wavelength, then this indicates rapid changes of continuous opacity, which may mean that the single layer model is no longer valid. This possibility can be investigated by examining the curve of growth residuals.

The infrared spectra, covering the region 7000 to 8800 Å, show a large number of high points, including all 8 of the continuum points, identified in the C star V460 Cygni, by Dominy et al. (1978). These high points were joined by straight lines. Care was taken to put the continuum on both spectra at the same time. This was done to make allowance for the random photometric errors present in the height of individual contiuum points.

The continuum to blue of 6900 Å is much more difficult to locate as there are no known continuum windows and the spectrum shows sharp fluctuations. Thirty-two high points were located and their heights, which correspond to an arbitary intensity scale, were measured on all the tracings. The log height was then formed, which enabled the results from the two 103aF plates to be combined. The log intensity

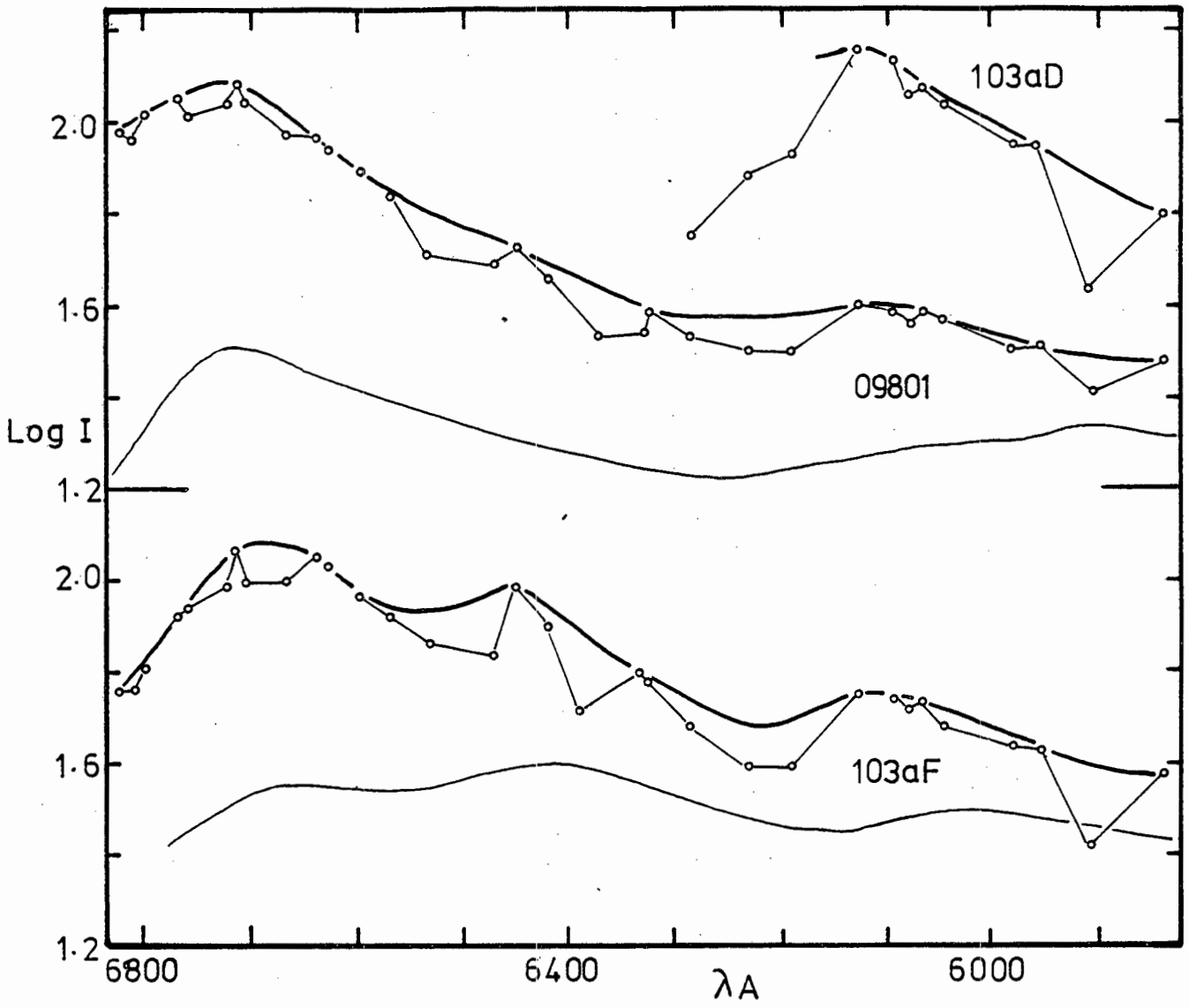

Figure 5.09

The heavy line represents the adopted continuum for the different emulsions. Note how the shape of this curve is similar to the emulsion sensitivity curves, illustrated by light lines under the 09801 and 103AF emulsions. The open circles represent individual continuum high points.

data in Table 5.01 is plotted in Fig. 5.09 against wavelength for the three emulsions. The published sensitivity curves of the Kodak 103aF and 09801 emulsions are drawn below the respective star intensity curves. There is a clear tendency for certain high points to be common to both spectra. There is also a tendency for the wavelength change of intensity to reflect the sensitivity curves of the two emulsions. The adopted continuum is shown by the heavy curve tangential to the highest points. There is clearly no guarantee that this continuum is 'correct', but we feel it is the most enlightenend way of drawing the continuum that is open to us. These curves were used to transfer the continuum onto the high dispersion tracings.

An independent estimate of the quality of the continuum fitting is given in the section dealing with the spectral scans.

5.11 Equivalent Widths

Equivalent widths and central depths were individually measured for 52 lines,all of which were chosen as having good profiles. The wavelengths and equivalent widths are listed in Table 5.02 and were measured on all the available plates by fitting trapezia. Fig.5.10 shows that different plates give systematically different equivalent widths. In Fig.5.10a, b, the best fitting line for each plate, denoted by plate number, is drawn heavy, while the light line corresponds to equality of equivalent width. The scales are the same in the two figures and Fig.5.10 is for the two IN emulsions. It is not clear what causes the effect as it seems to be independent of equivalent width but, since the densities of several of the plates are quite different, it may be related to the density intensity calibration. Individual central depth against equivalent width curves, were drawn for each plate, using only the calibration equivalent widths measured on that plate. These curves are shown in Fig. 5.11. The reason for not using mean equivalent widths for the calibration curves is to ensure that if a line is only measured on one spectrum, because the other plates are too weak, then it will have been measured on the best plate in which case the best calibration curve, appropriate to that plate, will prevail.

Central depths were then measured by hand for all the program lines.

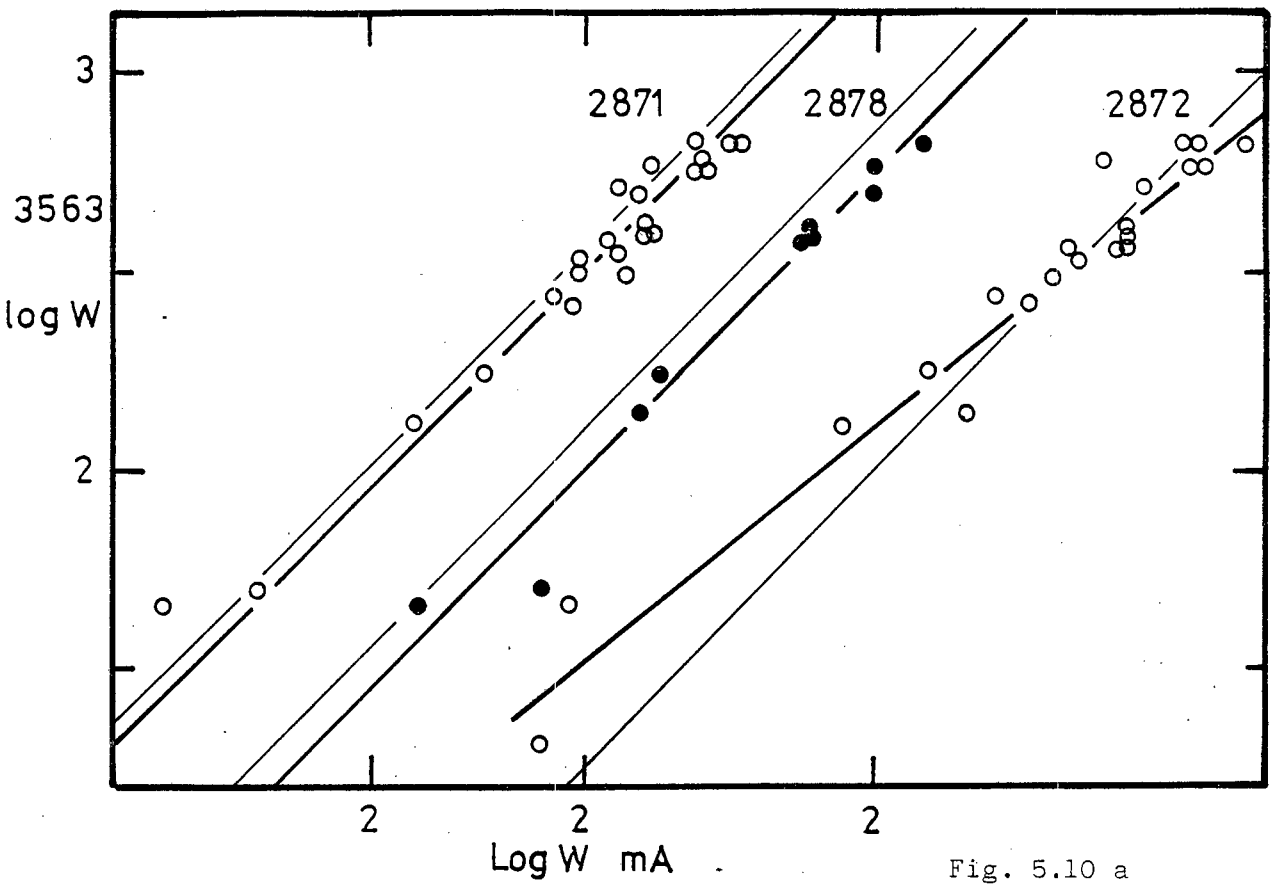

Fig. 5.10 a

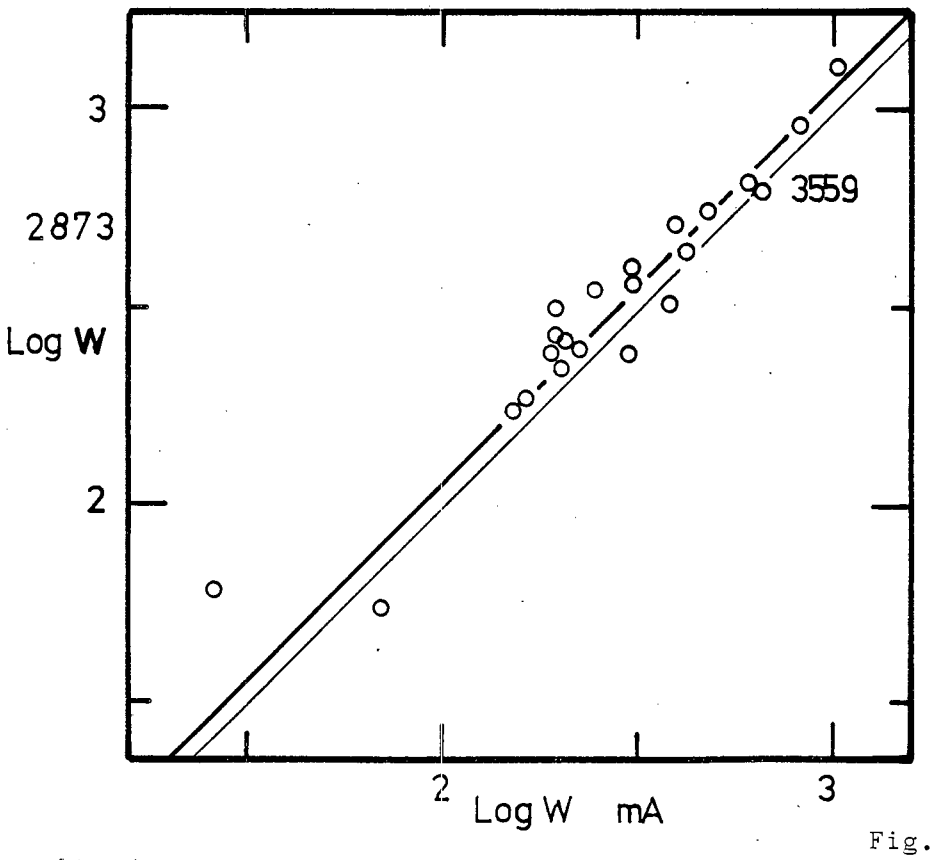

Fig. 5.10 b

This illustrates the systematic differences between equivalent widths measured on different plates. The light lines represent equivalence of equivalent width while the heavy lines are least squares fits. Fig. 5.10b is for the IN emulsions.

TABLE 5.02

List of Individual equivalent width measures

	log EW					
	IN	IN	103a-F	103a-F	09801	103aD
λ	2873	3559	2871	2872	3563	2878
5802.9						2.37
5809.5						2.58
5944.7			2.68		2.70	2.84
5955.3			2.72		2.77	2.84
5964.7			1.72		1.70	1.99
6025.3			2.61	2.65	2.57	2.67
6051.8						2.41
6062.9			2.95	2.96	2.82	2.97
6073.2						1.44
6079.5			2.30	2.14	2.25	2.29
6084.0				2.24	2.15	2.24
6085.2			2.71	2.65	2.59	2.67
6095.5			1.57	1.22	1.66	1.67
6117.7			2.71		2.62	2.67
6328.9				1.14	1.32	
6330.1			2.64	2.64	2.55	
6462.6			2.87	2.85	2.76	
6471.6			2.72	2.65	2.58	
6572.7			2.84	2.82	2.83	
6598.9			2.93	2.79	2.83	
6610.7					2.08	
6630.0			2.66	2.56	2.59	
6641.2			2.53	2.40	2.42	
6717.7			2.85	2.59	2.78	
6762.3			2.84	2.81	2.76	
6766.5			2.64	2.69	2.73	
6767.7			2.54	2.53	2.53	
6771.0			2.54	2.50	2.56	
6772.1			2.19			
6781.4			2.47	2.32	2.44	
6813.7			2.12	1.93	2.12	
7158.1	2.81	2.79				
7216.2	2.70	2.61				
7222.5	2.34	2.31				
7352.0	2.24					
7359.2	1.46					
7456.4	2.50	2.57				
7552.9	2.64	2.63				
7586.0	2.37	2.48				
7687.5	2.26	2.21				
7698.7	3.10	3.01				
7712.6	2.43	2.29				
7800.2	2.74	2.67				
8010.0	2.59	2.49				
8019.3		1.45				
8022.6		2.05				
8041.7	2.54	2.38				

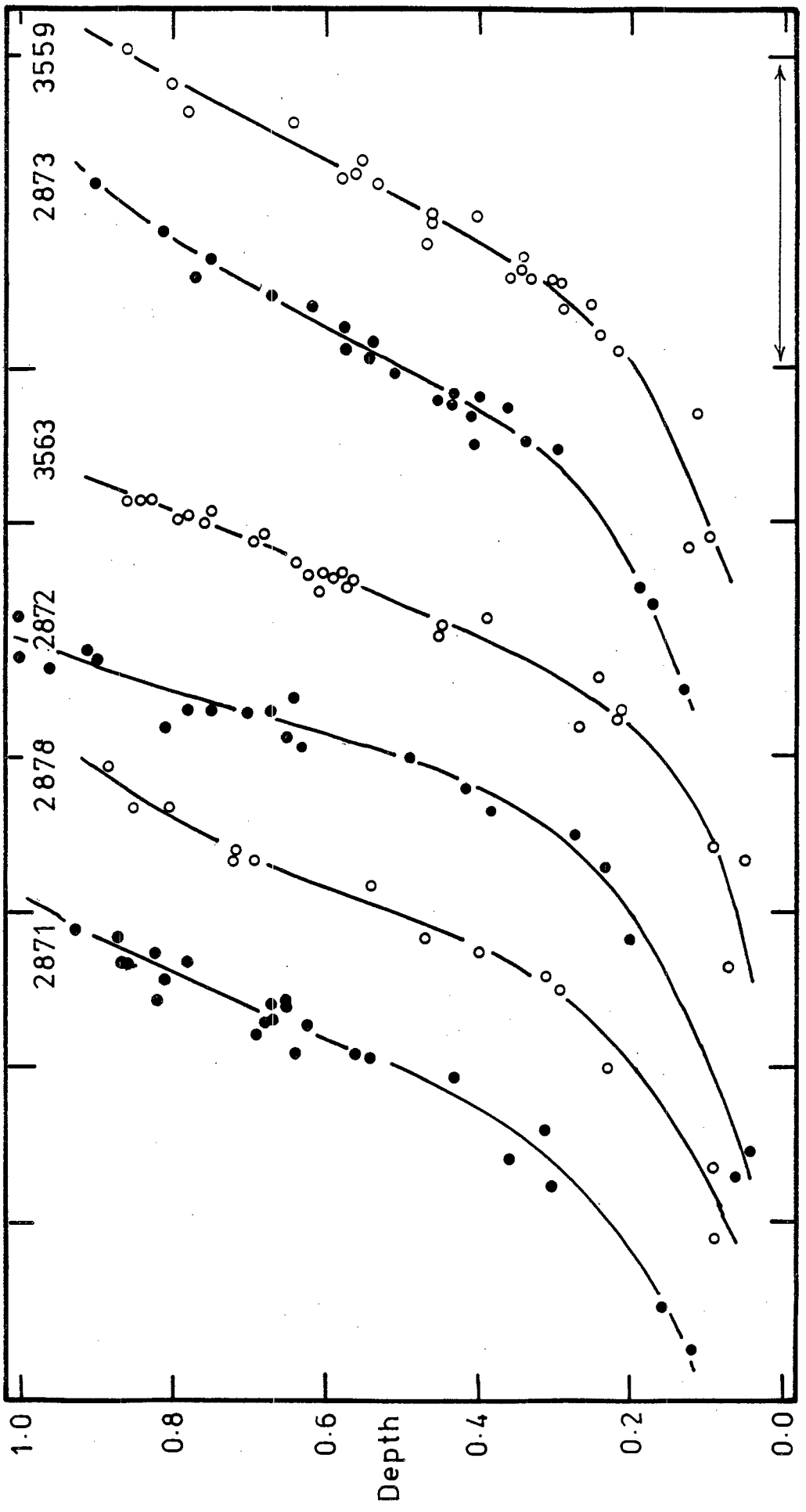

Figure 5.11

Central depth is shown as a function of equivalent width for the different plates. The scale is indicated by the arrow at the right hand side of the graph.

TABLE 5.02 Continued

λ	IN 2873	IN 3559	103a-F 2871	103a-F 2872	09801 3563	103aD 2878
8116.8	2.95	2.91				
8211.2	2.39	2.35				
8245.1	2.49	2.27				
8409.9	2.56	2.47				
8412.3	2.79	2.83				
8415.4	1.74	1.85				
8429.8	2.24	2.19				
8431.1		2.11				
8453.1	2.37	2.29				
8573.2	2.41	2.29				
8599.9	1.78	1.41				

These were converted to log W values via the calibration curves and finally mean values of log W/λ were formed for each line on all the plates.

Central depths were measured in preference to equivalent widths because they are more reliably measured, when the highest point in the wings of the line lies much below the continuum level. The only exceptions to this method of measuring equivalent widths were, the infra red CaII lines and the NaD lines. The CaII lines were measured directly on the tracings, by fitting trapezia, while the NaD line equivalent width was measured on a spectrum scan. The spectrum scan is described in section 5.13 and illustrated in Fig. 5.36. The continuum level adopted for the NaD lines corresponds to the level marked 1.0 in Fig. 5.36 and is lower than that adopted for the other lines. The justification for this is that the rapidly varying line absorption will look like an added source of continuous opacity to the more slowly varying NaD line opacity. This idea is investigated in the model atmosphere section.

Equivalent widths measured on photographic plates are traditionally considered to be no more accurate than a factor of two. It is difficult to estimate the errors, most of which are systematic and which include: scattered light in the spectrograph, uncertainties in the density intensity calibration, uncertainties in the location of the continuum, and grain noise in the photographic plate.

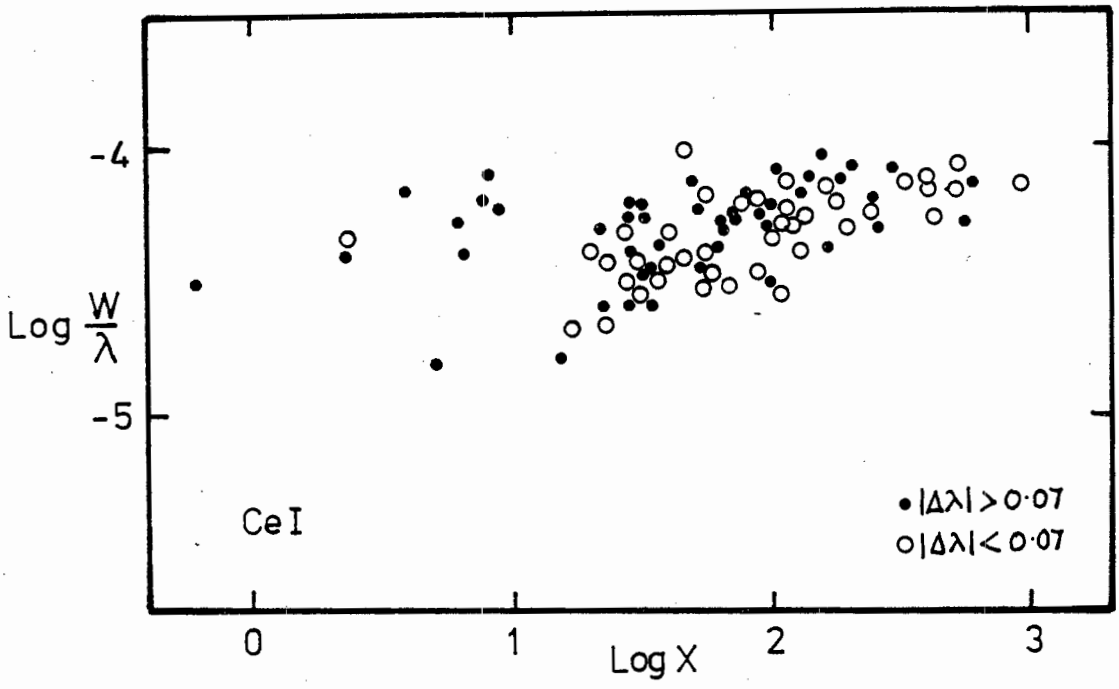

Figure 5.13

A curve of growth for CeI which shows that the lines having poor wavelength agreement and illustrated by filled symbols, are systematically shifted above and to the left of the others, indicating blending.

5.12 Selection of Lines

Initially all metal lines that had only one identification in Tables 2.04 and 2.05 were measured for equivalent width and used in the abundance analysis. However it is apparent that there is a slight systematic shift between those lines showing wavelength agreement within ± 0.07 Å of the laboratory values and the remainder. The effect, which is illustrated in Fig.5.13is in the sense that the poor agreement lines are slightly stronger indicating that they are probably blended.

With the exception of the elements NbI MoI PrII NdI SmI SmII EuI and HoI, for which, because of lack of data, we were obliged to accept all uniquely identified lines, the final selection of lines listed in Table5.08contains only lines with wavelength agreement within ± 0.07 Å.

No allowance has been made, in the initial line identification, for blending by ^{13}CN lines. Outside the region of the 2,0 band the effects should be negligable. Blending by unrecognised ^{12}CN and metal lines may be responsible for the wavelength shifts observed.

5.13 Spectrum Scans

Morphologically a spectrum scanner lies between high dispersion spectroscopy and narrow band photometry in that it provides good photometric accuracy, albeit with a loss of spectral information.

This is of great importance in UY Cen where we use scans to help fix the continuum across the boundaries between emulsions, as well as across the very broad spectral features found in such stars. Scans are also used to determine the profile and equivalent width of the NaD lines.

The scans were all obtained on the 0.75m telescope, during the commissioning of the scanner described by van Breda et al.(1978). The scanner is essentially a grating spectrograph with two entrance apertures and two exit apertures. Photomultipliers, coupled to pulse counting systems, are mounted below each exit aperture. The width of the exit apertures, located at the focal plane of the spectrograph camera, fixes the spectral resolution. The spectrum is scanned across the exit apertures by rotating the grating. The two entrance apertures enable star and sky to be observed simultaneously. Care must be taken

to use an appropriate entrance aperture and guiding technique, that strikes the right compromise between sacrificing spectral purity by being too large and photometric accuracy by being too small.

Normal observing technique is to observe the star first in one aperture and then in the other. The relative wavelength sensitivity of the two channels can be found and the sky background subtracted, to give an output in terms of counts per channel per second. The zenith distance is also recorded in order to allow for the effects of atmospheric extinction.

One very convenient aspect of the scanner software is that, provided the time required to do so does not fall outside predetermined limits, the dwell time per channel can be set to achieve a given number of counts. This allows a predetermined photometric accuracy to be achieved and as the instrumental sensitivity varies sharply with wavelength, thereby saves much observing time.

The UY Cen scans were converted to relative fluxes by calibration with an early type star of known flux distribution outside the earth's atmosphere. The technique for reduction is described in the next section.

Theory and Reduction of Scans

Let:

$N(\lambda)$ = The number of counts per second, recorded by the spectrometer, at wavelength λ.

$f(\lambda)$ = The flux distribution of the star above the earth's atmosphere.

$E(\lambda,Z)$ = The atmosphere transmission at wavelength λ and zenith distance Z.

$S(\lambda)$ = The sensitivity of the system. This includes the colour term of the optics, grating and photomultiplier.

The above terms are related by the two equations;

$$N(\lambda)_{STD} = f_{STD}(\lambda)\ E\ (\lambda,Z_{STD})S\ (\lambda) \qquad (5.77)$$

$$N(\lambda)_{UYC} = f_{UYC}(\lambda)\ E\ (\lambda,Z_{UYC})S\ (\lambda) \qquad (5.78)$$

The problem is, knowing $N(\lambda)_{STD}$, $N(\lambda)_{UYC}$, $f_{STD}(\lambda)$, to find $f_{UYC}(\lambda)$.

In order to do this we will also assume we know the behaviour of $E(\lambda,Z_{STD})$. Eliminating $S(\lambda)$ from equation 5.77 and 5.78 and expressing the result in terms of f_{UYC} we can write:

$$f(\lambda)_{UYC} = \frac{N(\lambda)_{UYC}}{N(\lambda)_{STD}} \frac{E(\lambda,Z_{STD})}{E(\lambda,Z_{UYC})} f_{STD} \qquad (5.79)$$

Since we are dealing with a simple absorption phenomena, $E(\lambda,Z_{STD})$ must be of the form $e^{-\tau_\lambda(z)}$, where $\tau_\lambda(z) = k_\lambda X$, where $X = \sec Z$. k_λ is the absorption coefficient per unit air mass, X is the number of unit air masses and z is the zenith distance. Hardie (1965 page 178) states that the wavelength variation of k_λ in the above equation is

$$k_\lambda \sim \frac{1}{\lambda^4}$$

If we make the further assumption that at $\lambda = \infty$ then $k_\lambda = 0$, we can write,

$$k_\lambda = \left(\frac{5000}{\lambda}\right)^4 k_{5000} \qquad (5.80)$$

where λ is in Å. We adopt the value $k_{5000}=0.159$ so that

$$E(\lambda,Z) = \exp\{0.159(5000/\lambda)^4 \sec Z\} \qquad (5.81)$$

All the terms in equation 5.79 are now known so we can solve for f_{UYC}. In order to eliminate the rapid wavelength variation of $f(\lambda)_{UYC}$ it is more convenient to express f_{UYC} in units of a given black body flux $f(\lambda)_{BB}$ equation 5.79 can now be rewritten as;

$$\frac{f(\lambda)_{UYC}}{f(\lambda)_{BB}} = \frac{f(\lambda)_{STD}}{f(\lambda)_{BB}} \frac{N(\lambda)_{UYC}}{N(\lambda)_{STD}} \exp\{0.159\left(\frac{5000}{\lambda}\right)^4 [\sec Z_{STD} - \sec Z_{UYC}]\} \qquad (5.82)$$

In practice $f_{STD}(\lambda)$ is only specified at intervals of about 300 Å, which means that it is necessary to interpolate the flux within each interval. This was done graphically and except in the regions of sharp stellar absorption features such as the NaD lines, is a good approximation for an early type star. We have simply interpolated the standard star counts across the Hα and NaD absorption regions, to obtain a smooth flux distribution. The atmospheric transmission function breaks down at the wavelengths of strong atmospheric absorption, for example within

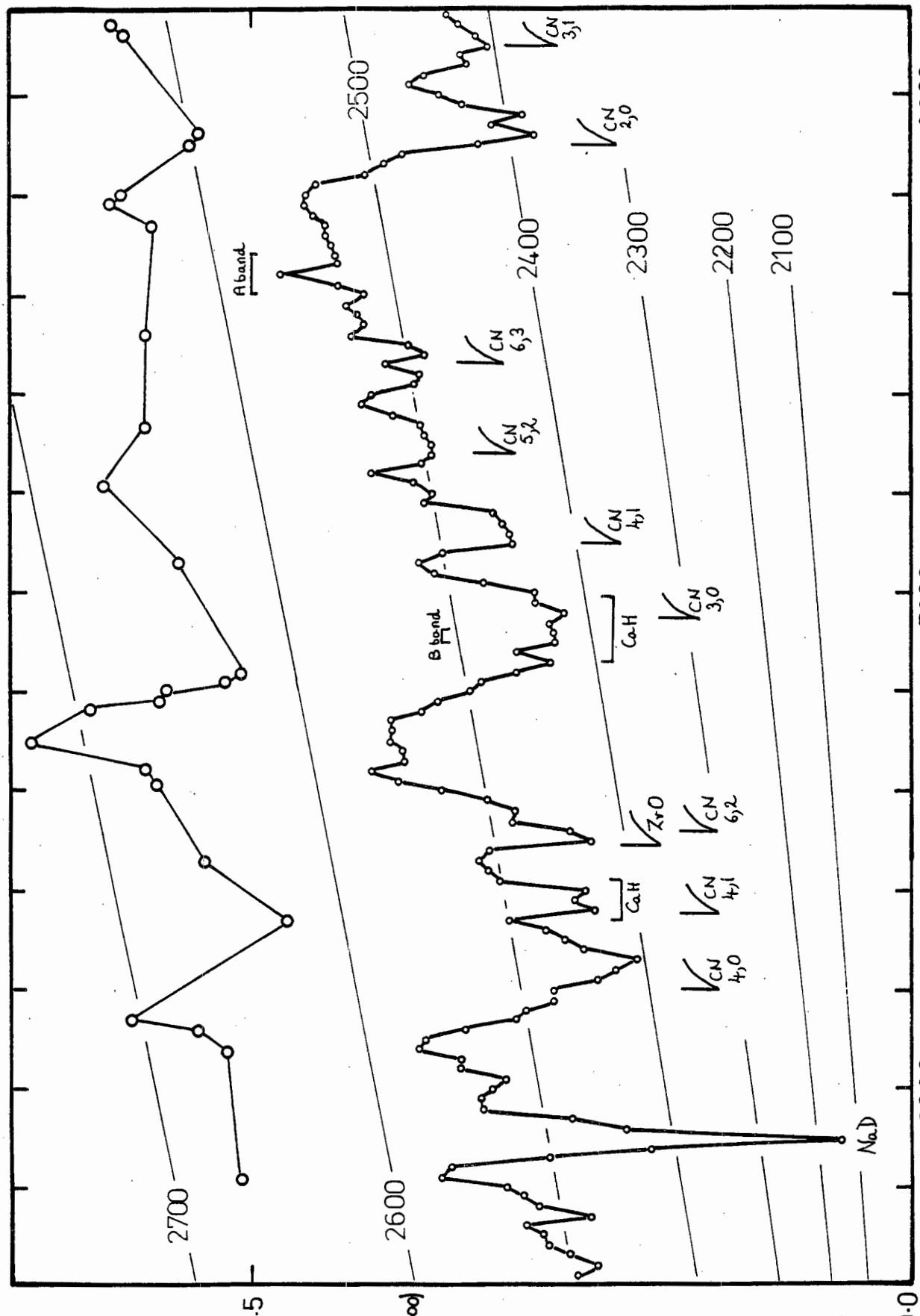

Figure 5.14

A spectrum scan of UY Cen with the most prominent molecular features marked. The scan is made with a 20Å window sampling every 20Å. The temperature calibration is discussed in the text.

the O_2 A and B bands. These regions have to be avoided in the interpolation as their modelling, as a function of sec Z, requires construction of appropriate curves of growth.

Results of Scans

Adopting the flux calibration of 109 Vir (Breger et al. 1976) as a standard, the spectral scans of UY Cen were reduced to arbitary flux units. Fig.5.14 shows a scan of UY Cen from 5600 Å to 8100, using a 20 Å exit window, sampling every 20 Å and normalised by a 3000° black-body. Fig.5.12 shows a scan of the NaD lines in UY Cen, normalised by a 2500° black body, obtained with an exit window of 8 Å and sampled every 5 Å. All scans were set to give a $\leq$ 1% photometric standard error.

For interest, various molecular features are identified in Fig.5.14. Bearing in mind the high density of atomic lines, the NaD and the CN2,0 features are the only two pure identifications. Note the slight over compensation of the atmospheric A band. The 3000° normalisation has clearly left a residual slope in the spectrum. We have overlayed a temperature grid normalised so that the 2500 black-body gives the best over all fit to the spectrum scan. This can be thought of as the best "Colour Effective Temperature". It will be remembered that 2500 was the best over all black-body colour fit to the broad band photometry. It must be emphasised that unless we have some independent estimate of angular diameter the temperature fitting depends on 'colour' which is not a very sensitive method as can be seen from the slow variation of slope in Fig. 5.14. However, once the colour temperature of one feature has been fixed the temperature scale within the diagram is also fixed. This is the basis for assigning a scale to the intensity axis and overlaying the temperature grid. The grid provides a standard of comparison by which to judge the intensity fluctuations.

5.14 Comparison of Photographic and Scan Continuum

Individual continuum points, as defined on the high dispersion coude tracings have been transfered onto the spectrum scan and are illustrated in Fig.5.14. Each tracing was divided into 20 Å wide windows to correspond in wavelength with the scanner bins. The area under the spectrum,

TABLE 5.03

$(\frac{B+A}{A})$

Plate Number

λ	2878	2871	2872	3563	Mean
5811	1.40	1.44			1.42
6071	1.46	1.41	1.41	1.34	1.41
6091	1.49	1.57	1.47	1.36	1.47
6111					
6131	2.13	1.97	2.16	1.85	2.03
6321					
6331		1.55	1.54	1.53	1.54
6451		1.74	1.79	1.46	1.66
6611		1.55	1.44	1.42	1.47
6631		1.52	1.43	1.42	1.42
6711		1.74	1.76	1.60	1.70
6751		1.68			1.68
6771		1.62	1.56	1.55	1.58
6791		1.75	1.66	1.66	1.69
6811		1.68		1.53	1.60
6821		1.86		1.54	1.70

	3559	2873			
7051	1.43	1.55			1.49
7211	1.57	1.68			1.62
7351	1.52	1.46			1.49
7511	1.35	1.38			1.36
7751	1.21	1.33			1.27
7771	1.27	1.37			1.32
7791	1.25	1.37			1.31
7891	1.57	1.75			1.66
7911	1.70	2.06			1.88
8111	1.71	1.90			1.80
8131	1.73	1.74			1.74

marked A in Fig. 5.15 was expressed as a fraction of the total area (A + B) under the continuum for each 20 A window. The spectrum scan was then scaled by the inverse of this fraction, at the appropriate wavelength and this defined the transferred continuum points which are illustrated in Fig. 5.14 by the large open circles. The areas A and B measured with a planimeter and individual values of $(\frac{A+B}{A})$ are given in Table 5.03.

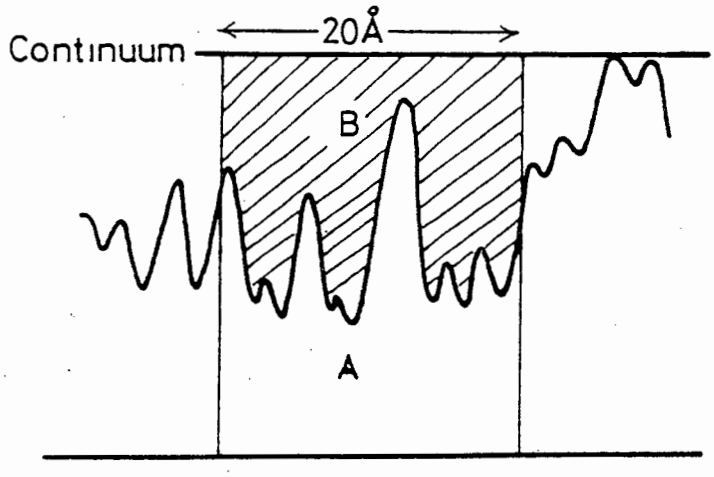

Figure 5.15

The definition of the areas A and B in terms of the spectrum and continuum.

If we accept the validity of the temperature grid then there is a tendency for the continuum, which is essentially a map of the highest points in the spectrum, to correspond to a cooler flux temperature toward longer wavelengths. This could be explained in terms of an increasing opacity toward longer wavelengths. There are quite marked variations in continuum height especially near 6900 Å, which corresponds to the join between the two emulsions where the spectrum is weak. There is also a tendency for the continuum to follow the underlying spectrum variations. Some of the variation undoubtedly reflects uncertainties in the original photographic density-intensity calibrations. This is apparent in Table 5.03 where systematic differences can be seen between different plates.

The over all fluctuation in the continuum of ± 10% about a smoothed curve is considered perfectly acceptable.

The continuum point at 6720 Å is of particular interst as the flux at this wavelength is 20% greater than the mean continuum level. This feature has the appearance of an emission line although there is no

reasonable identification. It appears consistantly bright in all the spectra and may represent the only true continuum point in the entire spectrum. This feature is not seen in other cool stars, which in general show much greater molecular absorption. In terms of the temperature grid drawn in Fig. 5.14 it has a brightness temperature of 2720° whereas the mean continuum level varies between 2675 in the blue to 2600 in the far red.

The results in Table 5.03 allow us to make an estimate of the total line blocking. This is an important parameter, required by those wishing to construct model atmospheres, who need to estimate what will be the effects of line opacity. The most appropriate estimate, which is least affected by individual molecular bands, is to compare the ratio of the flux beneath a smooth continuum and beneath a mean curve through the spectrum for which we adopt the 2500 black-body curve. This then gives the following results, which are expressed as percentage absorption of flux by lines

8000	30%
7000	38%
5800	46%

LABORATORY DATA

5.15 Partition functions and Lower energy levels

Partition functions are not listed here but have been taken from the following sources in order of priority; Cayrel and Jugaku (1963), Aller and Everett (1972) and Corliss and Bozman (1962)(hereafter NBS53).

Lower energy levels are given in electron volts and are taken from the following sources in order of priority; Moore (1959) Meggers et al. (1975) (hereafter NBS145) and Kurucz and Peytremann (1975).

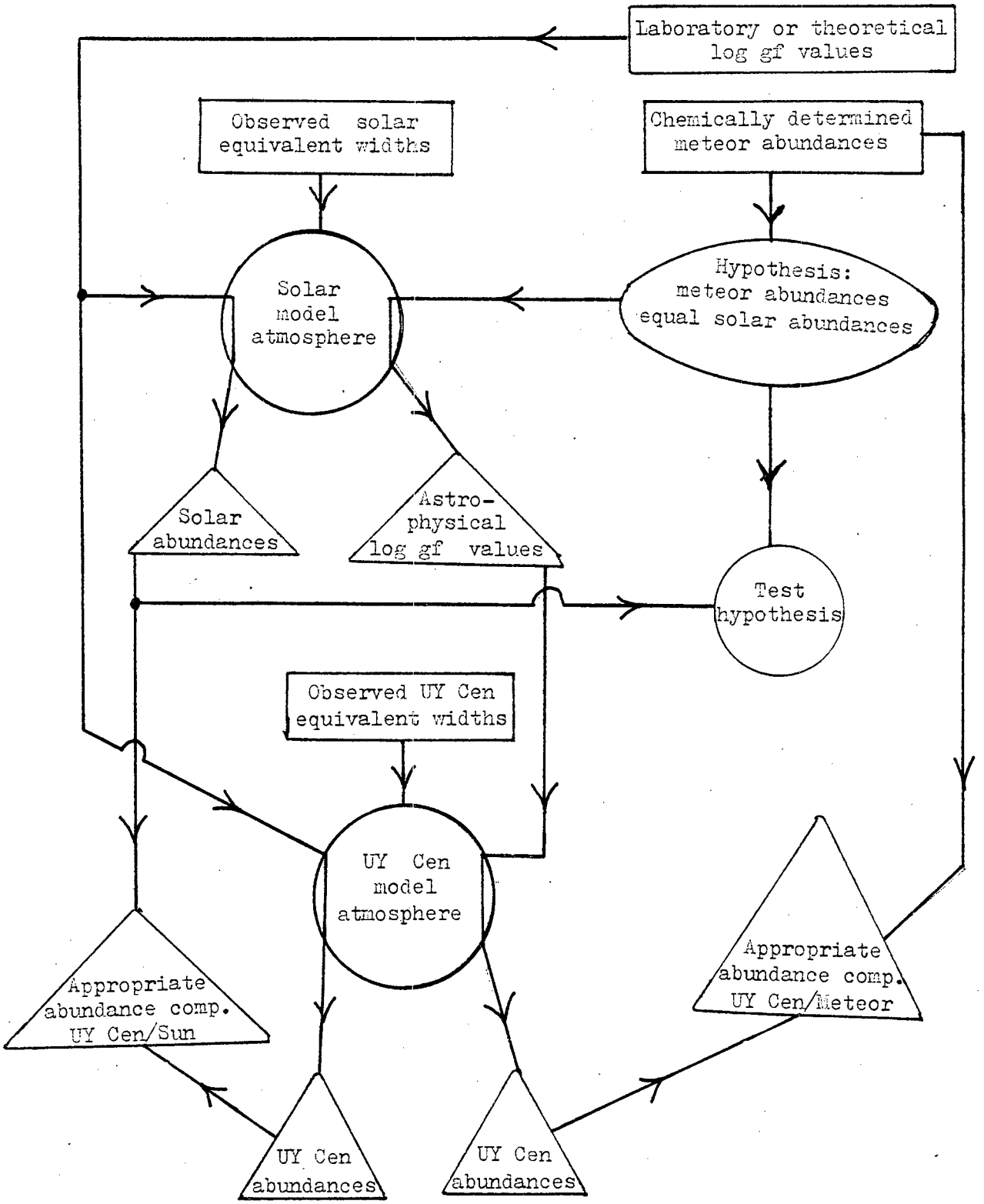

Figure 5.16

The flow diagram illustrates the correct relationship between the derived abundances and the methods used to find them.

5.16 Log gf Values

This section reviews and tabulates the log gf values used in the abundance analysis.

For many elements of interest, the quality and extent of laboratory determinations of log gf values still lags a long way behind the precision of solar line strengths and models. A good review of the situation, which is rapidly changing, is given by Biemont and Grevesse (1977). The Oxford group, under Blackwell, have produced log gf values with errors of order 1% for a number of Fe lines. However, for many of the elements beyond Ba, as well as for many lines of otherwise well determined elements, the best available data are those given in NBS53 (Corliss and Bozman(1962)and other publications of the NBS workers. Although the intensities from which the log gf values are derived are recognised to be good, these log gf values are now generally considered to contain fairly large systematic errors. For elements of the Fe group and lighter, a very large number of values of semi empirical log gf values have been calculated by Kurucz and Peytremann. These are considered relatively free of systematic errors but show large standard errors while for many heavy elements the Kurucz and Peytremann data is drawn directly from the NBS work. (In this analysis we hope to obtain abundances with errors due to log gf values of no more than 0.3 dex.)

The sun provides a convenient standard of comparison for abundance work and it should be possible to express stellar results on an absolute scale, by merely referring them to the appropriate solar calibration. If the same lines are observed in both the star and the sun then log gf values are not even required. However as soon as different lines and different ionization states, of a given element are found, as is the case with UY Cen, a knowledge of log gf values becomes essential. It is then important to ensure, that the adopted solar abundance pertains to the same set of log gf values used to find the stellar abundance. Recent atomic lifetime measurements by Andersen et al. (1975), for the elements, LaII, CeII, PrII, NdII, SmII, TmII,YbI,YbII and LaII indicates that the solar abundances of these elements are very similar to those found in meteors. This justifies us making a further extrapolation and assuming the meteor abundances are equal to the solar abundances which are then used to calibrate 'astrophysical' log gf values when required.

We have normalized Cameron's (1970) meteor abundances to the sun (on a scale where log N_H = 12) using Lambert and Luck's (1978) solar abundance determination for the elements Na, Mg, Al, Si, P, S, K and Ca. The solar abundances are then found by adding 1.54 to Cameron's meteor values.

The relationship between the log gf values and the appropriate solar and stellar abundances is summarised in Fig.5.16. In this diagram boxes correspond to observations, circles correspond to models and hypothesis, and triangles indicate results.

The policy used to obtain the appropriate log gf values and solar abundances is listed in order or priority below.

1) Use the best published log gf values directly and adopt the corresponding solar abundance.
2) Use the best available log gf or lifetimes to calibrate the NBS intensities. The appropriate solar abundance is that pertaining to the original log gf data.
3) Use meteor abundances, which become the appropriate solar abundances, to give astrophysical log gf values. These are in turn used to calibrate the NBS intensities.
4) Use the best available solar abundance and Kurucz and Peytremann log gf values.
5) As for 4 but use NBS log gf values.

The adopted log gf values and appropriate solar abundances are listed in tables 5.08 and 5.10 respectively. References to the origins of these data are given below the appropriate tables.

The following elements require special comment.

CaI

We adopt the relation

$$\log gf = \log gf_{NBS53} - 0.47 \ (\pm\ 0.06 \text{ s.e.})$$

based on Lambert and Luck's (1978) discussion of the Ca log gf data.

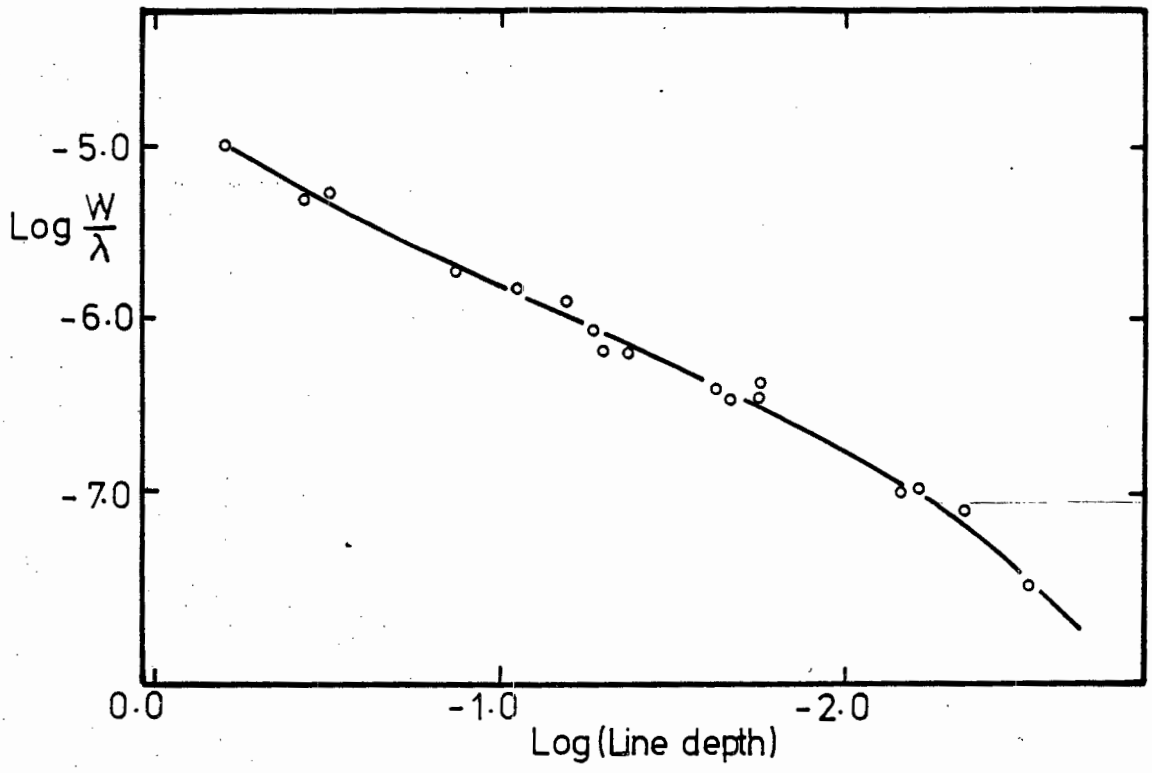

Figure 5.17

The calibration of equivalent width as a function of line depth, derived for the Delbouille et al. (1973) Solar Atlas.

NiI

We use the work of Lennard et al. (1975) to define the following mean corrections

$$\log gf_{LENNARD} = \log gf_{NBS53} - 0.67 = \log gf_{KURUCZ\ PEYT} - 0.09$$

YI

YI is present in the solar spectrum, so that the NBS log gf values can be compared directly with astrophysical log gf values found using a solar abundance $\log N_Y = 2.18 \pm .12$ ($\log N_H = 12.0$). This abundance was determined by Allen (1976) using theoretical log gf values for YII lines, given by Krueger et al. (1968) and is in close agreement with Cameron's renormalised abundance $\log N_Y = 2.22$.

28 YI lines are listed in the Rowland (Moore et al. (1966)) solar line list between 4039 and 6687 Å. Approximate equivalent widths were determined for each of the 150 lines taken from the KP line list which lie within ± 0.1 Å of the 28 YI lines. The YI lines which did not have competing identifications, as indicated by the KP lines, were then examined in the Delbouille et al. (1973) solar atlas. This left a total of 10 YI lines which had reasonable profiles, no competing identifications and wavelength agreement within ± 0.02 Å. Equivalent widths were determined for all these lines either by direct measurement (counting squares) or by using the log central depth against $\log W/\lambda$ calibration illustrated in Fig. 5.17. The Rowland wavelengths, wavelength differences between Rowland and the NBS data, NBS Intensities, solar $\log W/\lambda$, solar log gf values and lower excitation levels are listed in that order in Table 5.04.

The solar log gf values were obtained using the HSRA model atmosphere program as described above.

Equation 2 of NBS53 relates intensity to gf value as follows;

$$I = \frac{N}{U} \cdot \frac{8\pi^2 e^2 h}{m} \cdot \frac{gf}{\lambda^3} \cdot e^{-E/kT}$$

where N = particle density

e/m = the specific charge of the electron

E = the upper energy level

U = the partition function

λ = wavelength

T = Excitation temperature = 5040/θ

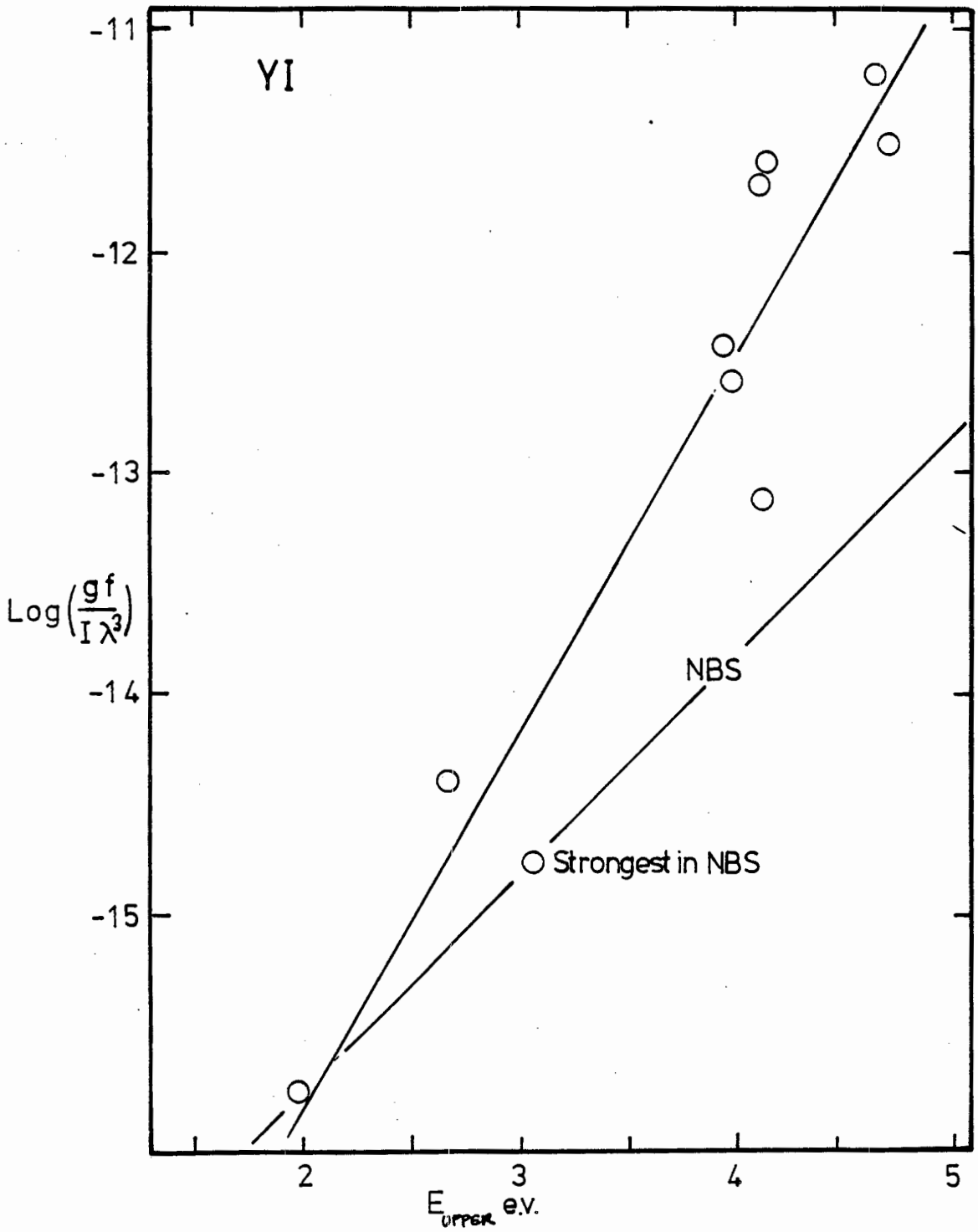

Figure 5.18

Calibration of the NBS53 intensities for YI using solar log gf values. The NBS solution is so marked.

This equation can be rewritten in a more convenient form

$$\text{as} \quad \log gf = 3 \log \lambda + \log I_{NBS} + C + \theta E_{upper} \qquad (5.83)$$

The constant C is discussed in NBS53 and can be broken down into various parameters specific to an individual ionization level, as well as a universal normalisation factor. NBS53 indicates that this normalisation is a function of upper energy level, although over the energy levels considered here it is taken as constant.

The solar log gf values and the NBS 145 intensities, of the 10 YI lines were used to solve for new values of θ and C, giving the solution;

$$\log gf = 3 \log \lambda + \log I_{NBS} - 19.29 + 1.706\ E_{UPPER} \qquad (5.84)$$

This is illustrated in Fig. 5.18 where the line is a least squares fit and where all the error is taken to be in the Y axis. The slope corresponds to an excitation temperature of 2954°. The line marked NBS is the solution given in NBS53, corresponding to an NBS arc temperature of 5100°. Note that the line with the greatest NBS intensity lies on this curve. The much lower temperature for the NBS arc derived from solar lines, could simply be a consequence of the high excitation lines, listed as present in the sun, being misidentifications. The solar solution predicts that the 4 volt YI line at 4852 Å should be observable with an equivalent width of 0.012 Å whereas the NBS53 log gf values predict it to be X10 weaker. Because 4852 is not seen in the sun we suggest, that despite the excellent wavelength agreement, the higher excitation lines are either misidentified or blended. We have therefore adopted the published NBS log gf values in the analysis.

If the astrophysical log gf values were used this would result in the abundance in UY Cen being increased by X1.44.

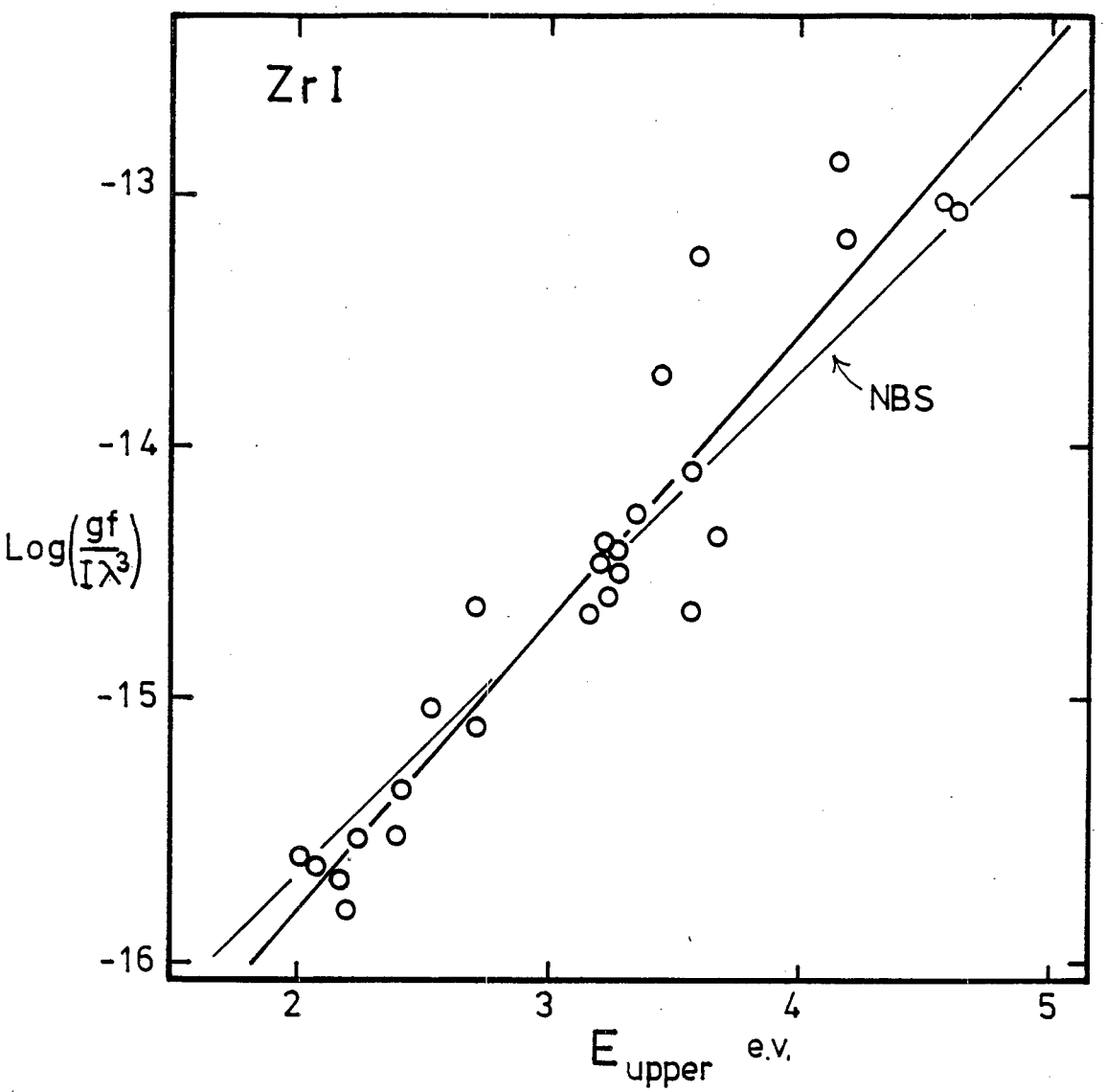

Figure 5.19

Calibration of the NBS53 intensities for ZrI using solar log gf values. Note how close the solution is to the NBS solution, indicated by the thin line.

TABLE 5.04

YI log $N_\odot$ = 2.18

$\lambda_{Rowland}$	$\lvert\Delta\lambda\rvert$	I_{NBS}	$Log\ W/\lambda_\odot$	log $gf_\odot$	χ_{lower}
4128.31	.00	8900	-5.69	0.04	0.06
4477.47	.02	160	-5.55	1.47	1.36
4487.26	.02	110	-5.62	1.40	1.37
4505.93	.02	500	-6.44	0.53	1.37
4513.58	.00	50	-6.01	1.48	1.90
4643.72	.02	2000	-5.76	-0.10	0.00
4819.64	.00	140	-6.21	0.76	1.36
4839.88	.01	770	-5.72	1.35	1.43
5135.18	.02	180	-6.00	1.88	2.29
6222.61	.02	300	-7.55	-1.94	0.00

ZrI

The solar spectrum was searched between 4000 and 7400 Å for all the ZrI lines listed in NBS145. Possible identifications were then compared with the KP line list and examined on the Delbouille at al. solar atlas. This left 26 good identifications which were combined with the renormalised meteor abundance of log N_o = 2.99, to give the astrophysical log gf values listed in Table 5.05. These log gf values were combined with the intensities in NBS145 to give the solution;

$$\log gf = 3 \log \lambda + \log I_{NBS} - 18.15 + 1.151\ E_{upper} \qquad (5.85)$$

which is illustrated in Fig. 5.19 and has been used to compute the log gf values used in the analysis. The NBS solution is also shown and is seen to be in remarkably close agreement. The UY Cen ZrI abundances would be reduced by only 7% if the NBS log gf values were used.

TABLE 5.05

Solar log gf values ZrI log $N_\odot$ = 2.99

λ	I_{NBS}	log $W/\lambda_\odot$	log $gf_\odot$	χ_{lower}
4030.04	490	-6.29	-0.86	0.60
4050.48	200	-5.53	-0.10	0.54
4055.70	600	-5.87	+0.53	1.58
4201.46	610	-5.90	-0.44	0.62
4241.69	1200	-6.19	-0.72	0.65
4431.49	160	-5.90	+0.27	1.35
4542.22	490	-6.07	-0.62	0.63
4575.52	490	-5.81	-0.97	0.00
4602.57	350	-6.16	+0.51	1.88
4683.42	260	-6.08	+0.26	1.53
4732.33	300	-6.34	-0.90	0.63
4739.48	1400	-5.91	-0.43	0.65
4772.31	870	-5.95	-0.50	0.62
4784.92	210	-6.56	-1.06	0.69
4805.87	260	-6.54	-1.04	0.69
4815.63	700	-6.20	-0.78	0.60
5680.90	120	-7.11	-1.77	0.54
5879.79	340	-6.70	-1.75	0.15
6127.44	680	-6.50	-1.54	0.15
6134.57	340	-6.56	-1.76	0.00
6140.46	100	-6.99	-1.67	0.52
6143.20	440	-6.54	-1.67	0.07
6489.64	110	-6.59	-0.23	1.55
7097.70	540	-6.59	-1.08	0.69
7102.91	280	-7.02	-1.56	0.65
7439.87	110	-7.55	-2.20	0.54

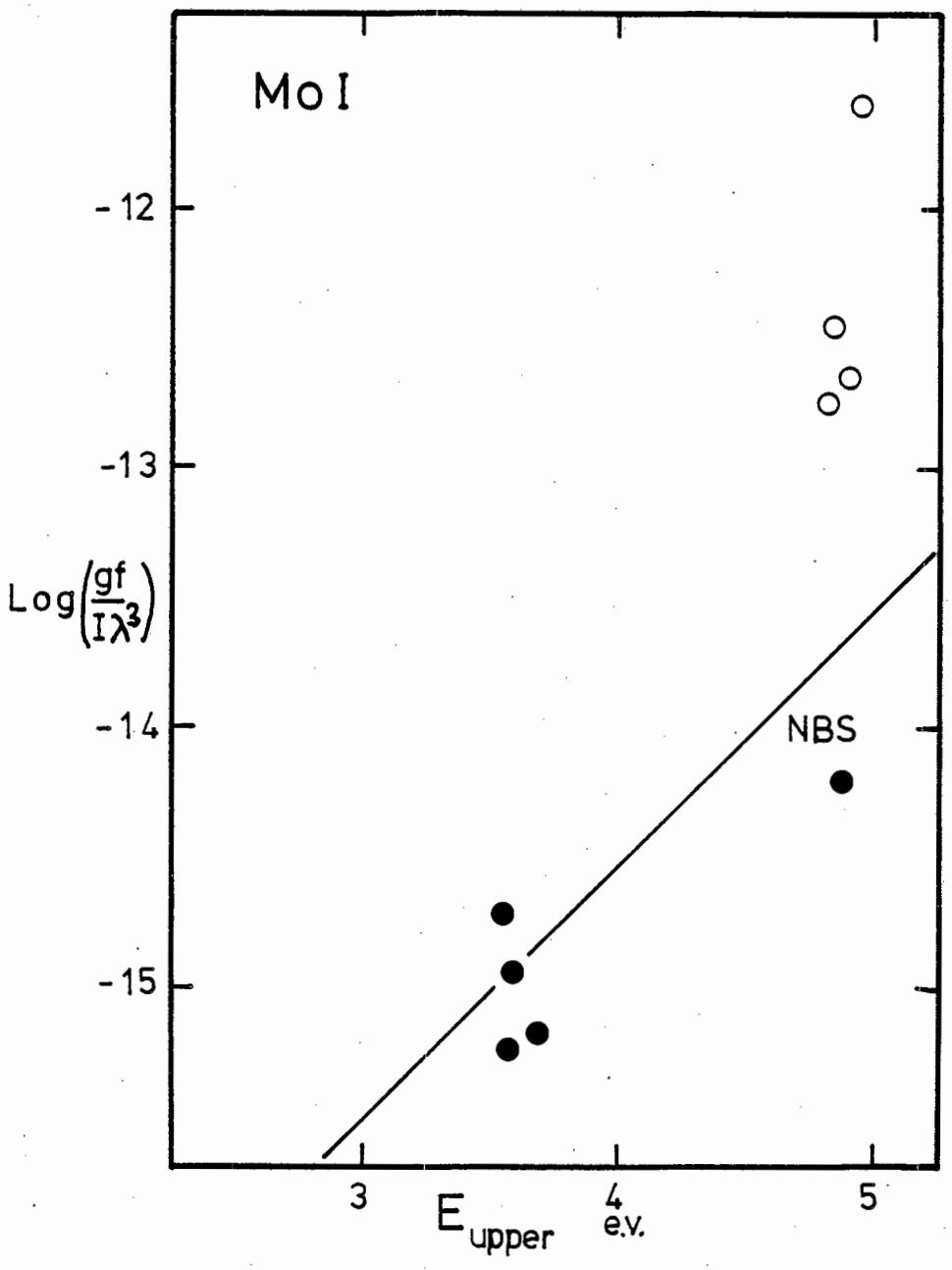

Figure 5.20

The strong MoI lines indicated by filled symbols have solar log gf values consistent with those given by the NBS solution, which is indicated by the line. The open symbols represent weak lines in the sun.

MoI

Nine MoI lines were found in the sun by the methods described above. These are listed in Table 5.06 along with astrophysical log gf values calculated on the basis of a meteor abundance of log N_{Mo} = 2.14. Fig 5.20 shows that the lines with the strongest NBS intensities, indicated by filled symbols, are all close to the NBS solution. We have therefore adopted the NBS log gf values since there are insufficient grounds for rejecting the NBS solution.

TABLE 5.06

λ	$\lvert\Delta\lambda\rvert$	I_{NBS}	log $W/\lambda_{\odot}$	log $gf_{\odot}$	χ_{lower}
4396.63	.03	140	-6.19	0.52	2.08
4468.30	.02	190	-5.95	0.77	2.08
4474.57	.01	630	-5.72	1.00	2.06
4411.59	.02	2500	-6.58	0.12	2.08
4627.49	.01	100	-5.57	1.39	2.28
5506.51	.02	7800	-6.04	-0.05	1.33
5533.04	.01	5200	-6.28	-0.30	1.33
5570.40	.05	2500	-6.06	-0.07	1.33
6030.68	.02	1300	-6.66	-0.49	1.53

LaI

Calibration of the NBS intensities in terms of log gf was done by methods similar to those described in the previous section using Molnar's (1972) observations of LaI lines in sunspots. Molnar uses Stellmacher and Wiehr's (1970) sunspot model to deduce abundances using NBS log gf values. We have inverted the procedure using a normalised meteor abundance, log N_{La} = 1.19. Because his results are only shown graphicaly, there is an ambiguity in knowing which of Molnar's abundances applies to which line. This ambiguity accounts for the arrows joining the points in Fig.5.21. It is clear that the ambiguity has little effect on the solution. The solution,

$\theta = 1.649 \pm 0.13$ $C = -17.07 \pm .40$

is seen, from Fig. 5.21, to be significantly different from the NBS solution, as the deduced

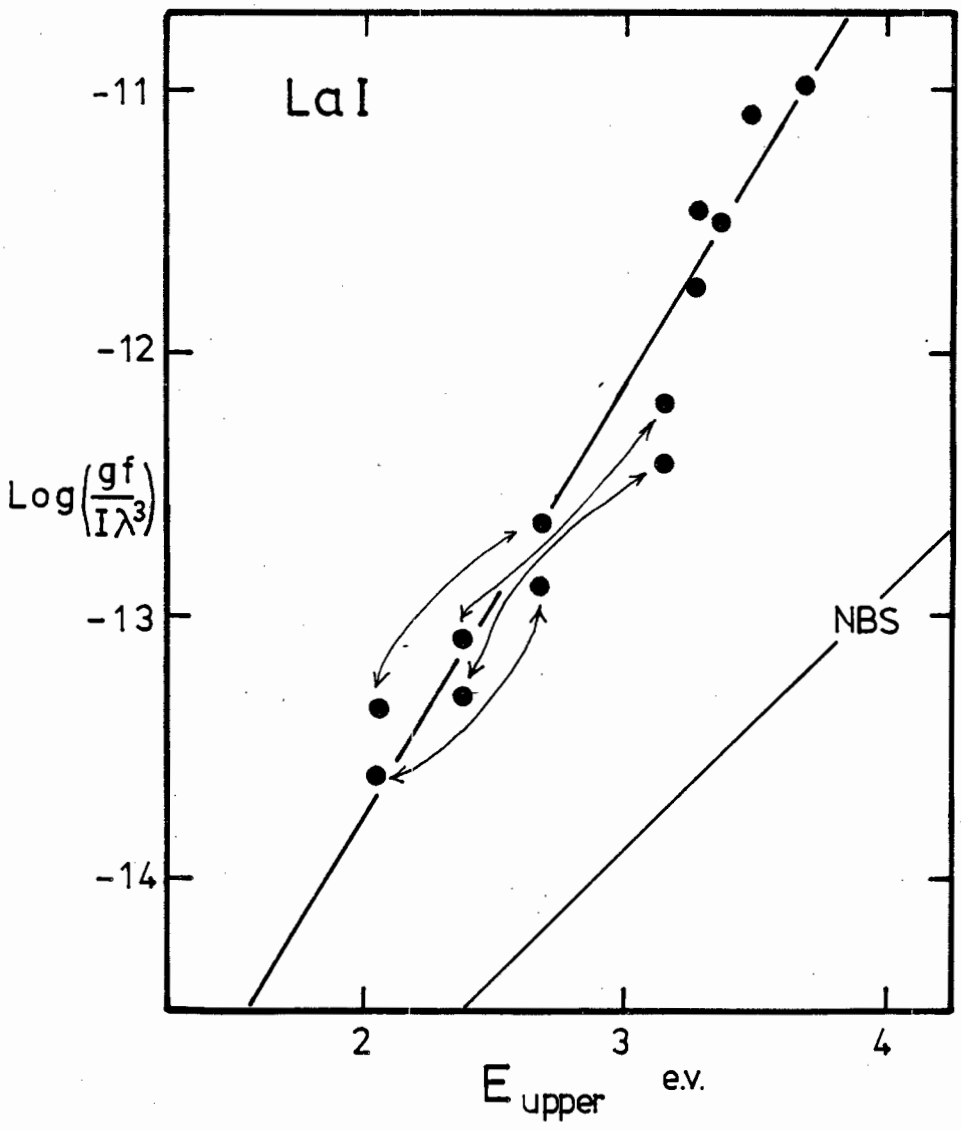

Figure 5.21

Calibration of the NBS53 intensities for LaI using published sunspot data. The arrows occur because of an ambiguity in the published data but clearly do not effect the solution.

log gf values are 1.4 dex larger. Despite the large correction, the La abundance given by the ionized and neutral lines in UY Cen, differs by only ~ 0.4 dex.

CeI

Log gf data have been derived from the intensities given in NBS 145 and the arc data given in NBS53, with the exception that an updated value of the ionization potential (χ_{ion} = 5.47) given in Allen (1973), was used.

LaII CeII NdII SmII PrII

Log gf values have been obtained for all these elements, by the methods outlined for YI, except that we have used the equivalent width and model atmosphere data, given by Grevesse and Blanquet (1969). In their paper, they compared the abundances they obtained from existing log gf data, with meteor abundances, whereas, we use the meteor abundances to derive log gf data. The constants, defined by equation 5.83 used to derive the log gf values in this analysis, are listed in Table 5.06. The solutions for individual elements are shown in Fig. 5.22.

TABLE 5.06

	θ	C
LaII	0.83 ± 0.09	-17.07 ± 0.31
CeII	1.05 ± 0.20	-17.37 ± 0.66
NdII	0.71 ± 0.12	-16.54 ± 0.40
SmII	0.75 ± 0.15	-16.52 ± 0.62
PrII	0.74 ± 0.24	-16.29 ± 0.58

SmI

Marek and Munster (1978) have measured lifetimes, for certain SmI energy levels, that can be used to check the NBS53 log gf values.

The lifetime Δt is related, to the Einstein coefficient of spontaneous emission A, by the relation

$$\Delta t = \frac{1}{\sum_{\ell<u} A_{u\ell}} \qquad (5.86)$$

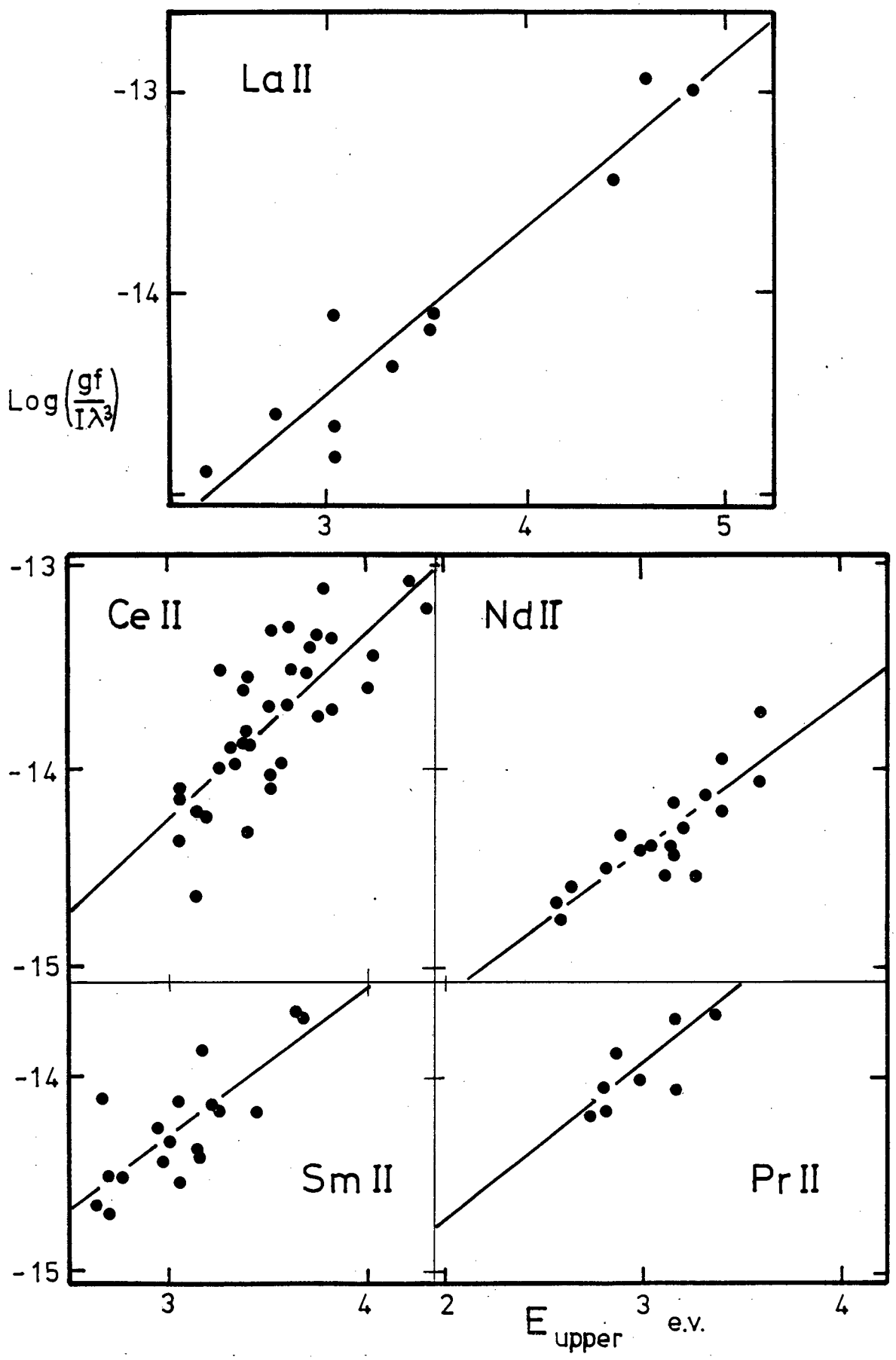

Figure 5.22

Calibrations of the NBS53 data for various elements using Grevesse and Blanquet's (1969) model and data.

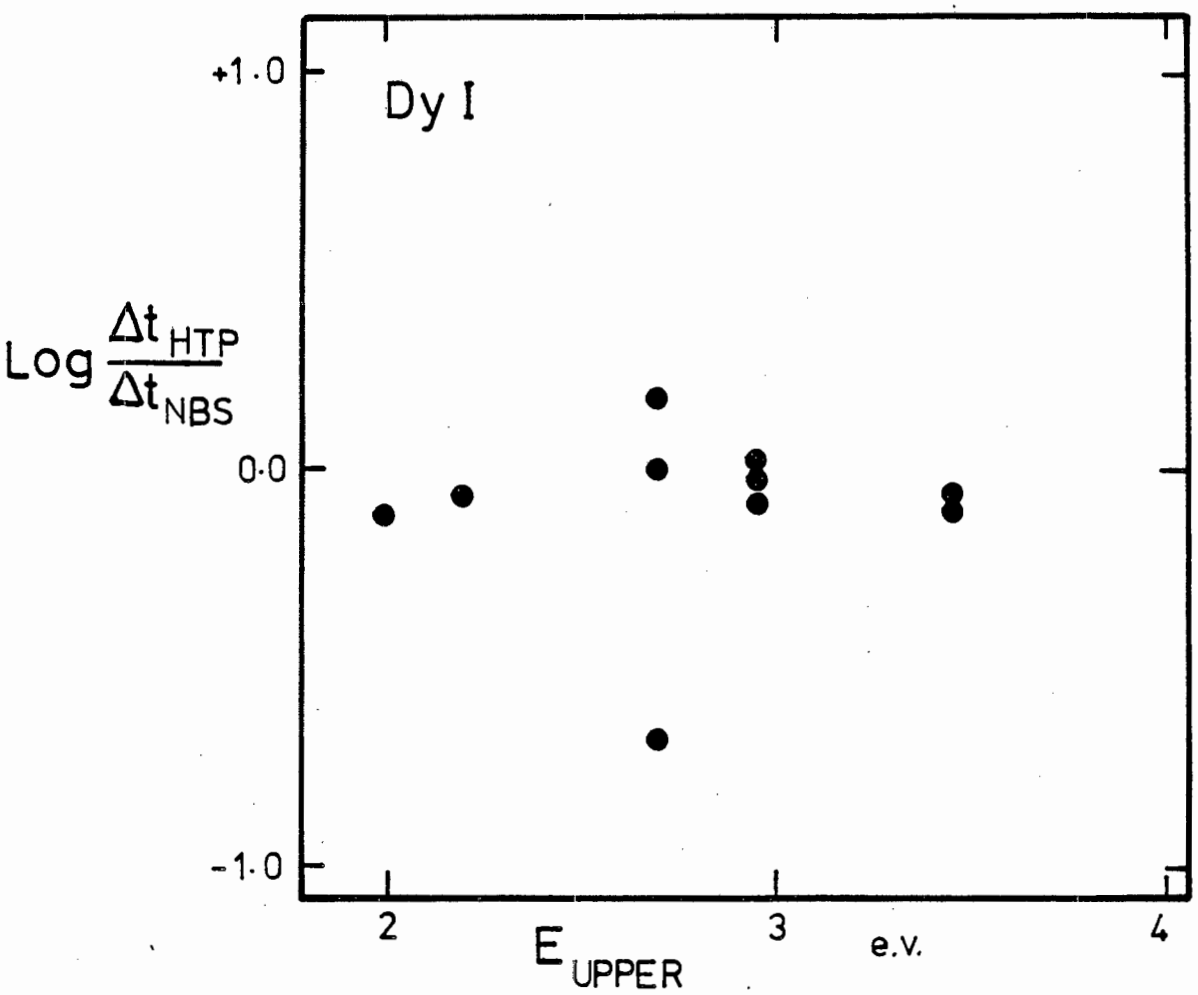

Figure 5.23

Comparison between Hotop and Marek's (1978) lifetimes and those deduced from the NBS53 intensities, using θ_{ex} = 0.83.

The summation takes place over all transitions having lower levels ℓ and a common upper level denoted by subscript u. The relationship between f value and $A_{u\ell}$, for λ in angstrom and $A_{u\ell}$ in sec^{-1} is;

$$f = 1.884 \times 10^{-15} \lambda^2 \frac{g_u}{g_\ell} A_{u\ell} \qquad (5.87)$$

Remember also that $-g_u f_{em} = g_\ell f_{abs} = gf$

In practice the summation was carried out for all the transitions listed in NBS53 having the appropriate common upper level. This obviously ignores many weak transitions but should not seriously overestimate the lifetimes. For the 11 levels considered, the lifetimes calculated from the NBS53 data do not differ from those listed by Marek and Munster (1978). There is too small a range in upper energy level to reveal any temperature error in the NBS SmI data. This result raises a slight problem because Molnar, using NBS53 log gf values, finds a sunspot SmI abundance 1.5 dex greater than the meteor abundance. On the other hand recent lifetime work by Andersen et al. (1975) for SmII gives a solar abundance 0.2 less than the meteor abundance. This leads us to the embarrassing situation of either doubting the SmI lifetimes or Molnars analysis, which we have previously used for LaI. Since Molnar finds a 1.5 dex overabundance in the sun compared with the meteors, there remains the very unlikely possibility that the sunspot SmI lines are misidentified. At present, the matter remains unresolved and we adopt the NBS53 log gf values for SmI.

DyI

Log gf values were calculated from NBS145 intensities using various values of θ. These log gf values were then compared with the lifetime measurements published by Hotop and Marek (1978) using the methods outlined in the previous section.

The best agreement was given by a value of $\theta = 0.83$, which is the mean excitation of the NBS arc found by us for the elements LaII, CeII, PrII, NdII, SmII, GdII, DyI and EuII. Log gf values were computed from equation 5.84 using the constants; $\theta = 0.831$, $C = -16.58$. The agreement between the Hotop lifetimes and lifetimes computed from these log gf values is shown in Fig. 5.23.

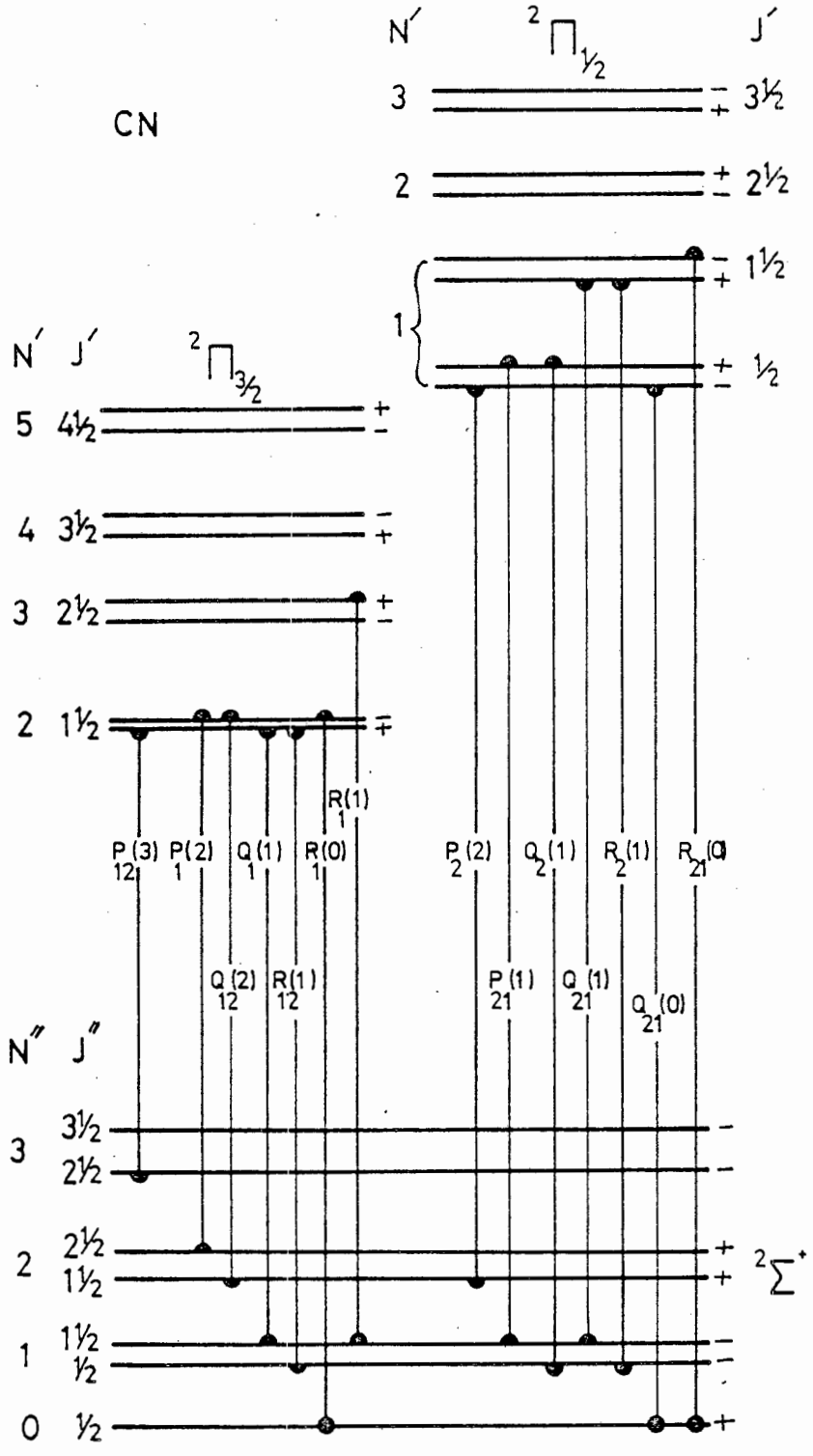

Figure 5.24

Term diagram for the lowest rotational transitions of CN.

HoI

No energy levels are available for HoI so we have assumed they are all ground state transitions and calculated log gf values using the arc data given in NBS53.

The finally adopted set of atomic line data is given in Table 5.07 The footnotes at the end of the table indicate the origin of individual log gf values.

5.17 CN, Extra Theory and Data

This section gives the theory and lists the sources of data used to compute the CN abaundance and $^{12}C/^{13}C$ isotope ratio.

The infra red CN bands used in this analysis arise from a $^2\Pi - ^2\Sigma^+$ electronic transition where the Σ state is the ground electronic state of the molecule and the $^2\Pi$ level is inverted. This is illustrated in Fig.5.24 along with a few rotational transitions. The notation and methods followed in this section are those adopted by Tatum (1967). Each CN vibrational transition consists of a triple headed band system degraded to the red. These are, from blue to red, an R_2 head an R_1 head and a Q_1 head, all led by a very weak satellite R_{21} head. The P_2, Q_2, P_1 and P_{12} systems do not form band heads. The satellite R_{12}, P_{21} and Q_{21} bands, shown on the term diagram, are not resolved from the Q_1 Q_2 and R_2 bands because of the very small doublet splitting of the $^2\Sigma$ level. The satellite branches are however extremely weak and can be ignored in the intensity calculations. Hund's case b coupling always pertains to a Σ level and the coupling of the upper level changes from a to b toward larger quantum numbers.

The line strength $\mathcal{S}$ of an individual rotational line is given by the relation

$$\mathcal{S} = \frac{\text{Hönl-london factor x S}}{(2-\delta_{o,\Lambda})(2s+1)(2J+1)} \qquad (5.88)$$

where S in the numerator is the band strength having dimensions [dipole moment]^2. The s and J in the denominator refer to the electron spin angular momentum and total angular momentum respectively. δ is the Kronecker delta symbol which is unity when the electron angular momentum $\Lambda = 0$, as in the case of Σ states, but is otherwise equal to zero. The line strength is related to the absorption

oscillator strength f_{12} by

$$f_{12} = \frac{8}{3} \frac{\pi^2 m\nu}{he^2 g} S \qquad (5.89)$$

where g is the electronic statistical weight, here equal to one. When S is given in atomic units (1 atomic unit = 2.542×10^{-16} cgs esu) and λ in angstrom, equations 5.88 and 5.89 give numerically

$$f_{12} = \frac{151.97}{(2J''+1)} \frac{(\text{Hönl london factor})}{\lambda} \times S \qquad (5.90)$$

The Boltzman equation for Hunds case b, which is analogous to equation 5.46 of section 5.03, is written;

$$\frac{N\ (\text{single rotational level})}{N_{total}} = \frac{2\emptyset(2J''+1)}{Q_{int}} e^{-\{Te+G(V'')+F(N'')\}\frac{hc}{kT}} \qquad (5.91)$$

For a ground electronic state the electronic excitation level Te equals zero and for a heteronuclear molecule with either Hunds case a or b, $\emptyset = \frac{1}{2}$. Q_{int} is the partition function, G(V'') and F(N'') are the vibrational and rotational excitation levels and (2J''+1) is the rotational statistical weight.

Using equations 5.42 of section 5.03 it is clear that we can combine equations 5.90 and 5.91 to express the absorption coefficient at the line centre K_o, in terms of N_{total} the total number of CN molecules per cc.

$$K_o = \frac{\sqrt{\pi}e^2 N_{total}}{m_e c\ \Delta\nu_D} \frac{151.97}{\lambda} (\text{Hönl london factor}) \times S \frac{e^{-\{G(V'')+F(N'')\}\frac{hc}{kT}}}{Q_{int}} \qquad (5.92)$$

If this equation is compared with the equivalent equation for an atomic line namely;

$$K_o = \frac{\sqrt{\pi}e^2}{m_e c} \frac{N_{total}}{\Delta\nu_D} \frac{gf}{u} e^{-\chi/kT}$$

it is clear that for the sake of uniformity of treatment we can tabulate:

$$\chi_{CN} = (G(V'')+F(N'')$$

$$gf_{CN} = \frac{151.97}{\lambda} (\text{Hönl-london factor}) \times S$$

and treat the CN lines in the same fashion as the atomic lines.

Dissociation

In general, molecular dissociation plays a much more important role than ionization, in relating the total number of C and N atoms, in the star's atmosphere, to the total number of CN molecules, N_{total}, given in equation 5.92. The solution of the dissociation equation

$$C + N \rightleftharpoons CN$$

is complicated by the fact that the whole network of possible reactions between C, N and all other atoms, must be considered. Calculation of this network is beyond the scope of this thesis; instead we rely on Greene's (1972) published results. These Tables give the number of CN molecules, as a function of pressure and temperature for various initial compositions. Although the calculations do not span the entire range of the Johnson model atmospheres, they do cover the range over which the absorption lines are mostly formed.

Sources of Molecular Data for CN

Partition functions Q_{int}, are taken from Tatum (1966) while the band strengths S, are taken from Arnold and Nicholls (1972). Hönl London factors are taken from Earls (1935). They have been normalised to obey the sum rule given by Tatum, which states that the sum of the factors for all the transitions which have a common lower level, must equal (2J"+1). The equations for the vibration and rotational energy levels are taken from Herzburg (1950). The values of the molecular constants used have been taken from Fay et al. (1971). Appropriate constant have been used used for ^{12}CN and ^{13}CN although the same partition function has been used for both molecules. Kilston (1975) quotes the change of partition function to be 5%, which is well within the errors expected from observational sources.

5.18 Listing of the CN and Atomic line Data

The data used in the curve of growth and model atmosphere analysis are listed in Table 5.07. The first two columns give the designation of the lower energy levels. The numbers in brackets naming individual rotational levels are the N" values illustrated in Fig. 5.24.

TABLE 5.07

Isotope	Lines Designation	λ UY Cen	log W/λ	χ_{lower}	Hönl-london factor	log gf
(2,0)	P_1 (19)	8033.7	-5.22	0.08	7.78	-2.23
	P_2 (19)	8019.3	-5.24	0.08	7.60	-2.24
	Q_1 (24)	8022.69	-4.86	0.13	22.74	-1.76
	R_2 (32)	8006.1	-5.33	0.24	15.84	-1.92
Normal lines						
(2,0)	P_1 (24)	8032.67	-4.48	0.14	10.42	-2.10
	P_2 (13)	7936.23	-4.58	0.04	4.70	-2.44
	Q_1 (22)	7968.50	-4.54	0.12	20.78	-1.80
	Q_1 (23)	7974.62	-4.55	0.13	21.84	-1.78
	Q_1 (28)	8010.07	-4.39	0.19	27.06	-1.68
	Q_1 (29)	8018.05	-4.48	0.20	28.10	-1.67
	Q_1 (59)	8407.15	-4.71	0.82	58.90	-1.37
	Q_2 (6)	7886.71	-4.63	0.01	4.02	-2.43
	Q_2 (8)	7892.09	-4.56	0.02	5.72	-2.36
	Q_2 (21)	7950.38	-4.42	0.11	18.72	-1.85
	Q_2 (25)	7977.22	-4.49	0.15	22.90	-1.76
	Q_2 (30)	8017.03	-4.54	0.22	29.00	-1.67
	Q_2 (34)	8054.02	-4.50	0.28	32.26	-1.61
	Q_2 (35)	8064.13	-4.50	0.29	33.30	-1.60
	Q_2 (40)	8118.82	-4.45	0.38	38.46	-1.54
	R_1 (31)	7967.11	-4.47	0.23	16.16	-1.91
	R_1 (40)	8038.05	-4.66	0.38	20.80	-1.80
	R_2 (10)	7875.89	-4.54	0.03	4.28	-2.48
	R_2 (17)	7890.58	-4.59	0.07	8.94	-2.16
	R_2 (34)	7979.73	-4.41	0.28	16.96	-1.88
(3,1)	P_1 (7)	8124.08	-4.93	0.27	2.02	-2.64
	Q_1 (28)	8211.26	-4.58	0.44	27.06	-1.51
(4,2)	P_2 (26)	8454.13	-4.65	0.67	11.22	-1.96
	Q_1 (29)	8431.11	-4.81	0.71	28.10	-1.53
	Q_2 (8)	8292.09	-4.69	0.52	5.72	-2.23
	Q_2 (30)	8429.89	-4.69	0.72	28.10	-1.53
	R_2 (17)	8291.19	-4.76	0.57	7.94	-2.08
(5,3)	Q_1 (22)	8595.64	-4.79	0.87	20.78	-1.84

Table 5.08 gives the data for the atomic lines. The wavelengths in column 1 are observed values in UY Cen. The lower excitation levels in column 3 are in electron volts and the letters in column 5 refer to the notes at the end of the table. The remaining entries are self explanatory.

TABLE 5.08

WAV	LOG W/L	CHI	LOG GF			WAV	LOG W/L	CHI	LOG GF		
6707.78	-3.94	0.00	0.00	a	LI 1	6064.65	-4.20	1.05	-1.68	g	TI 1
		0.00	-0.30	a	LI 1	6031.61	-4.01	0.05	-4.00	c	TI 1
						5990.59	-4.14	0.05	-4.44	c	TI 1
8183.27	-3.98	2.10	0.22	b	NA 1	5953.23	-4.21	1.89	-0.15	g	TI 1
6160.78	-4.31	2.10	-1.27	b	NA 1	5941.79	-4.08	1.05	-1.41	g	TI 1
5892.21	-2.15	0.00	0.11	b	NA 1	5739.43	-4.23	2.25	-0.31	e	TI 1
		0.00	-0.19	b	NA 1						
						8255.85	-4.22	1.06	-2.08	c	V 1
3806.77	-4.23	4.35	0.12	c	MG 1	3027.37	-4.13	1.06	-2.14	c	V 1
						6785.03	-4.23	1.05	-2.19	h	V 1
3773.94	-4.51	4.02	0.04	d	AL 1	6766.53	-4.20	1.06	-1.92	h	V 1
						6452.33	-4.23	1.19	-1.56	h	V 1
7698.77	-3.82	0.00	-0.18	d	K 1	6285.15	-4.08	0.28	-1.74	h	V 1
7664.80	-3.66	0.00	0.12	d	K 1	6251.77	-3.97	0.29	-1.52	h	V 1
						6245.12	-4.10	0.26	-2.45	c	V 1
6493.80	-4.05	2.52	-0.57		CA 1	6224.50	-4.01	0.29	-2.06	h	V 1
6471.62	-4.17	2.53	-1.16		CA 1	6213.87	-3.97	0.30	-2.10	h	V 1
6439.10	-4.07	2.53	-0.22		CA 1	6150.13	-4.01	0.30	-1.85	h	V 1
6169.52	-4.02	2.53	-0.89		CA 1	6039.73	-4.19	1.06	-0.94	h	V 1
6169.12	-4.02	2.53	-1.19		CA 1	6008.56	-4.30	1.18	-2.52	h	V 1
6102.70	-3.86	1.88	-1.26		CA 1	5737.08	-4.15	1.06	-0.79	h	V 1
8662.11	-3.56	1.69	-0.77		CA 2	5698.56	-4.11	1.06	0.03	h	V 1
8542.12	-3.47	1.69	-0.51		CA 2	5668.34	-4.17	1.03	-1.17	h	V 1
8498.20	-3.61	1.69	-1.46		CA 2	5627.62	-4.06	1.08	-0.38	h	V 1
6193.73	-4.10	0.00	-1.92	c	SC 1	6330.16	-4.19	0.94	-2.70	c	CR 1
						5798.43	-4.18	1.03	-3.98	c	CR 1
8819.41	-4.36	1.07	-3.19	c	TI 1						
8761.39	-4.66	1.74	-2.55	c	TI 1	8824.21	-4.12	2.20	-1.22	e	FE 1
8719.54	-4.47	1.74	-2.60	c	TI 1	8621.63	-4.48	2.95	-2.13	e	FE 1
8675.39	-4.19	1.07	-1.25	e	TI 1	8387.80	-4.13	2.18	-2.02	e	FE 1
8494.43	-4.46	1.74	-2.11	c	TI 1	7723.15	-4.48	2.28	-3.04	e	FE 1
8467.18	-4.41	2.12	-1.02	e	TI 1	7389.28	-4.43	4.30	-0.60	e	FE 1
8424.39	-4.51	2.10	-1.13	e	TI 1	6839.83	-4.27	2.56	-2.99	e	FE 1
8423.10	-4.50	1.88	-2.17	c	TI 1	6663.45	-4.25	2.42	-2.40	e	FE 1
8353.14	-4.22	0.81	-2.30	e	TI 1	6575.08	-4.29	2.59	-2.64	e	FE 1
8024.83	-4.36	1.88	-0.78	e	TI 1	6574.25	-4.09	0.99	-5.37	e	FE 1
7996.46	-4.67	3.34	0.24	e	TI 1	6358.71	-4.07	0.86	-4.47	i	FE 1
7852.70	-4.22	0.85	-2.87	c	TI 1	6280.67	-4.16	0.86	-4.39	i	FE 1
7834.50	-4.44	0.83	-4.19	c	TI 1	6254.27	-4.21	2.23	-3.07	e	FE 1
7796.45	-4.61	0.82	-4.84	c	TI 1	5943.49	-4.44	2.20	-4.28	c	FE 1
7791.34	-4.51	0.84	-4.37	c	TI 1	5778.41	-4.29	2.59	-3.23	c	FE 1
7773.74	-4.86	2.33	-2.60	c	TI 1						
7580.31	-4.50	2.23	-1.12	e	TI 1	7084.98	-4.20	1.88	-1.35	c	CO 1
7471.18	-4.33	0.81	-3.75	c	TI 1						
7469.94	-4.24	0.84	-3.30	c	TI 1	8770.64	-4.71	2.74	-3.27		NI 1
7466.37	-4.52	1.74	-3.17	c	TI 1	7385.29	-4.49	2.74	-2.01		NI 1
7424.50	-4.30	0.83	-3.49	c	TI 1	6914.52	-4.20	1.95	-2.46		NI 1
7423.15	-4.35	1.44	-2.64	f	TI 1						
7364.07	-4.16	1.43	-1.13	f	TI 1	7800.23	-4.20	0.00	0.14	j	RB 1
7337.72	-4.43	2.24	-1.53	c	TI 1						
7271.33	-4.32	1.44	-2.21	f	TI 1	7070.07	-4.31	1.83	-0.18	k	SR 1
7251.68	-4.16	1.43	-0.78	e	TI 1						
7138.05	-4.39	1.43	-2.27	c	TI 1	8800.61	-3.94	0.00	-2.58		Y 1
7065.12	-4.42	1.46	-2.46	c	TI 1	6793.70	-4.02	0.07	-2.14		Y 1
6556.01	-4.13	1.46	-0.97	g	TI 1	6534.88	-4.14	0.07	-3.04		Y 1
6554.17	-4.19	1.44	-1.19	e	TI 1	6557.35	-4.08	0.00	-2.62		Y 1
6336.14	-4.28	1.44	-1.48	e	TI 1	6222.54	-3.91	0.00	-1.95		Y 1
6215.17	-4.28	2.70	0.09	e	TI 1	6023.39	-4.00	0.00	-2.33		Y 1
6091.22	-4.39	2.27	-0.19	e	TI 1						

WAV	LOG W/L	CHI	LOG GF			WAV	LOG W/L	CHI	LOG GF		
8749.47	-4.14	0.60	-2.92	ZR	1	7219.86	-4.46	0.37	-0.73	LA	1
8453.12	-4.53	1.40	-1.38	ZR	1	7023.60	-4.26	1.00	0.90	LA	1
8063.06	-4.11	0.62	-1.77	ZR	1	6644.43	-4.12	0.13	-0.77	LA	1
8058.10	-4.31	0.62	-2.17	ZR	1	6600.13	-4.26	0.37	-0.36	LA	1
7940.47	-4.27	0.52	-2.76	ZR	1	6578.54	-4.08	0.00	-0.36	LA	1
7869.96	-4.28	0.69	-2.32	ZR	1	6454.54	-4.08	0.33	0.03	LA	1
7849.32	-4.21	0.69	-1.90	ZR	1	6411.03	-4.15	0.37	0.43	LA	1
7822.92	-4.51	1.75	-1.08	ZR	1	6394.19	-4.02	0.43	0.91	LA	1
7819.32	-4.43	1.82	-0.51	ZR	1	6325.84	-4.09	0.13	0.18	LA	1
7723.93	-4.35	0.60	-2.99	ZR	1	6293.46	-4.08	0.43	0.10	LA	1
7708.43	-4.67	1.58	-1.82	ZR	1	6249.90	-4.01	0.51	1.29	LA	1
7658.62	-4.20	0.54	-2.55	ZR	1	5789.15	-4.07	0.43	0.97	LA	1
7558.48	-4.42	1.55	-1.45	ZR	1	5631.26	-4.15	0.37	0.63	LA	1
7544.62	-4.56	1.58	-1.51	ZR	1	6774.22	-4.15	0.13	-1.88	LA	2
7383.56	-4.50	1.86	-1.07	ZR	1	6262.34	-4.16	0.40	-1.30	LA	2
7111.73	-4.07	0.52	-1.85	ZR	1	6172.71	-4.21	0.13	-2.39	LA	2
7102.98	-4.05	0.65	-1.56	ZR	1	5936.26	-4.28	0.17	-2.19	LA	2
7087.31	-4.03	0.60	-1.75	ZR	1						
7057.32	-4.49	1.58	-1.36	ZR	1	3810.87	-4.50	0.30	-1.31	CE	1
6990.79	-4.10	0.62	-1.68	ZR	1	8261.05	-4.56	0.30	-1.30	CE	1
6975.87	-4.50	1.44	-1.91	ZR	1	8245.17	-4.53	0.17	-1.66	CE	1
6762.35	-3.99	0.00	-2.68	ZR	1	8223.62	-4.55	0.59	-1.25	CE	1
6489.67	-4.21	1.55	-0.23	ZR	1	8171.38	-4.18	0.16	-1.74	CE	1
6484.35	-4.17	0.63	-2.75	ZR	1	7866.05	-4.30	0.17	-1.50	CE	1
6451.65	-4.17	0.62	-2.50	ZR	1	7842.66	-4.29	0.17	-1.42	CE	1
6407.05	-4.25	0.15	-2.78	ZR	1	7812.63	-4.69	0.72	-1.11	CE	1
6193.03	-4.15	0.54	-2.07	ZR	1	7806.83	-4.53	0.40	-1.67	CE	1
6140.45	-4.12	0.52	-1.67	ZR	1	7762.96	-4.66	0.52	-1.45	CE	1
6127.45	-4.00	0.15	-1.55	ZR	1	7732.30	-4.53	0.47	-1.20	CE	1
6124.83	-4.08	0.52	-1.94	ZR	1	7438.55	-4.45	0.55	-1.06	CE	1
6025.36	-4.11	0.15	-2.79	ZR	1	7421.03	-4.47	0.40	-1.48	CE	1
5995.32	-4.24	0.73	-2.36	ZR	1	7393.35	-4.40	0.59	-1.29	CE	1
5955.35	-3.95	0.00	-2.39	ZR	1	7017.23	-4.45	0.49	-1.30	CE	1
5680.98	-4.17	0.54	-1.77	ZR	1	6894.56	-4.42	0.29	-1.49	CE	1
5868.27	-3.97	0.15	-2.53	ZR	1	6749.48	-4.34	0.40	-1.37	CE	1
						6577.42	-4.49	0.17	-1.73	CE	1
5819.57	-4.95	1.61	-1.22 k	NB	1	6458.05	-4.17	0.17	-0.87	CE	1
						6253.65	-4.15	0.27	-1.12	CE	1
6733.82	-4.42	1.34	-1.83	MO	1	6228.21	-4.15	0.00	-1.61	CE	1
6619.20	-4.42	1.34	-1.50	MO	1	6187.94	-4.25	0.03	-1.35	CE	1
6030.61	-4.20	1.53	-0.49	MO	1	6123.72	-4.50	0.97	0.06	CE	1
5722.76	-4.32	1.42	-1.35	MO	1	6076.58	-4.34	0.95	-0.06	CE	1
						6066.73	-4.32	0.21	-0.93	CE	1
8520.90	-4.36	0.00	0.15 j	CS	1	6024.19	-4.16	0.40	-0.11	CE	1
						6006.77	-4.20	0.52	-0.28	CE	1
7911.35	-4.12	0.00	-2.00 c	BA	1	5992.60	-4.40	0.55	-0.34	CE	1
7780.44	-4.33	1.14	-0.23 c	BA	1	5972.75	-4.43	0.64	-0.85	CE	1
7392.44	-4.37	1.57	0.09 c	BA	1	5950.60	-4.34	0.41	-0.76	CE	1
6675.28	-4.18	1.14	-0.15 c	BA	1	5929.77	-4.22	0.55	-0.54	CE	1
6595.26	-4.29	1.12	0.15 c	BA	1	5926.33	-4.13	0.00	-0.79	CE	1
6110.77	-4.29	1.19	0.44 c	BA	1	5912.90	-4.23	0.59	-0.29	CE	1
5997.01	-4.37	1.12	-0.12 c	BA	1	5871.59	-4.06	0.27	-0.38	CE	1
5777.64	-4.31	1.67	0.72 c	BA	1	5812.91	-4.15	0.55	0.13	CE	1
6496.90	-3.98	0.60	-0.46 c	BA	2	5773.55	-4.14	0.00	-1.15	CE	1
						5692.97	-4.26	0.47	0.04	CE	1
8748.45	-4.36	0.33	-0.82	LA	1	5634.40	-4.20	0.21	-1.24	CE	1
8545.49	-4.19	0.37	-0.46	LA	1	5633.12	-4.29	0.41	-0.63	CE	1
8001.93	-4.24	0.37	-0.65	LA	1	8772.08	-4.58	0.36	-2.12	CE	2
7841.86	-4.39	0.43	-0.89	LA	1	7752.84	-4.55	0.33	-2.93	CE	2
7382.77	-4.42	1.20	0.83	LA	1	7746.62	-4.77	0.42	-2.85	CE	2

WAV	LOG W/L	CHI	LOG GF		
7717.63	-4.51	0.23	-2.84		CE 2
6051.86	-4.38	0.23	-2.25		CE 2
6043.36	-4.54	1.21	-0.60		CE 2
5609.02	-4.24	0.22	-1.59		PR 2
7094.11	-4.23	0.14	-1.67	k	ND 1
5749.80	-4.08	0.00	-1.47	k	ND 1
5675.87	-4.19	0.14	-0.61	k	ND 1
8839.04	-4.03	0.00	-2.47		ND 2
8249.61	-4.62	0.68	-2.54		ND 2
7863.07	-4.37	0.32	-2.43		ND 2
7808.50	-4.55	0.63	-2.29		ND 2
7773.04	-4.33	0.00	-2.96		ND 2
7751.02	-4.49	0.47	-2.40		ND 2
6790.36	-4.20	0.18	-2.14		ND 2
6740.09	-4.15	0.06	-2.10		ND 2
6428.69	-4.16	0.20	-2.34		ND 2
7104.71	-4.43	0.28	-1.30		SM 1
8048.80	-5.15	1.75	-0.75		SM 2
7042.15	-4.72	1.08	-0.91		SM 2
6732.15	-4.46	1.17	-0.71		SM 2
6472.53	-4.68	1.38	-0.98		SM 2
6864.72	-4.46	0.00	-1.46	c	EU 1
7733.54	-4.43	0.12	-1.79	k	GD 1
7168.33	-4.28	0.21	-1.17	k	GD 1
6730.80	-4.30	0.12	-1.59	k	GD 1
5856.27	-4.17	0.12	-1.02	k	GD 1
5851.66	-4.17	0.12	-1.14	k	GD 1
6579.36	-4.25	0.00	-1.36		DY 1
5974.48	-4.38	0.00	-1.45		DY 1
5651.98	-4.36	0.00	-1.60		DY 1
6133.56	-4.27	0.00	-1.82		HO 1
5973.48	-4.53	0.00	-1.69		HO 1
8409.92	-4.38	0.00	-1.91	k	ER 1
6308.84	-4.32	0.00	-1.43	k	ER 1
5762.83	-4.09	0.00	-1.01	k	ER 1
7845.22	-4.39	0.70	-1.66	k	HF 1
7740.21	-4.60	1.31	-1.49	k	HF 1
6185.08	-4.26	0.00	-3.08	k	HF 1

no entry: see Text for detailed remarks

a: Filipov, A.H., 1931. Z. Phys., 69, 526

b: Lambert, D.L., Warner, B., 1968. Mon.Not.R.astr.Soc., 138, 181

c: Kurucz, R.L., Peytremann, E., 1975. Smithsonian Astrophys. Obs. Special Report 362

d: Lambert, D.L., Luck, R.E., 1978. Mon.Not.R.astr.Soc., 183, 79

e: Smith, P.L., 1976. Mon.Not.R.astr.Soc., 177, 275

f: Kühne, M., Danzmann, K., Kock, M., 1978. Astron.Astrophys., 64, 111

g: Wiese, W.L., Fuhr, J.R., 1975. J.Phys.Chem.Ref.Data, 4, 263

h: Younger, S.M., Fuhr, J.R., Martin, G.A., Wiese, W.L., 1978. J. Phys. Chem. Ref. Data, 7, 495

i: Blackwell, D.E., Ibbetson, P.A., Petford, A.D., Shallis, M.J., 1979. Mon. Not. R. astr. Soc., 186, 633

j: Warner, B., 1968. Mon. Not. R. astr. Soc., 139, 115

k: Corliss, C.H., Bozman, W.R., 1962. Nat. Bureau Standards Monograph 53

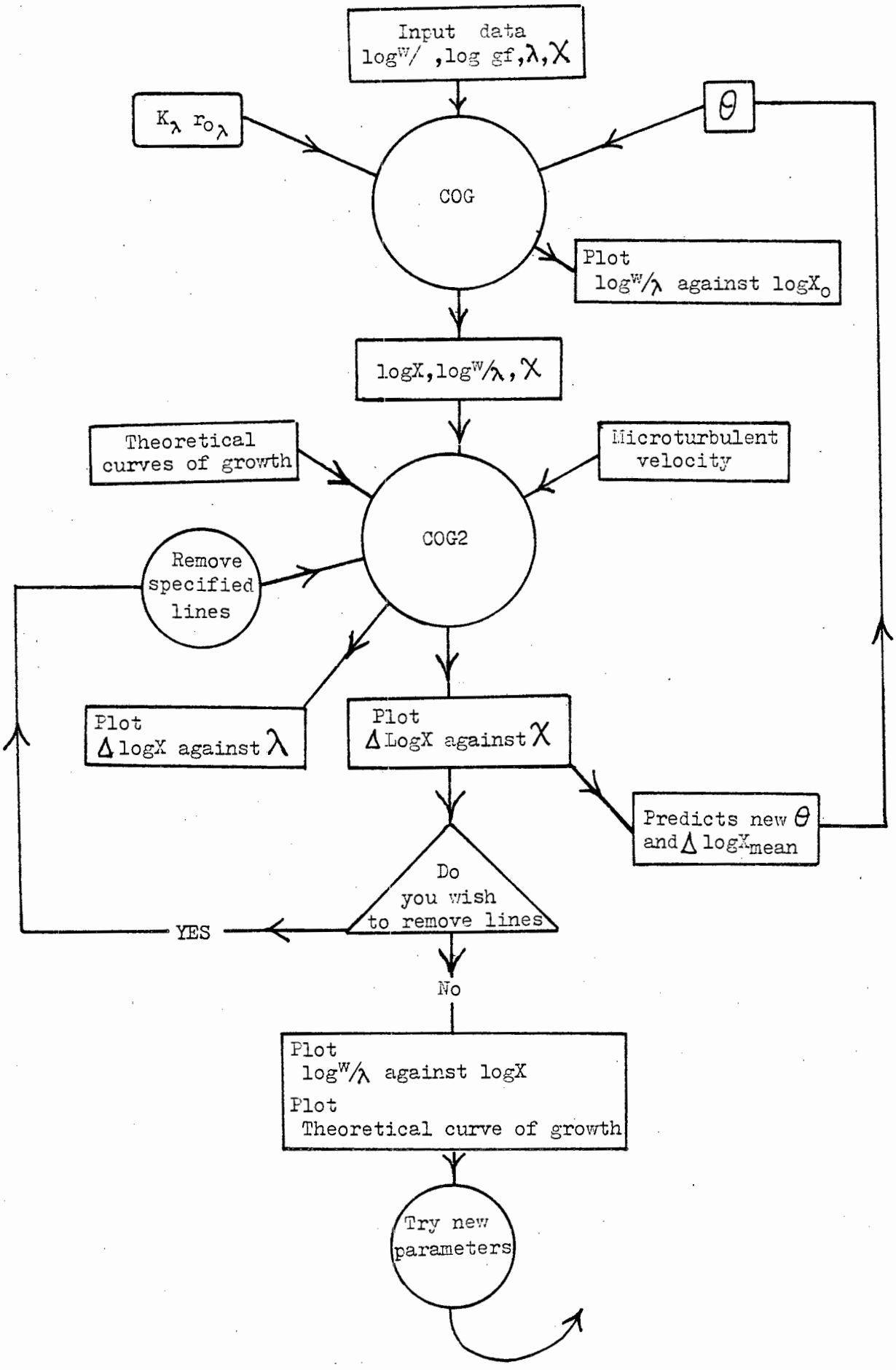

Figure 5.25

Flow chart for the programs used in the curve of growth analysis.

Results of the Abundance Analysis

5.19 Curve of Growth Analysis

Derivation of the Atmospheric parameters

The method used to define the excitation temperature θ, the wavelength variation of the opacity K and depth r_o, as well as the curve of growth parameters of microturbulent velocity ξ and damping, have been outlined in section 5.04. In practice the method is complicated by the fact that in cool stars it is very difficult to find lines on the linear part of the curve of growth and few elements have a good range of equivalent width, uncorrelated with either excitation or wavelength. This means that there is an unavoidable dependence of the various parameters on each other.

The molecule and elements, CN, TiI, VI, FeI, ZrI, LaI and CeI, all have a sufficient number of lines to define the curve of growth. However, of these; CN only has a small range of excitation, VI shows a strong correlation of line strength with excitation, FeI shows large scatter, and the log gf values of ZrI, LaI and CeI, may contain temperature terms. This leaves TiI, which shows a good mix of excitation and equivalent width uncorrelated with wavelength, but not many faint lines. The atmospheric parameters therefore depend heavily on TiI, but have been derived with the proviso, that the remaining elements should give consistent results, when described by the TiI parameters. To this end a program was written, which allows the user to investigate the effects of different temperatures, wavelength variation of the K, and r_o terms, microturbulent velocities and curves of growth. The flow diagram for the program is shown in Fig. 5.25.

The structure of the program allows the user to rapidly investigate the effects of changing the various parameters.

The slope of the ΔlogX against χ defines a new value of θ, which is determined by a least squares fit with all the error in ΔlogX. This implies that there is no error in the equivalent widths, which is of course not true and indicates the need to display the fit of the theoretical curve of growth as part of the program. The final mean values of ΔlogX used to derive the abundances, are found after fitting the theoretical curve of growth, by hand, to the data points. Allowance can then be made for the errors in $\log W/\lambda$ and systematic blending effects.

The broadband photometry discussed in chapter 2, as well as

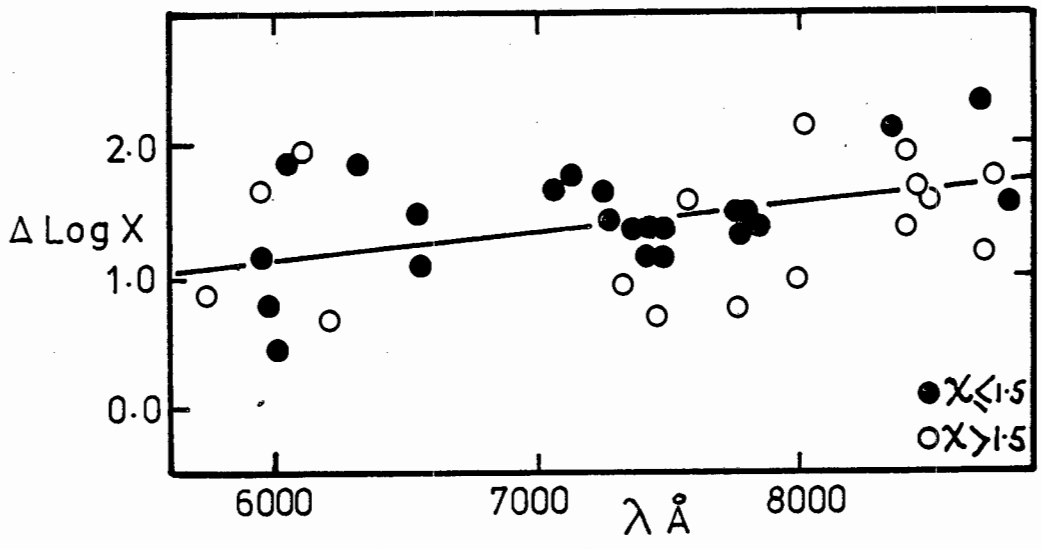

Figure 5.26

The trend of curve of growth residuals is shown as a function wavelength for TiI and amounts to almost an order of magnitude over the wavelength range. Note there is no difference between the high and low excitation lines.

Yamashita's (1973) work on GP Ori and FU Mon, indicates that the excitation temperature would lie close to $\theta = 2.0$. Curves of growth were plotted for TiI, for the range $1.6 < \theta > 2.5$, which all showed a strong convergence toward $\theta = 2.2$. When combined with the VI data, the resultant curve indicates a low value of the damping constant. The damping was set equal to $\Gamma_{classical}$ at 7000 Å.

The r_o and opacity terms were found by plotting the residuals $\Delta \log X$ against λ for titanium. This is illustrated in Fig.5.26 where we distinguish between the high and low excitation lines, which both show the same trend.

The least squares fit gives

$$\log\{K_H(\lambda)/K_H(\lambda_o)\} - \gamma \log\{r_o(\lambda)/r_o(\lambda_o)\} = 0.0002\lambda - 1.40$$

where λ_o = 7000 Å and λ is in angstrom units. This variation is much greater than the calculated variation of the continuous opacity and will be further discussed in chapter 6.

Both, van der Held curves of growth (pure absorption in a SS model) and Wrubel (1949) curves (pure scattering in a ME model) were used to investigate the data. The Wrubel curve with parameter $B_o/B_1 = 1/3$ showed a much smaller spread in θ between the various elements and is the curve used to derive the abundances. The Wrubel curve is very similar in shape to the curve of growth generated by the Johnson atmospheres, for 1.0 e.v lines, using pure absorption as the line forming mechanism. This illustrates the danger of using the shape of the curve of growth to deduce the method of line formation. Also, as far as relative abundance determinations are concerned, the curve of growth is simply an interpolation device between different elements and its shape is not important.

Both curves of growth gave essentially the same microturbulent velocity. The corresponding values of θ are given in Table 5.09 and with the exception of CN are very similar. The range of θ shown between the different elements will be discussed in chapter 6 dealing with stratification.

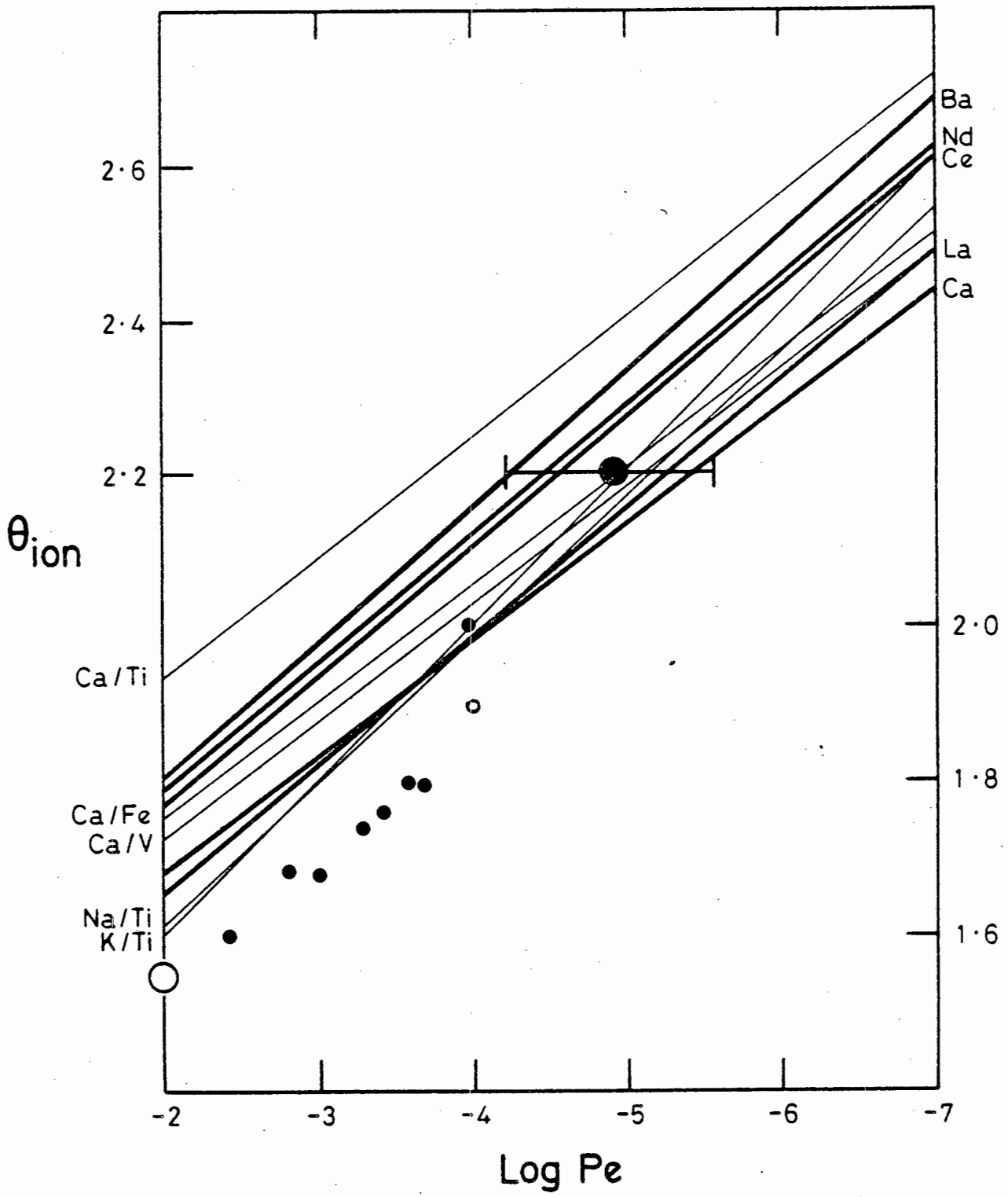

Figure 5.27

For the elements indicated along the right hand margin, the bold curves satisfy the condition that the ionized and neutral species give the same abundance. The light curves satisfy the condition that the abundance ratios, indicated along the left hand margin, are the same as in the sun. The error-barred filled symbol is the solution for UY Cen. The large open circle is for RZ Sgr, the cross for FU Mon and the small filled symbols are solutions for C stars given by Kilston (1975).

TABLE 5.09

	θ		No of lines
	Wrubel $\xi = 4.2$	van der Held $\xi = 4.24$	
CN	1.87	1.48	33
TiI	2.16	2.15	39
VI	1.97	2.27	17
FeI	1.90	1.97	14
ZrI	2.48	2.54	35
LaI	2.83	3.03	18
CeI	2.99	2.97	39
Weighted mean θ	2.36	2.35	

Ionization Correction

If LTE prevails then the ionization correction required to relate the observed number of atoms to the true number is governed by the Saha equation, which is defined by the electron pressure P_e and the ionization temperature T_{ion} (or θ_{ion}). There are then two methods that can be used to specify T_{ion} and P_e. The first involves satisfying the condition that the neutral and ionized species of a given element will give the same abundance. The second method is to make the assumption that certain abundance ratios are the same in UY Cen as in the sun.

The first method can be applied to the elements Ca, Ba, La, Ce and Nd, all of which have ionization potentials between 5 and 6 volts. Elements with higher ionization potentials are predominantly neutral and those lower are predominantly ionized. The condition that the neutral and ionized species should give the same abundances is illustrated by the appropriately labelled heavy lines in Fig. 5.27. The main drawback of the method is its sensitivity to zero point errors in the ionized and neutral log gf values. The second method is applied to the abundance ratios $^{Ca}/_{Ti}$, $^{Ca}/_{Fe}$, $^{Ca}/_{V}$, $^{Na}/_{Ti}$ and $^{K}/_{Ti}$ and is illustrated by the light lines in Fig. 5.27. The $^{Na}/_{Ti}$ ratio depends on the weak Na lines. The assumption that the abundance ratios will be solar is an obvious weakness of the method. On the other hand the correction required to make $[^{K}/_{Ti}] = 0$ is of order 3 dex so that consistency between the methods is a sensitive test of the validity of the LTE assumption.

As illustrated in Fig. 5.27 the $^{Ca}/_{Ti}$ and $^{K}/_{Ti}$ and $^{Na}/_{Ti}$ results very nicely bracket the (ion/neutral) results. It is also clear that since the lines are all parallel to each other there is no unique value of Pe and θ_{ion}. We therefore make the LTE assumption that $\theta_{ion} = \theta_{ex}$ which is indicated by the circle in Fig. 5.27 and gives log Pe = -4.9. It must be emphasised, that as several authors feel that there is no evidence to presume that $\theta_{ion} = \theta_{ex}$, this is not an appropriate argument for finding log Pe.

It is interesting to realise that, despite the great strength of the NaD lines, sodium is still at least 90% ionized in UY Cen. It would be interesting to observe a star in which Na was mainly neutral!

The small filled symbols in Fig. 5.27 are values of θ_{ion} and log Pe, deduced by Kilston (1975) for a number of carbon stars. He uses our second method of finding the ionization correction and makes the assumption that $\theta_{ex} = \theta_{ion}$. He finds the very close correlation of θ_{ion} with Pe highly significant but an alternative interpretation is that all his carbon stars have the same degree of ionization independant of their excitation temperatures. The fact that the points all lie below the UY Cen solution may indicate that his carbon stars are all somewhat less ionized than UY Cen. This is countered by the fact that Yamashita (1973) finds a similar degree of ionization for the SC star FU Mon (indicated by the cross in Fig. 5.27). The open circle is Catchpole and Feast's (1976) result for RZ Sgr where they followed Boesgaard's (1970) formula that for $\theta_{exc} > 1.50, \theta_{exc} - \theta_{ion} = 0.35$ and log Pe = -2.0. Catchpole and Feast nevertheless found that $[^{Ca}/_{K}] \simeq [^{Ti}/_{Ca}] \simeq 0.0$.

The Microturbulent Velocity

Struve and Elvey (1934) noted that the doppler width of stellar absorption lines in certain stars corresponded to temperatures far in excess of anything physically plausible. They attributed the broadening to small scale turbulence. This is not well understood in theoretical terms but is an important parameter through its influence on the shape of the curve of growth. The curve of growth provides the most sensitive means of determining the microturbulence required for the model atmosphere analysis. Synthetic line profiles, generated from the model atmosphere, are very insensitive to microturbulence because, for the typical 10 Å/mm spectra available, they are dominated by the instrumental profile.

For a similar reason it is not possible to detect any macroturbulent effects present in UY Cen.

The microturbulent velocity of 4.2 km s^{-1} found here, is within the range of 2 to 4.9 found in S stars by Boesgaard (1970) and similar to the value of 4.5 km s^{-1} found by Catchpole and Feast (1971) for the SLR S star RZ Sgr. These values, however, are all much less than the range of 6 to 11 km s^{-1} found by Utsumi (1970) and Kilston (1975) for C stars.

Empirically we found that raising the continuum level by 10% increased the derived microturbulent velocity by 1 km s^{-1}.

The $^{12}C/^{13}C$ ratio derived from the curve of growth is very sensitive to the microturbulent velocity simply because the ^{13}CN lines are on the linear part, while the ^{12}CN lines are on the transition part of the curve of growth. This is contrary to the conclusion of Climenhaga et al. (1977) who state that their model fitting results are not sensitive to microturbulence. The reason for this apparent contradiction, is that Climenhaga used velocities in the range 6.5 to 11.0 km s^{-1} which would place all our CN lines on the linear part of the curve of growth, where of course there is no sensitivity to microturbulence.

We have no grounds for doubting the high microturbulent velocities derived for carbon stars; we merely wish to draw attention to the sensitivity of model atmosphere results to the correct choice of velocity. As will be seen in a later section the derived Li abundances are also sensitive to the microturbulent velocity.

Final curve of Growth Parameters

The adopted parameters for the curve of growth analysis are

$\theta_{exc} = \theta_{ion} = 2.2$

$\log Pe = -4.9$

$\xi = 4.2$ km s^{-1}

Damping = $\Gamma_{classical}$ at 7000 Å

The adopted abundances relative to titanium are listed in Table 5.11 column 5. The abundance ratios in columns four and six are appro-

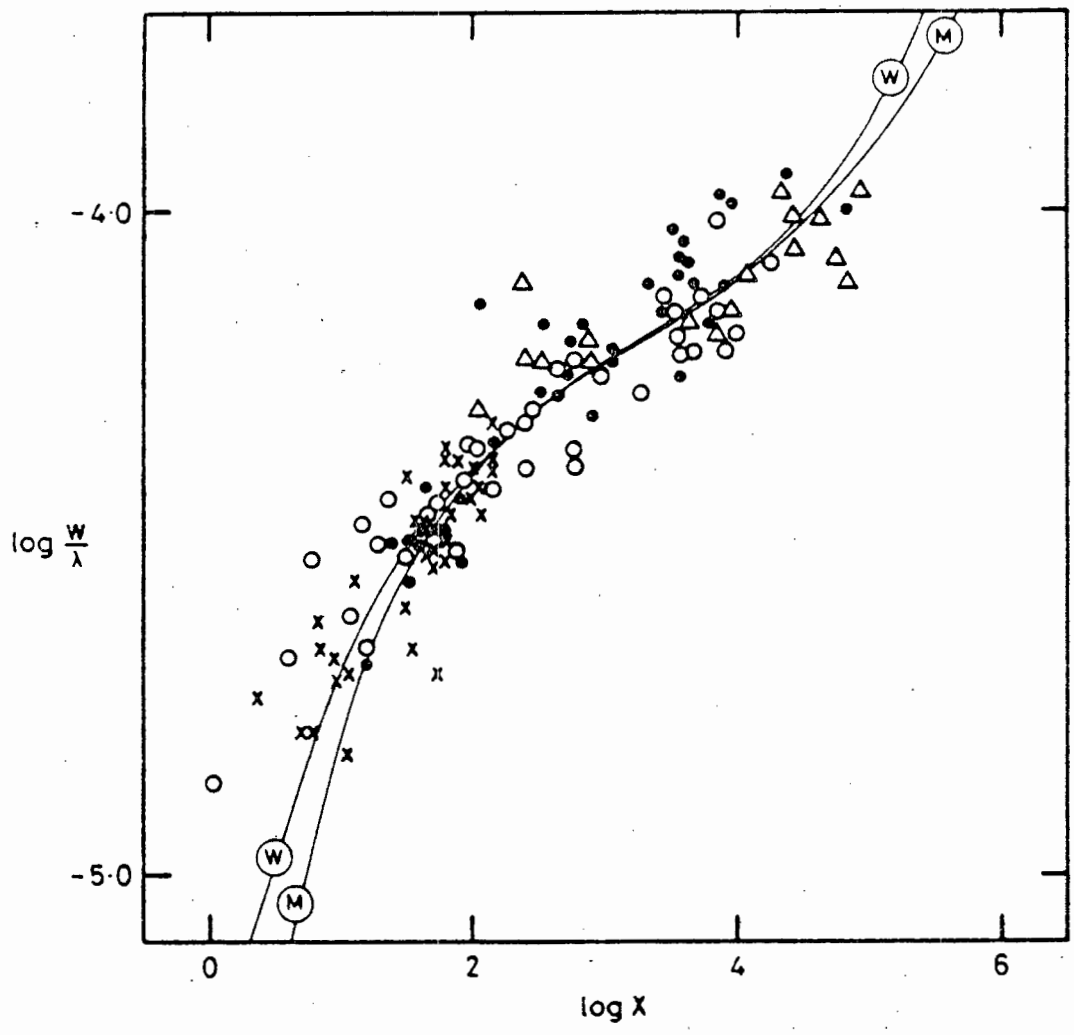

Figure 5.28

Curve of growth for CN = X, Ti = O, V = Δ and Zr = ● on an arbitrarily normalized log X scale. The curve marked W is a Wrubel curve, while the curve marked M is the curve of growth generated by the 2800 model atmosphere for a 1 e.v. TiI line. Both curves have a microturbulent velocity of 4.2 km s^{-1} and have been shifted to give the best fit to the data.

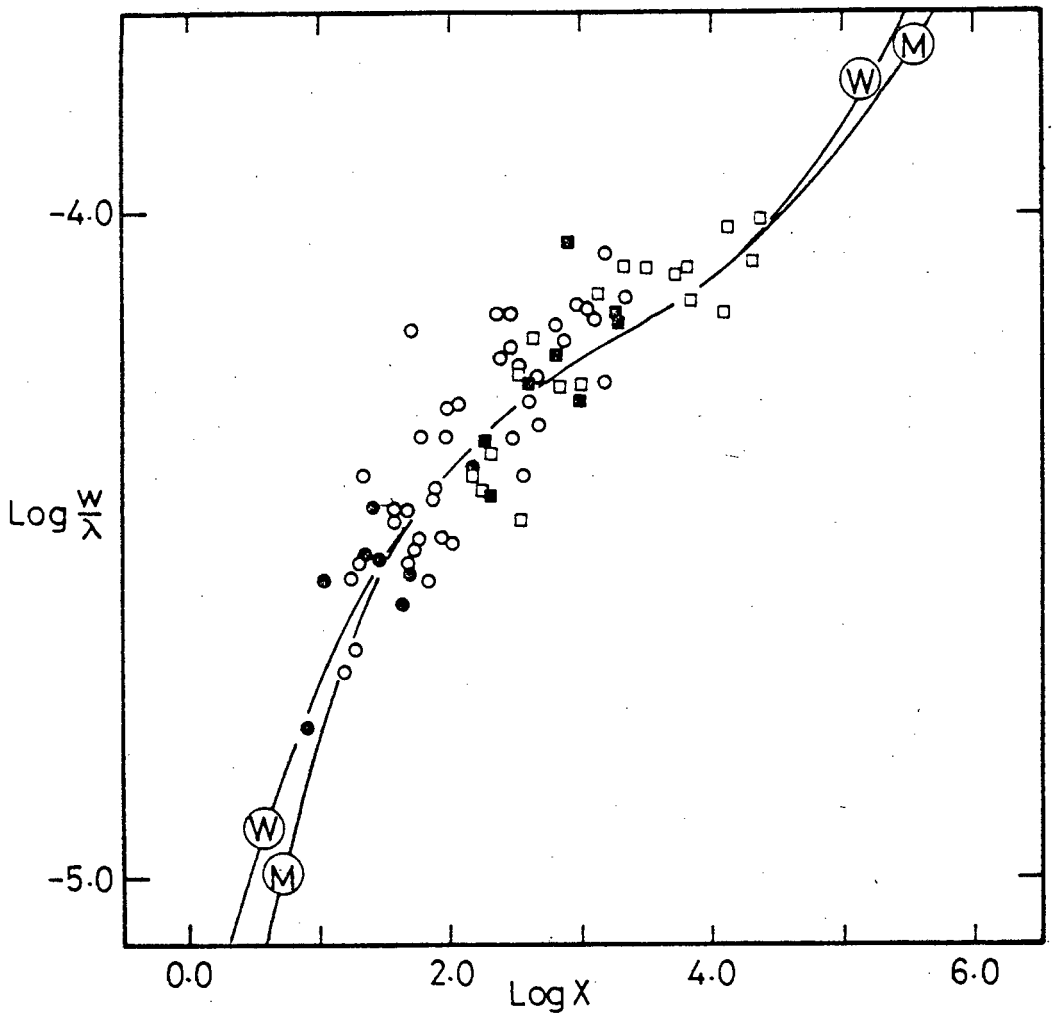

Figure 5.29

Identical to Fig. 5.28 but for CeI = O, CeII = O, LaI = □ and LaII = ■.

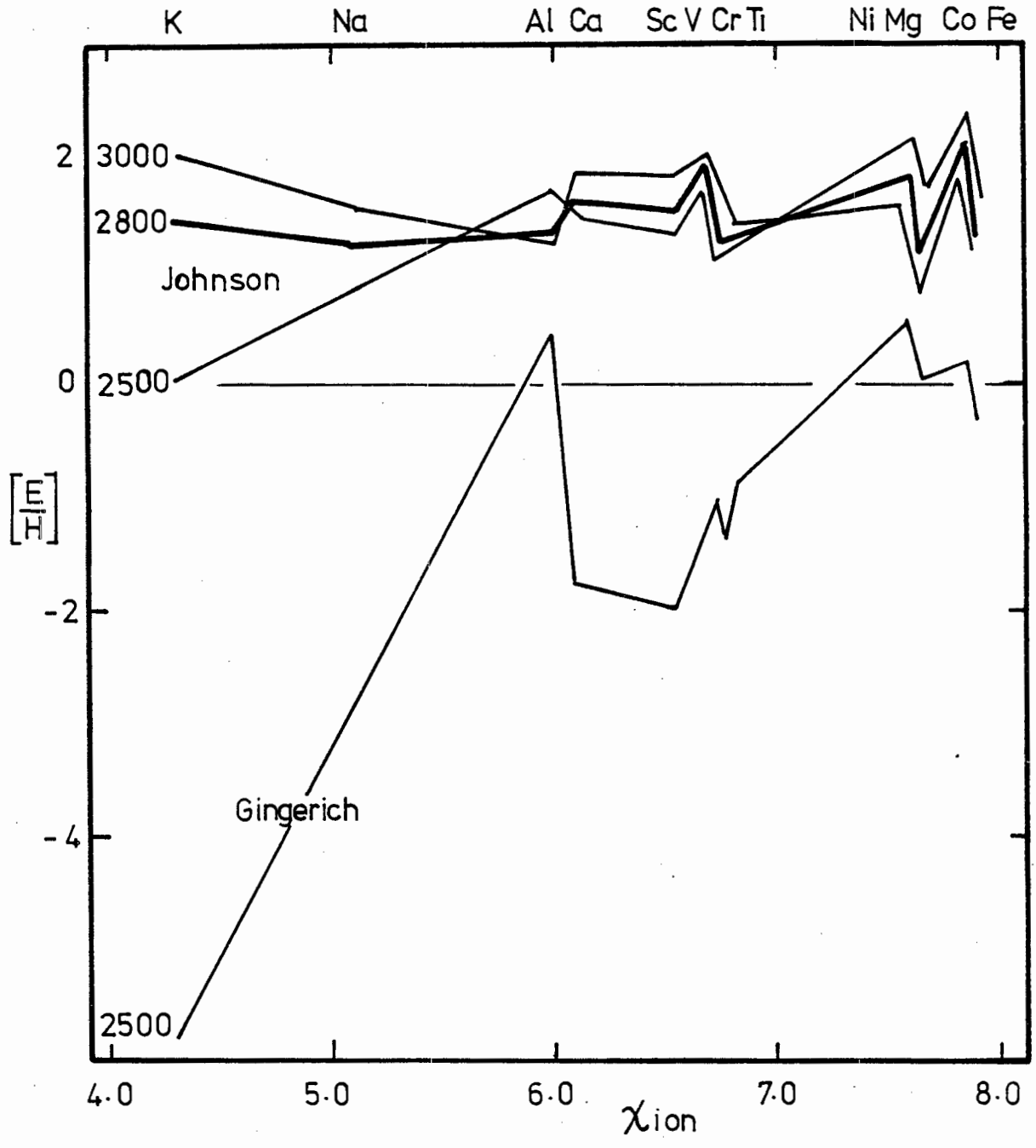

Figure 5.30

The abundance ratio compared with the sun is shown for the lighter elements as a function of their ionization potential. Note the much better fit shown by the Johnson models than by the Gingerich model, despite the near solar abundance predicted by the latter for the largely neutral atoms to right of Titanium.

priate to the ionization corrections corresponding to the ends of the error bars in Fig. 5.27.

Fig.5.28 gives a composite curve of growth for the elements, CN, TiI, VI and ZrI on an arbitrarily normalised log X scale. The adopted Wrubel curve of growth and the curve of growth generated by the 2800 model atmosphere for 1 volt TiI lines, are also shown. Both curves are slid to give a best fit to the data. Fig.5.29shows a composite curve of growth for LaI, LaII, CeI, CeII.

The results will be discussed further with those from the model atmosphere analysis in section 5.21.

5.20 Model Atmosphere Abundance Results

Using the Johnson model atmospheres, with a microturbulent velocity of 4.2km s^{-1}, abundances relative to the sun, mean temperatures and electron pressures, were derived for each line, by the techniques described in section 5.05.

The most appropriate model was found by examining both the trends of abundance with ionization potential, illustrated in Fig.5.30and the relative abundances of neutral and ionized atoms of the same element, given by each model and shown in Fig.5.31. It is clear from both Figures that the 2800 model gives the best fit to the data.

In Fig.5.30 we also show the abundance results obtained using the Gingerich et al.(1966) 2500 model, which was used to model the flux distribution in chapter 3. It is interesting to note that this model gives solar abundances for the elements Ni, Mg, Co and Fe, which are all completely neutral, but predicts that Na and K are very underabundant. The reason is that the atmosphere has a very low opacity, so that the line forming region is at a very much higher electron pressure than in a Johnson atmosphere, of similar effective temperature. This means that even Na and K will be neutral, in which case the observed lines are far too weak.

The abundances, mean pressures and temperatures, as defined in section 5.08 , are given in Table 5.10for the 2800, log g = 1.0 model atmosphere. The mean abundances for the three atmospheres are given in Table 5.11.

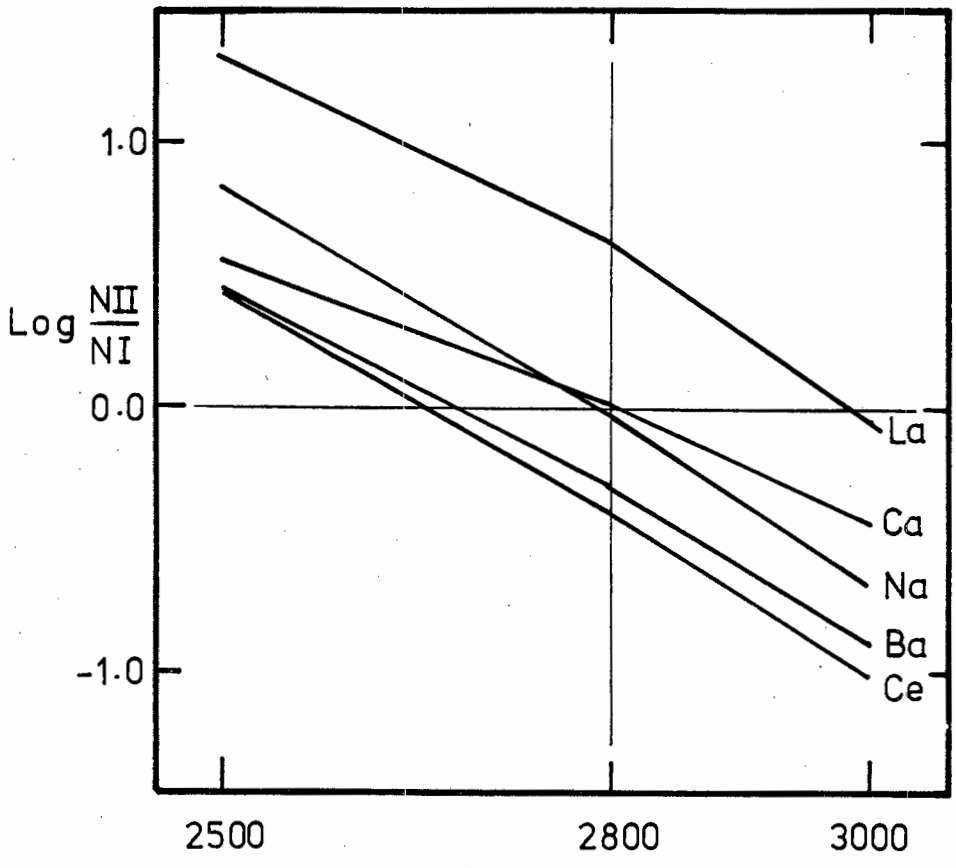

Figure 5.31

The abundance ratios, given by the ionized and neutral species of the element indicated on the right hand side, is shown for the three Johnson models, each indicated by its effective temperature.

TABLE 5.10

WAV	ION	CHI	LOG W/L	LOG GF	THETA	LOG PE	LOG [E]
NA LOG SOLAR ABUNDANCE=6.32							
8183.27	1	2.10	-3.98	0.22	2.53	-6.03	1.90
6160.78	1	2.10	-4.31	-1.27	2.25	-4.56	0.80
MG LOG SOLAR ABUNDANCE=7.62							
3806.77	1	4.35	-4.23	0.12	2.04	-3.95	1.59
AL LOG SOLAR ABUNDANCE=6.49							
3773.94	1	4.02	-4.51	0.04	1.96	-3.65	1.61
K LOG SOLAR ABUNDANCE=5.12							
7698.77	1	0.00	-3.82	-0.18	2.53	-6.49	1.35
7664.80	1	0.00	-3.66	0.12	2.40	-6.00	1.47
CA LOG SOLAR ABUNDANCE=6.34							
6493.80	1	2.52	-4.05	-0.57	2.43	-5.20	1.60
6471.62	1	2.53	-4.17	-1.16	2.33	-4.83	1.35
6439.10	1	2.53	-4.07	-0.22	2.44	-5.20	1.19
6169.52	1	2.53	-4.02	-0.89	2.44	-5.24	2.12
6169.12	1	2.53	-4.02	-1.19	2.44	-5.24	2.42
6102.70	1	1.88	-3.86	-1.26	2.44	-5.57	1.85
8662.14	2	1.69	-3.56	-0.77	2.08	-4.02	1.61
8542.12	2	1.69	-3.47	-0.51	2.05	-3.94	1.53
8498.20	2	1.69	-3.61	-1.46	2.09	-4.02	2.17
SC LOG SOLAR ABUNDANCE=3.04							
6193.73	1	0.00	-4.10	-1.92	2.61	-6.18	1.58
TI LOG SOLAR ABUNDANCE=5.05							
8819.41	1	1.07	-4.36	-3.19	2.25	-4.57	1.64
8761.39	1	1.74	-4.66	-2.55	1.97	-3.69	1.18
8719.54	1	1.74	-4.47	-2.60	2.08	-4.05	1.87
8675.39	1	1.07	-4.19	-1.25	2.48	-5.33	0.86
8494.43	1	1.74	-4.46	-2.11	2.08	-4.05	1.40
8467.18	1	2.12	-4.41	-1.02	2.10	-4.11	1.31
8424.39	1	2.10	-4.51	-1.13	2.02	-3.87	0.92
8423.10	1	1.88	-4.50	-2.17	2.04	-3.92	1.56
8353.14	1	0.81	-4.22	-2.30	2.45	-5.28	1.07
8024.83	1	1.88	-4.36	-0.78	2.15	-4.25	0.80
7996.46	1	3.34	-4.67	0.24	1.88	-3.39	1.33
7852.70	1	0.85	-4.22	-2.87	2.43	-5.20	1.66
7834.48	1	0.83	-4.44	-4.19	2.15	-4.26	1.66
7796.45	1	0.82	-4.61	-4.84	2.03	-3.90	1.74
7791.34	1	0.84	-4.51	-4.37	2.09	-4.07	1.60
7773.84	1	2.33	-4.86	-2.60	1.85	-3.31	1.85
7580.31	1	2.23	-4.50	-1.12	1.99	-3.77	1.09
7471.13	1	0.81	-4.33	-3.75	2.26	-4.59	1.67
7469.94	1	0.84	-4.24	-3.30	2.38	-5.02	1.87
7466.37	1	1.74	-4.52	-3.17	2.00	-3.80	2.10
7424.50	1	0.83	-4.30	-3.49	2.29	-4.72	1.63
7423.15	1	1.44	-4.35	-2.64	2.16	-4.30	1.72
7364.07	1	1.43	-4.16	-1.13	2.42	-5.16	1.53
7337.72	1	2.24	-4.43	-1.53	2.03	-3.88	1.77
7271.38	1	1.44	-4.32	-2.21	2.20	-4.40	1.45
7251.68	1	1.43	-4.16	-0.78	2.42	-5.16	1.16
7138.05	1	1.43	-4.39	-2.27	2.11	-4.14	1.08
7065.12	1	1.46	-4.42	-2.46	2.08	-4.04	1.17
6556.01	1	1.46	-4.13	-0.97	2.42	-5.17	1.56
6554.17	1	1.44	-4.19	-1.19	2.34	-4.87	1.23
6336.14	1	1.44	-4.28	-1.48	2.19	-4.39	0.78
6215.17	1	2.70	-4.28	0.09	2.07	-4.03	1.61
6091.22	1	2.27	-4.39	-0.19	1.99	-3.77	0.41
6064.65	1	1.05	-4.20	-1.68	2.35	-4.91	0.76
6031.61	1	0.05	-4.01	-4.00	2.55	-6.25	2.53
5990.59	1	0.05	-4.14	-4.44	2.57	-5.84	2.06
5953.23	1	1.89	-4.21	-0.15	2.22	-4.48	0.76
5941.79	1	1.05	-4.08	-1.41	2.50	-5.54	1.51
5739.43	1	2.25	-4.23	-0.31	2.14	-4.23	1.38

WAV	ION	CHI	LOG W/L	LOG GF	THETA	LOG PE	LOG [E]
V LOG SOLAR ABUNDANCE=4.02							
8255.85	1	1.06	-4.22	-2.08	2.42	-5.16	2.60
8027.36	1	1.06	-4.13	-2.14	2.52	-5.58	3.35
6785.03	1	1.05	-4.23	-2.19	2.33	-4.86	2.33
6766.53	1	1.06	-4.20	-1.92	2.38	-5.02	2.36
6452.33	1	1.19	-4.23	-1.56	2.29	-4.70	1.96
6285.15	1	0.28	-4.08	-1.74	2.58	-6.03	1.61
6251.77	1	0.29	-3.97	-1.52	2.48	-6.05	2.02
6245.12	1	0.26	-4.10	-2.45	2.57	-5.94	2.07
6224.50	1	0.29	-4.01	-2.06	2.54	-6.10	2.33
6213.87	1	0.30	-3.97	-2.10	2.48	-6.05	2.61
6150.13	1	0.30	-4.01	-1.85	2.54	-6.09	2.13
6039.73	1	1.06	-4.19	-0.94	2.35	-4.93	1.33
6008.56	1	1.18	-4.30	-2.52	2.16	-4.30	2.33
5737.08	1	1.06	-4.15	-0.79	2.39	-5.06	1.46
5698.56	1	1.06	-4.11	0.03	2.45	-5.29	0.94
5668.34	1	1.08	-4.17	-1.17	2.36	-4.95	1.69
5627.62	1	1.08	-4.06	-0.38	2.47	-5.42	1.73
CR LOG SOLAR ABUNDANCE=5.71							
6330.16	1	0.94	-4.19	-2.70	2.37	-5.00	0.56
5798.43	1	1.03	-4.18	-3.98	2.34	-4.89	1.99
FE LOG SOLAR ABUNDANCE=7.50							
8824.21	1	2.20	-4.12	-1.22	2.34	-4.88	1.00
8621.63	1	2.95	-4.48	-2.13	1.98	-3.73	1.19
8387.80	1	2.18	-4.13	-2.02	2.34	-4.85	1.66
7723.15	1	2.28	-4.48	-3.04	1.97	-3.70	0.65
7389.23	1	4.30	-4.43	-0.60	1.91	-3.49	2.20
6839.83	1	2.56	-4.27	-2.99	2.08	-4.06	2.08
6663.45	1	2.42	-4.25	-2.40	2.10	-4.11	1.30
6575.08	1	2.59	-4.29	-2.64	2.04	-3.94	1.56
6574.25	1	0.99	-4.09	-5.37	2.47	-5.40	2.70
6358.71	1	0.86	-4.07	-4.47	2.48	-5.49	1.64
6280.67	1	0.86	-4.16	-4.39	2.40	-5.11	0.88
6254.27	1	2.28	-4.21	-3.07	2.13	-4.21	1.86
5943.49	1	2.20	-4.44	-4.28	1.89	-3.44	1.47
5778.41	1	2.59	-4.29	-3.23	1.97	-3.71	1.85
CO LOG SOLAR ABUNDANCE=4.90							
7084.98	1	1.88	-4.20	-1.35	2.25	-4.59	2.34
NI LOG SOLAR ABUNDANCE=6.28							
3770.00	1	2.74	-4.71	-3.27	1.86	-3.35	2.37
7385.00	1	2.74	-4.49	-2.01	1.93	-3.56	1.66
6914.00	1	1.95	-4.20	-2.46	2.23	-4.52	2.16
RB LOG SOLAR ABUNDANCE=2.60							
7800.23	1	0.00	-4.20	0.14	2.69	-6.33	1.61
SR LOG SOLAR ABUNDANCE=2.90							
7070.07	1	1.83	-4.31	-0.18	2.35	-4.88	2.04
Y LOG SOLAR ABUNDANCE=2.18							
8800.61	1	0.00	-3.94	-2.58	2.47	-6.40	4.14
6793.70	1	0.07	-4.02	-2.14	2.57	-6.40	3.46
6584.88	1	0.07	-4.14	-3.04	2.61	-6.03	3.41
6557.35	1	0.00	-4.08	-2.62	2.63	-6.36	3.39
6222.54	1	0.00	-3.91	-1.95	2.44	-6.23	3.48
6023.39	1	0.00	-4.00	-2.33	2.57	-6.33	3.44
ZR LOG SOLAR ABUNDANCE=2.99							
8749.47	1	0.60	-4.14	-2.92	2.57	-5.85	3.97
8453.12	1	1.40	-4.53	-1.38	2.05	-3.95	1.72
8063.06	1	0.62	-4.11	-1.77	2.57	-5.91	3.06
8058.10	1	0.62	-4.31	-2.17	2.33	-4.84	1.91
7940.47	1	0.52	-4.27	-2.76	2.40	-5.10	2.53
7869.96	1	0.69	-4.28	-2.32	2.36	-4.97	2.38
7849.32	1	0.69	-4.21	-1.90	2.46	-5.35	2.47
7822.92	1	1.75	-4.51	-1.08	2.02	-3.85	2.12

WAV	ION	CHI	LOG W/L	LOG GF	THETA	LOG PE	LOG CE
ZR CONTINUED							
7819.32	1	1.82	-4.43	-0.51	2.07	-4.02	2.02
7723.93	1	0.60	-4.35	-2.99	2.27	-4.65	2.42
7708.42	1	1.58	-4.67	-1.82	1.94	-3.61	2.04
7658.62	1	0.54	-4.20	-2.55	2.49	-5.45	2.87
7558.48	1	1.55	-4.42	-1.45	2.09	-4.07	2.43
7544.62	1	1.58	-4.56	-1.51	1.99	-3.76	2.01
7383.56	1	1.86	-4.50	-1.07	2.00	-3.80	2.30
7111.73	1	0.52	-4.07	-1.85	2.57	-5.96	3.09
7102.98	1	0.65	-4.05	-1.56	2.54	-5.91	3.19
7087.31	1	0.60	-4.03	-1.75	2.55	-6.00	3.45
7057.32	1	1.58	-4.49	-1.36	2.01	-3.83	2.03
6990.79	1	0.62	-4.10	-1.68	2.56	-5.83	2.92
6975.87	1	1.44	-4.50	-1.91	2.01	-3.83	2.26
6762.35	1	0.00	-3.99	-2.68	2.52	-6.25	3.30
6489.67	1	1.55	-4.21	-0.23	2.29	-4.72	2.33
6484.35	1	0.63	-4.17	-2.75	2.47	-5.37	3.33
6451.65	1	0.62	-4.17	-2.50	2.47	-5.38	3.06
6407.05	1	0.15	-4.25	-2.78	2.40	-5.12	1.73
6193.03	1	0.54	-4.15	-2.07	2.50	-5.52	2.62
6140.45	1	0.52	-4.12	-1.67	2.53	-5.65	2.41
6127.45	1	0.15	-4.00	-1.55	2.54	-6.13	2.33
6124.83	1	0.52	-4.08	-1.94	2.56	-5.88	3.07
6025.36	1	0.15	-4.11	-2.79	2.57	-5.89	2.86
5995.32	1	0.73	-4.24	-2.36	2.32	-4.82	2.50
5955.35	1	0.00	-3.95	-2.39	2.47	-6.19	3.19
5680.98	1	0.54	-4.17	-1.77	2.44	-5.26	2.05
5868.27	1	0.15	-3.97	-2.53	2.48	-6.09	3.52
NB LOG SOLAR ABUNDANCE=1.69							
5819.57	1	1.61	-4.95	-1.22	1.79	-3.11	2.21
MO LOG SOLAR ABUNDANCE=2.14							
6733.82	1	1.34	-4.42	-1.83	2.03	-3.90	2.68
6619.20	1	1.34	-4.42	-1.50	2.03	-3.88	2.32
6030.61	1	1.53	-4.20	-0.49	2.25	-4.57	2.90
5722.76	1	1.42	-4.32	-1.35	2.06	-3.99	2.63
CS LOG SOLAR ABUNDANCE=1.13							
8520.90	1	0.00	-4.36	0.15	2.49	-5.47	2.69
BA LOG SOLAR ABUNDANCE=2.07							
7911.35	1	0.00	-4.12	-2.00	2.76	-7.00	3.24
7780.44	1	1.14	-4.33	-0.23	2.50	-5.49	2.34
7392.44	1	1.57	-4.37	0.09	2.38	-5.01	2.74
6675.28	1	1.14	-4.18	-0.15	2.65	-6.13	3.27
6595.26	1	1.12	-4.29	0.15	2.52	-5.57	2.08
6110.77	1	1.19	-4.29	0.44	2.50	-5.47	1.91
5997.01	1	1.12	-4.37	-0.12	2.40	-5.10	1.91
5777.64	1	1.67	-4.31	0.72	2.38	-5.01	2.49
6496.90	2	0.60	-3.98	-0.46	2.44	-5.56	2.20
LA LOG SOLAR ABUNDANCE=1.19							
3748.45	1	0.33	-4.36	-0.82	2.52	-5.55	2.10
8545.49	1	0.37	-4.19	-0.46	2.68	-6.36	3.01
3001.93	1	0.37	-4.24	-0.65	2.63	-6.05	2.74
7841.80	1	0.43	-4.39	-0.89	2.46	-5.34	2.25
7382.77	1	1.20	-4.42	0.83	2.33	-4.82	2.03
7219.86	1	0.37	-4.46	-0.73	2.40	-5.13	1.70
7023.60	1	1.00	-4.26	0.90	2.52	-5.56	2.39
6644.43	1	0.13	-4.12	-0.77	2.70	-6.68	3.36
6600.18	1	0.37	-4.26	-0.36	2.59	-5.85	2.26
6578.54	1	0.00	-4.08	-0.36	2.71	-6.87	3.09
6454.54	1	0.33	-4.08	0.03	2.69	-6.73	3.42
6411.03	1	0.37	-4.15	0.48	2.69	-6.45	2.40
6394.19	1	0.43	-4.02	0.91	2.63	-6.70	3.17
6325.84	1	0.13	-4.09	-0.18	2.70	-6.81	3.14

WAV	ION	CHI	LOG W/L	LOG GF	THETA	LOG PE	LOG CE
LA CONTINUED							
6293.46	1	0.43	-4.08	0.10	2.68	-6.67	3.57
6249.90	1	0.51	-4.01	1.29	2.61	-6.64	2.93
5789.15	1	0.43	-4.07	0.97	2.67	-6.62	2.68
5631.26	1	0.37	-4.15	0.63	2.68	-6.40	2.23
6774.22	2	0.13	-4.15	-1.83	2.43	-5.20	3.52
6262.34	2	0.40	-4.16	-1.30	2.36	-4.94	3.27
6172.71	2	0.13	-4.21	-2.39	2.32	-4.80	3.39
5936.26	2	0.17	-4.28	-2.19	2.20	-4.42	2.78
CE LOG SOLAR ABUNDANCE=1.61							
8810.87	1	0.30	-4.50	-1.31	2.48	-5.43	2.40
8261.05	1	0.30	-4.56	-1.30	2.45	-5.30	2.25
8245.20	1	0.17	-4.53	-1.66	2.48	-5.42	2.38
8223.62	1	0.59	-4.55	-1.25	2.41	-5.14	2.88
8171.38	1	0.16	-4.18	-1.74	2.73	-6.68	4.26
7866.05	1	0.17	-4.30	-1.50	2.64	-6.08	3.08
7842.59	1	0.17	-4.29	-1.42	2.65	-6.13	3.06
7812.63	1	0.72	-4.69	-1.11	2.33	-4.85	2.77
7806.83	1	0.40	-4.53	-1.67	2.44	-5.27	2.92
7762.96	1	0.52	-4.66	-1.45	2.37	-5.01	2.72
7732.30	1	0.47	-4.53	-1.20	2.43	-5.23	2.61
7438.55	1	0.55	-4.45	-1.06	2.46	-5.34	2.87
7421.03	1	0.40	-4.47	-1.48	2.47	-5.38	2.89
7393.35	1	0.59	-4.40	-1.29	2.49	-5.45	3.36
7017.23	1	0.49	-4.45	-1.30	2.46	-5.35	2.97
6894.56	1	0.29	-4.42	-1.49	2.51	-5.53	2.80
6749.48	1	0.40	-4.34	-1.37	2.56	-5.74	3.26
6577.42	1	0.17	-4.49	-1.73	2.48	-5.43	2.57
6458.05	1	0.17	-4.17	-0.87	2.73	-6.65	3.49
6253.65	1	0.27	-4.15	-1.12	2.73	-6.68	4.18
6228.21	1	0.00	-4.15	-1.61	2.75	-6.80	4.06
6187.94	1	0.03	-4.25	-1.35	2.68	-6.30	2.95
6123.72	1	0.97	-4.50	0.06	2.34	-4.83	2.52
6076.58	1	0.95	-4.34	-0.06	2.47	-5.38	3.16
6066.73	1	0.21	-4.32	-0.98	2.60	-5.88	2.54
6024.19	1	0.40	-4.16	-0.11	2.71	-6.57	3.35
6006.77	1	0.52	-4.20	-0.28	2.68	-6.29	3.39
5992.60	1	0.55	-4.40	-0.34	2.47	-5.38	2.31
5972.75	1	0.64	-4.43	-0.85	2.43	-5.24	2.92
5950.60	1	0.41	-4.34	-0.76	2.55	-5.69	2.68
5929.77	1	0.55	-4.22	-0.54	2.66	-6.16	3.54
5926.33	1	0.00	-4.13	-0.79	2.74	-6.86	3.38
5912.90	1	0.59	-4.23	-0.29	2.64	-6.09	3.30
5871.59	1	0.27	-4.06	-0.38	2.69	-6.88	4.14
5812.91	1	0.55	-4.15	0.13	2.70	-6.53	3.55
5773.55	1	0.00	-4.14	-1.15	2.74	-6.82	3.63
5692.97	1	0.47	-4.26	0.04	2.62	-5.99	2.48
5634.40	1	0.21	-4.20	-1.24	2.70	-6.43	3.66
5633.12	1	0.41	-4.29	-0.63	2.59	-5.83	2.82
8772.06	2	0.36	-4.58	-2.12	2.08	-4.02	2.34
7752.84	2	0.33	-4.55	-2.93	2.07	-3.99	3.11
7746.62	2	0.42	-4.77	-2.85	1.95	-3.64	2.70
7717.63	2	0.23	-4.51	-2.84	2.10	-4.11	2.94
6051.86	2	0.23	-4.38	-2.25	2.12	-4.17	2.64
6043.46	2	1.21	-4.54	-0.60	1.91	-3.51	2.27
PR LOG SOLAR ABUNDANCE=0.71							
5609.02	2	0.22	-4.24	-1.59	2.24	-4.55	3.22
ND LOG SOLAR ABUNDANCE=1.43							
7094.11	1	0.14	-4.23	-1.67	2.68	-6.31	3.47
5749.80	1	0.00	-4.08	-1.47	2.73	-6.95	4.41
5675.87	1	0.14	-4.19	-0.61	2.70	-6.44	2.76
8839.10	2	0.00	-4.03	-2.47	2.55	-6.01	4.98

WAV	ION	CHI	LOG W/L	LOG GF	THETA	LOG PE	LOG [E]
ND CONTINUED							
8249.68	2	0.68	-4.62	-2.54	2.00	-3.80	3.05
7863.07	2	0.32	-4.37	-2.43	2.22	-4.47	3.12
7808.50	2	0.63	-4.55	-2.29	2.03	-3.89	2.86
7773.04	2	0.00	-4.33	-2.96	2.29	-4.72	3.20
7751.02	2	0.47	-4.49	-2.40	2.08	-4.05	2.85
6790.36	2	0.18	-4.20	-2.14	2.40	-5.10	3.52
6740.09	2	0.06	-4.15	-2.10	2.48	-5.42	3.67
6428.69	2	0.20	-4.16	-2.34	2.44	-5.23	4.04
SM LOG SOLAR ABUNDANCE=0.89							
7104.71	1	0.28	-4.43	-1.30	2.42	-5.19	2.63
8048.80	2	1.75	-5.15	-0.75	1.77	-3.04	2.72
7042.15	2	1.08	-4.72	-0.91	1.89	-3.43	2.30
6732.15	2	1.17	-4.46	-0.71	1.99	-3.77	2.96
6472.53	2	1.38	-4.68	-0.98	1.86	-3.33	2.94
EU LOG SOLAR ABUNDANCE=0.70							
6864.72	1	0.00	-4.46	-1.46	2.42	-5.20	1.81
GD LOG SOLAR ABUNDANCE=1.01							
7733.54	1	0.12	-4.43	-1.79	2.35	-4.93	2.31
7168.33	1	0.21	-4.28	-1.17	2.49	-5.47	2.60
6730.80	1	0.12	-4.30	-1.59	2.46	-5.37	2.67
5856.27	1	0.12	-4.17	-1.02	2.61	-6.03	3.05
5851.66	1	0.12	-4.17	-1.14	2.61	-6.03	3.17
DY LOG SOLAR ABUNDANCE=1.10							
6579.36	1	0.00	-4.25	-1.36	2.56	-5.76	2.42
5974.43	1	0.00	-4.38	-1.45	2.39	-5.09	1.76
5651.98	1	0.00	-4.36	-1.60	2.40	-5.13	1.99
5641.56	2	0.10	-4.22	-2.74	2.20	-4.42	3.99
HO LOG SOLAR ABUNDANCE=0.44							
6133.56	1	0.00	-4.27	-1.82	2.50	-5.49	3.59
5973.48	1	0.00	-4.53	-1.69	2.25	-4.59	2.40
ER LOG SOLAR ABUNDANCE=0.76							
8409.92	1	0.00	-4.38	-1.91	2.42	-5.18	2.40
6308.84	1	0.00	-4.32	-1.43	2.44	-5.26	2.13
5762.83	1	0.00	-4.09	-1.01	2.64	-6.49	3.62
8367.50	2	0.06	-4.91	-3.76	1.37	-3.39	3.19
HF LOG SOLAR ABUNDANCE=0.80							
7845.22	1	0.70	-4.39	-1.66	2.20	-4.42	3.22
7740.21	1	1.31	-4.60	-1.49	1.97	-3.69	3.45
6185.08	1	0.00	-4.26	-3.08	2.38	-5.08	3.72

TABLE 5.11

UY Cen $\left[\frac{E}{Ti}\right]$

Element	Solar Abundance $\log N_{HYDROGEN} = 12.0$ $\log N_{ELEMENT}$	Reference	Curve of Growth $\theta = 2.2$ $\log P_e$ -4.3	-4.9	-5.6	Model Atmosphere $\log g = 1.0$ T_e 2500	2800	3000	Quality
Li I	1.1	1	-	-	-	See Text			B
Na I	6.32	2	-0.9	-0.2	0.4	-0.5	-0.1	0.2	B
Mg I	7.62	2	1.0	1.0	1.0	0.7	0.2	-0.2	C
Al I	6.49	2	0.8	0.9	1.0	0.5	0.2	0.0	B
K I	5.12	2	-0.7	-0.1	0.5	-2.0	0.0	0.5	B
Ca I	6.34	2	0.0	0.2	0.7	0.2	0.3	0.5	A
Ca II			1.4	0.8	0.5	0.7	0.3	0.1	C
Sc I	3.04	3	0.0	0.0	0.1	-0.1	0.2	0.4	B
Ti I	5.05	3	0.0	0.0	0.0	0.0	0.0	0.0	A
V I	4.02	3	0.4	0.4	0.4	0.5	0.6	0.7	A
Cr I	5.71	3	0.0	0.0	0.0	-0.2	-0.1	-0.1	C
Fe I	7.50	3	0.3	0.3	0.3	0.2	0.1	-0.1	A
Co I	4.90	3	1.1	1.1	1.1	1.0	0.9	0.8	C
Ni I	6.28	4	1.0	1.0	1.0	0.9	0.6	0.4	B
Rb I	2.60	3	-0.1	0.5	1.2	-1.4	0.2	0.8	B
Sr I	2.90	3	0.7	0.7	1.3	0.2	0.6	1.0	C
Y I	2.18	5	1.6	1.7	1.8	1.9	2.1	2.4	A
Zr I	2.99	6	0.8	0.8	0.8	1.1	1.2	1.2	A
Nb I	1.69	6	0.8	0.8	0.8	0.8	0.8	0.8	D
Mo I	2.14	6	1.4	1.4	1.3	1.3	1.2	1.1	C
Cs I	1.13	6	1.1	1.6	2.3	-0.2	1.3	1.8	C
Ba I	2.07	7	0.7	1.3	1.9	0.3	1.1	1.6	A
Ba II			0.7	0.7	0.6	0.8	0.8	0.7	B
La I	1.19	6	0.5	1.1	1.7	0.6	1.3	1.8	A
La II			1.6	1.4	1.4	2.0	1.9	1.7	A
Ce I	1.61	6	0.9	1.5	2.1	0.9	1.7	2.2	B
Ce II			1.2	1.2	1.1	1.3	1.3	1.2	A
Pr II	0.7	6	1.8	1.7	1.6	1.9	1.8	1.7	D
Nd I	1.43	6	1.5	2.0	2.7	1.3	2.1	2.7	C
Nd II			1.7	1.6	1.5	2.2	2.1	2.0	A
Sm I	0.89	6	0.6	1.1	1.7	0.6	1.2	1.7	D
Sm II			1.6	1.4	1.3	1.5	1.3	1.2	C
Eu I	0.70	3	-0.3	0.2	0.8	-0.3	0.4	0.9	C
Gd I	1.01	6	0.8	0.9	1.3	0.9	1.3	1.7	B
Dy I	1.10	6	0.2	0.5	1.0	0.1	0.6	1.1	B
Ho I	0.44	6	0.9	1.1	1.6	1.1	1.6	2.0	D
Er I	0.76	3	0.7	0.9	1.4	0.8	1.3	1.7	C
Hf I	0.80	3	2.0	2.0	2.0	2.0	2.0	2.0	C

REFERENCES

1 Müller, E A., Peytremann, E., de la Reza, R., 1975. Solar Phys. 41, 53.

2 Lambert, D.L., Luck, R.E., 1978. Mon. Not. R. astr. Soc., 183, 79.

3 Ross, J.E., Aller, L.H., 1976. Science, 191, 1223.

4 Lennard, W.N., Whaling, W., Scalo, J.M., Testerman, L., 1975. Astrophys. J. 197, 517.

5 Allen, M.S., 1976. Publ. astr. Soc. Pacific, 88, 338.

6 Cameron (1970) see text for details.

7 van Paradijs, J., 1975. Astron. Astrophys. 44, 295.

5.21 Comparison of Curve of Growth and Model Abundances

Table 5.11 gives the final abundances, $[\frac{E}{Ti}]$ which are defined by

$$[\frac{E}{Ti}] = \log (\frac{N_{Element}}{N_{Ti}})_{UY\ Cen} - \log (\frac{N_{Element}}{N_{Ti}})_{Sun}$$

where N refers to the number of atoms of a given element. The appropriate solar abundances are given in column 2 with their references numbered in column 3 and listed below the Table. The values in column 5 are the finally adopted curve of growth abundances; the values in columns 4 and 6 show the effects of changing the electron pressures to the values corresponding to the ends of the error bars in Fig. 5.27. The values in columns 7, 8 and 9, are results given by the three model atmospheres. Column 10 is an assessment of the quality of the abundance determination, dependent on the quality of the laboratory log gf data, the number of star lines and the appearance of the curve of growth. The scale is defined below.

A; $\geq$ 4 star lines, good log gf, well definded curve of growth.
B; either $\geq$ 4 star lines, uncertain log gf
or $<$ 4 star lines, good log gf.
C; either $<$ 4 star lines, poor log gf
or $<$ 4 star lines, good log gf, but uncertain identification.
D; either 1 line,
or uncertain identification and poor log gf.

With the exception of the elements Mg, Al and CaII, the agreement between the two methods is considered excellent. It is somewhat surprising that the curve of growth method should give good relative abundances when both the model and the star show evidence of stratification. Stratification effects are described in chapter 6. It is interesting to realise that the degree of ionization in the curve of growth analysis, can be represented by one temperature and one pressure. Table 5.11 further shows that the abundances given by the ionized lines are much less sensitive to changes in the atmospheric parameters, than their corresponding neutral species. This occurs because, with the exception of CaII, the ion, when observed, is the dominant species and the abundance is there-

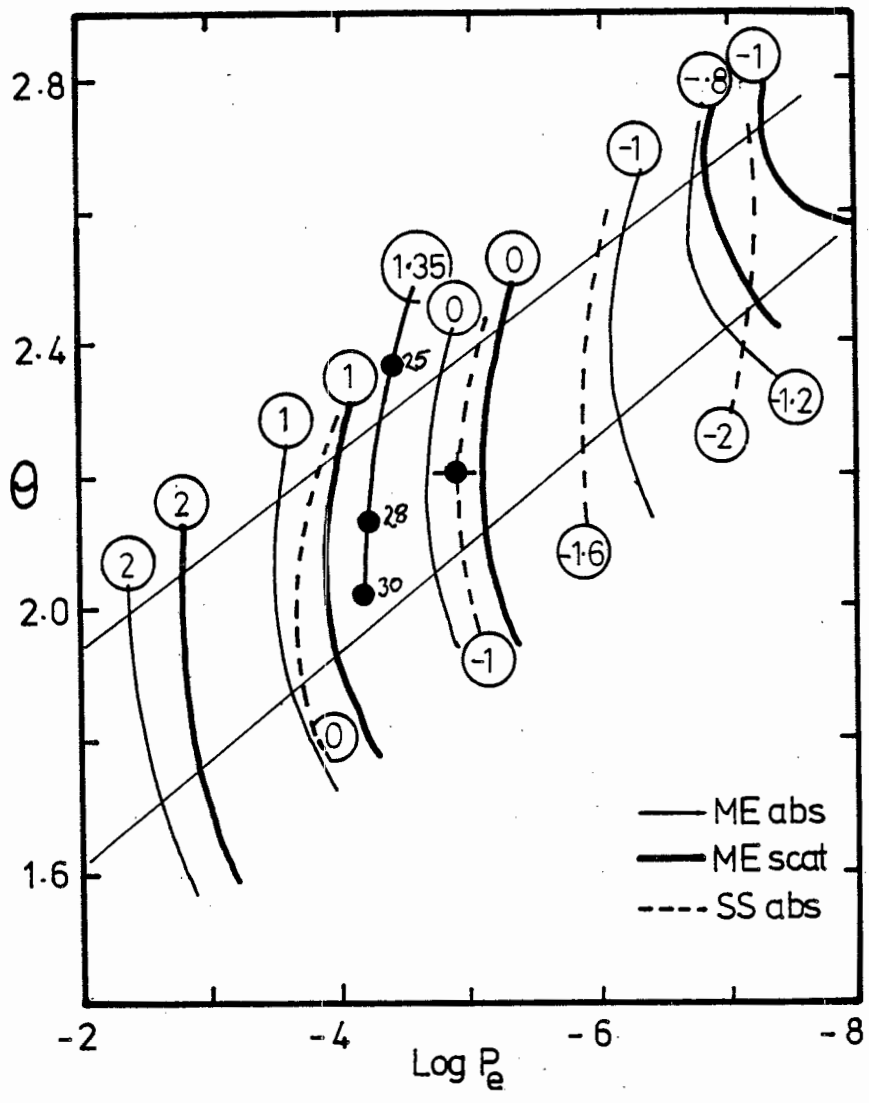

Figure 5.32

The loci of the solutions, for various values of Ti/H indicated in the circles, are shown for the various curve of growth models as a function of temperature and pressure. The mean solutions for the Johnson models, indicated 25, 28 and 30 and for the curve of growth analysis, indicated by the crossed circle, are also shown. The straight lines demarcate the solutions for various elements given in Fig. 5.27.

fore much less sensitive to changes in the degree of ionization. Ions have a second advantage in that they are usually also present in the sun, which greatly facilitates abundance comparison. The change over from predominantly ionized to predominantly neutral elements occurs at about 6.5 volts.

5.22 Absolute Abundances relative to hydrogen

The results in Table 5.11 are logarithmic abundances relative to the sun, normalised by the assumption that the $^{Ti}/H$ ratio is the same in both the sun and UY Cen. This assumption is generally made because of the great difficulty in determining the absorption coefficient per hydrogen atom in a cool star, where there are many unknown sources of opacity.

Equation 5.59, which relates the curve of growth shift $\Delta\log X$ to the $^{Ti}/H$ ratio is rewritten below, where all the terms between the curly brackets are functions of θ and or Pe.

The log UI and log r_0 terms are only slowly dependent on θ.

$$\log \frac{Ti}{H} = 20.05 - \Delta\log X - \log \tau_2 + \{\log UI - \gamma \log r_0(7000) + \log K(7000) + \log(1+a)\}$$

The inverse slope of the curve of growth has the value $\gamma = 5.52$ while $r_0(7000)$ has different values for the SS and ME models. The derivation and variation of r_0 and γ is described in chapter 6. The observed value for Ti is $\Delta\log X = 1.35$. We assume $\tau_2 = 1$ where τ_2 is the continuum optical depth above which the absorption lines are formed in the SS model. The opacities dependant on hydrogen, are found using the appropriate model atmosphere subroutine.

Fig.5.32 shows values of $[^{Ti}/H]$ for various models, as a function of θ and log Pe. The parallel lines contain the Saha ionization solutions that satisfy NI = NII for the appropriate elements given in Fig.5.27, while the filled crossed circle corresponds to the adopted curve of growth parameters. The differences of $[^{Ti}/H]$ between the different models is a consequence of the different values of r_0, while the variation with θ and log Pe, is mainly a result of the change of opacity.

The ME models, with pure absorption and pure scattering, predict $[^{Ti}/H]$ abundances of respectively -0.2 and +0.2. On the other hand

the SS model indicates $[^{Ti}/H]$ = -1.0,or alternatively if we accept that $[^{Ti}/H]$ = 0.0 then the SS model implies that the opacity is much higher than the hydrogen opacity alone.

We have also plotted,the mean values of log Pe and θ and the $[^{Ti}/H]$ ratio,given by the three Johnson model atmospheres. These are labelled 30, 28 and 25,according to their effective temperatures. If the opacity variation scales with log Pe and θ in the same way as for the ME and SS models, then the Johnson models predict $[^{Ti}/H]$ = 0.8 for UY Cen extrapolated to the curve of growth values of θ and Pe. This may indicate an overestimate of the opacity in the model, possibly a consequence of using a model atmosphere for which C/O ≠ 1.0. It must be remembered, that we have simply scaled the tabulated opacity at 10000 Å, by the wavelength variation of the hydrogen opacity. It is also important to appreciate the wide range of θ and log Pe, given by individual Ti lines in the model atmosphere, which is illustrated in Fig. 6.04.

Within the very large uncertainties of this type of argument there is no evidence to suppose that the $^{Ti}/H$ ratio is other than solar.

5.23 Abundances of Li, Na and CN

The last part of this chapter is concerned with the abundances of Li, Na and CN, all of which require special consideration. The abundances are derived using the 2800 Johnson model atmosphere.

Li

The Li abundance is of considerable astrophysical interest because it gives important clues and sets limits on the evolutionary history of a star. The Li line strength also shows considerable variation amongst otherwise rather similar stars, which must reflect variations in Li abundance.

There are two important effects that influence the derived Li abundance. These are; the model used to describe the Li line formation and the effect of blending by other elements. Non LTE effects may also be important and this point will be discussed briefly below.

The extent to which the various methods used to deal with the low atomic weight and the doublet nature of the 6707 Li line breakdown has not always been appreciated, by the various workers in the field. The

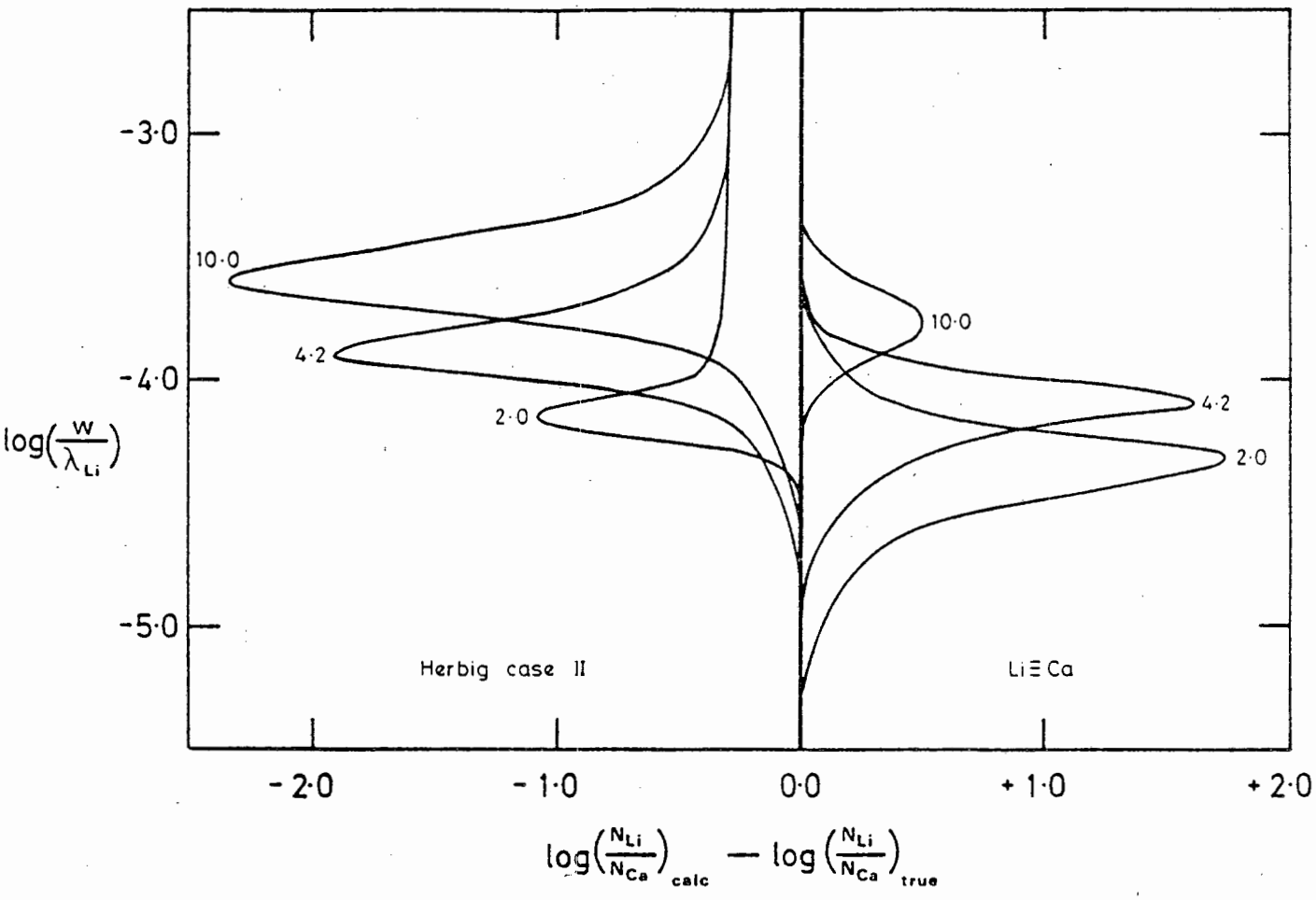

Figure 5.33

The different abundances, given by different theories of Li line formation, are shown as a function of Li equivalent width for various values of the microturbulent velocity.

problem was clearly stated by Herbig (1965), who then showed that for his stars, where the Li line was very weak, the three different methods gave essentially the same result. In Fig.5.33 we plot the difference between the calculated and true number of Li atoms as a function of the Li equivalent width, for various values of the microturbulent velocity. These curves are based on curves of growth produced for Ca and Li, using the Johnson 2800 model atmosphere. Three Li line formation theories are used. The first is Herbig's case II, in which the two doublet components are considered to be physically separate and extrinsically blended by low resolution or microturbulance. The second theory, which we believe gives the 'true' abundance, and provides the standard of comparison in Fig.5.33 corresponds to Herbig's case I. In case I the absorption coefficients of the doublets must be added and the sum used to compute the equivalent width. This assumes that the 'microturbulent velocity', deduced from the curve of growth, can indeed be combined with the thermal velocity, to define the doppler width required by the line broadening theory. The third theory ignores the doublet nature and the difference in atomic weight and assumes that the Li and Ca curves of growth are therefore identical. This is the situation that prevails when the Li 6707/Ca 6573 line ratio is used as an estimate of the Li abundance. Examination of Fig.5.33 shows that for both weak and strong Li lines all theories give substantially the same result. However for Li lines of intermediate strength, which applies to the majority of S and C stars, the results are very sensitive to theory and the adopted microturbulent velocity. The microturbulent velocities cover the range found by various workers for S and C stars. The actual amplitude of the deviation will depend on the damping which is low in both UY Cen and the model atmosphere. The seriousness of the effect is apparent in the case of UY Cen with $\log W/\lambda = -3.94$ and $\xi = 4.2 \text{km s}^{-1}$, for which the Li abundance would be underestimated by 2 dex using Herbigs case II instead of his case I.

The derived Li abundance is very sensitive to the effects of blending by other lines. This is clearly a problem in the case of the sun and other stars, where the Li line is intrinsically very weak. It remains an important problem in UY Cen, because of the shape of the curve of growth, which means that a 0.1 dex change in equivalent width will

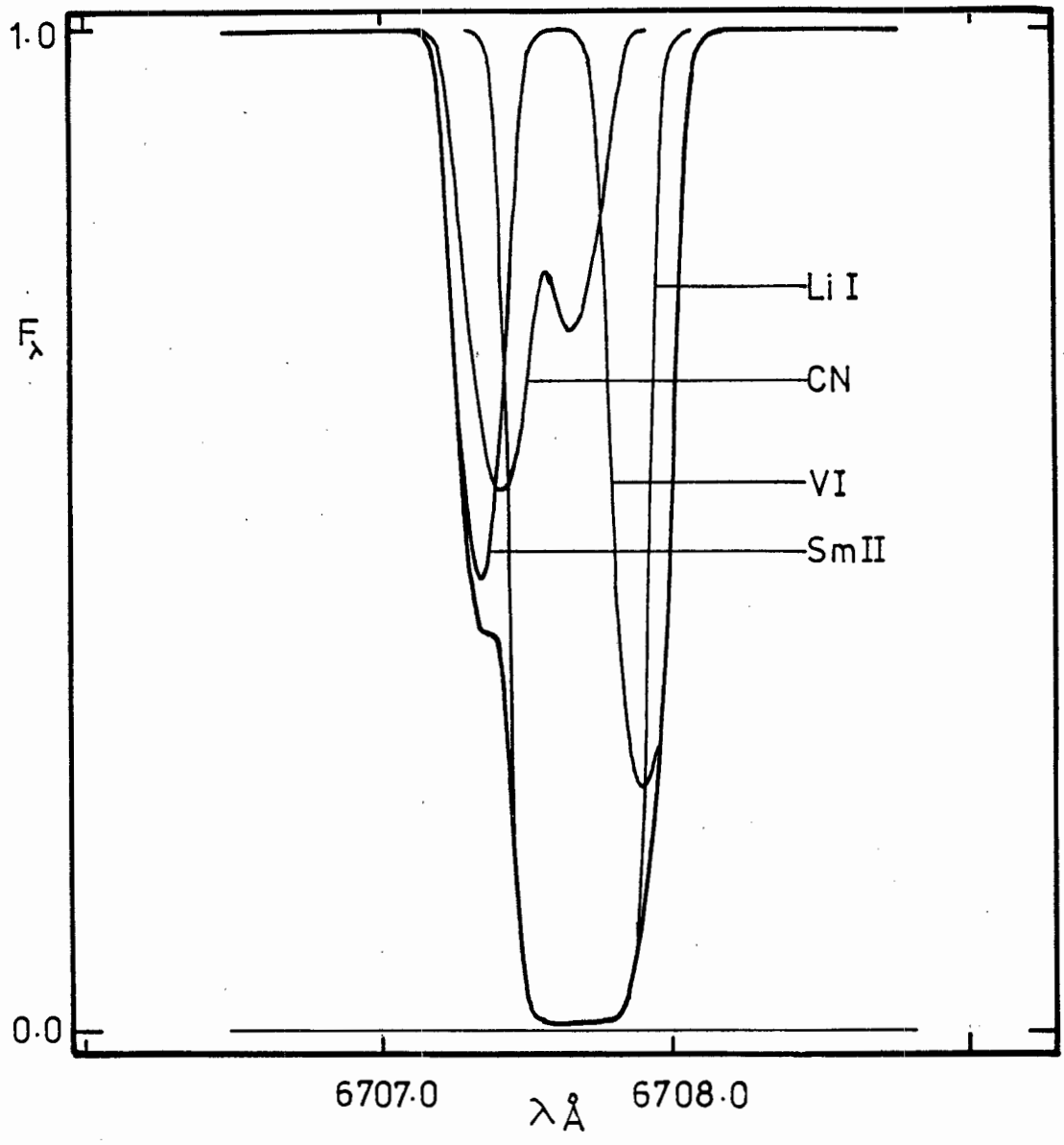

Figure 5.34

The outer envelope shows the line profile, generated by the 2800 atmosphere using the contributors indicated, that matches the observed equivalent width. The other profiles show the individual contributors as if they were the only line present. The Li doublet is not resolved.

correspond to a 1.0 dex change of abundance.

We have re-examined the line identification sources, in the light of our abundance analysis, for possible blends with the Li line. We have also examined all the lines, which include a number of ^{13}CN lines, given by Luck (1977) as blending with Li. Of these the lines listed in Table 5.12 below are considered important.

TABLE 5.12

Element	λ	lower excitation level	log gf	log W/λ
SmII	6707.45	0.92	-1.65	-4.74
$^{12}CN(6,2)Q_2(44)$	6707.529	0.96	-1.75	-4.60
$^{12}CN(5,1)R_1(64)$	6707.816	1.21	-2.05	-4.94
VI	6708.100	1.22	-2.99	-4.51
LiI doublet				-4.07
Equivalent width of entire feature				-3.94

The Table also gives the excitation levels, log gf values and the equivalent width, that each of the contributors would have were it the only line present. The log gf values are drawn from the sources given in the data sections. The equivalent widths have been calculated using the 2800 Johnson atmosphere and adopting the abundances given in column 8 of Table 5.11. The CN strengths are also appropriately normalised. The remaining blending lines listed by Luck (1977), all have log W/λ < -5.10 and have been ignored. Ignoring the background of weaker lines will compensate for the fact that they have been ignored throughout the analysis and manifest themselves as an added source of opacity throughout the spectrum.

The model atmosphere program was modified to allow for the combination of all the lines listed in Table 5.12 according to Herbig's case I (added absorption coefficients).

The number of Li atoms was altered with the Johnson 2800 atmosphere to match the observed log W/λ = -3.94 and gave a final value of $[\frac{Li}{Ti}]$ = -0.8.

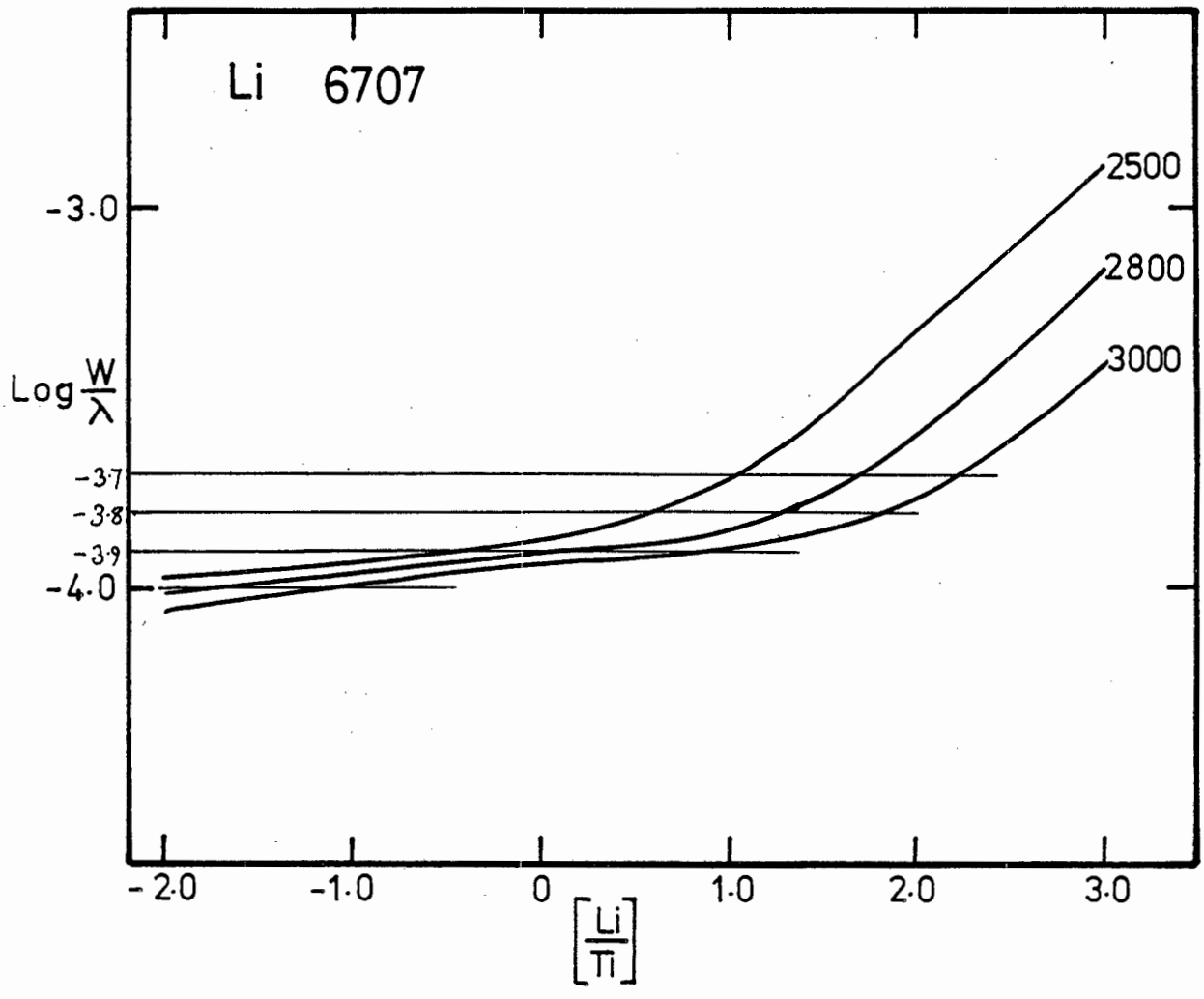

Figure 5.35

Curve of growth generated by the 2800 atmosphere for the Li feature illustrated in Fig. 5.34.

This can be compared with a value $[\frac{Li}{Ti}] = +0.7$ which would have been obtained if the blending lines had been ignored. Fig. 5.34 shows the resulting Li line profile as well as the profiles of the blending lines were they the only line.

The half width of the feature is 14% greater than for a line of the same equivalent width produced only by lithium, a difference that cannot be detected on our tracings. The mean wavelength is 6707.796 Å which is in much better agreement with the measured wavelength of 6707.78 Å ± 0.025 s.e. than with the mean wavelength for a pure ^{7} Li line of 6707.846 Å.

Fig.5.35 shows a series of curves of growth for the Li feature including the blends, for the three different model atmospheres. This illustrates the insensitivity of the equivalent width to the [Li/Ti] abundance in the region of the observed Li equivalent width. It is clear that we can claim little more than that the Li abundance in UY Cen is less than or close to the solar value, with an uncertainty of about ± 1 dex. It is also clear that for observed $\log W/\lambda > \sim -3.70$ there is no doubt that Li is overabundant. This is the situation found in the SLR SC stars.

The Sodium D Lines

The NaD lines were modelled by adding the absorption coefficients appropriate to each component, at each wavelength across the profile.

Fig. 5.36 shows profiles given by the three Johnson model atmospheres, each satisfying the condition that $[\frac{Na}{Ti}] = 0.0$. The $[^{Ti}/H]$ ratio remains essentially constant for each model and is the value given by the UY Cen TiI equivalent widths. The rapid change in NaD equivalent width is a consequence of the changing degree of ionization. It is clear that while the profiles generated by the models encompass the profile given from the spectral scan, the detailed fit is not very good in either shape or central depth. The poor shape fit suggests that the NaD lines are heavily blended by some large scale feature.

The theoretical profiles have been normalised to fit the spectrum scan continuum, which is about 30% lower than the continuum given by the coude spectra. This implies that the NaD lines are formed in a higher opacity environment than individual metal lines and it has already been

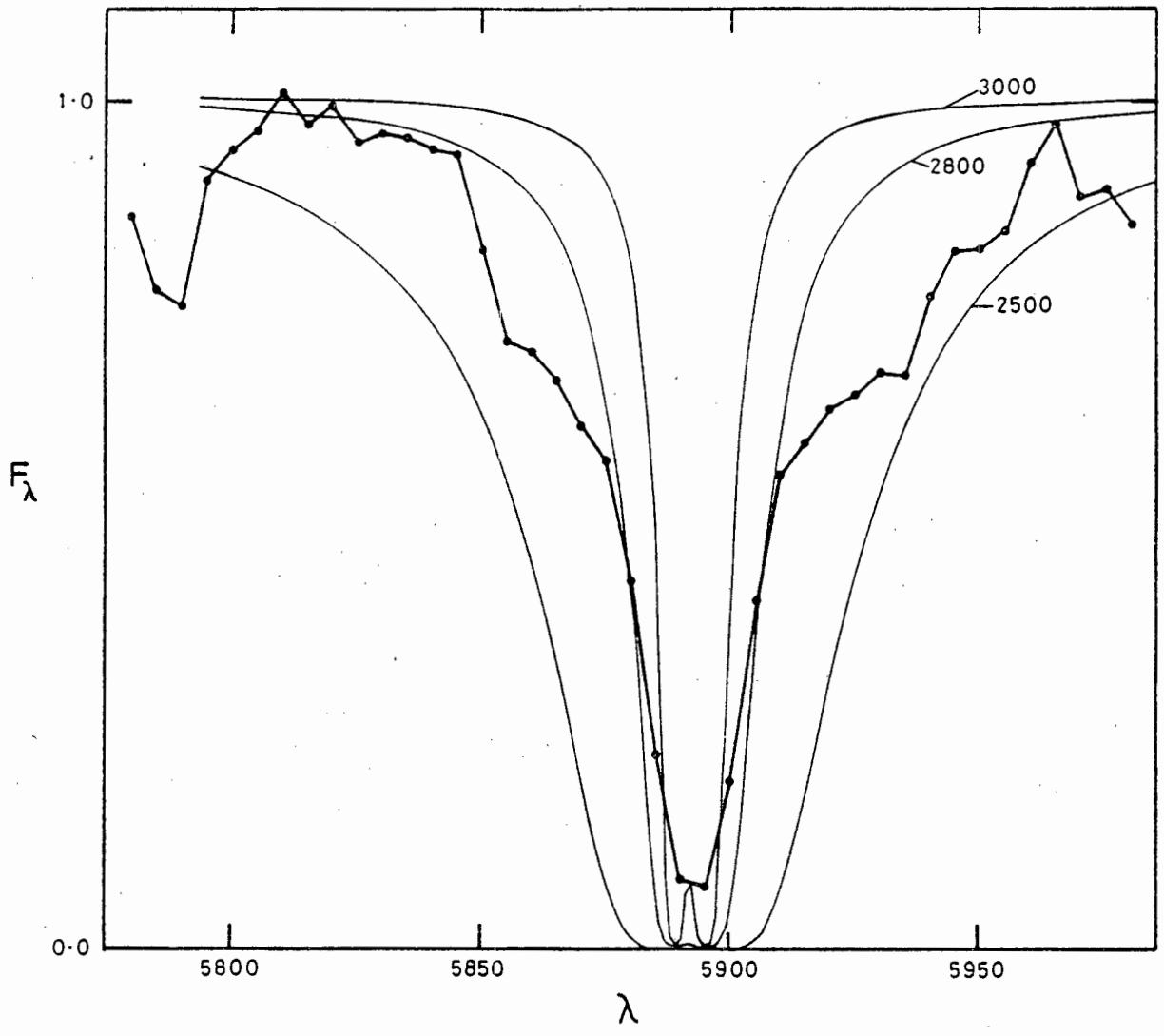

Figure 5.36

The spectrum scan of the Na D lines, normalized by a 2500 black-body is compared with profiles generated by the three Johnson model atmospheres each satisfying the condition that [Na/Ti] = 0. Note the marked change of equivalent width from model to model.

pointed out that to the broad NaD lines individual metal lines will look like an added source of continuous opacity. In order to model this we have taken the density contribution function, given by a 0.9 ev TiI line with log $^{W}/\lambda$ = -4.2 and used it to modify the continuous opacity at depth τ, according to the expression;

$$K_c(\tau) = K_c(\tau)(1 + \alpha F(\tau))$$

Here $F(\tau)$ is the density contribution function and α is a constant which is found by satisfying the condition that the emergent flux in the continuum will be reduced by the observed factor (here 30%). When this is done it has a less than 1% effect on either the shape or the equivalent width of the NaD line. Reducing the emergent flux by 80% still only reduces the equivalent width by about 20%.

The explanation for this insensitivity is given by stratification effects, which show that even the wings of the NaD lines are formed high in the atmosphere, above the region where the TiI lines have much effect.

The discrepancy between the observed and predicted central depth can be understood to indicate that, either the surface of UY Cen is hotter than the model or possibly that there is evidence for an extended atmosphere, in which case the area of the upper levels are much greater.

CN

Greene (1972) has calculated partial pressures for the CN molecule for two total pressures and a series of temperatures and C/O ratios, appropriate to the SC stars. He calculates the CN partial pressure by solving for 23 different molecules. The C/O ratio is changed, by either diluting a solar composition mix with CNO, or 3α processed material. In otherwords only the C, N and O abundances change. Piccrillo (1980) shows that the CN pressure calculations will not be sensitive to the fact that solar abundances have been used for the enhanced heavy elements of periods 5 and 6.

Unfortunately the Greene partial pressures do not cover the entire range of temperature and gas pressure found in the model atmospheres. Greene's results have therefore required considerable extrapolation and interpolation. Examination of Greene's curves of partial pressure

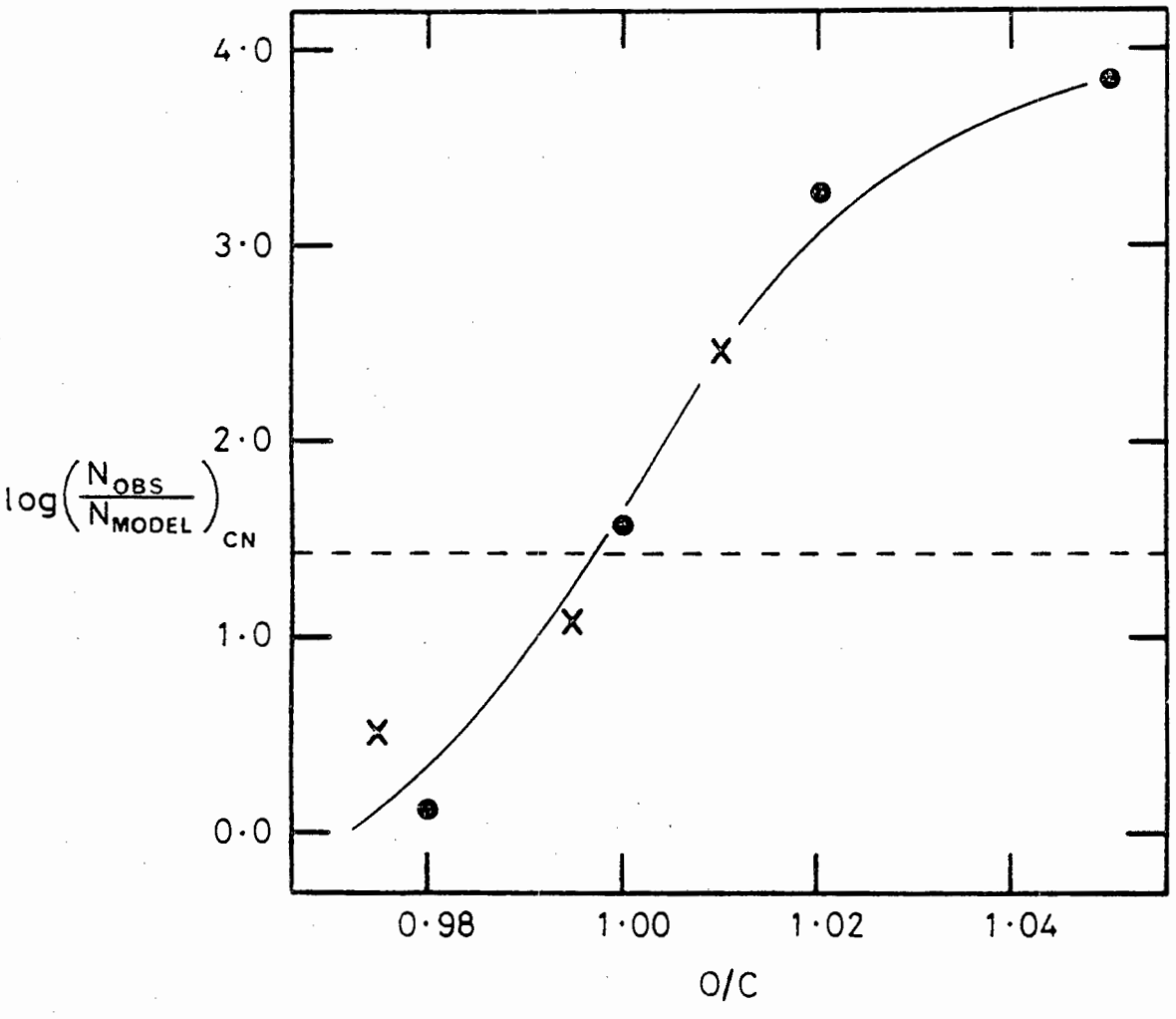

Figure 5.37

The factor by which the CN abundances, predicted by the model, must be multiplied in order to reproduce the observed CN equivalent widths, is shown as a function of the O/C ratio. The dotted line is the same factor for Ti. The crosses are for a carbon weak CNO mixture while the filled circles are for a carbon rich 3α mixture. Note the lack of discrimination between the two mixtures and the fact that the two curves intersect at O/C = 1.

as a function of temperature, shows that for a given C/O ratio, the curves for the two total pressures are of identical shape but displaced in the partial pressure temperature plane. On the other hand there is quite rapid variation of shape with C/O ratio.

The two total pressure curves were interpolated and extrapolated to cover the entire range of pressure and temperature within the model atmosphere, by transforming to a new coordinate system. This was a rotated system of axes such that lines joining points of equal slope lay parallel to one axis. The angle of rotation was an input variable and it was simple to see how the resulting abundances varied with the angle of rotation of the coordinate system. The major weakness of the whole process is that there is no way of knowing that the curves do indeed transform in this way. However, the observed effects discussed are gross and the CN lines are mainly formed in regions close to one of the total pressure curves, so that the poor definition of the partial pressures should not be too serious.

The CN abundance

The partial pressure of CN was found for every level of the model atmosphere by the methods given in the previous section. These partial pressures were then used by the model atmosphere program, along with other appropriate atomic data, to calculate equivalent widths. The number of CN atoms was scaled, without of course altering their relative depth distribution, until the calculated equivalent width equalled the observed value. The calculated variation of CN strengths was found to depend much more strongly on O/C ratio and carbon abundance than on the effective temperatures of the different model atmospheres, so that we only need consider the results for the 2800 atmosphere. Fig.5.37 shows the factor, by which the CN abundances must be multiplied to give the observed $\log W/\lambda$ for CN, as a function of the C/O ratio. The dotted line shows the same factor for Ti, which is of course the [Ti/H] ratio given by the model. The crosses are for the nitrogen rich CNO mixture, while the circles correspond to the carbon rich 3α mixture. The correspondence of the two sets of points, on the same curve, indicates that the CN strength alone will not discriminate between either the CNO or the 3α origin of the CN. It is interesting to note the rapid variation of the

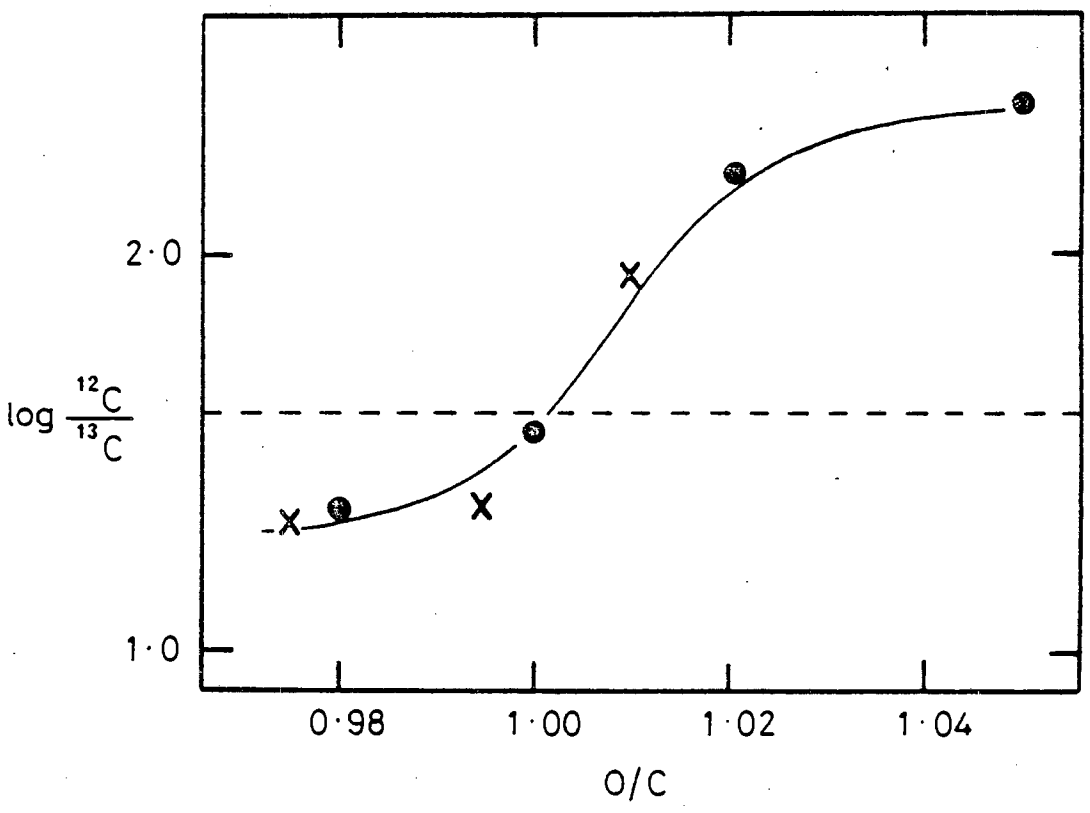

Figure 5.38

The derived $^{12}C/^{13}C$ ratio is shown as a function of O/C ratio. The dotted line shows the curve of growth result.

CN strength as a function of O/C. This corresponds to the well known rapid increase of CN strength on passing from S to C stars.

If we assume that the observed [Ti/H] ratio is a consequence of an incorrect opacity rather than due to an enhanced Ti abundance, then we can say that the point where the Ti and CN curves intersect, gives the O/C ratio at which the observed and calculated CN strengths are equal. It is satisfying to note, that within the errors of the CN log gf values, this is at O/C = 1.0, which ties in neatly with the idea that the SC stars have O/C ≃ 1.0. The N/C ratio then takes the value 27.0 or 0.10 depending on whether the CNO or 3α abundances prevail.

The $^{12}C/^{13}C$ ratio

The atmosphere parameters derived by Catchpole (1979) for UY Cen are somewhat different from those given here. The present curve of growth analysis gives a $^{12}C/^{13}C$ ratio of 40 (1.6) dex. The major uncertainty in determining the $^{12}C/^{13}C$ ratio is that all the (2,0) ^{13}CN lines are weaker than any of the (2,0) ^{12}CN lines. This means that in order to define the curve of growth, intrinsically weaker ^{12}CN lines arising from higher excitation levels, must be used. This in turn makes the results sensitive to the adopted band strengths and excitation temperature. Greene (1969) notes a discrepancy between the observed and predicted band strengths of CN in both the sun and α Ser. Day et al. (1973) re-analised α Ser and concluded that the discrepancy, between the (4,0) and (2,0) bands, was a consequence of systematic errors in Greene's equivalent widths, which were measured in different spectral regions. However this can not explain the difference between the (2,0) and (3,1) bands which are both in the red. If Greene's observed band strengths are used then the $^{12}C/^{13}C$ ratio will be lowered by about 0.2 dex.

The model atmosphere results are very interesting in that they show that the predicted isotope ratio will depend on the O/C ratio. This is illustrated in Fig. 5.38, where the dotted line is the result given by the curve of growth analysis.

The variation of the isotope ratio is a consequence of the fact that the number of CN molecules per hydrogen atom is not uniform throughout the atmosphere. The actual distribution depends on the O/C ratio

in the sense that for O/C < 1.0 there are proportionally far more CN molecules higher in the atmosphere. This variation of distribution is important because of stratification by equivalent width, which means that the very much weaker ^{13}CN lines are formed much deeper in the atmosphere. If this effect is confirmed by more detailed model atmosphere calculations it will have important consequence in determining the isotope ratios for C and S stars.

The curve of growth and model atmosphere results are in good agreement for O/C ≈ 1.0 which is somewhat fortuitous.

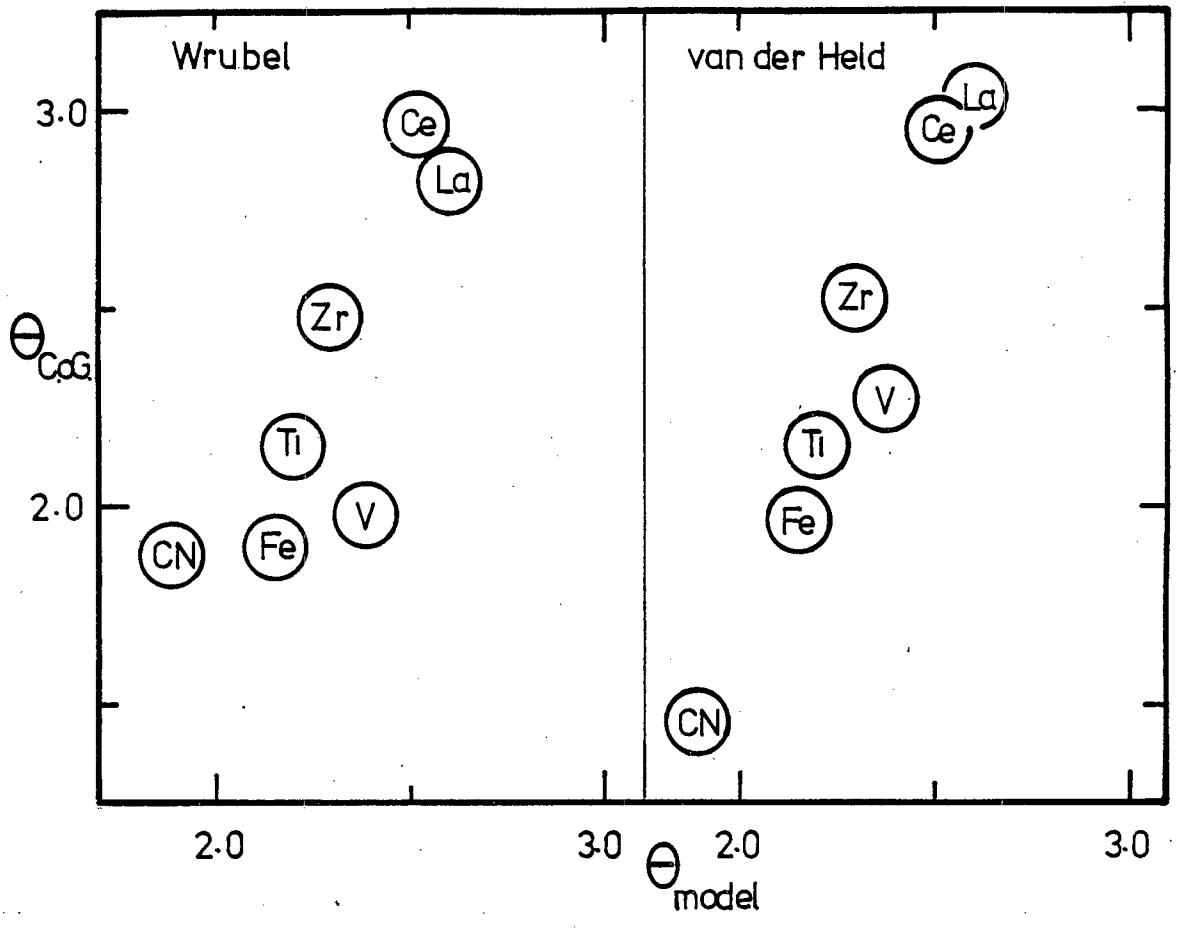

Figure 6.01

The mean θ, for individual elements, given by the curve of growth analysis, is shown as a function of the mean stratification temperature given by the Johnson 2800 atmosphere. The correlation indicates that stratification is present in UY Cen.

CHAPTER 6

The Stratification and R_o Term

6.01 Introduction

In this chapter we use the ME, SS and Johnson model atmosphere, to investigate the effects of stratification and the origin of the r_o term in UY Cen.

There are two indications that stratification may be present in the UY Cen atmosphere. The first is the range of mean excitation temperature, found for different elements, during the curve of growth analysis. The second indication is the discrepancy between the curve of growth and model atmosphere abundances, for the elements Mg and Al, both of which have high lower excitation levels.

6.02 The Excitation temperature Stratification effect

Equation 5.76, in the contribution function section, has been used to define the values of θ, given for each line in Table 5.10. Mean values of θ were formed for each element and are compared, in Fig. 6.01, with the results given by the curve of growth analysis in Table 5.09. There is a clear correlation which gives direct evidence for the existence of stratification in UY Cen. The method of estimating θ in the curve of growth analysis is quite different from the method used with the model atmosphere. In the curve of growth analysis θ is given by the slope of $\Delta \log X$ against χ and it is obvious that this can depend rather critically on the set of log gf values used. On the other hand the θ, estimated by the model atmosphere, depends on how atoms are distributed in the atmosphere and is therefore quite independent of the log gf value, depending only on the equivalent width, ionization and excitation level involved. Since the excitation levels, which are the only data common to both methods, are very well known it is highly improbable that the θ correlation can be a spurious effect. We therefore conclude that the atmosphere of UY Cen is more accurately described by the model atmosphere than by either the SS or ME models.

It is noteworthy that the range of θ given by the curve of growth is much greater than that given by the model, which one might say shows that stratification is even more important in UY Cen than is indicated by the model. However it is not possible to confirm this idea. A second point of interest is that the small value of θ, given by CN with the van der Held curve, does not deviate from the trend of the remaining elements, although the range of 1.5 in θ was taken as grounds for prefering the Wrubel curve. We show below that stratification depends on wavelength, excitation, ionization and equivalent width, so there is no simple way of improving the curve of growth method to allow for these effects.

With the possible exception of the KI lines, there is no evidence for a correlation of the wavelength residuals, of the lines used in the abundance analysis, with the θ depth of formation. This indicates a stable atmosphere. The two KI lines show a mean blue shift of 6 km s^{-1} but both lines are blended so that no great significance can be attached to this observation.

6.03 Stratification Effects in the model

In this section we use the model atmospheres to predict and illustrate the relative importance of the different effects which contribute to the over all stratification of a given absorption line. The stratification level is very conveniently indicated by the weighted mean θ for the line, defined by equation 5.76 for the density contribution function (DCF). The important contributors are; excitation level, wavelength, log W/λ and ionization potential. The technique used is to vary only one contributor at a time holding all the others constant by, where necessary changing the total number of atoms. The standard data set is given by;

The 2800 atmosphere, ξ = 4.2 km s^{-1}, log W/λ = -4.30, χ_{lower} = 1.50 e.v. χ_{ion} = 6.82 e.v., λ = 7000 Å. These data, as well as the partition function and atomic weight, correspond to that of a typical titanium line.

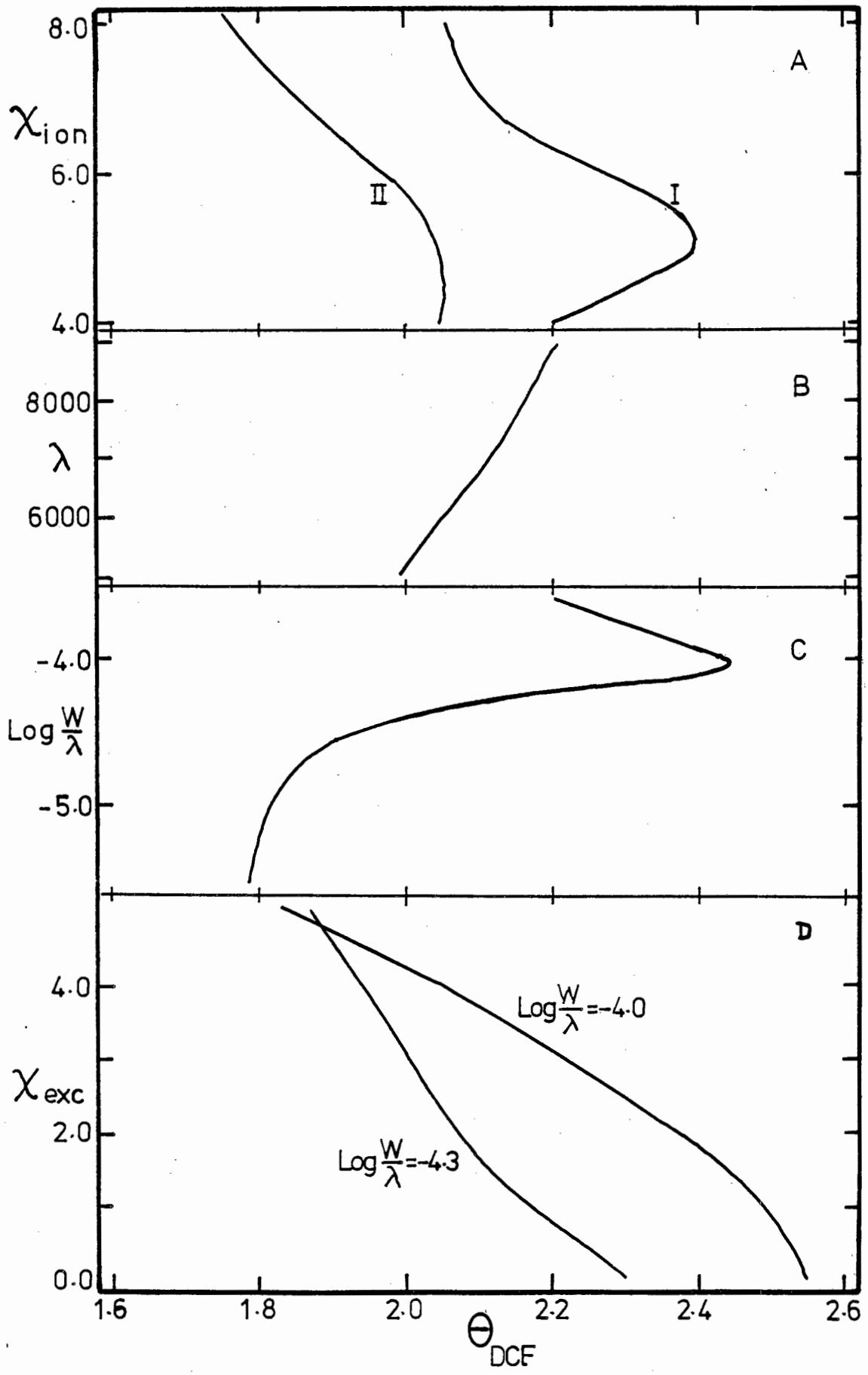

Figure 6.02

The depth of line formation, indicated by θ_{DCF} is shown as a function of various important line formation parameters. As each is varied the remainder are held constant.

The results are shown graphically in Figs. 6.02 A to D.
The two curves in Fig. 6.02A correspond to an ionized and a neutral line. From 4.0 to 8.0 e.v., the atoms change from being 99.99% ionized to being 99.84% neutral. The tendency for the ionized lines to be formed deeper is a consequence of the higher excitation environment. It is difficult to forsee how stratification will depend on ionization potential because the effects of temperature and electron pressure work against each other.

The wavelegnth dependence of the depth of line formation is illustrated in Fig. 6.02B. This is partly a consequence of the variation of the continuous opacity, but much more important, it is a consequence of the change in gradient of the Planck function with wavelength. This will be more fully dealt with in the section on the variation of r_o but can be described as follows. Within the line forming region as the wavelength increases, both the gradient of the Planck function and the total flux become greater. This means that a line of constant central depth or 'contrast' must be formed much shallower in the atmosphere at the longer wavelength. An absorption line of constant log W/λ has a slightly smaller central depth but is nevertheless still formed higher in the atmosphere at the longer wavelength.

The effect that weak lines are formed deeper than strong lines is well known and is illustrated in Fig. 6.02C. The turnover, shown by lines on the squareroot part of the curve of growth, is a consequence of our weighting method and illustrates the increased importance of the wings in contributing to the total equivalent width. The wings are always formed deeper than the line centre.

Depth depencence of different lower excitation levels is shown in Fig. 6.02D for two log W/λ values. The depth dependence is a simple consequence of the higher excitation levels requiring higher excitation temperatures to be populated.

It is clear from Fig. 6.02 a to d that the various effects are of about equal importance, so that it is really impractical to demonstrate the effects of any one type of stratification, without a very large body of observational data. The fact that the two curves in Fig. 6.02d are not of identical shape with a constant relative displacement, suggests that cross terms exist between the various stratification effects. The elements giving

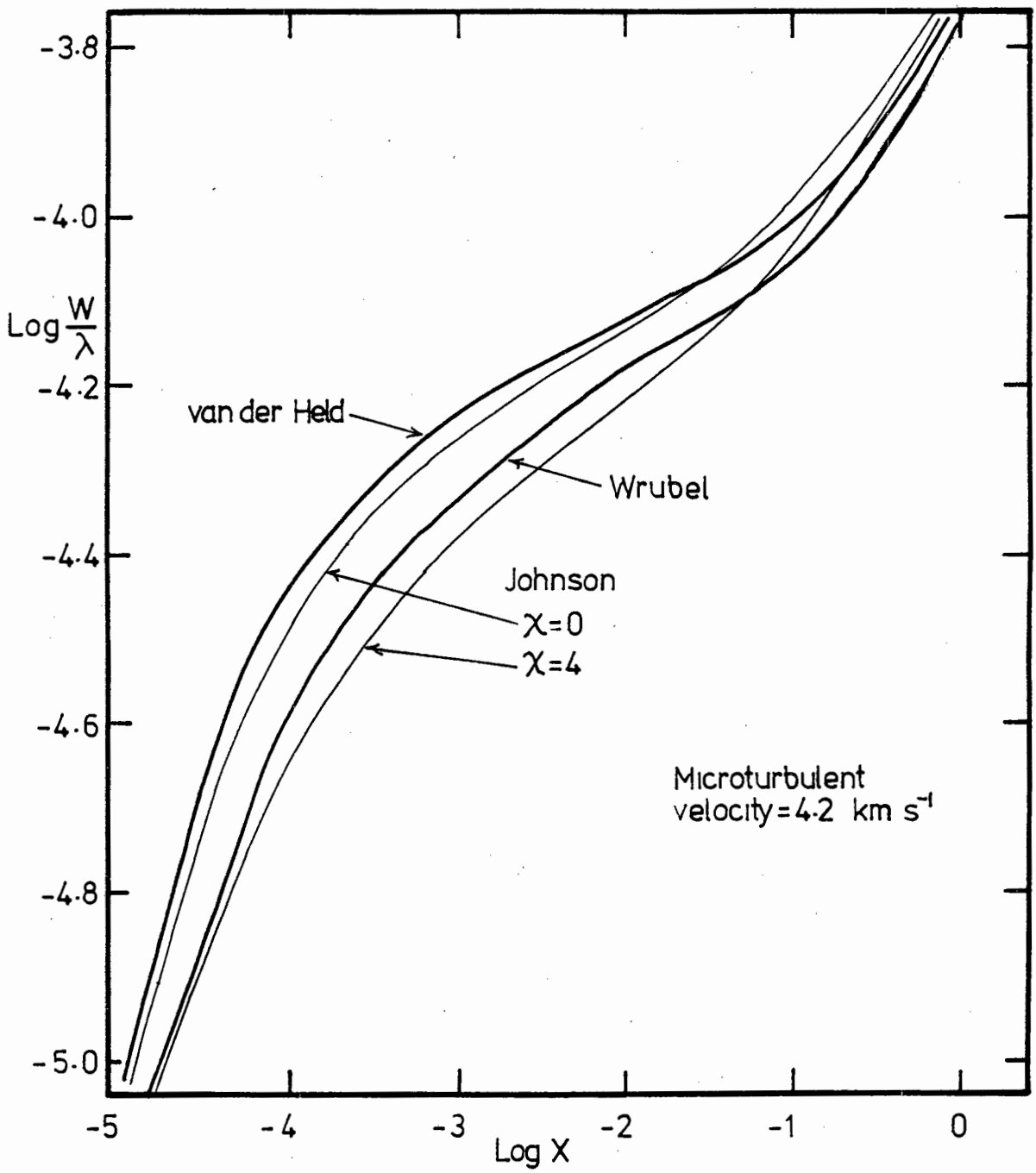

Figure 6.03

The difference in shape of different curves of growth is shown. All the curves have been normalized so that log W/λ = log X for faint lines.

rise to the different values of θ_{ex} from the curve of growth, do indeed show a hetrogeneous distribution of log $W/\lambda, \chi_{lower}$ and ionization potential.

Another aspect of stratification is shown by the theoretical curves of growth produced by the model atmosphere. Two theoretical curves, given by the 2800 atmosphere for TiI, with $\xi = 4.2$ km s^{-1}, for $\chi = 0$ and $\chi = 4.0$ e.v., are shown in Fig. 6.03. Also shown are the Wrubel curve, with $B^o/_{B^1} = 1/3$ and the van der Held curve, with $\xi = 4.2$ and $\Gamma = \Gamma_{classical}$. All the curves have been normalised to satisfy the condition that log W/λ faint = log X. The splitting of the model atmosphere curves is a consequence of the effects illustrated in Fig. 6.02C and D and simulates a difference of microturbulent velocity. An apparent increase of microturbulent velocity with decreasing lower excitation, has been noted by Utsumi (1970) in his analysis of 22 C stars. In a curve of growth analysis with few weak or strong lines, the apparent separation of the curve of growth, by an amount proportional to excitation level, would be interpreted as a wrong choice of excitation temperature. An increase of θ by ~ 0.17 brings the curves into coincidence. Fig. 6.03 also shows the good agreement in shape, between the model atmosphere and the Wrubel curves. The van der Held and Johnson curves are generated by pure absorption while the Wrubel curve is for pure scattering, which as mentioned before, illustrates the danger of using the form of the curve of growth to interpret the method of line formation. Fig. 6.03 also indicates that if the log W/λ data is confined to the transition part of the curve of growth, as is usually the case for cool stars, then compared with the van der Held curve, the Wrubel curve will overestimate the absolute abundances by ≃ 0.55 dex.

Fig. 6.04 illustrates the wide range of θ and Pe at which individual star lines are formed in the 2800 model. The graph is drawn for the elements, Ti, V, Fe, Zr, La and Ce, which all show considerable overlap and are not distinguished. The lines cooler than $\theta = 2.6$ are all either La or Ce lines. The turnover at low temperature is caused by the stratification effect shown in Fig. 6.02C. The large open circle illustrates the curve of growth solution, while the pair of lines contain the ionization

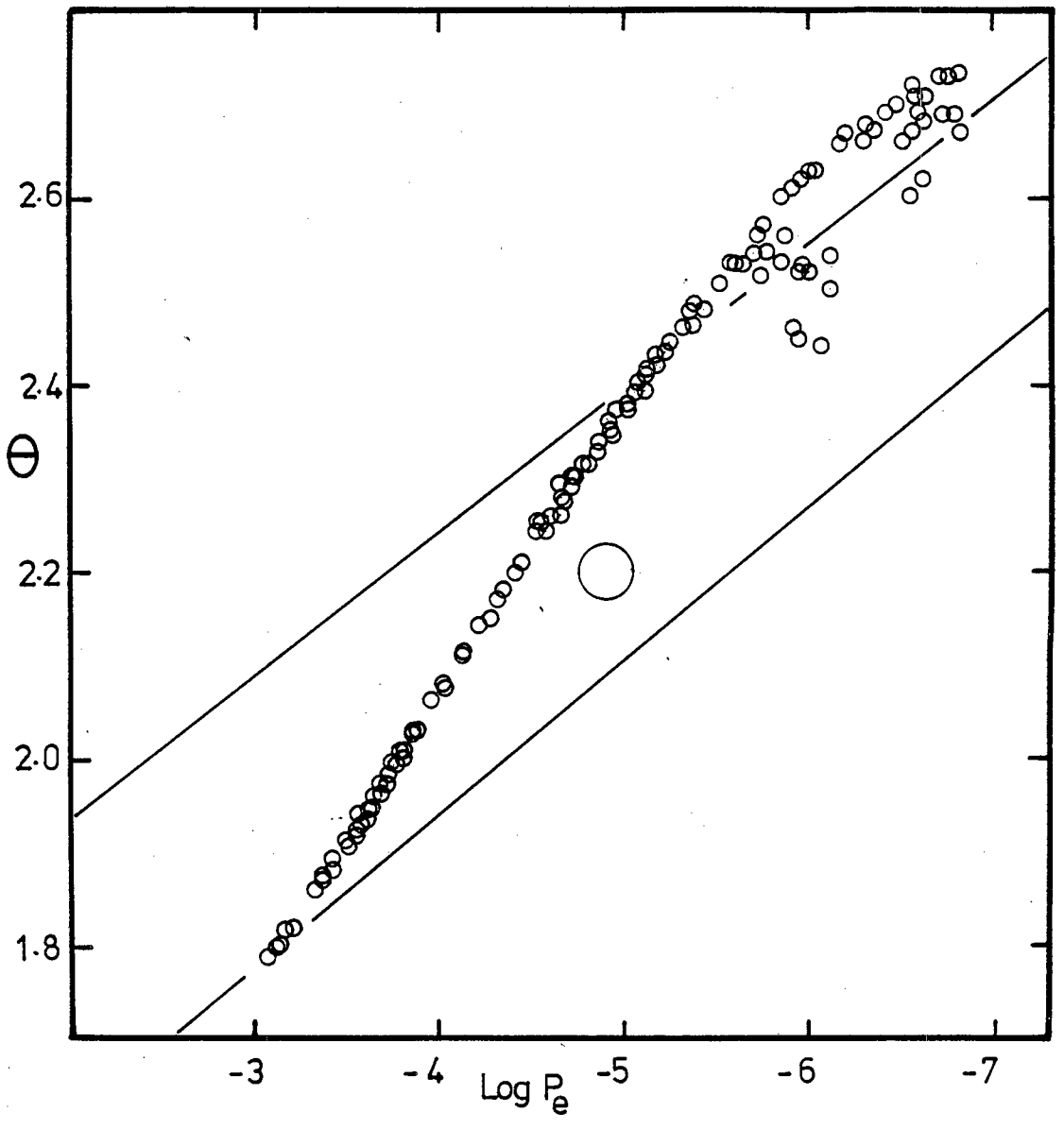

Figure 6.04

This Fig. shows the wide range of θ and P_e, as defined by the DCF, over which individual lines are formed in the 2800 model atmosphere. The large open circle gives the adopted curve of growth parameters while the two straight lines demarcate the curve of growth ionization solutions given in Fig. 5.27.

solutions illustrated in Fig. 5.27 for the curve of growth analysis.

Apart from the mean θ effect, evidence for stratification in UY Cen is provided by Mg, Al and CaII, all of which are significantly more abundant in the curve of growth analysis, compared with the model atmosphere. This is because they are high excitation lines and tend to group toward the high temperature, high pressure end of Fig. 6.04.

6.04 The Wavelength variation of the r_o Term

The Variation in the ME and SS Models

In section 5.19 we empirically determined the wavelength variation of the K and r_o terms. This is an important correction amounting to 0.66 dex over the wavelength range considered. Fig. 6.05 shows the individual log N values for Ti given by the 2800 atmosphere. There is clearly no trend with wavelength in contrast with Fig. 5.26 for the curve of growth residuals.

Using the model atmosphere opacity routine it is possible to calculate the variation of the H^- opacity, which amounts to 0.12 dex over the wavelength range. This leaves 0.54 dex to be explained by the r_o term. The great importance of the r_o term is a consequence of the low damping, with the result that γ, the inverse slope of the curve of growth, takes the value 5.52 in the region where most of the lines are formed.

The appropriate formulae for r_o were derived in section 5.03 and all given again below.

SS pure absorption

$$r_o = 1 - \frac{B_{\text{Line forming level}}}{B_{\text{contnuum forming level}}}$$

ME pure abs

$$r_o = \frac{\frac{B_1}{B_o}}{\sqrt{3} + \frac{B_1}{B_o}}$$

ME pure scattering

$$r_o = \frac{\frac{3}{2} + (1+\sqrt{3})\frac{B_1}{B_o}}{(\sqrt{3}+2)(\sqrt{3} + \frac{B_1}{B_o})}$$

where

$$\frac{B_1}{B_o} = \frac{3}{8}\,\frac{h\nu}{kT_o}\,(1 - e^{-h\nu/kT_o})^{-1}$$

which is derived from solution of the equations; $T^4(\tau) = T_o^4\,(1 + \frac{3}{2}\tau)$ and $B(\tau) = B_o + B_1\,\tau$, at the limit $\tau \to 0$. T_o is

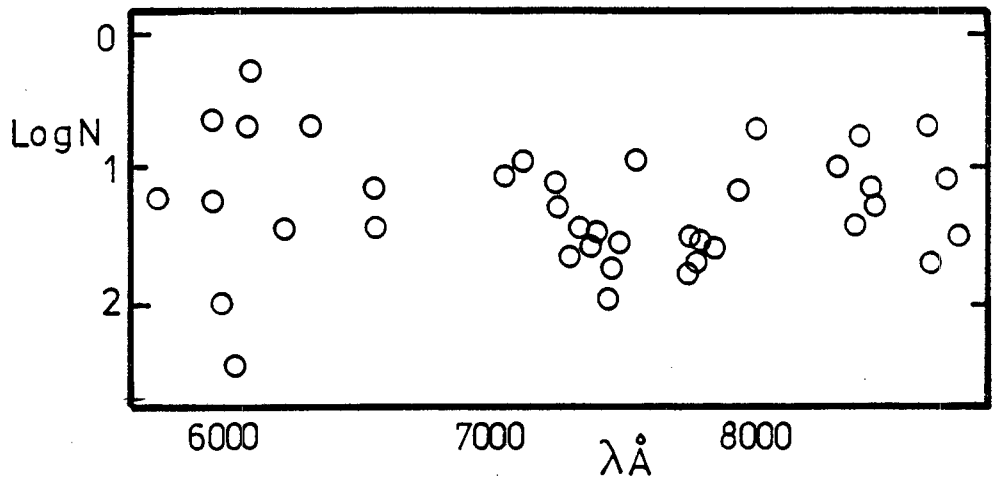

Figure 6.05

The model atmosphere residuals for TiI are shown as a function of wavelength. Note the lack of any wavelength dependence and compare this with the results for the curve of growth analysis given in Fig. 5.26.

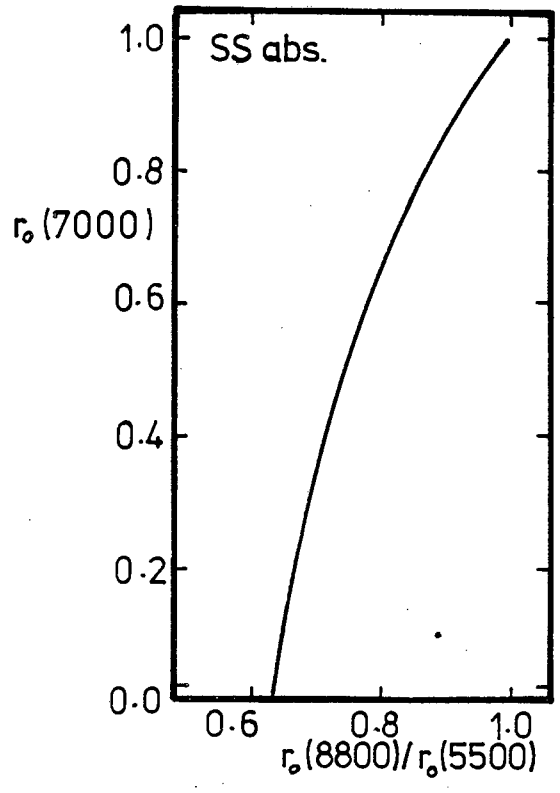

Figure 6.06

For the SS model, the maximum central depth at 7000A is shown as a function of the ratio of maximum depths at 8800 and 5500A.

the boundary temperature, related to the effective temperature by

$$Te = 1.19T_o$$

We require the value of r_o at our standard wavelength of 7000 Å as well as the wavelength variation of r_o.

In the case of pure absorption in the SS model, r_o can be discovered empirically by finding the limiting central depth of a strong line. In which case the emissivity in the line centre will be given by the value of the Planck function in the reversing layer, from which the continuum temperature can be deduced or vice-versa. The relationship between the maximum central depth $\equiv r_o$ and the ratio of $r_o(8800)/r_o(5500)$ is shown in Fig. 6.06. This relationship is found to be independent of the actual temperatures of the line and continuum forming regions. Comparing the central depth of the sodium D lines with the continuum level, deduced from the coude plates, indicates that $r_o = 0.95$ at 5900 Å. This corresponds to $r_o(7000) = 0.924$ and $r_o(8800)/r_o(5500) = 0.91$.

For the ME atmospheres, both $r_o(7000)$ and the wavelength variation change only slowly with boundary temperature. Values are given in Table 6.01.

TABLE 6.01

T_o	7000 r_o	ME pure abs. $r_o(8800)/r_o(5500)$	7000 r_o	ME pure scat. $r_o(8800)/r_o(5500)$
1000	0.82	0.92	0.64	0.95
2000	0.69	0.87	0.58	0.92
2400	0.65	0.85	0.56	0.92
2600	0.63	0.84	0.55	0.91
2800	0.61	0.84	0.54	0.90
20000	0.26	0.86	0.36	0.95

The boundary temperature appropriate to UY Cen is assumed to be 2200°.

Comparing the three models gives the following result.

Observed variation = 0.66 dex

Calculated variation in SS with pure Abs + H^-(0.12 dex) = 0.35 dex

Calculated ME with pure Abs + H^-(0.12 dex) = 0.51 dex

Calculated ME with pure scattering + H^-(0.12 dex) = 0.32 dex

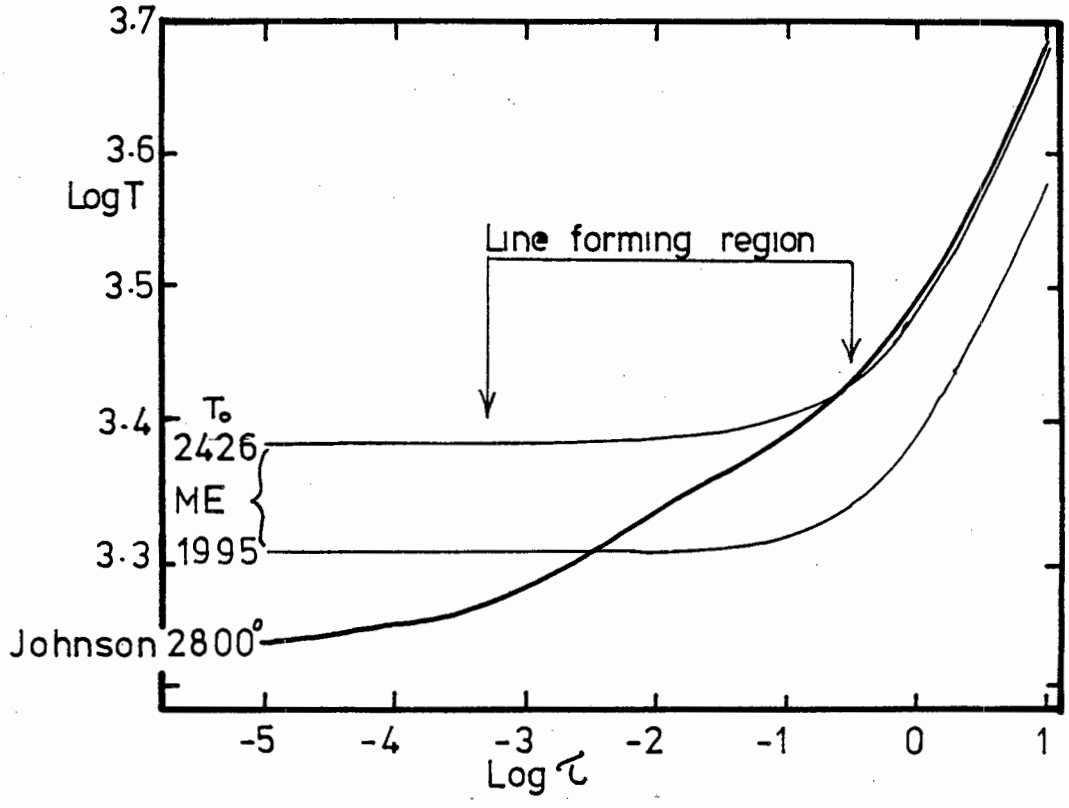

Figure 6.07

The variation of temperature with optical depth is shown for the ME and Johnson model atmospheres. Note how they differ over the important line forming region.

It is apparent that the three models all underestimate the effect, but the best agreement is shown by the ME atmosphere with pure absorption.

The r_o effect in the Model Atmosphere

Fig. 6.07 compares the log T against log τ variation in the 2800 model atmosphere with the variation in two ME atmospheres, identified by the appropriate values of T_o. The 2426 ME model gives a good fit to the model atmosphere for log $\tau > -1.0$ but only a poor fit in the outer layers. The arrows indicate the limits within which, according to the model atmosphere and the contribution functions, most of the UY Cen lines are supposed to be formed. It is clear that the ME atmosphere deviates significantly in this region. It is therefore to be expected that the two models will give different results.

Two experiments were performed with the model atmosphere. In the first, the continuous opacity was set constant at all wavelengths. The behaviour of a 0.0 and a 3.0 volt TiI absorption line was then examined at 5500 and 8800 Å. Both lines were set to have log $W/\lambda = -4.30$ at 5500 Å and a series of lines at 8800 Å were defined to satisfy various conditions of similarity. These conditions are defined in Fig. 6.08 and illustrated in terms of their depths of formation in the atmosphere, indicated by θ. It is evident that a line formed by the same number of atoms, which satisfies the condition that log gf λ_{8800} = log gf λ_{5500}, is formed at the same depth, but has a smaller value of log W/λ at 8800. It is clear that the difference in the equivalent width is apparently dependent on depth. Taking the mean difference in equivalent width and multiplying by the γ factor (5.52) and adding the 0.12 dex for the H^- opacity variation gives 0.67, in good agreement with the observed value. Since we have shown that not all the elements are formed at the same effective temperature, the apparent dependence of the correction on depth, suggests another pitfall of the curve of growth analysis. Unfortunately, elements other than TiI are not suitable for investigating the effect. Fig. 6.08 rather dramatically illustrates the effects of keeping various other parameters constant. For instance in order to keep log W/λ constant requires a 0.75 dex and 0.36 dex increase respectively, in the number of atoms forming the $\chi = 0.0$ and $\chi = 3.0$ e.v., lines at 8800 Å.

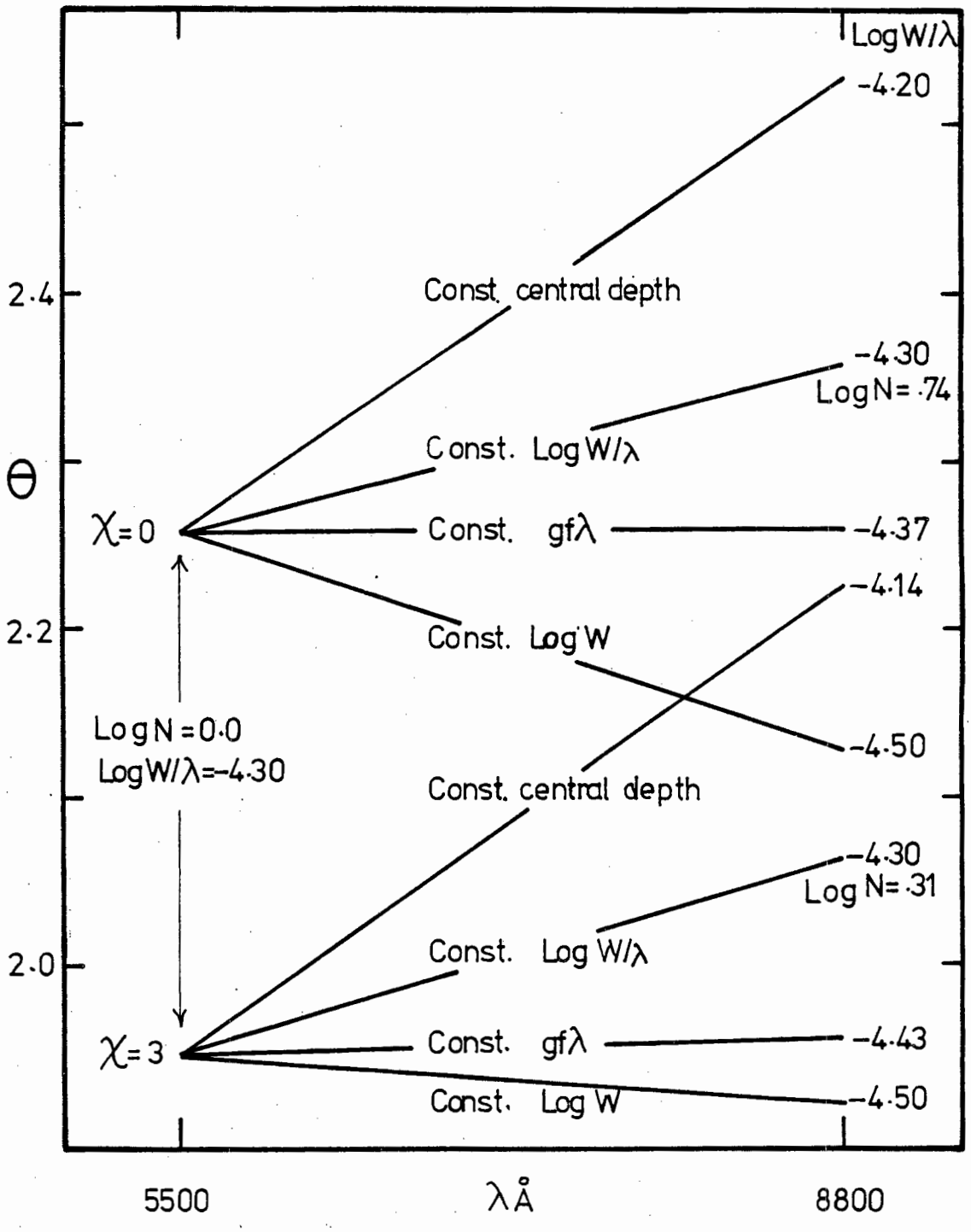

Figure 6.08

Depths of formation in the 2800 atmosphere, defined by θ_{DCF} are shown as a function of wavelength for various parameters as specified.

The second experiment was to set the wavelength to 5500 Å for the Planck function at 8800 Å and also to suppress the wavelength variation of the opacity. In this case, the log W/λ values, numbers of line forming atoms, central depths and stratification depths, of the two lines were identical. The results of this experiment are illustrated in Fig. 6.09 which also illustrates the different doppler widths and equivalent widths appropriate to the two regions, when using the same number of line forming atoms and a microturbulent velocity of 4.2 km s^{-1}.

From the experiments with the model we conclude, that apart from the opacity variation, the variation with wavelength seen in the equivalent widths is entirely a consequence of the depth gradient of the Planck function varying with wavelength. The effect is especially conspicuous in UY Cen as a result of the very flat curve of growth, itself a consequence of the low damping. The wavelength variation of r_o is much better described by the Johnson model than by either the SS or the ME models. It is interesting to note that the ME model with pure absorption, describes the effect better than the pure scattering model.

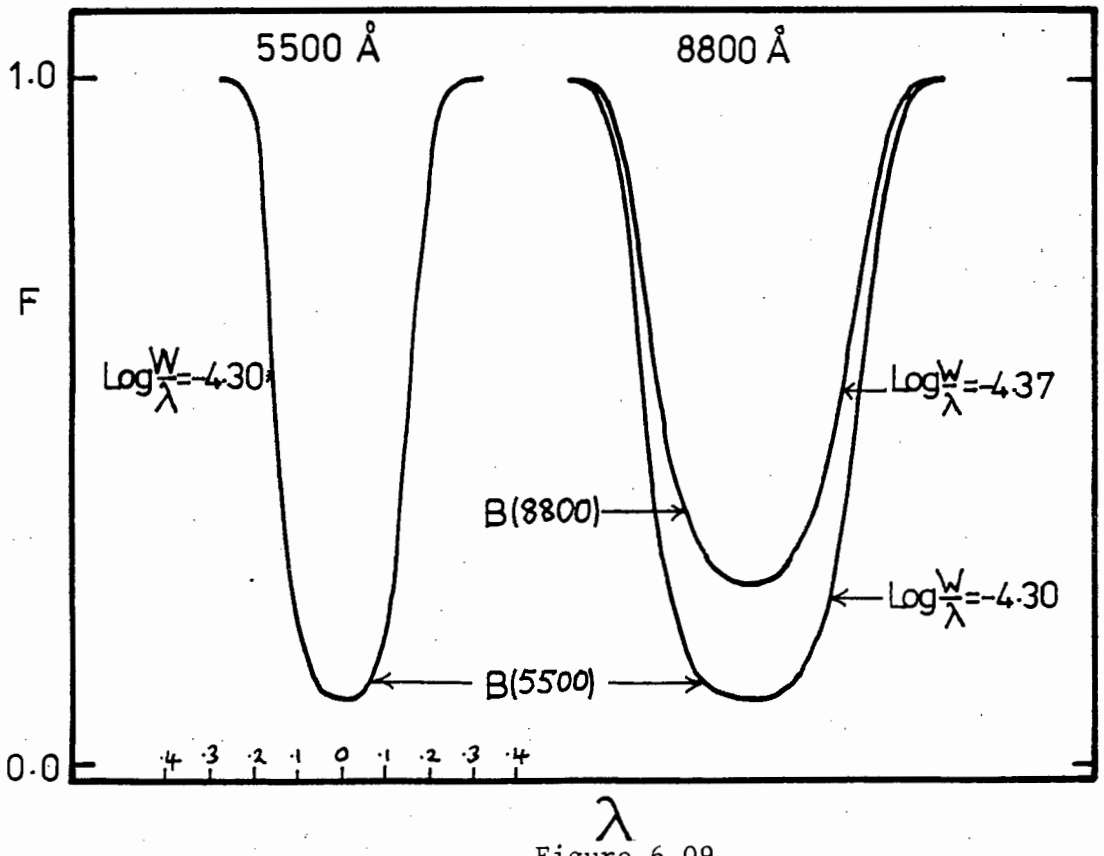

Figure 6.09

Line profiles, generated by the 2800 model atmosphere with no continuous opacity variation and with the same number of line forming atoms, are shown at two wavelengths. For the case where the log W/λ are identical, the Planck function at 8800 is equal to that at 5500 A.

CHAPTER 7
RESULTS AND FUTURE WORK

7.01 Introduction

In this chapter we summarize the results of the abundance analysis, discuss the parameters describing UY Cen and finally examine the astrophysical significance of our work.

7.02 Summary of the Abundance Section

The curve of growth analysis provides a good first approximation to the abundances in UY Cen, while the model atmosphere provides a second approximation that allows for the effects of stratification. The agreement between the two methods, shown by the results in Table 5.11 is very encouraging and gives us confidence that we may be obtaining valuable results by extending the model atmosphere to interpretation of the Li and CN abundances. However it is important to recognise the limitations of these methods. Two of which are; the geometrical limitations of the model atmosphere and the fact that we have only considered line formation by pure absorption. Pure absorption is probably a poor approximation in the low densities prevelant in the model atmosphere, especially in the central regions of strong lines, which are formed high in the atmosphere. Another limitation is that the model is itself based on solar atmospheric abundances rather than on abundances appropriate to C/O = 1. Piccirillo (1980) reports the results of using atmospheres with C/O = 1 and shows that the pressure is increased at a given optical depth. This is similar to the effect seen in the Gingerich et al. (1966) atmosphere, which although giving solar Ti/H abundances gives a very poor representation of the largely ionized elements. Molecular hydrides indicate that hydrogen is certainly present in UY Cen although Hα is not seen probably due to a balance between absorption and emission. Hydrogen emission would indicate the presence of a chromosphere which is again not modelled. Another important restriction is our failure to consider non LTE effects. Luck (1977) shows that non LTE models by comparison with LTE models, increase the Li abundances he finds in G and K supergiants, by up to 0.7 dex. Auman and Woodrow (1975) show that this is a result of the much greater degree of ionization given by

their statistical equilibrium models compared with the equivalent LTE models. In our analysis any non LTE effect may be compensated by the fact that the observed degree of ionization was the parameter used to select the appropriate model. The non LTE effect would rather suggest that our derived pressure and temperature parameters had little physical meaning.

One of the few direct checks on the validity of the model, is given by the correlation between the curve of growth excitation temperatures and the mean model atmosphere temperatures, found for various elements.

The fact that there exists a solution of the Saha equation and also a model atmosphere, that gives abundances for the period 3 and 4 elements consistant with the sun, despite their range in ionization potential, is very encouraging and suggests that the models give useful abundances.

There is a strong correlation between the abundance residuals given by the curve of growth and by the model atmosphere. This suggests that a considerable improvement could be obtained in the results, without any refinement of the model, by simply improving the accuracy of the equivalent widths and the laboratory log gf data.

7.03 Internal agreement of Parameters

In this section we examine the internal consistency between various directly determined and derived parameters, describing UY Cen. These, particularly the mass, luminosity and temperatures, are of great importance in placing UY Cen in an Hertzsprung Russell (HR) diagram and in relating its position to current evolutionary theory.

Table 7.01 illustrates the interdependence of the different parameters and should be read as follows. The derivation of, for instance the gas pressure Pg, depends on the electron pressure and some model relating gas to electron pressure. The derivation of the radius R depends on the bolometric magnitude and the effective temperature T. This diagram is not complete, in for example the case of the bolometric magnitude, which also depends on the apparent magnitude, reddening and distance.

TABLE 7.01

The derivation of	Depends on							
	M_{BOL}	T	P_e	P_g	R	M	K_o	Model
P_g			X					X
g					(X)	X		
R	X	X						
M				X	(X)		X	

The ringed parameters may be loosely described as the directly observed parameters, which are reasonably certain. The radius R also falls into this category as it depends only on directly observed parameters. One of the most interesting parameters,we would like to know about, is the mass. This can be either deduced from the kinematic arguments,given in chapter 4 or more specifically from the spectroscopic data. The weak link in the spectroscopic derivation,lies in the relationship between the electron and gas pressures.

Table 7.02 summarizes the available data, all of which have been discussed and derived in previous sections.

TABLE 7.02

M_{BOL} = best compromise = -4.5

T = 2500° continuum fitting.

= 2300° excitation C of G.

$\log P_e$ = -4.9 Assumption $\theta_{ex} = \theta_{ion}$ from C of G.

M = 1.0 to 1.5 (units of solar mass) from kinematics.

$\log K_o$ = -27.00 per H atom, from SS model $[^{Ti}/H] = 0$.

The Radius

The radius R, in cm, is directly related to the effective temperature and bolometric magnitude via the Planck function by;

$$5 \log R = 96.56 - 10 \log T_e - M_{BOL} \qquad (7.01)$$

for $M_{BOL} = -4.5$ This gives

$R = 377R_0 = 2.68 \times 10^{13}$cm

The gravity g

We obtain g from the relation

$$\log g = \log G + \log M_* - 2\log R \qquad (7.02)$$

where G is the gravitational constant. Assuming a one solar mass star and the above value of R we obtain;

$$\log g = -0.71$$

This is a low gravity, but consistant with the values expected for very cool giants and supergiants. The model atmospheres were based on $\log g = +1.0$, which combined with a 2800 effective temperature and a bolometric magnitude of -4.5, would imply a mass of 32 M_0. This is quite unrealisticaly large for young disk population objects and again illustrates the danger of too literal adoption of the model parameters.

The Mass M_*

The spectroscopic mass can be obtained from equation 5.54 in chapter 5 which, by making the substitutions given in that section, can then be rewritten as,

$$\tau_{cont} = \frac{K_o P_g}{M g}$$

where M = the average mass of an atom

K_o = the abs coefficient per atom.

Substituting for g and assuming that $\tau_{cont} = 1$ we obtain

$$M = \frac{K_o P_g R^2}{Gm} \qquad (7.03)$$

Taking the usual cosmic mix, $N_H = 12.0$, $N_{He} = 11.16$, gives $M = 2.31 \times 10^{-24}$ gm and $\log K_o = -27.06$.

This leaves us with the problem of relating the electron pressure to the gas pressure. The ratio P_g/P_e depends on the ratio of ionized atoms to the total number of atoms. Probably the best estimates of this are given by the model atmospheres and are summarized below:

Figure 7.01

The logarithmic overabundance of individual elements on UY Cen, compared with the sun, is shown as a function of atomic weight. Cowley and Downs' theoretical "s" process abundance curves are also shown for various values of the neutron exposure τ.

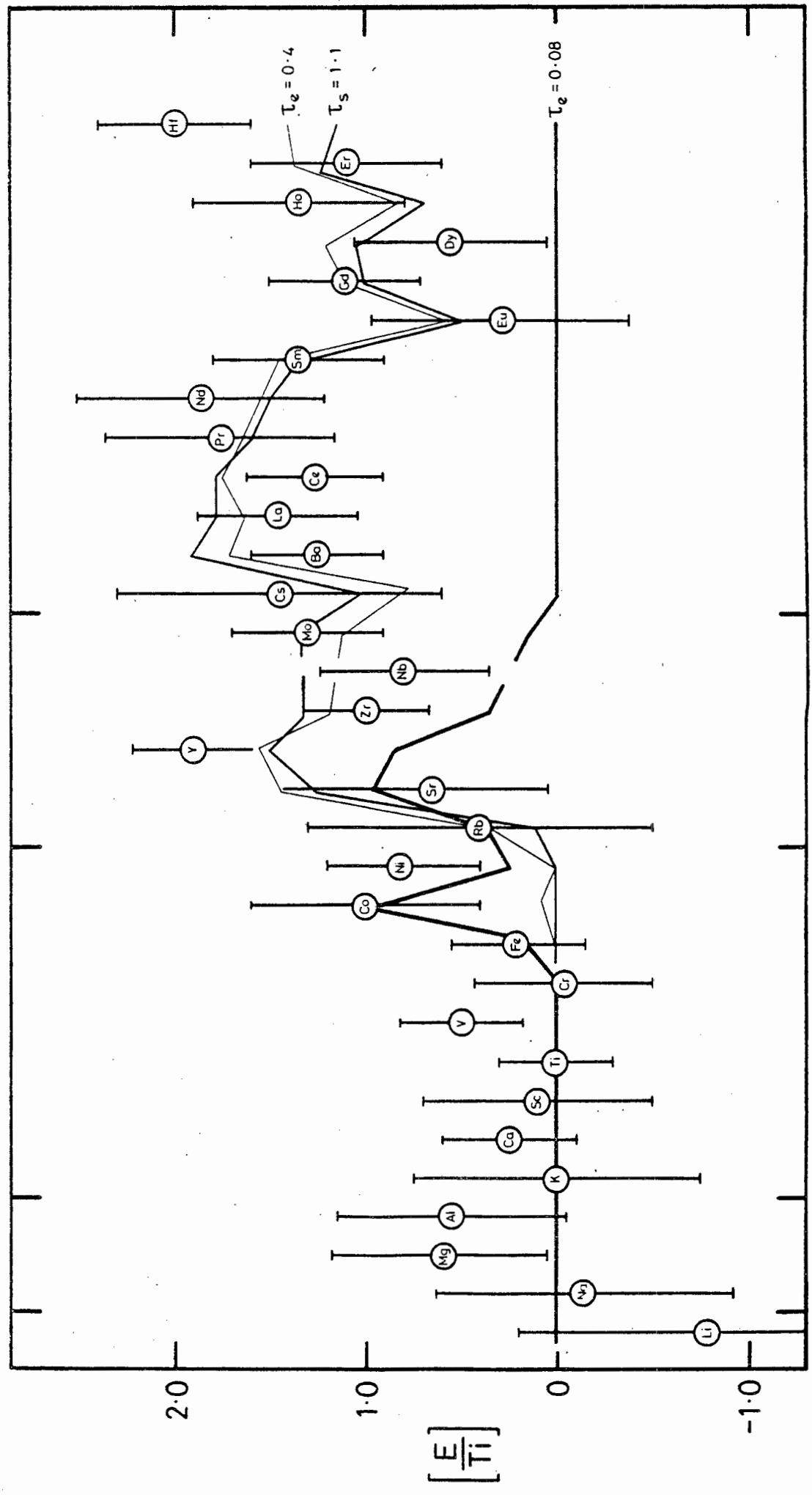

	τ = 0.5	τ = 1.0		
log P_g/P_e	7.20	6.93	log g = 1	Gingerich et al. (1966)
	7.49	7.12	log g = 3	
	5.38	5.19	log g = 1	Johnson 2800 (1974)

The ratios do not depend too strongly on either optical depth or gravity but do differ quite markedly between the Johnson and Gingerich atmospheres.

Substituting for these values in the equation for M gives;

M = 0.46 $M_\odot$ Gingerich model

M = 0.01 $M_\odot$ Johnson model

The difference between the two values illustrates the uncertainties of the method, but the values do indicate that UY Cen is a low mass object. The condition that the microturbulent velocity can not be greater than the escape velocity predicts a lower limit of 0.02 $M_\odot$, which is again unrealistically low.

7.04 Comparison with other Workers and Discussion

In this section we compare our abundances with other work and discuss the astrophysical implications of these abundances.

The final best set of abundances differences with respect to the sun and normalized to Ti, are illustrated in Fig.7.01. The results are plotted in order of increasing atomic weight and the X axis is marked by period, as defined in the periodic table of elements. The abundances are means of the curve of growth and 2800 atmosphere results, with preference given to the ionized lines, where appropriate. The error bars, which if anything should be an overestimate of the true error, contain the following 3 components. These are; the observed scatter about the best fitting curve of growth, the effects of changing the ionization by the amounts given in column 4 and 6 of Table 5.1 and an additional 'factor of two'. The 'factor of two' allows for uncertainties in the log gf data, blending and other unrecognised sources of error. The errors are correlated for the elements, Li, Na, K, Rb and Cs, that are still mostly ionized, in the sense that changing the degree of ionization

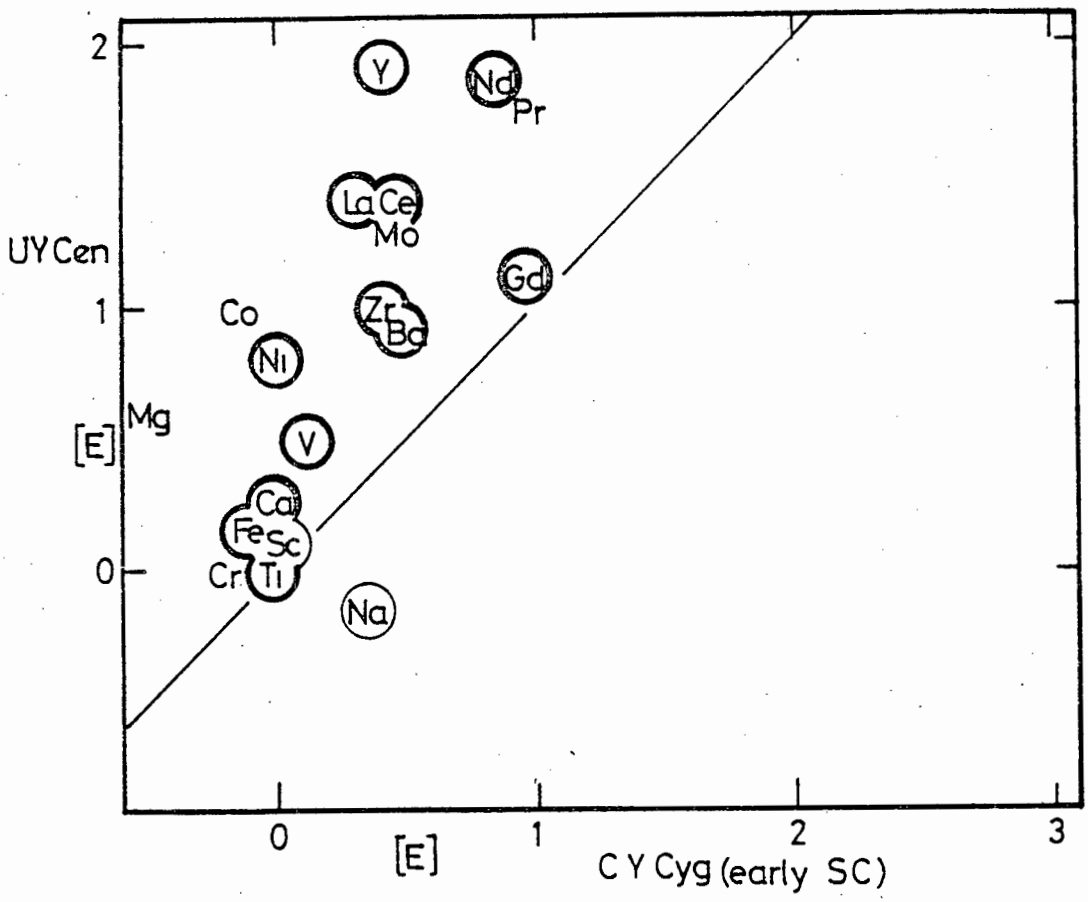

Fig. 7.02

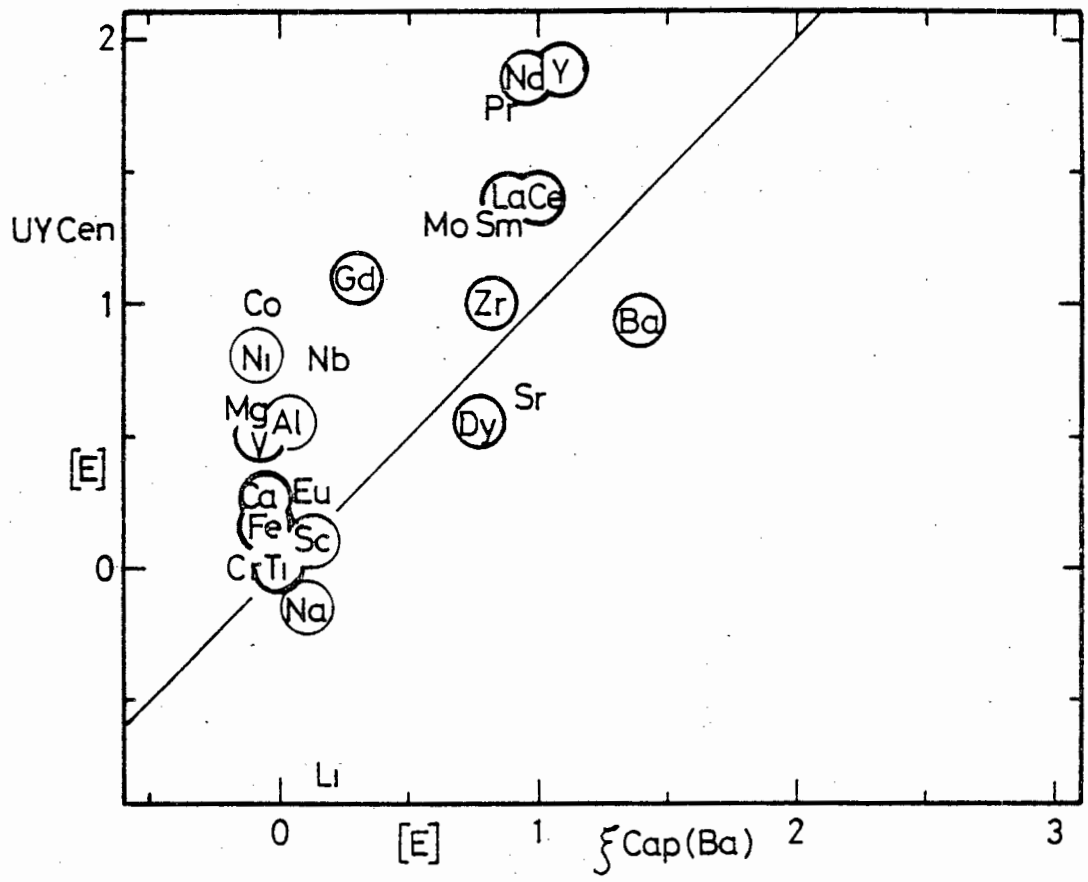

Fig. 7.03

Element overabundances in UY Cen, compared with the sun, are plotted against those found in various other representative stars. The heavy circles indicate good quality determinations in UY Cen.

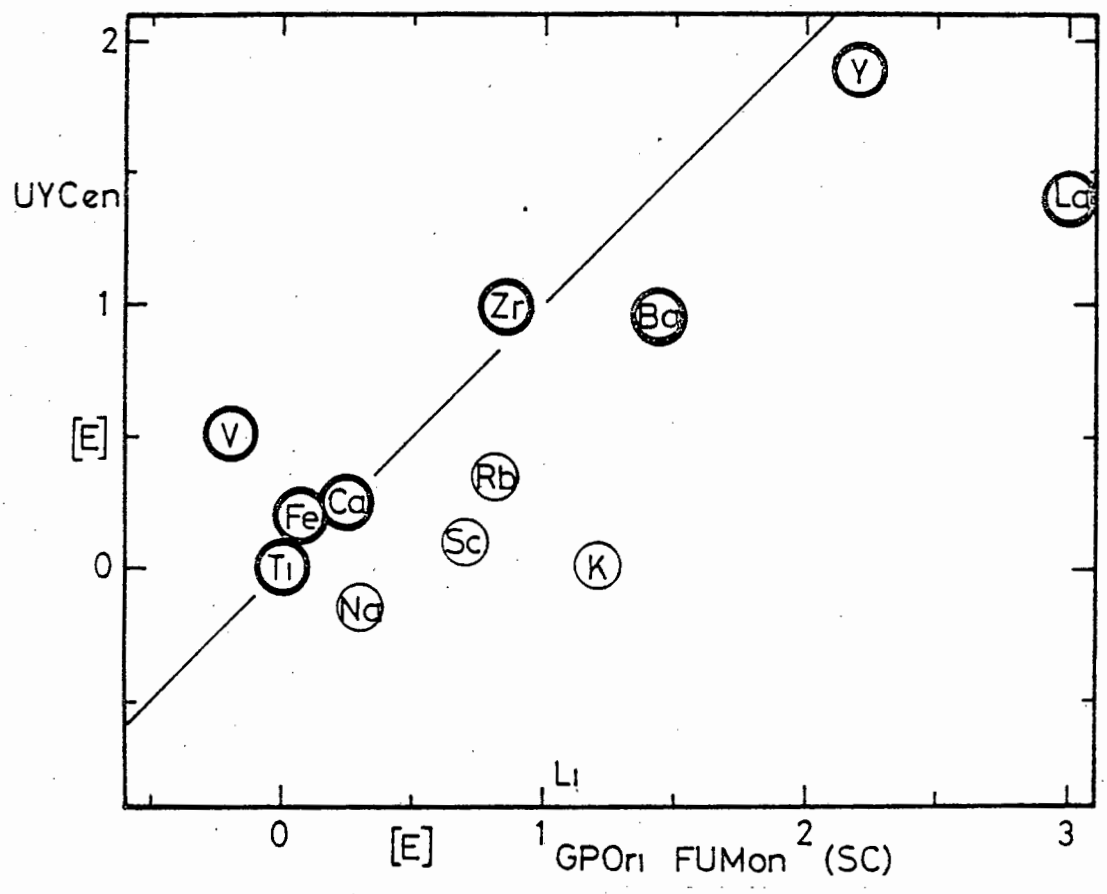

Fig. 7.04

Element overabundances in UY Cen, compared with the sun, are plotted against those found in various other representative stars. The heavy circles indicate good quality determinations in UY Cen.

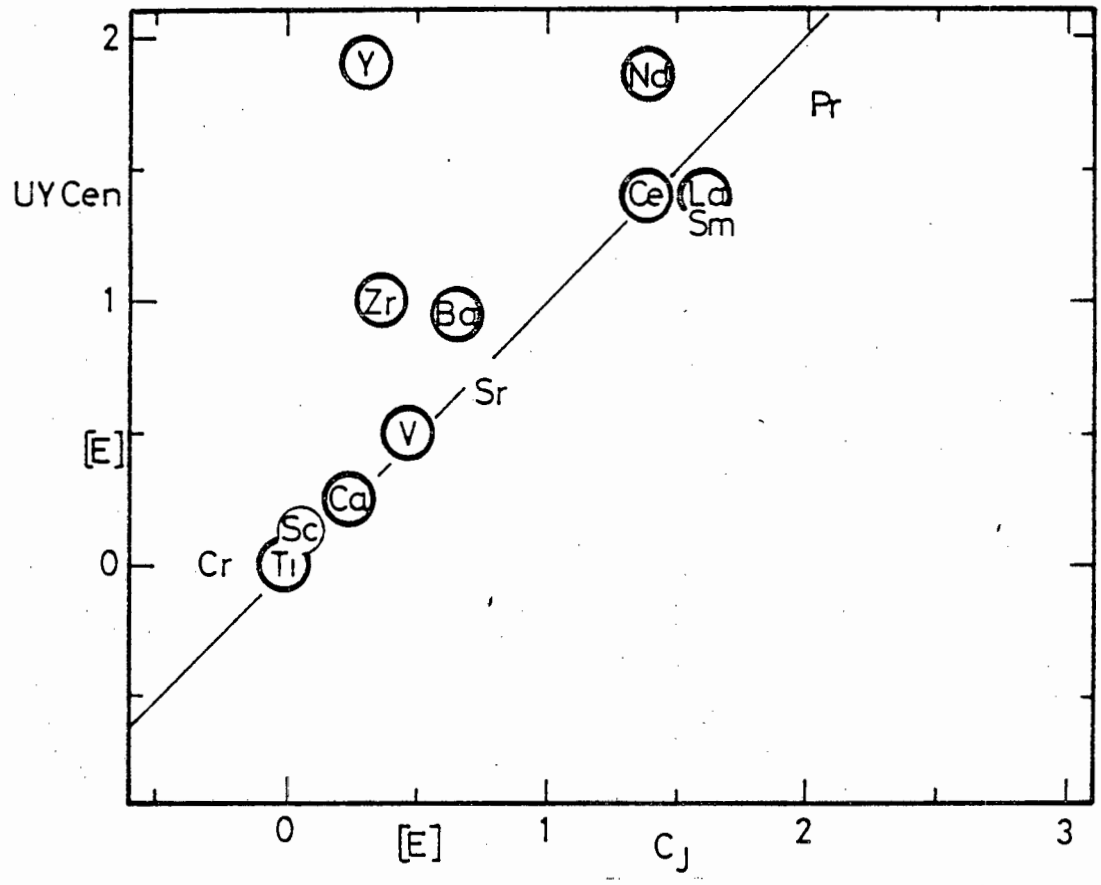

Fig. 7.05

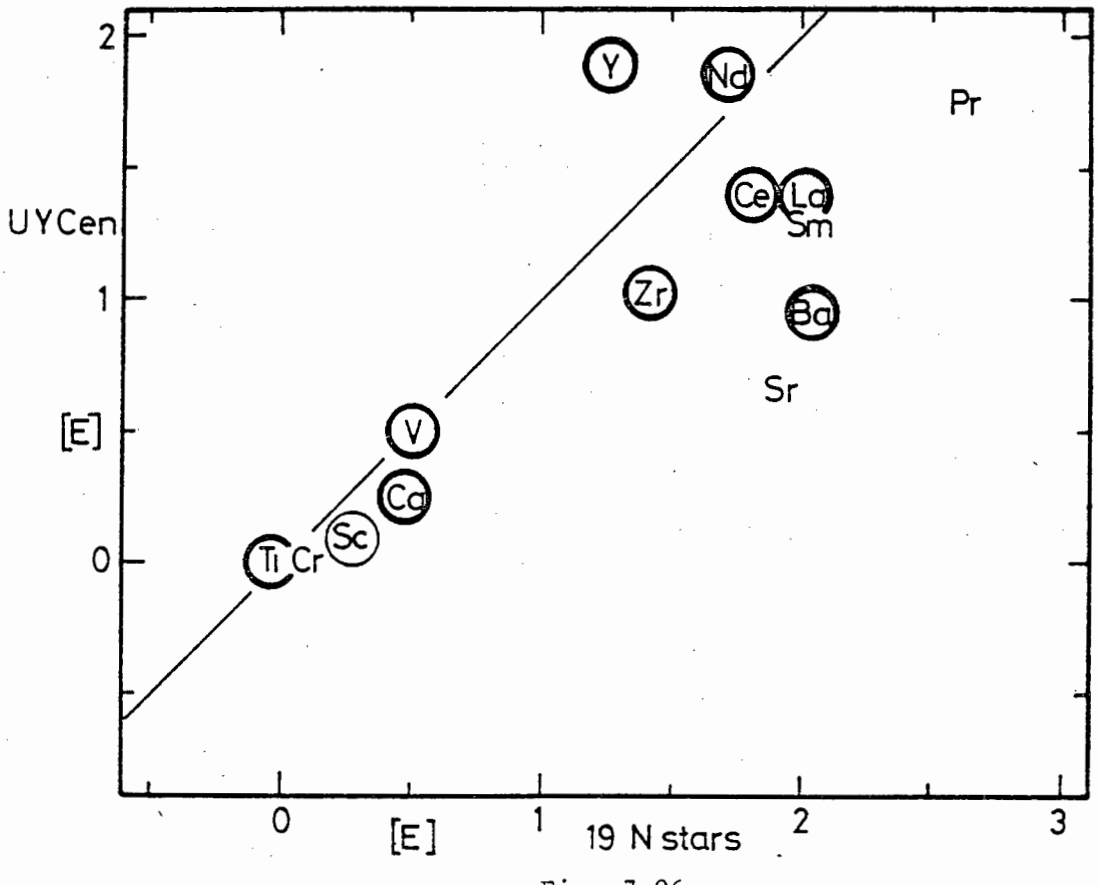

Fig. 7.06

Element overabundances in UY Cen, compared with the sun, are plotted against those found in various other representative stars. The heavy circles indicate good quality determinations in UY Cen.

will cause them to move in phase up or down their error bars.

In Fig. 7.02 to 7.06 we compare the abundances given here with those found by other authors, for a representative sample of stars of type BaII, SC, C and C_J. In these Figs. the abundances are relative to the sun and normalized to Ti.

A plain atomic symbol indicates the determination in UY Cen is of quality C or D, a light circle indicates quality B and a heavy circle indicates quality A. The quality assessment is given in section 5.21.

Broadly speaking Fig. 7.02 to 7.06 show a trend of increasing heavy metal (periods 5 and 6) enhancement as one progresses from the BaII star to the C stars. One of the most conspicuous effects is the great abundance of Y in UY Cen compared with any of the other stars except for the cool SC stars. The fact that Yamashita finds a similar enhancement of Y in the otherwise very similar SC stars GP Ori and FU Mon, gives us confidence in accepting this as a real effect. Fig. 7.05 and 7.06 clearly show the abundance differences between the ^{13}C rich J stars and normal cool carbon stars, both data are taken from Utsumi (1970). The mean abundances for the four ^{13}C rich stars, including the super lithium rich star WZ Cas, show proportionally lower abundances for the 5th period elements Y, Zr and Sr, than do the cool carbon stars.

The UY Cen abundances appear to be most similar to those of the C stars.

The heavy metal abundances are weaker in CY Cygni than in UY Cen. Keenan and Boeshaar (1980) classify CY Cygni as being a warmer SC star but with a similar NaD strength when compared with UY Cen. Culver's (1971) analysis confirms this classification, as he finds a higher excitation temperature, but a similar degree of ionization. The similar degree of ionization will account for the similar NaD strengths. Although the enhancements are less in CY Cygni, they occur in both the 5th and 6th periods as they do in UY Cen.

7.05 Comparison with Nucleosynthesis Theory

Elements beyond the iron peak are thought to be formed by three methods known as the r, s and p process. The p process is the least understood and the least important by abundance, but is required to explain certain nuclides which can not be explained by the other methods.

The p process relies on the presence of r and s nuclides which absorb positrons that then transform neutrons into protons. The positrons are produced by photon decay at temperatures of order 10^9K.

The r and s process both rely on neutron capture by iron peak nucleii followed by β decay, in which the captured neutron is transformed into a proton, thereby producing elements of increasing atomic number. The r process is thought to occur in an explosive environment where there is a high density of rapid neutrons. This allows several neutron captures to take place between β decays and synthesises a sequence of neutron rich nuclides.

The s process, which is the best understood process, is thought to occur in red giants, under stable conditions, where the neutrons are supplied by such reactions as;

$^{22}Ne(\alpha,n)^{25}Mg$ $^{13}C(\alpha,n)^{16}O$

In this case β decay takes place between successive neutron captures, generating a series of stable nuclides.

Each process generates a characteristic abundance distribution and in theory it is possible to reconstruct the neutron exposure history from the observed distribution. Analysis of terrestial heavy elements shows that it is necessary to propose a distribution of neutron exposures to explain their abundances. It should be remembered, that for any given element, certain isotopes will be produced by the r process and others by the s process. When elements are referred to as being of r or s origin this presupposes that they show the same isotope mix as that found on earth. In the solar system, Eu is considered to be predominantly produced by the r process and the fact that Eu is not enhanced in UY Cen and the BaII stars, strongly suggests that the s process is the source of element enhancement in these stars.

Cowley and Downs (1980) have recently produced a set of tables giving the distribution of abundances with atomic number, normalised to Sr = 10^{20}, resulting from the exposure of ^{56}Fe nucleii to neutrons. Summing over all isotopes of a given element, makes the data more easily comparable with stellar abundances, for which we have no isotope data. They use two models for the neutron exposure, a decreasing exponential exposure and a single exposure, parameterized by τ_e and τ_s respectively.

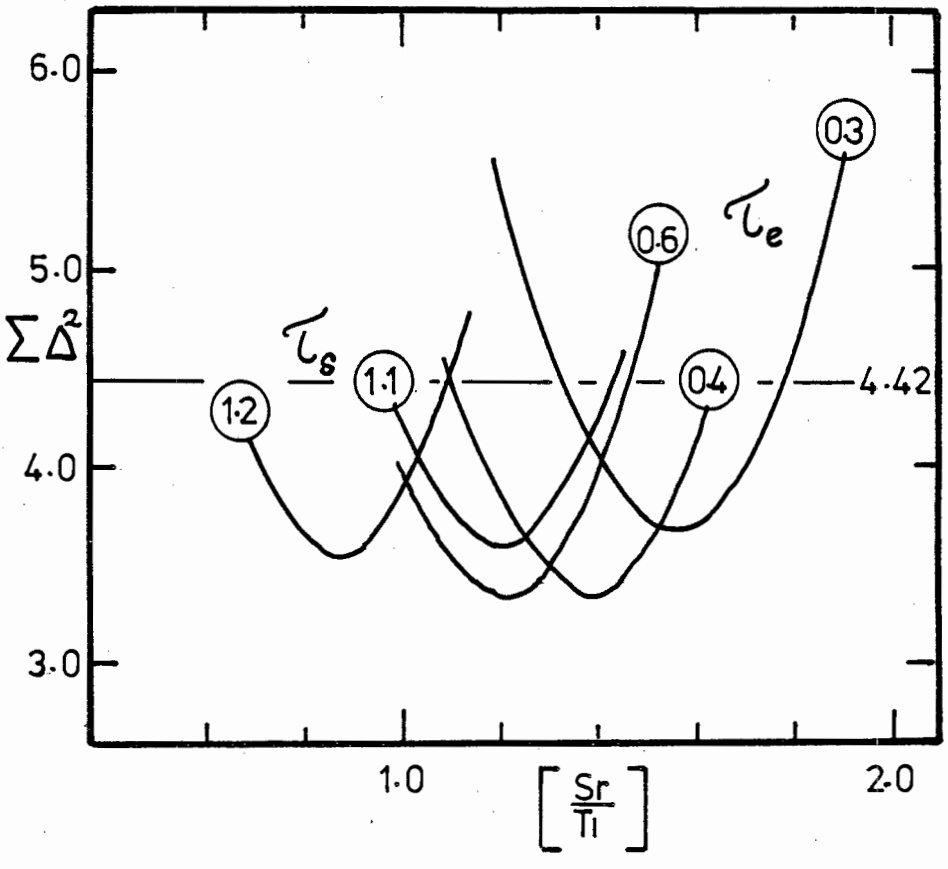

Figure 7.07

The sum of the squares of the differences, between the observed and calculated "s" process abundance distributions, are shown as a function of the Sr overabundance, for the various values of τ indicated in the circles. The straight line at 4.42 is the value assuming a uniform overabundance of 1.2 dex.

The parameter τ is essentially a measure of neutron exposure.

We use a model of a stellar atmosphere, which initially has the solar abundance distribution and to which is added a certain amount of material that was initially pure ^{56}Fe. We then calculate the resulting abundances for a given value of τ and a given number of ^{56}Fe, which is however more conveniently parameterized by the Sr overabundance.

The model

Let N_*Sr = the number of Sr atoms per H atom in the star

" $N_{\odot Sr}$ = the number of Sr atoms per H atom in the sun

Then the overabundance of Sr in the star $E_{Sr} = N_{*Sr}/N_{\odot Sr}$

The excess number of Sr atoms in the star compared with the sun

$$= N_{*Sr} - N_{\odot Sr}$$

$$= N_{\odot Sr}(E_{Sr}-1)$$

The Cowley Downs tables tabulate, for a given τ, the $\log_{10}$ of the number of atoms of element M, denoted C_M, produced per 10^{20} Sr atoms.

$\therefore$ the total number of atoms of element M produced per Sr atom $= 10^{(C_M-20)}$

$\therefore$ for a given E_{Sr}, the extra number of atoms of M $= 10^{(C_M-20)}(E_{Sr}-1)\ N_{\odot Sr}$

$\therefore$ The total number of atoms of M in the star

$$= 10^{(C_M-20)}(E_{Sr}-1)N_{\odot Sr} + N_{\odot M}$$

$\therefore$ The overabundance of M in the star denoted E_M

$$= \frac{N_{\odot Sr}}{N_{\odot M}}(E_{Sr} - 1)10^{(C_M-20)} + 1 \qquad (7.04)$$

Fig. 7.01 shows three sets of values of E_M for different values of τ. Further comparison is made in Fig. 7.07 where the sum of the squares of the differences of the theoretical and observed log overabundances are shown as a function of the adopted value of log E_{Sr}, for various

values of τ_e and τ_s.

With the exception of Nb, which is not calculated by Cowley and Downs, the differences are calculated for the period 5 and 6 elements.

The line at $\Sigma\Delta^2 = 4.42$ corresponds to the difference found by assuming that the solar abundances are simply scaled by 1.21 dex, which is the mean overabundance of these elements.

The deviation about the theoretical curves is clearly less than about the mean curve. It is possible to test the statistical significance of this comparison using the variance ratio test. The observed ratio is 1.34, whereas the predicted ratio at the 5% level is ~ 2.5. From a statistical point of view, this would not be considered very strong evidence for accepting the model results, in place of the statement that the abundances of the heavy elements are simply in the solar ratio but scaled by 1.21 dex. However, we have made the test unduly stern by omitting the fact that the model predicts no enhancement of the 3 and 4th period elements.

Examination of Figs. 7.01 and 7.07 shows that it is clearly impossible to distinguish between the single exposure and exponential models. This is similar to the situation found by Cowley and Downs for the Ba star abundances. One of the best fits is shown by the Ba star ζ Cap for which they find a value of $\tau_e = 0.3$. The best fit for UY Cen is for a somewhat greater value of $\tau_e = 0.6$. This indicates that the overabundance of heavy elements is correlated with neutron exposure.

The most obvious model would be one in which the entire surface material has been s processed. However as Cowley and Downs point out, in such a model one would expect the iron peak abundance to be modified in the sense that the Sc low (in cosmic abundance) would be shifted to larger atomic number. They do not observe this effect in ζ Cap and nor do we observe it in UY Cen. The alternative idea, that completely processed material is added to the atmosphere, is not explained by current stellar evolution theory. It is however worth realising that because the cosmic number density of Fe is so much greater than Y or Zr, abundance enhancements of Y or Zr of up to 4.0 dex, will cause a quite negligable reduction in Fe abundance.

The τ_e = 0.08 curve in Fig. 7.01 shows an enhancement of both Co and Ni which are not normally considered to be 's' process elements. According to Bond et al. (1979) U Aqr shows Sr and Y enhancements relative to Fe, of the order of 2 dex while the heavier elements appear normal. It would be very interesting to know whether U Aqr also shows an overabundance of Co.

The large Y/Zr and Y/Sr ratios are clearly not explained by any of the Cowley Downs models. If the rather poorly determined Sr abundance has been underestimated then it is possible that the high Y/Zr ratio, which is relatively well determined, might be explained by a second phase of neutron capture.

The remaining period 5 and 6 element abundances follow the theoretical curves reasonably well, although the rather low Ba abundance is somewhat unexpected.

7.06 Individual Element Abundances of particular interest

In this section we consider individual element abundances of interest.

Li

Despite its apparent strength, the fact that the Li abundance in UY Cen is less than that in the sun is of considerable interest. With the exception of the SLR objects, Catchpole and Feast (1971) showed that the SC stars, including UY Cen, have Li/Ca 6573 line strengths ≃ 1.0. On a simple model this placed them amongst the minority of S and C stars that have Li abundances greater than the sun. The present analysis shows that mainly as a consequence of blending, this is no longer true.

The subsolar Li abundance now indicated for the SC stars, fits into the general trend of decreasing Li abundance with decreasing temperature, observed in the majority of giants and supergiants. (Wallerstein Conti 1969). This is probably a consequence of the destruction of Li by convection and is illustrated by the stars in the lower part of Fig. 7.08, taken from Boesgaard (1970).

If we consider the range of stars that are defined as SC stars by Keenan and Boeshaar, then we find that 4/28 are SLR, a much higher proportion than found amongst the S and C stars. The SLR SC stars are Richer's SC star in LMC, Henize 166, VX Aql and WZ Cas.

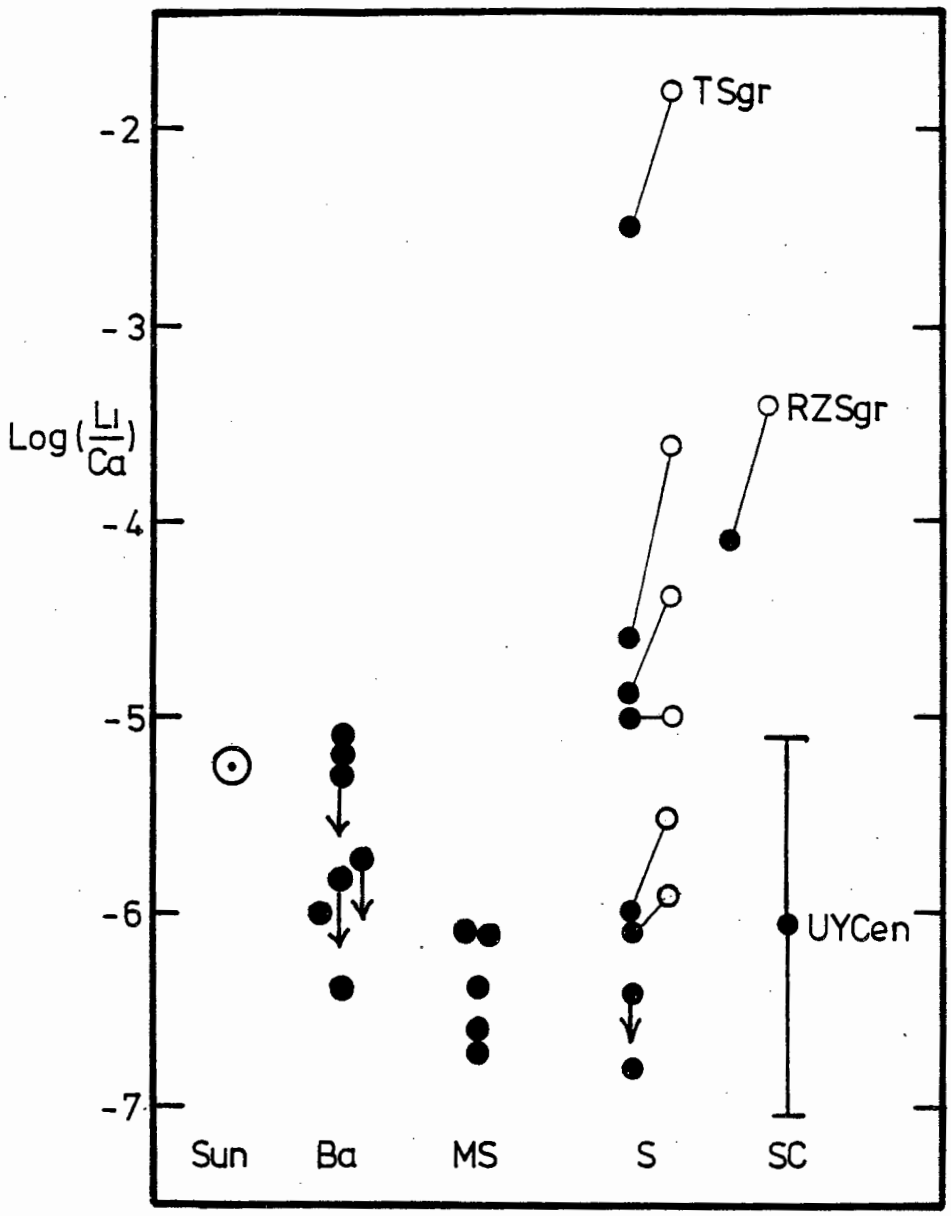

Figure 7.08

The Li abundance is shown for various types of object based on Boesgaard's (1970) work. The open circles show the effect of using the correct theory for the Li doublet. Arrows indicate upper limits.

This analysis does not cast doubt on the reality of these high Li abundances.

Improper modelling and failure to allow for blending, must have some effects on the Li abundances of S and C stars given in the literature. Boesgaard's (1970) analysis of S stars made no allowance for blending and used Herbig's case II. Fig. 7.08 shows the changes that would apply to her abundance using Herbig's case I. The corrections are made using her published microturbulent velocities but assuming the damping found for UY Cen. The correction for blending has not been included but will not be as severe as found for UY Cen because the CN lines are not present at 6707 Å in the S stars. The net result is that the blending and theory effects may tend to cancel for the S stars.

Torres-Peimbert and Wallerstein's (1966) analysis of Li in C stars allowed for blending but used the Li ≡ Ca theory. The net result may therefore be that they have slightly overestimated the Li abundance.

Na

One of the consequences of the abundance analysis is that, despite their enormous strength, the NaD lines are consistent with a solar Na/Ti abundance.

KI, CaII

Richer (1971) in his classification of C star spectra, noted that WZ Cas (SLR N star, Keenan Boeshaar SC star) is a member of a small group of peculiar stars, which simultaneously show strong KI and CaII lines. Low dispersion spectra of our SC stars show a similar effect which, since UY Cen has normal K and Ca abundances, suggest the effect is caused by an unusual opacity.

V

Vanadium is found to be about 0.3 dex overabundant in Warner's (1965) analysis of BaII stars, Utsumi's (1970) work on C stars and Culver's (1971) analysis of the S star CY Cygni. This suggests that the overabundace seen here may be significant although we can offer no explanation as to the cause of it.

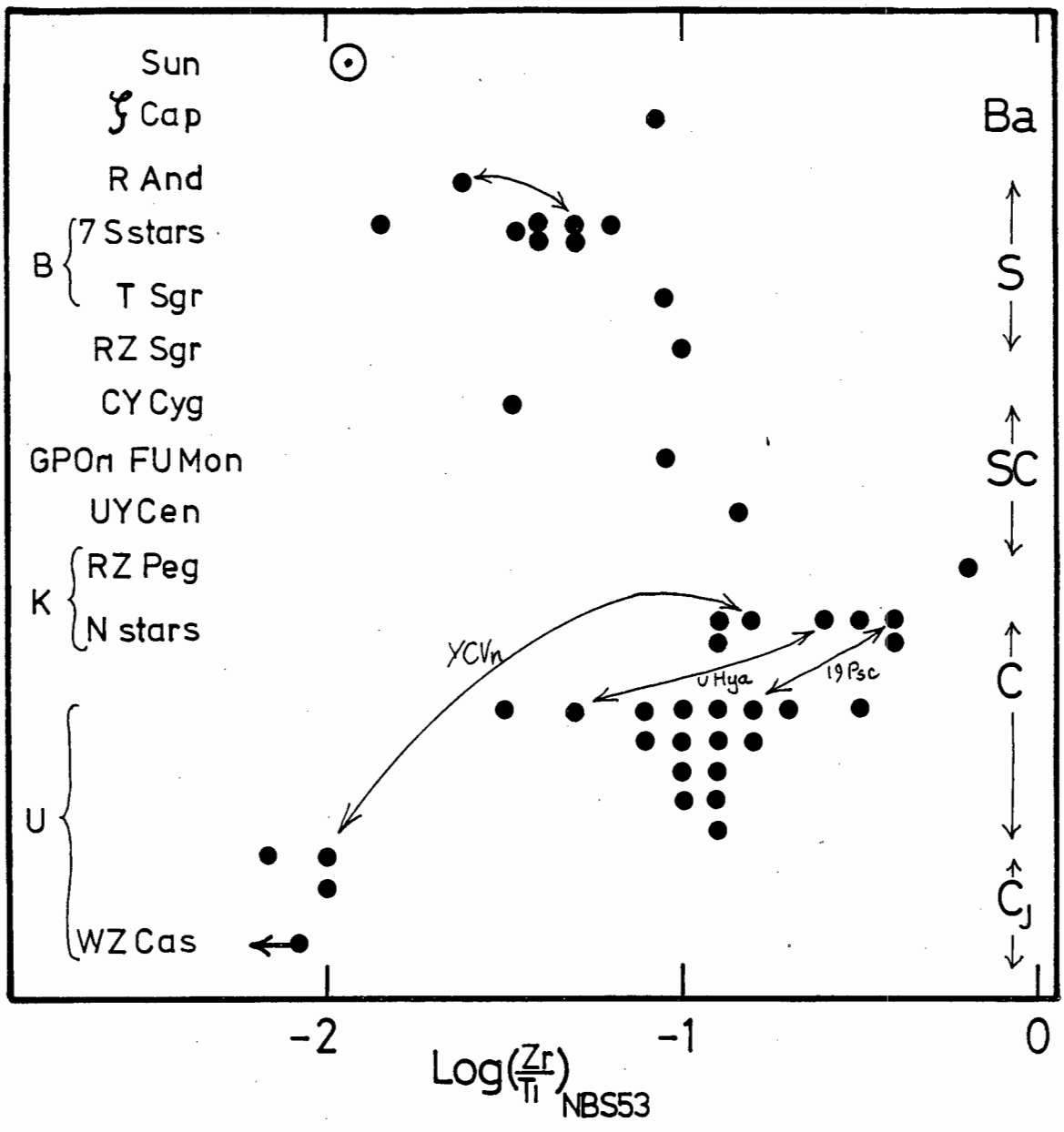

Figure 7.09

Zr abundances, on the NBS53 system, are shown for various types of star. Note the poor agreement found for the same star by different observers. Sun from Aller (1965). ζ Cap from Tech (1971). R And from Davis (1979). B indicates Boesgaard (1970). RZ Sgr from Catchpole and Feast (1976). CY Cyg from Culver (1971). GP Ori and FU Mon from Yamashita (1973). K indicates Kilston (1975). U indicates Utsumi (1970).

Zr

Fig. 7.09 illustrates the Zr/Ti abundance ratios obtained by the authors listed. The abundances have been converted to the system of abundances given by Corliss and Bozman (1962) in NBS53, using the corrections given by Catchpole and Feast (1976). This is done for the sake of convenience, because the majority of the abundances given were obtained using the NBS53 log gf values and it is much easier to convert our results onto their system than the other way around. The difficulty arises because other authors have used lines for which we do not have log gf values in our system. For differential analyses e.g. ζ Cap and CY Cygni the appropriate solar abundance indicated is that found using the NBS53 log gf values and is given by Aller (1965). There is a residual uncertainty in this method of comparison, in that different subsets of the NBS53 data will not all give the same abundances. This effect is well within the intrinsic uncertainties of the individual determinations. On the NBS53 system the UY Cen $\log\left(\frac{Zr}{Ti}\right) = -.84$, compared with our best estimate, given in Table 5.11, of -1.06. Fig. 7.08 shows that the N stars have higher Zr/Ti abundance ratios than the S stars, while the SC and SLR S stars lie somewhere in between. Earlier work on N stars by Utsumi (1970) agrees with this picture except that he finds a number of N stars, notably the ^{13}C rich and the SLR star WZ Cas, have Zr abundances less than the S stars. It is unfortunate to note that for the three stars common to Kilston and Utsumi, Kilston finds Zr enhancements in excess of Utsumi's by between 1.2 and 0.4 dex. In the case of YCVn this causes the star to span the entire range of observed S star Zr/Ti abundances. However there seems no doubt, that at least in the case of WZ Cas, the Zr abundance is low as Peery (private communication) fails to find any Zr lines in high dispersion spectra. This further serves to caution against bracketing the SLR SC Stars and WZ Cas, despite the fact that they may both have C/O ratios close to 1. In the section below, where we discuss the evolution of cool stars, we suggest that there might be two occasions when a star C/O $\simeq$ 1.

It is clear that although there are probably very interesting abundance patterns in these cool stars they are still partly hidden by 'observational' error.

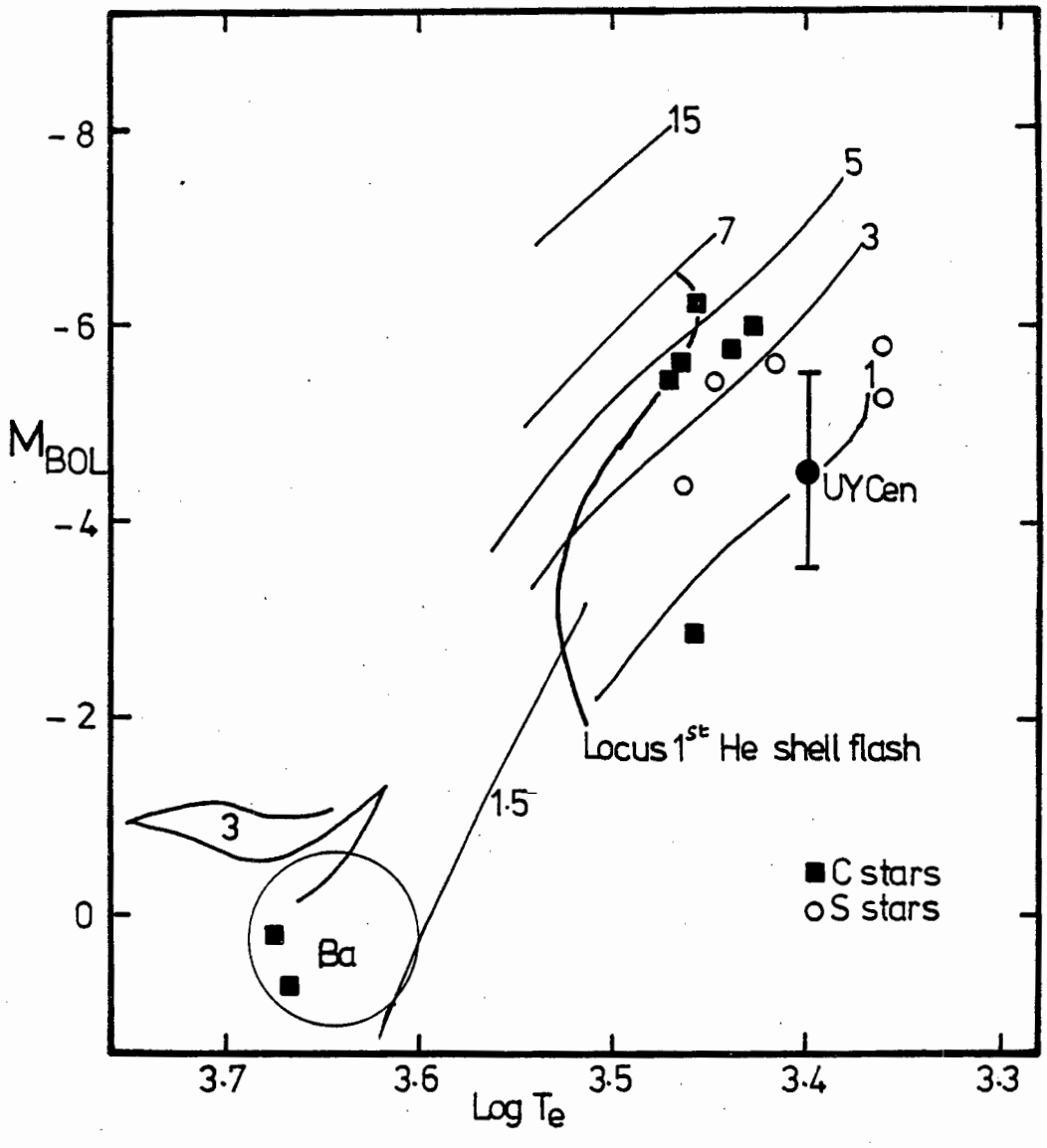

Figure 7.10

A composite HR diagram for cool evolved stars based on Scalo (1976). The evolutionary tracks are labelled by solar mass and are upper right; for the 2nd ascent double shell burning models and lower left; for 1st ascent core He burning models. Note that TT9 is the S star below the label 1.

PrII

Allan and Cowley (1974) show that hyperfine structure is important for PrII and it is possible that the abundance of this element has been overestimated by our failure to allow for the effect. The large error assigned to the Pr abundance will adequately cover this contingency and does not justify detailed calculation.

Ho

The Holmium abundance is very uncertain.

7.07 Evolutionary History and Position in the HR Diagram

In this section we place UY Cen in the HR diagram and relate its position to current theories of stellar evolution. We also suggest a possible relationship between the M, S, SC and N stars.

Unless otherwise acknowledged the evolutionary theory and information regarding the star data relies heavily on the following sources: Scalo (1976) Baschek (Liege 1979) and Scalo and Miller (1979).

Fig. 7.10 gives a composite HR diagram for peculiar and cool stars and indicates the position of UY Cen given by the parameters found in this thesis. Data is for stars with individually determined distances taken from Scalo (1976) and from Feast et al.(1976). Best fitting blackbodies have been used to assign temperatures to the Feast et al.data. The error bar illustrates the range of uncertainty found for the mean absolute magnitude of the SC stars. It is apparent that UY Cen occupies a position towards the red end of the distribution of the stars but that it is somewhat less luminous than carbon and S stars of similar temperature.

Although the Ba, S and C star phenomena probably covers a wide range of masses, as exemplified by ζ Cap (5-50 $M_\odot$) Scalo (1976) and TT9, the SLR S star in η Car (Catchpole and Feast (1976)), it seems probably that the majority of such stars have masses between 1 and 5 solar masses as discussed by Scalo and Miller (1979). The broad outlines of post main sequence evolution for stars in this mass range are now reasonably well understood and can be summarised as follows.

As a star exhausts its hydrogen burning core it leaves the main sequence moving to higher luminosities and lower effective temperature. This trend continues as the star makes its first ascent of the giant branch developing a hydrogen burning shell, which moves slowly outward, leaving a degenerate He core. At the same time the surface convective

envelope grows deeper and sweeps up ^{13}C rich material, generated during core H burning. Dearborn et al.(1976) show that for initial $^{12}C/^{13}C$ ratios in the range 40 to 90 convection can give surface values of $^{12}C/^{13}C$ in the range 20 to 30. For stars of less than between 2 and 3 solar mass, the first ascent of the giant branch is terminated dramatically by the He core flash (Iben 1965) and the onset of core He burning. This event is probably accompanied by mass loss,which also plays an important part throughout a stars post main sequence life. The He core flash may be accompanied by extensive mixing although this is not predicted by present theory. Such mixing could cause the star to return all the way to the H burning main sequence and has been suggested by Sneden and Bond (1976) as the origin of the subgiant CH stars. If the star is a Pop II object the onset of core He burning causes it to return to the hotter and less luminous horizontal branch while Pop I objects move to the slightly cooler Pop I clump region.

Towards the end of core He burning the star once more ascends the giant branch, this time with concentric He and H burning shells. Theory predicts that as the star crosses the line illustrated in Fig.7.10 it will begin to experience regular He shell flashes. The upper mass limit for this phenomena is considered to be between 10 - 15 $M_{\odot}$ by Scalo and Miller (1979). This stage of evolution continues until the commencement of core carbon burning.

It will be clear from this brief outline that one of the fundamental problems of relating evolutionary status to position in the HR diagram is the considerable overlap by quite different evolutionary phases.

One of the most striking aspects of Fig. 7.10 is the fact that the majority of cool C and S stars all lie to the right of the locus of the onset of He shell flashes, while the early C stars and Ba stars lie at lower luminosities. It is very tempting to conclude that the early C stars and Ba star peculiarities are formed during the core He flash, while the remaining peculiar surface abundances of the late C, S and SC stars, are formed as a result of the He shell flashes. This idea has been investigated by Scalo and Miller (1979) who relate the observed mass amd spece densities of peculiar stars to possible birthrates and evolutionary theory.

They conclude that the space densities of R and Ba stars are consistant with their being partly mixed during the core He flash and that only 2-3% of all stars experiencing the flash, need become R and Ba stars. They note that the actual space densities of the S, SC and N stars are very uncertain but are in about the ratio of the intervals of C/O covered by each class. They further conclude that the data for these stars are marginally consistant with their having originated during the He shell flash stage. They admit that their arguments are not very strong and note that there are some N and S stars which are too massive to experience either He core or shell flashes. Iben and Truran (1978) go further and on the basis of evolutionary models emphatically state; ".... the bulk of all N and S stars do not owe their high surface abundances of ^{12}C and s process elements, to the thermal pulse ^{22}Ne source mechanism which produces large enhancements of ^{12}C and s process elements only when M_{BOL} is brighter than -6.0". Yet further doubt is provided by the position of TT9 in Fig. 7.10 which despite its membership of a very young cluster lies at the end of a 1 solar mass evolutionary track.

The most convincing evidence that the s process abundances are produced during the double shell burning phase is the presence of Tc, discovered in some N and S stars by Merrill (1952, 1956). This indicates that these stars must have undergone nuclear synthesis within the last $\sim 10^5$ years, which is far too short a time for them to move from the He core to the He shell flashing stage. It seems very probable that there is some extra parameter, related to the stars structure, that has yet to be included in the stellar evolution calculations. An important clue may exist in the observation by McClure et al. (1980) that all Ba stars may be spectroscopic binaries.

Despite the rather pessimistic impression regarding the agreement between theory and observation it is worth looking, in slightly more detail, at the broad predictions of the He shell burning theory and how it may relate to UY Cen.

Iben (1976) and papers cited therein, show that during double shell burning ^{13}C will be diluted by newly formed ^{12}C and s process rich material. The ^{12}C and s process synthesis occurs in a deep convective shell that is formed during thermal pulses and is brought to the surface between thermal pulses by the outer convective envelope. At this stage it is possible that sufficient carbon is produced to give $C/O \geq 1$ and form carbon stars. This is consistent with Catchpole and Feast's (1976) confirmation that N stars have larger Zr/Ti ratios than S stars.

It is also consistent with Fujita's and Tsuji's (1977) suggestion that ^{13}C is low in all N stars compared with normal giants. The process of ^{12}C enhancement continues until the temperature at the base of the convective envelope becomes high enough to convert ^{12}C into ^{13}C and then into ^{14}N by proton capture. This will reduce the overall carbon abundance while increasing the relative ^{13}C abundance. This phase of evolution corresponds to the deep convection or "hot bottom" phase described by Scalo et al. (1975) when it is possible to generate $^{12}C/^{13}C$ ratios less than 20 and is also a possible site for lithium production. This evolutionary model suggests to us that there are two times when SC stars may be formed. The first is at low luminosity, when carbon and s process abundances are increasing and C/O reaches unity for the first time. The second will be at much higher luminosity, when carbon is being destroyed in the hot bottom phase. A simple model of the variation of $^{12}C/^{13}C$ with C/O can be constructed by assuming first, that as ^{12}C is added to a star's atmosphere there is no change in $^{13}C/O$ and second, that as ^{12}C is burnt to ^{13}C and ^{14}N there is no change in the oxygen abundance. Some of the predictions of this model are compared with observations in Fig.7.11. The open circles and crosses are supergiants and giants, from Luck (1978) and Lambert and Ries (1977) respectively. The squares represent carbon stars, with $^{12}C/^{13}C$ taken from the sources given below and with C/O ratios from Gow (1977), UY Cen is represented by the triangle and an assumed C/O = 1. A logarithmic scale is appropriate for $^{12}C/^{13}C$ as an error of say a factor two represents a constant interval in such a diagram. The diagonal lines in Fig. 7.11 represent the predicted loci of stars with increasing ^{12}C and different but constant $^{13}C/O$. They are drawn to include the extreme values of $^{12}C/^{13}C$ and C/O observed amongst the supergiants. It is seen that a number of the N stars with the highest $^{12}C/^{13}C$ ratios, as well as UY Cen, lie between these lines. This implies that they could have been produced by simply adding ^{12}C to the atmospheres of normal giants or supergiants. The near vertical lines, on the right hand side of Fig. 7.11 are the predicted loci of stars which are burning their atmospheric carbon. The dashes across these curves correspond to equal intervals of time. The inverval being the time for one quarter of the ^{12}C to be burnt. It is apparent that once a star starts to burn carbon and again approaches C/O = 1 it rapidly reduces its $^{12}C/^{13}C$

ratio. This behaviour is insensitive to both the initial $^{12}C/^{13}C$ ratio and the burning rates which are set at (^{13}C burn rate) = 3.44 (^{12}C burn rate). Within the observational uncertainties the distribution of carbon stars in Fig. 5.10 is consistent with the model. The stars are expected to lie between the diagonal lines or near the vertical tracks and preferably near their base where the stars should spend most of their time. In this model UY Cen is apparently at the stage where C/O = 1 for the first time, which is consistent with our statistically determined value of M_{Bol} = -4.5. Since we only expect a high lithium abundance in the hot bottom phase of evolution (cf. Scalo et al.1975) we would anticipate that the super lithium rich SC and CS stars, LMC 89 Henize 166 and Case 621, might be in this phase and at the point where C/O reaches unity for the second time. They might thus be expected to show much higher ^{13}C abundances. We have examined the red and infrared 80 Å mm^{-1} spectra on Henize 166 and Case 621 stars but neither show ^{13}C. Unfortunately this only places a very high upper limit on the ^{13}C abundance as CN is intrinsically not very strong in these stars so this suggestion can not be confirmed at present. It is not possible to say anything about the ^{13}C abundance in LMC 89 but it is noteworthy that its M_{Bol} is a magnitude brighter than the galactic SC stars, possible evidence that it is at the C/O = 1 phase for the second time. Red and infrared 80 Å mm^{-1} spectra are also available for the SC stars GP Ori and FU Mon. Both stars are spectroscopically very similar to UY Cen and likewise do not show the 6260 Å ^{13}CN feature. This disagrees with Yamashita (1972) who classifies both as J stars.

The mild S star χ Cyg has a $^{12}C/^{13}C$ ratio consistent with its being at a stage of evolution intermediate between that of the normal M stars and the SC stars. The strong Mira S star, R And presents something of a problem. It has an s process rich spectrum and shows Tc, which implies that it is probably undergoing regular thermal pulses and has a low $^{12}C/^{13}C$ (= 6) ratio which suggests it is also undergoing hot bottom convection. This is not however consistent with the low M_{Bol} = -4.9 found by Feast et al.(1976). A further interesting problem arises with WZ Cas which shows no Zr (Peery private communication) but does show enhancements of 6th period elements. This situation could only arise with the continued exposure of heavy elements beyond the point where all the Fe had been exhausted, when the s abundance peak would shift to larger atomic weights. Since Fe is clearly present in WZ Cas, this model would require the added complication that the s processing has to be confined to one small region of the star's surface.

7.08 Suggestions for Future Work

The theory of stellar evolution is still very uncertain in explaining the position of peculiar red giants in the HR diagram, in all but the broadest outline. It would therefore be of great value to obtain more accurate data for all the parameters of mass luminosity age and composition, discussed in this thesis and so provide the theoreticians with further clues.

The statistical properties of the SC stars would be better defined by obtaining a larger sample. The advent of modern detectors means that velocity and spectral information could be obtained for stars discovered on much deeper objective prism surveys. This would be especially worthwhile in the Magellanic Clouds where the distance modulus is well known. It must be remembered that the Cloud peculiar red giants may be intrinsically different from the Galaxy ones.

It would be worth determining the $^{12}C/^{13}C$ ratios for the SLR, SC and CS stars. This might indicate whether these stars are at a different phase of evolution to normal SC stars.

Our analysis indicates that more accurate abundances could be obtained for the heavy elements, by improving the quality of the observational and laboratory data,without necessarily having to use a more sophisticated theory. This would allow more detailed comparison with the theoretical s process distributions.

Modern photon counting detectors would allow a search for Tc to be made to much fainter magnitudes. This is probably the simplest diagnostic of current s process production. Modern detectors also allow us to search for spectroscopic binaries and see whether the frequency is as high as that suggested amongst the Ba stars. This might provide a clue as to the perturbation necessary to generate a peculiar giant or even whether some peculiar giants have acquired their s process elements from evolved faint companions via mass transfer.

This thesis indicates that the problem of determining Li abundances in cool stars is subject to large uncertainties. Resolving these uncertainties will probably require much more sophisticated model atmospheres which allow for non LTE and sphericity effects.

References

Allen, C.W., 1973. Astrophysical Quantities, 3rd edition, Athlone Press.

Allen, M.S., 1976. Publ. astr. Soc. Pacific., 88, 338.

Allen, M.S., Cowley, C.R., 1974. Astrophys. J., 190, 601.

Aller, L.H., 1963. The Atmospheres of the Sun and Stars. 2nd edition. Ronald Press New York.

Aller, L.H., 1965. Advances in Astronomy and Astrophysics, Vol. 3, page 1. Editor Zdenek Kopal, Academic Press New York London.

Aller, M.F., Everett, H.M., 1972. Astrophys. J., 172, 447.

Andersen, T., Poulsen, O., Ramanujam, P.S., Petrakiev Petkov, A., 1975. Solar Phys., 44, 257.

Arnold, J.O., Nicholls, R.W., 1972. J. Quant. Spectrosc. Rad. Trans., 12, 1435.

Auman, J.R., Woodrow, J.E.J., 1975. Astrophys. J., 197, 163.

Balona, L.A., Feast, M.W., 1974. Mon. Not. R. astr. Soc., 167, 621.

Barnes, T.G., Evans, D.S., 1976. Mon. Not. Roy. astr. Soc., 174, 489.

Barnes, T.G., Evans, D.S., Moffell, T.J., 1978. Mon. Not. Roy. astr. Soc., 183, 285.

Baschek, B., 1979. Les Elements et leurs Isotopes dans l'Univers. (Liege Colloquium), 327.

Becker, W., Fenkart, R., 1970. IAU Symposium, 38, 205. Reidel.

Bessell, M.S., 1979. Publ. astr. Soc. Pacific, 91, 589.

Bidelman, W., 1950. Astrophys. J., 112, 219.

Bidelman, W., 1953. Les Processus Nucleaires dans les Astres (Liege Colloquium) page 402.

Biemont, E., Grevesse, N., 1977. Physica Scripta, 16, 39.

Blaauw, A., 1965. Stars and Stellar Systems. Vol. 5, page 435 Editors Blaauw, A., Schmidt, M., University Chicago Press.

Blanco, V.M., 1965. Stars and Stellar Systems 5, 241. Edited Blaauw, A., Schmidt, M., University Chicago Press.

Boesgaard, A.M., 1970. Astrophys. J., 161, 163.

Bond, H.E., Luck, R.E., Newman, M.J., 1979. Astrophys. J., 233, 205.

van Breda, I.G., Carr, D.M., Edwin, R.P., Partridge, J.H., 1978. ESO/SRC Conference on Application of Camac to Astronomy.

Breger, M., 1976. Astrophys. J. Suppl., 32, 1.

Burbidge, E.M., Burbidge, G.R., Fowler, W.A., Hoyle, F., 1957. Rev. mod. Phys., 29, 547.

Cameron, A.G.W., 1970. Space Science Reviews, 15, 121.

Cannon, A.J., Pickering, E.C., 1918. Ann. astr. Obs. Harvard College, 91 to 99.

Carbon, D.F., Gingerich, O., 1969. Theory and Observation of Normal Stellar Atmospheres, p.377, editor O. Gingerich, M.I.T. Press.

Catchpole, R.M., 1975. Publ. astr. Soc. Pacific, 87, 397.

Catchpole, R.M., 1979. Les Elements et leurs Isotopes dans l'Univers (Liege Colloquium) 381.

Catchpole, R.M., 1981. Mon. Not. R. astr. Soc., in press.

Catchpole, R.M., Feast, M.W., 1971. Mon. Not. R. astr. Soc., 154, 197.

Catchpole, R.M., Feast, M.W., 1971b. Observatory, 91, 29.

Catchpole, R.M., Feast, M.W., 1976. Mon. Not. R. astr. Soc., 175, 501.

Catchpole, R.M., Glass, I.S., 1974. Mon. Not. R. astr. Soc., 169, 69.

Catchpole, R.M., Robertson, B.S.C., Lloyd Evans, T.H.H., Feast, M.W. Glass, I.S., Carter, B.S., 1979. South African astr. obs. Circular 1, 61.

Catchpole, R.M., Robertson, B.S.C., Warren, P.R., 1977. Mon. Not. R. astr. Soc., 181, 391.

Cayrell, R., Jugaku, J., 1963. Ann. d'Astrophys., 26, 648.

Clegg, R.E.S., Wyckoff, S., 1977. Mon. Not. R. astr. Soc., 179, 417.

Climenhaga, J.L., 1966. Colloquium on Late Type Stars, editor M. Hack p.54.

Climenhaga, J.L., Harris, B.L., Holts, J.T., Smolinski, J., 1977. Astrophys. J. 215, 836.

Corliss, C.H., Bozman, W.R., 1962. Nat. Bureau Standards Monograph 53.

Cowley, C.R., 1970. The Theory of Stellar Spectra.University of Michigan Press.

Cowley, C.R., Cowley, A.P., 1964. Astrophys. J., 140, 713.

Cowley, C.R., Downs, P.L., 1980. Astrophys. J., 236, 648.

Culver, R.B., 1971. An Analysis of the Spectrum of the Irregular Variable CY Cygni 5000-6700 Å, PhD, Ohio State University.

Davis, D.N., 1971. Astrophys. J., 167, 327.

Davis, D.N., 1979. Les Elements et leurs Isotopes dans l'Univers (Liege Colloquium) 365.

Davis, S.P., Phillips, J.G., 1963. The Red System of the CN Molecule, University of California Press.

Day, R.W., Lambert, D.L., Sneden, C., 1973. Astrophys. J., 185, 213.

Dean, C.A., 1976. Astron. J., 81, 364.

Dearborn, D.S.P., Eggleton, P.P., Schramm, D.N., 1976. Astrophys. J., 203, 455.

Delbouille, L., Neven, L., Roland, G., 1973. Photometric Atlas of the Solar Spectrum from λ 3000 to λ 10000 Å. Liege.

Delhaye, J., 1965. Stars and Stellar Systems. Vol. 5 page 61.Editors Blaauw, A., Schmidt, M., University Chicago Press.

Dominy, J.F., Hinkle, K.H., Lambert, D.L., Hall, D.N.B., Ridgway, S.T., 1978. Astrophys. J., 223, 949.

Dubois, I., 1977. Astron. Astrophys. 57, 51.

Earls, L.T., 1935. Phys. Rev. 48, 423.

Eggen, O.J., 1972. Astrophys. J., 177, 489.

Fay, T., Marenin, I., van Citters, W., 1971. J. Quart. Spectrosc. Rad. Trans., 11, 1203.

Feast, M.W., 1954. Les Particules Solides dans les Astres (Liege Colloquium) page 280.

Feast, M.W., 1956. Les Molecules dan les Astres (Liege colloquium) page 301.

Feast, M.W., 1963. Mon. Not. R. astr. Soc., 125, 367.

Feast, M.W., Catchpole, R.M., Glass, I.S., 1976. Mon. Not. R. astr. Soc., 174, 81.

Feast, M.W., Robertson, B.S.C., Catchpole, R.M., Lloyd Evans, T.H.H., Glass, I.S., Carter, B.S., 1980. Submitted to Mon. Not. R. astr. Soc.

Fowler, A., 1909. Mon. Not. R. astr. Soc., 69, 508.

Fujita, Y, Tsuji, T., 1977. Publ. Astron. Soc. Japan, 29, 711.

Fujita, Y., Tsuji, T., Maehara, H., 1966. Proc. Japanese, Acad. 42, 765.

Gasson, R.E.M., 1966. Ph.D. Thesis, Cambridge University.

Gatterer, A., Junkes, J., Salpeter, E.W., 1957. Molecular Spectra of Metallic Oxides, Vatican Observatory.

Gingerich, O., Kumar, S.S., 1964. Astron. J. 69, 139.

Gingerich, O., Latham, D.W., Linsky, J., Kumar, S.S., 1966. Trieste Colloquium on Late Type Stars, p.291, editor Hack, M.

Gingerich, O., Noyes, R.W., Kalkofen, W., Cuny, Y., 1971. Solar Phys., 18, 347.

Glass, I.S., 1974. Mon. Not. astr. Soc. Sth. Africa, 33, 53.

Gow, C.E., 1977. Publ. Astron. Soc. Pacific, 89, 510.

Gray, D.F., 1976. The Observation and Analysis of Stellar Photospheres, Wiley Interscience.

Greene, A.E., 1972. Contributions Perkins Obs. Series II, 31, 1.

Greene, T.F., 1969. Astrophys. J. 157, 737.

Grevesse, N., Blanquet, G., 1969. Solar Physics, 8, 5.

Hardie, R.H., 1962. Stars Stellar Systems. Vol. 2, page 178. Editor Hiltner, W.A., University of Chicago Press.

Harrison, G.R., 1939. Massachusetts Institute of Technology Wavelength Tables. John Wiley and Sons, New York.

Havnes, O., van der Hewvel, E.P.J., 1972. Astron. Astrophys. 19, 283.

Held, E.F.M. van der, 1931. Zs. Phys., 70, 508.

Herbig, G.H., 1965. Astrophys. J., 141, 588.

Herk, G. van, 1965. Bull. astr. Inst. Netherl., 18, 71.

Herzberg, G., 1950. Spectra of Diatomic Molecules 2nd edition. Van Nostrand Reinhold Company.

Hjerting, F., 1938. Astrophys. J., 88, 508.

Hotop, R., Marek, J., 1978. Zeits für Physik. A, 287. 15.

Iben, I., 1965. Astrophys. J., 142, 1447.

Iben, I., 1976. Astrophys. J., 208, 165.

Iben, I., Truran, J.W., 1978. Astrophys. J., 220, 980.

Johnson, H.L., 1965. Com. Lunar. Planet. Lab.,3, 73.

Johnson, H.L., 1966. Ann. Rev. Astr. Astrophys.,4, 193.

Johnson, H.L., 1968. Stars Stellar Systems. Vol. 7, page 167. Editors Middlehurst, B.M., Aller, L.H. University Chicago Press.

Johnson, H.R., 1974. NCAR-TN/STR 95 NCAR Technical Note.

Johnson, H.R., Kelch, W.L., 1972. Bull. A.A.S. 4, 323.

Johnson, H.R., Mendez, M.E., 1970. Astrophys. J., 75, 785.

Keenan, P.C., 1954. Astrophys. J., 120, 484.

Keenan, P.C., 1958. Handbuch der Physik, Vol. 50, page 101. Springer-Verlag, Berlin.

Keenan, P.C., Boeshaar, P.C., 1980. Astrophys. J. Supp. 43, 379.

Kilston, S., 1975. Publ. astr. Soc. Pacific, 87, 189.

Krueger, T.K., Aller, L.H., Ross, J., Czyzak, S.J., 1968. Astrophys. J., 152, 765.

Kurucz, R.L., Peytremann, E., 1975. Smithsonian Astrophys. Obs. Special Report 362.

Lambert, D.L., Luck, R.E., 1978. Mon. Not. R. astr. Soc., 183, 79.

Lambert, D.L., Ries, L.M., 1977. Astrophys. J., 217, 508.

Lambert, D.L., Warner, B., 1968. Mon. Not. R. astr. Soc., 138, 181.

Lennard, W.N., Whaling, W., Scalo, J.M., Testerman, L., 1975. Astrophys. J., 197, 517.

Luck, R.E., 1977. Astrophys. J., 218, 752.

Luck, R.E., 1978. Astrophys. J., 219, 148.

Marek, J., Münster, P., 1978. Astron. Astrophys., 62, 245.

Marenin, I., 1970. Bull. A.A.S., 2, 329.

McClure, R.D., Fletcher, J.M., Nemec, J.M., 1980. Astrophys. J. Lett., 238, L35.

Meggers, W.F., Corliss, C.H., Scribner, B.F., 1975. Nat. Bureau Standards Monograph 145.

Meggers, W.F., Scribner, B.F., 1950. J. Res. Nat. Bureau Standards, 45, 476.

Merrill, K.M., Stein, W.A., 1976. Publ. astr. Soc. Pacific., 88, 285.

Merrill, P.W., 1923. Publ. astr. Soc. Pacific., 35, 216.

Merrill, P.W., 1952. Astrophys. J., 116, 21.

Merrill, P.W., 1956. Publ. astr. Soc. Pacific., 68, 70.

Mihalas, D., 1977. Stellar Atmospheres. University of Chicago Press.

Molnar, H., 1972. Astron. Astrophys., 20, 69.

Moore, C.E., 1959. Nat. Bureau Standards, Technical note 36.

Moore, C.E., Minnaert, M.G.J., Houtgast, J., 1966. The Solar Spectrum 2935 to 8770 Å., Nat. Bureau Standards Monograph 61.

Morgan, W.W., Keenan, P.C., Kellman, E., 1943. An Atlas of Stellar Spectra, University of Chicago Press, plate 55.

Oort, J.H., 1965. Stars and Stellar Systems. Vol. 5 page 455. Editors Blaauw, A., Schmidt, M., University Chicago Press.

Pearse, R.W.B., Gaydon, A.G., 1975. The Identification of Molecular Spectra, Fourth edition, Chapman Hall, London.

Peery, B.F., Jr., 1971. Astrophys. J., 163, L.1.

Phillips, J.G., Davis, S.P., 1976a. Astrophys. J., 206, 632.

Phillips, J.G., Davis, S.P., 1976b. Astrophys. J. Suppl., 32, 537.

Piccirillo, J., 1980. Mon. Not. R. astr. Soc., 190, 441.

Powell, A.L.T., 1969. R. Obs. Bull., 152.

Reader, J., Davis, S.P., 1967. J. Res. Nat. Bureau Standards, 71A, 587.

Richer, H.B., 1971. Astrophys. J., 167, 521.

Richer, H.B., Frogel, J.A., 1980. Astrophys. J., 242, L9.

Ridgway, S.T., Wells, D.C., Joyce, R.R., Allen, R.G., 1979. Astron. J., 84, 247.

Robertson, B.S.C., 1980. Master Science Thesis. University of Cape Town.

Robertson, B.S.C., Catchpole, R.M., 1981. Mon. Not. astr. Soc. South Africa, 39, 82.

Russell, H.N., Bowen, I.S., 1929. Astrophys. J., 69, 196.

Scalo, J.M., 1976. Astrophys. J., 206, 474.

Scalo, J.M., Despain, K.H., Ulrich, R.K., 1975. Astrophys. J., 196, 805.

Scalo, J.M, Miller, G.E., 1979. Astrophys. J., 233, 596.

Smart, W.M. Text-book of Spherical Astronomy. 5th edition 1962, page 109. Cambridge University Press.

Sneden, C., Bond, H.E., 1976. Astrophys. J., 204, 810.

Stellmacher, G., Wiehr, E., 1970. Astron. Astrophys., 7, 432.

Stephenson, C.B., 1967. Astrophys. J., 150, 543.

Stephenson, C.B., 1976. Pub. Warner and Swasey Obs. Vol 2 No 2.

Struve, O., Elvey, C.T., 1934. Astrophys. J., 79, 409.

Tatum, J.B., 1967. Astrophys. J. Supp., 14, 21.

Tech, J.L., 1971. Nat. Bureau Standards Monograph 119.

Terrill, C.L., 1969. Astron. J., 74, 413.

Teske, R.G., 1956. Publ. astr. Soc. Pacific., 68, 520.

Torres-Peimbert, S., Wallerstein, G., 1966. Astrophys. J., 145, 724.

Tsuji, T., 1962. Publ. astr. Soc. Japan, 14, 222.

Utsumi, K., 1970. Publ. astr. Soc. Japan, 22, 93.

Walker, A.R., 1976. Ph.D. Thesis. University of Cape Town.

Walker, A.R., 1979. South African astr. circ., 1, 112.

Wallerstein, G., Conti, P.S., 1969. Ann. Rev. Astr. Astrophys. 7, 99.

Wilson, W.J., Schwartz, P.R., Neugebauer, G., Harvey, P.M., Becklin, E.E., 1972. Astrophys. J., 177, 523.

Wojslaw, R.S., Peery, B.F., Jr., 1976. Astrophys. J. Suppl., 31, 75.

Wrubel, M.H., 1949. Astrophys. J., 109, 588.

Wrubel, M.H., 1960. Aller in Stars and Stellar Systems. Vol. 6, page 199. Editor Greenstein, J.L. University Chicago Press.

Wyckoff, S., Clegg, R.E.S., 1978. Mon. Not. R. astr. Soc., 184, 127.

Wyckoff, S., Wehinger, P.A., 1977. Astrophys. J., Lett., 212, L319.

Wyller, A.A., 1966. Astrophys. J., 143, 828.

Yamashita, Y., 1972. Ann. Tokyo Astron. Obs., 13, 169.

Yamashita, Y., 1973. Publ. astr. Soc. Japan, 25, 511.

Yamashita, Y., Unno, W., 1963. Publ. astr. Soc. Japan, 15, 230.

Yorka, S.B., 1976. A Catalogue of S Type Stars and a Study of their Galactic Distribution. MSc Thesis, Ohio State University.